E. V. ARMENSKY
G. B. FALK

FRACTIONAL-HORSEPOWER ELECTRICAL MACHINES

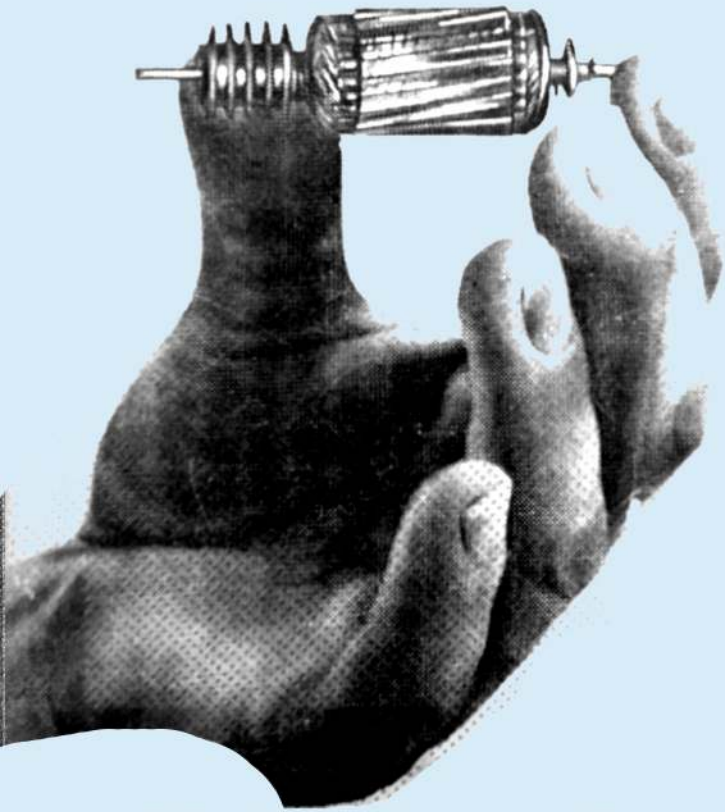

Mir Publihsers Moscow

This book is concerned with the theory of, and physical processes occurring in, miscellaneous fractional-horsepower electrical machines; special attention is given to static and dynamic characteristics of these machines; the book also presents design and construction features of fractional-horsepower electrical machines and gives illustrative examples of their application.

Along with general-purpose fractional-horsepower machines of a large-scale production, the book deals with a number of promising types, such as contactless fractional-horsepower d.c. motors, low-inertia machines, amplifier motor-generator sets and synchro-motor units, fractional-horsepower synchronous harmonic-drive motors, fractional-horsepower steromotors, etc.

The book is intended for use in the curriculum for electrical-engineering students and may be of interest for electrical engineers dealing with fractional-horsepower electrical machines.

E. V. ARMENSKY
G. B. FALK

FRACTIONAL-HORSEPOWER ELECTRICAL MACHINES

ИЗДАТЕЛЬСТВО
МИР

Е. В. АРМЕНСКИЙ, Г. Б. ФАЛК

ЭЛЕКТРИЧЕСКИЕ МИКРОМАШИНЫ

ИЗДАТЕЛЬСТВО «ВЫСШАЯ ШКОЛА»
МОСКВА

MIR PUBLISHERS • MOSCOW

E. V. ARMENSKY
G. B. FALK

FRACTIONAL-HORSEPOWER ELECTRICAL MACHINES

Translated from the Russian
by

O. B. VOLODINA

First published 1978
Revised from the 1975 Russian edition

The Greek Alphabet

Α α	Alpha	Ι ι	Iota	Ρ ρ	Rho
Β β	Beta	Κ κ	Kappa	Σ σ	Sigma
Γ γ	Gamma	Λ λ	Lambda	Τ τ	Tau
Δ δ	Delta	Μ μ	Mu	Υ υ	Upsilon
Ε ε	Epsilon	Ν ν	Nu	Φ φ	Phi
Ζ ζ	Zeta	Ξ ξ	Xi	Χ χ	Chi
Η η	Eta	Ο ο	Omicron	Ψ ψ	Psi
Θ ϑθ	Theta	Π π	Pi	Ω ω	Omega

The Russian Alphabet and Transliteration

А а	a		К к	k		Х х	kh
Б б	b		Л л	l		Ц ц	ts
В в	v		М м	m		Ч ч	ch
Г г	g		Н н	n		Ш ш	sh
Д д	d		О о	o		Щ щ	shch
Е е	e		П п	p		Ъ ъ	''
Ё ё	yo		Р р	r		Ы ы	y
Ж ж	zh		С с	s		Ь ь	'
З з	z		Т т	t		Э э	e
И и	i		У у	u		Ю ю	yu
Й й	y		Ф ф	f		Я я	ya

На английском языке

© «Высшая школа», 1975 г.
© English translation, Mir Publishers, 1978

Contents

PREFACE 7

INTRODUCTION 9

0.1. Classification of Fractional-Horsepower Electrical Machines and Their Functions in State-of-the-Art Engineering 9
0.2. Basic Technical and Economic Requirements to Fractional-Horsepower Electrical Machines 12
0.3. General Problems of Fractional-Horsepower Machine Reliability 13

Chapter One. ROTARY AMPLIFIERS 22

1.1. General Information and Classification 22
1.2. Self-Excited Rotary Amplifier 24
1.3. Cross-Magnetized Rotary Amplifier (Amplidyne). Mechanical Design and Principle of Operation 31
1.4. Amplidyne Static and Dynamic Characteristics . . . 36
1.5. Application of Rotary Amplifiers 44

Chapter Two. FRACTIONAL-NORSEPOWER ELECTRIC MOTORS 48

2.1. General Information and Classification 48
2.2. Fractional-Horsepower D.C. Servo Motors. Mechanical Design and Principle of Operation 49
2.3. Methods of Control of Fractional-Horsepower D.C. Servo Motors 63
2.4. Dynamic Characteristics of Fractional-Horsepower D.C. Servo Motors 77
2.5. Universal Fractional-Horsepower Commutator Motors 82
2.6. Fractional-Horsepower Induction Servo Motors. Mechanical Design and Principle of Operation . . . 87
2.7. Methods of Control of Fractional-Horsepower Induction Servo Motors 100
2.8. Dynamic Characteristics of Fractional-Horsepower Induction Servo Motors 112
2.9. Continuous-Running Fractional-Horsepower Synchronous Motors 116
2.10. Stability of Fractional-Horsepower Synchronous Motor Speed 138
2.11. Continuous-Running Low-Speed Synchronous Motors 145
2.12. Stepper Motors 161

2.13. Auxiliary Fractional-Horsepower Single-Phase Motors 176
2.14. A. C. Motor Sets 186
2.15. Application of Servo Motors 192

Chapter Three. TACHOGENERATORS 198
3.1. General Information and Classification 198
3.2. Direct-Current Tachogenerators 199
3.3. A.C. Induction Tachogenerators 208
3.4. Alternating-Current Synchronous Tachogenerators . . 221
3.5. Dynamic Characteristics of Tachogenerators 222
3.6. Application of Tachogenerators 224

Chapter Four. SYNCHROS 230
4.1. General Information and Classification 230
4.2. Mechanical Design of Single-Phase Synchros . . . 231
4.3. Synchro Indicators 237
4.4. Synchro Transformers 247
4.5. Differential Synchros in Indicating Transmission Systems 252
4.6. High-Torque Indicating Transmission System . . . 254
4.7. Dynamic Characteristics of Synchro Indicators . . 256
4.8. Application of Synchros 259

Chapter Five. ROTARY TRANSFORMERS 265
5.1. General Information and Classification 265
5.2. Mechanical Design of Rotary Transformers 266
5.3. Sine-Cosine Rotary Transformers 269
5.4. Rotary Transformer Balancing Adjustment 275
5.5. Linear, Scale, and Vector-Computing Rotary Transformers 280
5.6. Rotary Transformer Errors 291
5.7. Sine-Cosine Rotary Transformers as Parts of Remote High-Accuracy Angular Displacement Transmission Systems 294
5.8. Application of Rotary Transformers 300

BIBLIOGRAPHY. 306

APPENDICES 307

INDEX 333

Preface

The fractional-horsepower electrical machines ranging from fractions of a watt to 750 watts are essential parts of automatic control and regulation systems, computers, gyroscopes and domestic appliances.

Most papers and text-books concerning electrical machines and fractional-horsepower machines of automatic-control systems give a comprehensive analysis of their theory, mechanical design, and calculations. Among them are the books of Soviet authors, such as, Kostenko M.P., Piotrovsky L.M., Iosifyan A.G., Chechet Yu.S., Khrushchev V.V., and also the works of foreign authors: Cron G., White D., Woodson G., Seely S., Robisho L., and others.

The authors of this book are not going to show how to design, calculate, and manufacture fractional-horsepower electrical machines. The primary aim of this book is to familiarize future electrical engineers with the principle of operation, construction and, in particular, with characteristics and options of automatic control elements based on electrical machines, to teach them to properly select an appropriate element and to use it in state-of-the-art automatic-control systems. The text has been written on the assumption that the students are already familiar with the general theory of electrical machines. The book is based on the lectures read by the authors at the Moscow electronic machinery institute.

Introduction

0.1. Classification of Fractional-Horsepower Electrical Machines and Their Functions in State-of-the-Art Engineering

According to their application, the fractional-horsepower electrical machines are available of the following two groups:

(1) a *group of general-purpose fractional-horsepower machines* (Fig. 0.1) that incorporates commutator, induction, and synchronous fractional-horsepower motors meant for individual or tandem operation to drive miscellaneous mechanisms and units, domestic appliances, etc.;

Fig. 0.1. Classification of general-purpose fractional-horsepower electrical machines

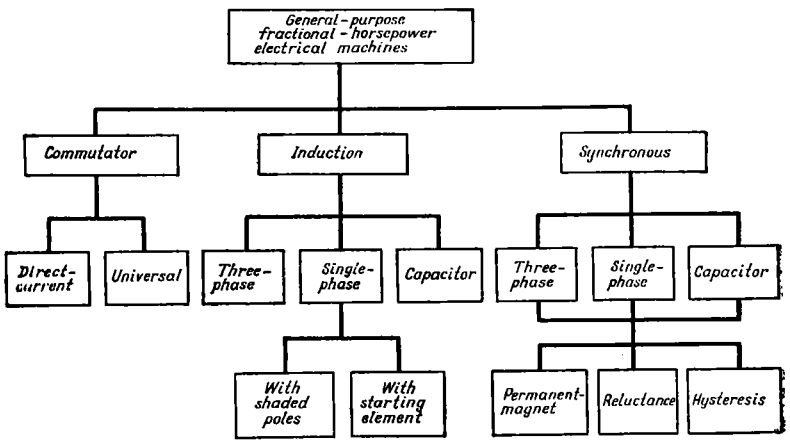

(2) *fractional-horsepower electrical machines for automatic-control systems and units* (Fig. 0.2) that can be subdivided into the following four groups according to their functions:

(a) power machines converting electric power into mechanical energy;

(b) information machines converting the angle of turn, angular velocity, and angular acceleration into an electric signal;

(c) gyro machines incorporated in gyroscopic units and devices;

(d) current and voltage converters, frequency changers, and power amplifiers.

The importance and function of fractional-horsepower electrical machines in modern automatic-control units can be evaluated by studying their operation as part of a servo system.

Figure 0.3 shows a simple servo system. Two potentiometers R_1 and R_2 connected into a bridge circuit are used as a driving and a comparison element. The potentiometers

Fig. 0.2. Classification of fractional-horsepower electrical machines for automatic-control units and devices

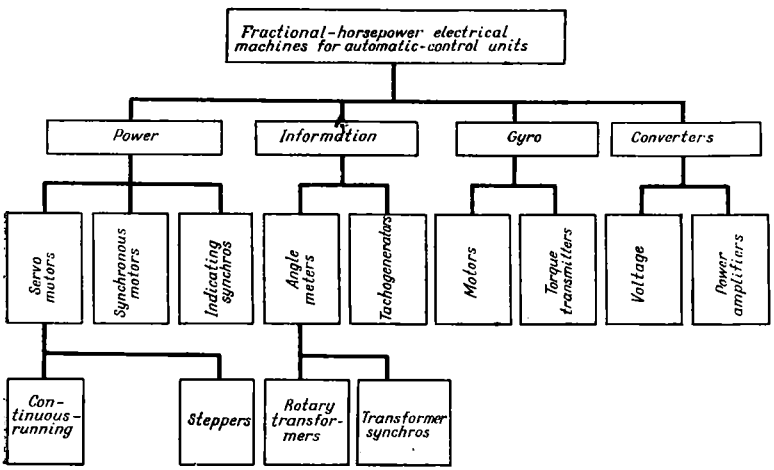

are connected to a d.c. voltage source V. A signal picked off the potentiometer wipers is applied, whenever required, to the converter C, amplified by the amplifier A, and arrives at the servo motor SM. The motor imparts its motion via the reduction unit RU to the equipment under control CE and at the same time moves the wiper of the potentiometer R_2. With the wipers of the potentiometers R_1 and R_2 placed originally in a position, say, I, the potential difference across these wipers will be zero and the system will not pass any signal. Under such a condition the system is said to be in an equilibrium state.

Shifting the wiper of the potentiometer R_1 to position II causes a signal to appear across the converter input; the amplitude of this signal depends on the amount of motion (in our case, it is proportional to the distance between positions I and II) and its polarity depends on the direction of motion (in our case, a positive potential will be picked off the potentiometer R_1 and a negative potential, off the potentiometer R_2). Upon conversion and amplification, the signal will actuate the servo motor and the latter will drive the equipment under control CE and the wiper of the potentiometer R_2. This motion will be in progress until the potentiometer wiper reaches position II. In actual servo systems, a feedback element is incorporated to improve dynamic properties. In our case, the feedback element FBE is provided for the servo motor and the amplifier.

For a direct-current system of this type, a d.c. amplidyne can be used as an amplifier, a d.c. machine as a servo motor,

Fig. 0.3. Servo system

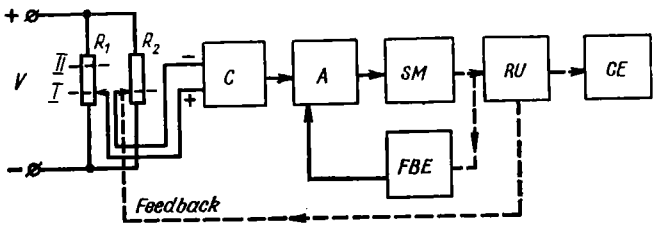

and a d.c. tachogenerator as a feedback element. For an a.c. system, potentiometers can be superseded by synchros or rotary transformers, with an induction motor serving the function of a servo motor and an induction tachogenerator used as a feedback element.

0.2. Basic Technical and Economic Requirements to Fractional-Horsepower Electrical Machines

The basic technical and economic requirements to fractional-horsepower electrical machines can be classified as follows.

1. General requirements disregarding the machine functions, mechanical design, and principle of operation. For general-purpose machines, these requirements are as follows:

(a) high efficiency and power factor;
(b) long service life;
(c) low cost;
(d) simple construction and manufacturing technique;
(e) repairability.

These requirements are not of primary importance for fractional-horsepower machines of automatic-control units and devices. Basic requirements to them are as follows:

(a) high accuracy of conversion of original values;
(b) stability of performance;
(c) fast response;
(d) high reliability.

The basic requirements to information and gyro machines are accuracy and stability of their characteristics. Power machines and converters must have high efficiency and power factor along with sufficient accuracy and fast response.

2. Requirements to fractional-horsepower electrical machines depending on their application and operating conditions:

(a) minimum size and mass at desired performance, essential for airborne equipment;

(b) resistance to vibrations and shocks, essential for transport and agricultural machines and also for airborne equipment;

(c) resistance to environmental effects and radiation, essential for machines operating in nuclear reactors, space vehicles, in tropics;

(d) explosion safety, essential for mine machines;

(e) low noise, essential for recording and reproducing appliances;

(f) low radio interference, essential for machines running in conjunction with electronic equipment or in radar sets;

(g) low amount of gas escaped, essential for machines used in vacuum equipment.

0.3. General Problems of Fractional-Horsepower Machine Reliability

Reliability of a fractional-horsepower electrical machine is the probability that the machine will perform adequately for the length of time intended and under the operating environment encountered.

Reliability is one of basic technical and economic characteristics of the machines. High reliability is most important for fractional-horsepower machines used in short-lived or one-shot devices or in special-purpose apparatus (military equipment, etc.).

Reliability of fractional-horsepower machines intended for a long service life is to be ensured on a reasonable level with due regard for economic factors, that is, the best level of reliability is that obtained at minimum cost.

The quantitative estimate of fractional-horsepower machine reliability is made by using the probability and mathematical statistics methods.

All the pieces of equipment, according to the reliability theory, are classified as *repairable* and *nonrepairable*, that is, the ones that can be repaired upon failure and those that cannot. A failure is an event involving a full or partial loss of serviceability (mechanical or electric trouble, performance degradation, repair outages, etc.). Fractional-horsepower electrical machines are practically repairable pieces of equipment, but they may fall into either of the classes depending on application.

In the theory of reliability failures are usually treated as random events, therefore, all the quantitative characteristics are of probabilistic nature. The most suitable characteristics for the analysis of fractional-horsepower electrical machines, and nonrepairable ones in particular, are as follows.

Probability of trouble-free operation $P(t)$, that is, the probability that the trouble-free running time of a machine till failure is longer than or equal to the specified time interval.

Statistical estimation of the no-failure probability is made by using the formula (on condition that the machines failed are neither repaired nor replaced by new ones):

$$P^*(t) = \frac{N_0 - n(t)}{N_0} \tag{0.1}$$

where N_0 is the number of machines in the beginning of test; $n(t)$ is the number of machines failed within time t.

The probability of fractional-horsepower machine failure

$$Q(t) = 1 - P(t) \tag{0.2}$$

Intensity of failures, $\lambda(t)$, that is, the probability of failures of a machine per time unit after a predetermined moment, equals the failure probability density to no-failure probability ratio:

$$\lambda(t) = \frac{\frac{d}{dt} Q(t)}{P(t)} \tag{0.3}$$

Statistical estimation of the intensity of failures is made from the formula

$$\lambda^*(t) = \frac{n(t)}{\Delta t N_{av}} \tag{0.4}$$

where $n(t)$ is the number of machines failed within the time interval Δt; N_{av} is the average number of machines operating trouble-free within the time internal Δt.

A typical characteristic of the intensity of failures, $\lambda(t)$, obtained for fractional-horsepower electrical machines by experience is illustrated in Fig. 0.4. A relatively high intensity of failures is within portion 0-t_1, but it reduces rather abruptly. This portion illustrates an early-failure period

within which failures occur due to manufacturing defects. The portion t_1-t_2 shows a period of normal operation. Upon the expiration of time t_2 the intensity of failures suddenly increases due to mechanical or electrical wear of the machine components.

Hence, the intensity of failures for a period of normal operation of the machine may be assumed constant, *viz.*, $\lambda = \text{const}$. In such a case, the probability of trouble-free operation obeys the exponential law

$$P(t) = e^{-\lambda t} \tag{0.5}$$

Average time of trouble-free operation t_{av}, that is, mathematical expectation of no-trouble service time of the machine

$$t_{av} = \int_0^\infty P(t)\, dt \tag{0.6}$$

defines an average time interval between the beginning of operation and the first failure.

At $\lambda = \text{const}$, the average no-trouble time

$$t_{av} = 1/\lambda \tag{0.7}$$

may, likewise, characterize the average no-trouble time between two failures.

For a statistical estimation of the average no-trouble time, use is made of the formula

$$t^*_{av} = \frac{\sum_{i=1}^{N_0} t_i}{N_0} \tag{0.8}$$

where t_i is the no-trouble time of an ith specimen.

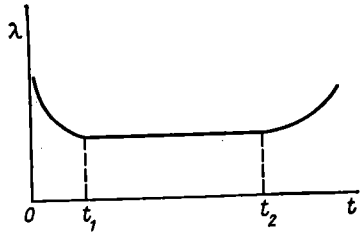

Fig. 0.4. Failure intensity characteristic

Fractional-horsepower electrical machines are less reliable than contactless elements of automatic-control systems, which are free from movable parts.

Intensity of Failures of Automatic-Control System Elements per Hour

Fractional-horsepower electrical machines	$(0.01\text{-}8.0) \times 10^{-4}$
Transformers	$(0.0002\text{-}0.64) \times 10^{-4}$
Resistors	$(0.0001\text{-}0.15) \times 10^{-4}$
Semiconductor devices	$(0.0012\text{-}5.0) \times 10^{-4}$

It is evident from experience that most failures occur due to troubles in the main parts of fractional-horsepower electrical machines or changes in their characteristics.

Given below are most probable troubles in the main parts of fractional-horsepower machines:

Sliding contact:

(a) mechanical damage to brush holders;

(b) damage to commutator or slip rings caused by brushes;

(c) poor contact between commutator or slip rings and brushes due to wear of brushes or insufficient pressure of brush stud on brush.

Bearings:

(a) broken cage;

(b) wedging of bearing due to poor condition of bearing lubricant.

Windings:

(a) broken turns or leads as a result of burning due to overloads, mechanical strain due to temperature fluctuations or electrical corrosion action, especially at high humidity;

(b) earth or turn-to-turn fault of insulation as a result of poor electric strength, especially at high humidity and severe thermal conditions.

Magnetic system:

(a) changes in magnetic characteristics due to shocks, vibrations, and strain;

(b) changes in electromagnetic characteristics as a result of short circuits between stampings, electrical corrosion, etc.

The condition of bearings and sliding contacts greatly depends on the speed of rotation of the machine rotor. Wear of most parts, commutator and brushes in particular,

increases with the rotation speed, hence, the reliability of these parts and of the machine as a whole reduces.

Figure 0.5 illustrates the average no-trouble time t_{av} of some direct-current fractional-horsepower commutator motors as a function of speed ω (solid line) at which they were tested; the rated speed and the time within which they were tested are assumed as unity.

So, the service life that can be guaranteed by the manufacturer depends on the motor rated speed. For example, the guaranteed service life of the series ДПР fractional-horsepower commutator motors will be as follows:

2,000 to 3,000 h for the rated speed of 2,500 r/min;

200 to 600 h for the rated speed of 9,000 r/min.

It means that a higher reliability of fractional-horsepower electrical machines can be attained by dispensing with sliding contacts, that is, by developing contactless constructions. The guaranteed service life of series МБ fractional-horsepower contactless motors rated at speeds as high as 12,500 r/min amounts to approximately 10,000 h while that of direct-current fractional-horsepower commutator motors, series ДПМ, ДПР, and the like, does not exceed 3,000 h even at much lower speeds.

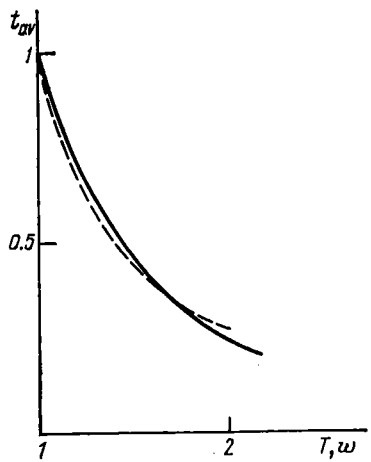

Fig. 0.5. Average time of trouble-free operation of fractional-horsepower direct-current commutator motors as function of temperature and speed

Reliability of machine insulation greatly depends on ambient temperature, relative humidity, and on the temperature of the machine proper. Insulation electric strength decreases with an increase in humidity and absolute temperature with the result that the intensity of failures rises due to earth insulation breakdown and turn-to-turn faults.

Deviations of temperature and humidity from specified operational limits produce a detrimental effect on many parts of machines, and not only on their insulation. Experiments with a number of d.c. and a.c. fractional-horsepower machines have shown that failures due to excessive humidity, high or low temperature amount to approximately 70-100 per cent of the total number of failures resulting from operating the machines under unspecified conditions.

Figure 0.5 illustrates the average no-trouble time t_{av} of some direct-current fractional-horsepower commutator motors *versus* ambient temperature T (dash line) at which they were tested (the rated ambient temperature and the time corresponding to this temperature are assumed as unity).

These are important factors in establishing the service life guaranteed by the manufacturer of fractional-horsepower electrical machines. For example, the service life guaranteed for series ДИД-А fractional-horsepower induction servo motors is 500 h at up to 100°C ambient but it may be raised to 1,000 h if these motors will operate at an ambient temperature not over 70°C.

Operating the machines at temperatures beyond the specified limits worsens their output characteristics in addition to increasing the probability of their troubles. In the case of information machines, this causes an increase in phase and amplitude errors. The power-type machines do not gain the desired speed at inadmissible absolute heating temperatures, etc.

Hence, in selecting fractional-horsepower electrical machines for a particular unit, their thermal conditions must be given a serious consideration. Service conditions of the machines must be also taken into account.

1. The fractional-horsepower electrical machines are commonly manufactured of a totally enclosed type. When this is the case, the temperature rise above ambient is

primarily determined by the amount of power loss per unit area of the machine frame. When mounted in the equipment, the frame may be joined to a metal panel or any other element to improve the conditions of heat transfer.

2. The fractional-horsepower electrical machines may be installed in enclosed units or in compartments accommodating other heat-emitting pieces of equipment. When this is the case, it is most essential to properly calculate the surrounding temperature at which the machine is expected to operate. An increase in the ambient temperature causes an increase in the absolute temperature of the machine, which influences the machine reliability and accuracy of operation, as has been already stated.

3. The power-type fractional-horsepower machines, rotary power amplifiers, induction tachogenerators, general-purpose motors are themselves intensive heat sources. In calculating their thermal conditions, it is important to take into account their operating conditions, such as continuous no-load or full-load running, frequent starts and reversals (intermittent duty), etc. The inherent power losses of information machines, such as rotary transformers or d.c. tachogenerators, are usually lower and their thermal conditions depend primarily on the ambient temperature.

Reliability of fractional-horsepower electrical machines may reduce in the course of service due to vibrations, shocks, and too low atmospheric pressure.

To increase their reliability the following measures should be taken:

(a) improvement of mechanical design;

(b) improvement of manufacturing technique;

(c) increase of heat resistance, mechanical and electrical properties of insulation;

(d) use of machines under specified operating conditions.

Reliability of fractional-horsepower electrical machines is associated with their mechanical and electrical *endurance*. The mechanical and electrical endurance of a machine may be determined by the service life of this machine from the beginning of its operation till its depreciation. The mechanical and electrical endurance is usually a criterion evaluating general-purpose fractional-horsepower machines and other repairable machines. The service life of fractional-

Table 0.1

Machine type	λ, failures per hour	T_g, h
Type ДПМ d.c. fractional-horsepower permanent-magnet commutator motors:		
2,500 r/min	$(1.3\text{-}8)\times10^{-4}$	1,000
9,000 r/min	—	50-300
Type ДПР d.c. fractional-horsepower permanent-magnet commutator motors with a hollow nonmagnetic armature:		
2,500 r/min	—	2,000-3,000
9,000 r/min	—	200-600
Type ПЯ d.c. fractional-horsepower permanent-magnet disk-armature motors	0.1×10^{-4}	500
Type МБ fractional-horsepower permanent-magnet contactless motors	—	10,000
Fractional-horsepower induction servo motors with a nonmagnetic hollow rotor:		
АДП	—	1,500-2,000
ЭМ-М	—	400
ДИД	2.9×10^{-4}	500
Series ДКМ fractional-horsepower squirrel-cage induction servo motors	—	1,000
Type УАД general-purpose fractional-horsepower induction motors	—	3,000
Type АПН high-reliability induction motors	$(0.2\text{-}0.4)\times10^{-4}$	5,000
Domestic single-phase fractional-horsepower induction motors:		
ДАО	1.7×10^{-4}	—
КД-40	1.35×10^{-4}	—
КД-3-5А (with slide bearings)	8.2×10^{-4}	—

Table 0.1 (cont.)

Machine type	λ, failures per hour	T_g, h
Type ДСР fractional-horsepower synchronous reducing motors (rotor speed 115 r/min) with built-in reduction unit of 115/60 or 115/2 gear ratio	0.008×10^{-4}	10,000
Type ДСД fractional-horsepower split-pole synchronous motors (rotor speed 3,000 r/min) with built-in reduction unit of 3,000/60 or 3,000/2 gear ratio	$(1.7\text{-}2.6) \times 10^{-4}$	—
Type ДС permanent-magnet synchronous motors	—	3,000
Type Г fractional-horsepower hysteresis synchronous motors	—	2,000
Permanent-magnet stepper synchronous motors:		
ШД1	10^{-4}	—
ДШ	—	1,000
Type ШД 300 reluctance stepper synchronous motors	0.75×10^{-4}	—
Type БД-160А and БС-155А single-phase magslips with intervening toroidal transformer	0.06×10^{-4}	5,000

horsepower machines is established with due account of their purpose, operating conditions, and economic considerations (this especially concerns general-purpose machines).

An optimum endurance of fractional-horsepower electrical machines, so far as economic considerations are concerned, is such a service life that involves minimum maintenance and running charges throughout the entire service period, as referred to the running time.

Table 0.1 gives approximate reliability characteristics and service life T_g guaranteed by the manufacturer for some types of fractional-horsepower electrical machines.

Chapter

1 ROTARY AMPLIFIERS

1.1. General Information and Classification

An *amplifier* is a unit meant to control rather heavy power (output value) by means of a low-power signal (input value). The output value is a function of the input signal and amplification is afforded by the energy of an external source.

According to the type of energy controlled, the amplifiers are classified as *electrical*, *pneumatic*, *hydraulic*, and *mechanical* amplifiers.

The electrical amplifiers are, in their turn, classified as *electronic*, *thyratron*, *transistorized*, *magnetic*, *segnetoelectric*, and *rotary* amplifiers. The former five are static machines and the latter is an amplifier with a rotating armature.

The output (controlled) power of the rotary amplifiers is produced due to mechanical power of the drive motor.

The *rotary amplifiers* are essentially direct-current commutator machines.

Depending on the method of excitation, the amplifiers are classified as *direct-magnetized* amplifiers and *cross-magnetized* amplifiers or amplidynes.

The *direct-magnetized amplifiers*, in which the main flux is along the direct axis of the machine, are as follows:

(1) independent amplifiers;
(2) self-excited amplifiers;
(3) motor-amplidyne sets;
(4) double-commutator amplifiers;
(5) two- and three-stage direct-magnetized amplifiers.

The *cross-magnetized amplifiers* (*amplidynes*), in which the main flux is along the quadrature axis of the machine, are as follows:

(1) full-pitch winding amplidynes;
(2) half-pitch winding amplidynes;
(3) segregated magnetic system amplidynes.

The lighter the amplifier control power, the lower are the mass and overall dimensions of control gear. Therefore, the most important characteristic of the machine is the amplification or gain factor. The amplifier is characterized by a power gain, a current gain, and a voltage gain.

The *amplidyne power gain* k_P is the output-to-control power ratio:

$$k_P = P_{out}/P_{cont}$$

The *amplidyne current gain* k_I is the ratio of current through the amplidyne output circuit to the control current:

$$k_I = I_{out}/I_{cont}$$

The *amplidyne voltage gain* is the ratio of voltage across the output circuit to the control voltage:

$$k_V = V_{out}/V_{cont}$$

Hence,

$$k_I k_V = k_P$$

The rotary amplifiers may have a rather high power gain (10^3 to 10^5).

One more important characteristic is the *amplifier response* characterized by the time constants of its circuits.

The time constant is determined by the field energy varying in the course of regulation. The time constant of an electric circuit

$$\tau = L/R$$

where L is the circuit inductance and R is the circuit resistance.

The amplifier time constant $\tau = 0.02$ to 0.2 s.

The best amplifier is that having a high power gain and a fast response, that is, minimum time constants. Since the amplifier time constant is proportional to the power gain, different amplifiers can be compared by one more characteristic, a quality factor k_q which is the ratio of the power gain to the sum of time constants of the amplifier stages:

$$k_q = k_P/\Sigma\tau$$

An essential feature of amplifiers operating in automatic-control systems is linearity of their output characteristics,

that is, output *vs* input characteristic curves. When this requirement is complied with, the amplifier gain remains constant irrespective of the control signal.

The rotary amplifiers are used in automatic-control systems as power amplifiers operating primarily during transients, when considerable overload currents are likely to occur. Therefore, one more important characteristic of the rotary amplifiers is their overload capacity.

It is, likewise, very important for the rotary amplifiers to possess high reliability in operation and stability of their characteristics.

Characteristics of rotary amplifiers required under different operating conditions are set forth under Section 0.2.

Where light power is required, cross-magnetized amplidynes are employed, while some special-purpose systems incorporate self-excited rotary amplifiers.

Independently excited amplifiers are similar to independently excited direct-current generators as far as their mechanical design and circuit arrangement are concerned. Independently excited amplifiers possessing a rather low power gain have not found a wide application. In Ward-Leonard systems, however, where a wide range of motor speed control is essential, the generator runs as an independently excited amplifier. Multistage direct-magnetized amplifiers are not actually used in the range of low powers.

1.2. Self-Excited Rotary Amplifier

Self-excited amplifiers have been developed to obtain a high power gain. The self-excited amplifier is distinguished by construction from the independently excited machine in that its field poles carry a self-excitation winding mounted coaxially with the control windings and connected in parallel (Fig. 1.1*a*) or in series (Fig. 1.1*b*) with the armature winding.

The operating principle of the self-excited amplifier can be best understood from the analysis of operation of a direct-current shunt-wound generator. Figure 1.2*a* shows a no-load characteristic of the machine, $E = f(I_f)$, that is, its electromotive force E as a function of the field current I_f, and current-voltage characteristics $I_f R_f = f(I_f)$ of the

field circuit, *1* and *2*, that determine the voltage drop across the resistor R_f inserted in this circuit.

Let the angle of slope of the no-load characteristic linear portion be designated through α_3 and the slopes of the field-circuit current-voltage characteristics through α_1 and α_2.

The angle of slope of the field-circuit current-voltage characteristic depends on the field-circuit resistance, because

$$\tan \alpha = \frac{I_f R_f}{I_f} = R_f \qquad (1.1)$$

The characteristics of Fig. 1.2*a* show that when $\alpha_1 > \alpha_3$ the machine will not be excited since, according to the characteristics, the generator will produce an electromotive force E_1 at a certain value of magnetomotive force, say, F_1, and to produce such an mmf, a voltage $V_1 > E_1$ must be applied to the field winding. At $\alpha_2 < \alpha_3$ the machine will get excited to point C. The angle of slope α_3 at the origin of the no-load characteristic is referred to as a critical angle α_{cr}. So, the condition under which the machine will be excited can be expressed through the angles

$$\alpha \leqslant \alpha_{cr} \qquad (1.2)$$

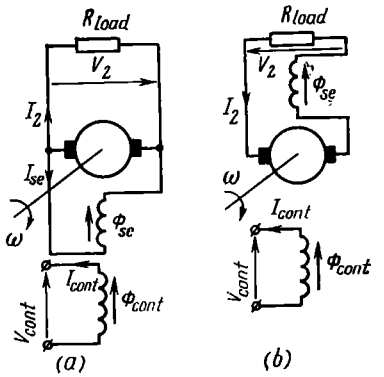

Fig. 1.1. Circuit diagrams of self-excited rotary amplifiers

The resistance of the amplifier self-excitation winding circuit is selected so that in the absence of a signal across the control winding the amplifier is not excited, that is, $\alpha > \alpha_{cr}$ (straight line *1* on Fig. 1.2*b*). If a signal causing an mmf $F_{cont} = I_{cont} w_{cont}$ is applied to the control winding having w_{cont} turns, the current-voltage characteristic will be displaced parallel to the straight line *1* and will occupy the position of the straight line *2*, the amplifier will get excited to point *A*, and an emf *E* will be induced in the armature winding. It can be easily understood that the emf *E* is induced due to a magnetic flux of a magnitude determined by the total excitation mmf:

$$F_f = F_{cont} + F_{se} \tag{1.3}$$

where $F_{se} = I_{se} w_{se}$ is the mmf of the self-excitation winding; w_{se} is the number of turns of this winding.

Substitute a straight line ($\angle AOB \approx \alpha_{cr}$) for the *OA* section on the characteristic curve of Fig. 1.2*b* and analyse the triangles *OAB* and *CAB*:

for the triangle *OAB* we have

$$E = F_f \tan \alpha_{cr} \tag{1.4a}$$

for the triangle *CAB*

$$E = F_{se} \tan \alpha \tag{1.4b}$$

Fig. 1.2. Characteristics
(*a*) self-excited generator; (*b*) self-excited rotary amplifier

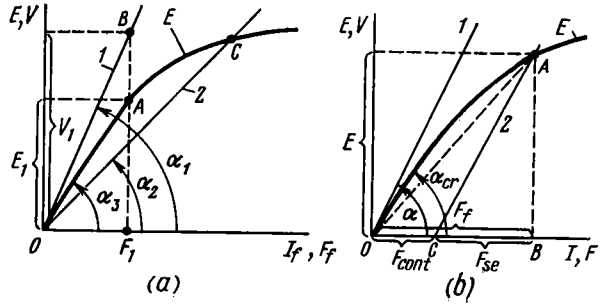

From a joint solution of equations (1.3), (1.4*a*), and (1.4*b*) we find the mmf gain:

$$k_F = \frac{F_f}{F_{cont}} = \frac{1}{1 - \frac{\tan \alpha_{cr}}{\tan \alpha}} \tag{1.5}$$

An increase in the power gain k_P with the magnetomotive force is greater in self-excited amplifiers than in independently excited machines. The relation between the control powers of the two machines both at equal current densities and with an average length of turns of the control windings is as follows:

$$\frac{P_{cont\ ind}}{P_{cont}} = \frac{F_{cont\ ind}}{F_{cont}}$$

where P_{cont} and F_{cont} are, respectively, the control power and mmf of a self-excited amplifier; $P_{cont\ ind}$ and $F_{cont\ ind}$ are, respectively, the control power and mmf of an independently excited amplifier.

In order to obtain an equal power in both the amplifiers, $F_{cont\ ind}$ must be equal to F_f where F_f is to be found from equation (1.3). Then, in view of equation (1.5) we obtain

$$\frac{k_{P\ ind}}{k_P} = \frac{P_{cont}}{P_{cont\ ind}} = \frac{F_{cont}}{F_{cont\ ind}} = \frac{1}{k_F}$$

or

$$k_P = k_F k_{P\ ind} \tag{1.6}$$

where $k_{P\ ind}$ is the power gain of the independently excited amplifier.

As can be understood from equations (1.5) and (1.6), the closer the angle of slope of the self-excitation winding current-voltage characteristic approaches the critical angle α_{cr}, the higher is the power gain of the amplifier. With an angle of slope α equal to the critical angle α_{cr} the power gain k_P will be infinity.

In the event of $\alpha < \alpha_{cr}$ the self-excited amplifier becomes uncontrollable due to a spontaneous self-excitation in the absence of a signal across the control winding. Since the amplifier magnetic circuit possesses residual magnetism, the value of α must not be selected too close to α_{cr} to avoid

self-excitation. Therefore, in practice the slope of the current-voltage characteristic for rotary amplifiers is selected 3 to 5 per cent larger than the critical angle of the E versus $f(F)$ curve.

With such characteristics the power gain of the self-excited amplifiers may be as high as 1,500 to 2,000.

In order to determine the dynamic properties of the shunt-wound self-excited amplifiers, we shall analyse the self-excitation process occurring in the machine under no-load conditions.

Assume that the B-H curve is of a linear form (straight line OA, Fig. 1.2*b*), the generator rotates with a constant speed, eddy currents are negligible, the inductance and resistance of the armature winding are much lower than those of the self-excitation winding.

Let voltage V_{cont} (see Fig. 1.1*a*) be applied to the control winding. Under such conditions, the following equation of emf balance will be valid for the self-excited amplifier:

$$V_{cont} = i_{cont} R_{cont} + L_{cont} \frac{di_{cont}}{dt} + M \frac{di_{se}}{dt} \qquad (1.7)$$

where i_{cont}, i_{se} are currents through the control and self-excitation windings; L_{cont}, R_{cont} are control winding inductance and resistance; M is mutual inductance between the control and self-excitation windings.

For the self-excitation circuit we have

$$e_A = i_{se} R_{se} + L_{se} \frac{di_{se}}{dt} + M \frac{di_{cont}}{dt} \qquad (1.8)$$

where e_A is the armature emf; L_{se}, R_{se} are the inductance and resistance of the self-excitation winding.

The armature emf can be found from the triangle AOB (Fig. 1.2*b*):

$$e_A = i_f \tan \alpha_{cr} = (i'_{cont} + i_{se}) R_{cr} \qquad (1.9)$$

where $i_f = i'_{cont} + i_{se}$ is the equivalent field current corresponding to the mmf F_f; $i'_{cont} = k_{tr} i_{cont}$ is the control current referred to the number of turns of the self-excitation winding; $k_{tr} = w_{cont}/w_{se}$ is the winding-to-winding transformation ratio; $R_{cr} = \tan \alpha_{cr} = E_A/I_f$ is the critical resistance of the excitation circuit.

Assume that there is a full magnetic linkage between the control and self-excitation windings, that is,

$$M = \sqrt{L_{cont} L_{se}} \tag{1.10}$$

Then

$$L_{cont} = k_{tr}^2 L_{se};\ M = L_{se} k_{tr};\ L_{cont} = k_{tr} M \tag{1.11}$$

Write equations (1.7) and (1.8) of emf balance in the form of operators. To this end, transform the terms of these equations with regard to equations (1.9) through (1.11):

$$\left.\begin{aligned} L_{cont} p i_{cont} + M p i_{se} &= k_{tr} M p i_{cont} + M p i_{se} \\ &= M p (i_{cont} + i_{se}) = \frac{M}{R_{cr}} p e_A \\ L_{se} p i_{se} + M p i_{cont} &= L_{se} p i_{se} + k_{tr} L_{se} p i_{cont} \\ &= L_{se} p (i_{se} + i'_{cont}) = \frac{L_{se}}{R_{cr}} p e_A \end{aligned}\right\} \tag{1.12}$$

where $p = d/dt$ is the operator.

Upon transformation, the emf equilibrium equation takes the form

$$R_{cont} i_{cont} + \frac{M}{R_{cr}} p e_A = V_{cont} \tag{1.13}$$

$$R_{se} i_{se} + \frac{L_{se}}{R_{cr}} p e_A - e_A = 0 \tag{1.14}$$

Upon solving equations (1.13) and (1.14) with due account of equations (1.5) and (1.9), we obtain a differential equation of the armature emf [in equation (1.5) $\tan \alpha_{cr} / \tan \alpha = R_{cr}/R_{se}$]

$$e_A + k_F (\tau_{cont} + \tau_{se}) p e_A = k_F \frac{k_{tr} R_{cr}}{R_{cont}} V_{cont} \tag{1.15}$$

where $\tau_{cont} = L_{cont}/R_{cont}$ and $\tau_{se} = L_{se}/R_{se}$ are electromagnetic time constants of the control and self-excitation circuits.

If the armature emf at the initial moment ($t = 0$) is assumed to be also zero, equation (1.15) will take the form

$$e_A = k_F \frac{k_{tr} R_{cr}}{R_{cont}} V_{cont} \left[1 - \exp\left(-\frac{t}{k_F (\tau_{cont} + \tau_{se})}\right)\right] \tag{1.16}$$

As can be understood from equation (1.16), the emf of the self-excited amplifier will rise according to an exponential law (solid line on Fig. 1.3) with an equivalent time constant

$$\tau = k_F (\tau_{cont} + \tau_{se}) \tag{1.17}$$

when a control voltage V_{cont} is applied to its control winding.

From the comparison of equations (1.6) and (1.17) we can see that an increase in the power gain k_P with k_F causes a decrease in the amplifier speed. Since $k_F \gg 1$, the equivalent time constant τ is much higher than the sum of time constants of the self-excitation and control windings. That is why the self-excited amplifiers are used when a high speed of response is not required.

The steady-state value of the amplifier emf can be determined by using equation (1.16) and solving the following equation:

$$E_A = k_F \frac{k_{tr} R_{cr}}{R_{cont}} V_{cont} \tag{1.18}$$

The amplifier voltage gain can be found by using equation (1.18):

$$k_V = \frac{E_A}{V_{cont}} = k_F \frac{k_{tr} R_{cr}}{R_{cont}} \tag{1.19}$$

Fig. 1.3. Transient characteristic of self-excited rotary amplifier
——— emf rise curve; - - - - - tangent to the emf rise curve at the origin of coordinates

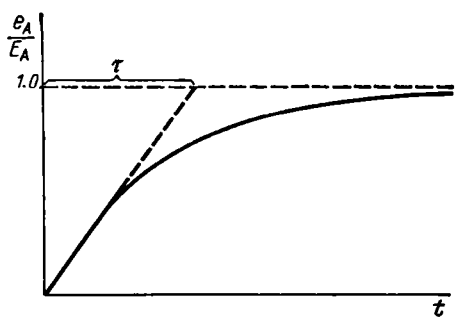

Equation (1.15), with due account of equations (1.17) through (1.19), may take the form

$$e_A + \tau p e_A = k_V V_{cont} \tag{1.20}$$

Now it can be easily understood that the self-excited amplifier is an aperiodic component with a transfer function

$$W(p) = \frac{e_A}{V_{cont}} = \frac{k_V}{\tau p + 1} \tag{1.21}$$

1.3. Cross-Magnetized Rotary Amplifier (Amplidyne). Mechanical Design and Principle of Operation

This Section covers full-pitch amplidynes. As distinct from the independently excited and self-excited amplifiers, where the main-field flux is a direct flux along the field poles, the amplidynes are cross-magnetized machines where the main-field flux is the quadrature armature-reaction flux.

Figure 1.4*a* illustrates the amplidyne schematic diagram. The amplidyne is essentially a d.c. generator with

Fig. 1.4. Amplidyne schematic diagram

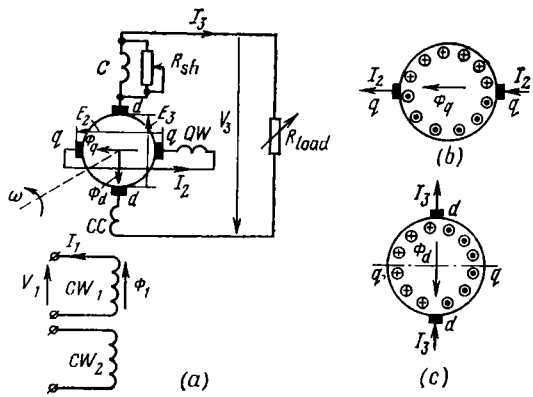

an additional set of short-circuited brushes occupying a position along the quadrature axis of the machine, *qq*. The amplidyne stator carries a number of windings, *viz*, control windings *CW* (usually two or four) arranged along the direct axis *dd*, and a compensating winding *C* mounted coaxially with the former. The degree of compensation afforded by the compensating winding *C* is controlled by means of a shunt resistor R_{sh}.

The same circuit comprises a commutating winding *CC* to improve commutation. Sometimes, a magnetizing quadrature winding *QW* having a low resistance is connected in the quadrature-axis circuit in series with the armature.

The principle of operation of the amplidyne is as follows. Assume that the drive motor runs at a rated speed, that is, $\omega = \omega_r$ and a d.c. voltage V_1 is applied to one of the control windings. Under such conditions, the small field flux Φ_1 (that is small due to a low power applied to the amplidyne input at high amplification) causes emf $E_2 = k_m \omega \Phi_1$ in the armature quadrature-axis circuit *qq* that is also relatively small (k_m is a design factor). The armature quadrature-axis circuit carries a current I_2 of a rather high magnitude as the circuit resistance is low.

Figure 1.4*b* shows the direction of current I_2 flowing in the armature winding that produces a quadrature armature-reaction flux Φ_q. This flux causes an emf $E_3 = k_m \omega \Phi_q$ in the direct-axis circuit of the armature, *dd*. This emf is picked off by the direct-axis brushes. The emf E_3 causes a current I_3 with the result that a voltage drop V_3 occurs across the resistor R_{load}.

Figure 1.4*c* shows the direction of I_3 current flow in the armature conductors. The direct armature-reaction flux Φ_d due to this current opposes the control flux Φ_1. If the machine were left in this condition the flux Φ_d, that is high in magnitude, would nullify the original short-circuit current and no amplification would take place. To alter the situation so that the machine may display amplifier characteristics, a compensating field *C* (see the above description) is placed on the stator poles.

The direct armature-reaction flux Φ_d is proportional to the mmf

$$F_d = I_3 w_A \qquad (1.22)$$

where w_A is the number of turns in the parallel circuit of the armature winding.

It can be easily understood from equation (1.22) that the direct-axis mmf F_d and, hence, the flux Φ_d that is proportional to the former, vary with the current I_3, that is, they depend on the value of the load resistor R_{load}. Good compensating action of the winding C is obtained when the mmf F_c of this winding also depends on the value of current I_3. That is why the winding C is inserted in the direct-axis circuit of the machine in series with the armature winding. Then the compensating winding mmf

$$F_c = I_3 w_c \tag{1.23}$$

where w_c is the number of turns in the compensating winding.

The degree of amplidyne compensation is characterized by the compensation factor

$$k = F_c/F_d \tag{1.24}$$

The amplidyne may run under one of the following three conditions:

(1) at $k = 1$, when the machine is compensated, that is, the direct-axis armature-reaction mmf equals the compensating winding mmf;

(2) at $k < 1$, when the machine is undercompensated, that is, the direct-axis armature-reaction mmf is higher than the compensating winding mmf;

(3) at $k > 1$, when the machine is overcompensated, that is, the direct-axis armature-reaction mmf is lower than the compensating winding mmf.

The amplidynes are usually produced slightly overcompensated, that is, with the compensating winding mmf approximately 5 per cent higher than the direct-axis armature-reaction mmf or with $k = 1.05$.

As has been already stated, the degree of compensation is adjusted by means of the shunt resistor R_{sh}. With due account of the R_{sh} resistance, the compensating winding mmf

$$F_c = I_3 w_c \frac{R_{sh}}{R_c + R_{sh}} \tag{1.25}$$

To improve commutation in the direct-axis circuit of the armature, commutating poles are arranged on the stator along the *dd* axis. To improve commutation in the quadrature-axis circuit of the armature, the current I_2 is reduced and the quadrature-axis flux is maintained by placing a magnetizing quadrature winding *QW* on the stator (Fig. 1.4*a*). This winding produces a flux Φ_{QW} that is cumulative with the quadrature armature-reaction flux.

Hence, when a magnetizing quadrature winding *QW* is inserted in the quadrature-axis circuit, the quadrature flux

$$\Phi'_q = \Phi_q + \Phi_{QW}$$

Figure 1.5 illustrates the stator and armature stampings as well as the arrangement of windings in a two-pole cross-magnetized amplidyne. The control windings *1* are placed in the large slots of the stator along the quadrature axis

Fig. 1.5. Arrangement of stator and armature fields in amplidyne

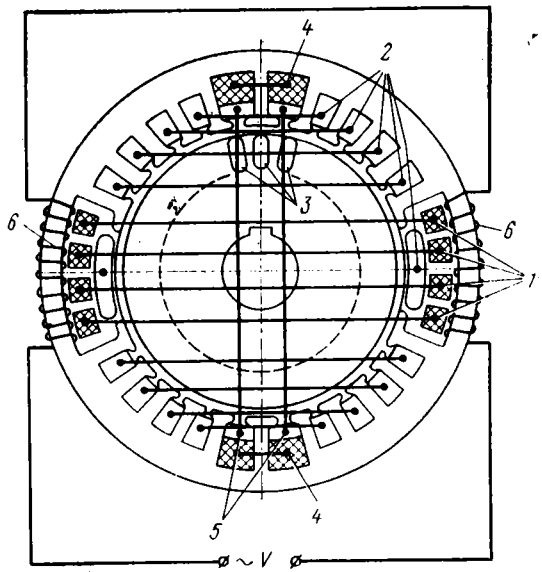

Fig. 1.6. Amplidyne УДМ-150

1—amplidyne stator; *2*—amplidyne armature; *3*—amplidyne brush gear; *4*—compensating winding shunt resistor; *5*—drive motor stator; *6*—motor armature; *7*—motor brush gear; *8*—fan; *9*—frame

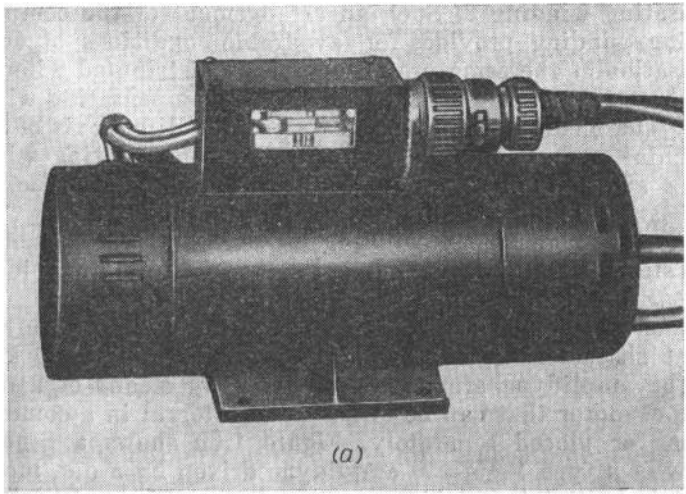

(*a*)

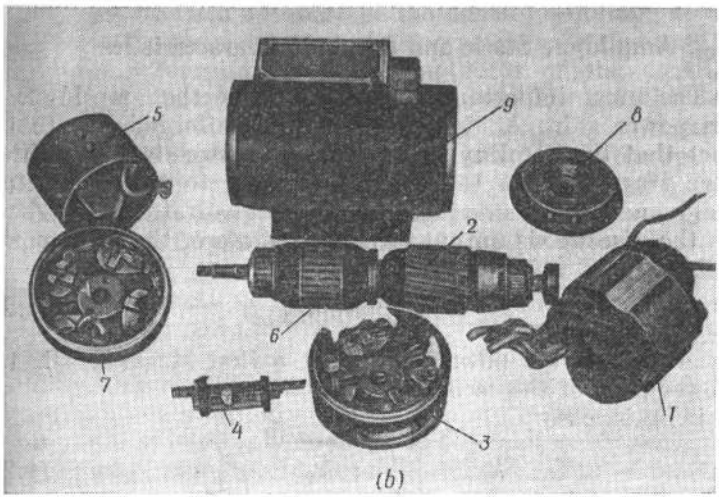

(*b*)

of the machine. Each of these windings consists of four concentrated coils.

A portion of the large quadrature-axis slot as well as the small slots of the stator accommodate the distributed compensating winding *2*. Such an arrangement of the compensating winding provides for favourable conditions of compensation as the armature also carries a distributed winding *3* whose flux is compensated for by the compensating winding. The medium slots arranged along the direct axis of the machine accommodate a concentrated commutating winding *4* and a magnetizing quadrature winding *5*. The back of the large slot carries a demagnetizing winding *6*.

The demagnetizing winding *6* serves to demagnetize the stator by alternating current so as to eliminate residual voltage due to hysteresis.

Such a mechanical design of the stator and armature is most characteristic of amplidynes rated at up to 20 kW.

The amplidyne armature is rotated by means of a d.c. or a.c. motor that can be either built integral in a common frame or placed separately. Figure 1.6*a* shows a general view of a type УДМ-150 amplidyne driven by a d.c. motor that is built integral in a common frame. Figure 1.6*b* illustrates the exploded view of this amplidyne.

1.4. Amplidyne Static and Dynamic Characteristics

The most important characteristic of the amplidyne is its power gain. A high power gain is afforded due to the fact that the amplidyne functions as a two-stage amplifier. One stage is from the control winding to the quadrature field and the other stage, from the quadrature field back to the direct-axis output circuit. Therefore, the total power gain

$$k_P = k_{P1} k_{P2} \tag{1.26}$$

where k_{P1} is the power gain of the first stage, k_{P2} is the power gain of the second stage;

in this case

$$k_{P1} = \frac{V_2 I_2}{V_1 I_1}; \quad k_{P2} = \frac{V_3 I_3}{V_2 I_2} \tag{1.27}$$

Substituting the power gains of the stages in equation (1.26) we obtain

$$k_P = \frac{V_3 I_3}{V_1 I_1} = \frac{I_3^2 R_{load}}{I_1^2 R_1} \tag{1.28}$$

where R_1 is the control field resistance.

The power gain for each stage can be expressed through basic characteristics of the machine and the load. To this end, the currents flowing in the direct- and quadrature-axis armature circuits are expressed according to the Ohm's law through the armature emfs and resistances, the armature emf through the speed of rotation and the magnetic flux, the latter through the current and inductance of the windings creating this flux.

When the amplidyne is fully compensated ($k = 1$), the resultant-power gain equation obtained as a result of the said transformation takes the form

$$k_P = c \frac{\Lambda_d \Lambda_q \omega^4 R_{load}}{R_2 (R_3 + R_{load})} \tau_1 \tau_2 \tag{1.29}$$

where c is a design factor; Λ_q, Λ_d are, respectively, quadrature-axis and direct-axis permeances of the machine; R_2, R_3 are, respectively, quadrature and direct resistances of the amplidyne; ω is the angular velocity of the armature; $\tau_1 = L_1/R_1$ is the time constant of the control winding; $\tau_2 = L_2/R_2$ is the time constant of the quadrature-axis circuit; L_1, L_2 are, respectively, the inductances of the control winding and the quadrature-axis circuit of the amplidyne.

Consequently, the less the magnetic circuit is saturated (the higher the Λ_d and Λ_q values) and the higher the speed of rotation of the amplidyne, the higher is its power gain. The speed of rotation cannot be increased to a high degree as this would impair conditions of commutation at the direct-axis and quadrature-axis brushes and reduce the mechanical strength of the machine.

The power gain k_P is proportional to the time constants of the control and quadrature windings, that is, the requirements to high amplification and extremely rapid response are mutually contradictive.

The power gain greatly depends on the load resistance and the degree of the amplidyne compensation (Fig. 1.7). In

rent I_3 and differs from the emf E_3 by the value of voltage drop across the internal resistor R_3 inserted in the direct-axis circuit of the amplidyne.

In the case of an overcompensated machine ($k > 1$), the output voltage may be maintained constant irrespective of an increase in the load current I_3. Moreover, it may rise with this load current.

With the machine undercompensated ($k < 1$), the output voltage decreases with an increase in the load current I_3 more abruptly than in the case of a fully compensated machine.

The amplidyne working characteristics show the output voltage and current as functions of the control current at $\omega = \text{const}$ and $R_{load} = \text{const}$ (Fig. 1.9). The type of these characteristics depends on the shape of the *B-H* curve of the machine.

At low control currents, nonlinear curves and, as a consequence, varying gain factors are due to a residual emf. At heavy control currents, these phenomena occur as a result of the magnetic circuit saturation.

When the amplidyne is incorporated in a closed-loop control system (stabilizers, regulators, servo systems), it must run slightly undercompensated ($k = 0.97$ to 0.99), otherwise overcompensation may cause disturbances in the working system due to excess mmf of the compensating winding with the result that self-sustained oscillations will appear in the system.

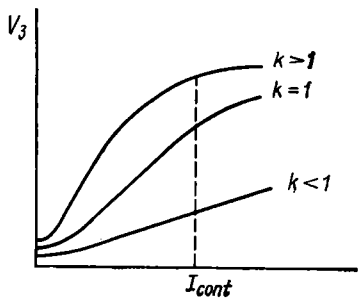

Fig. 1.9. Amplidyne working characteristics

The dynamic properties of the amplidyne are characterized by transient processes, that is, by the rise of the direct-axis voltage as a function of time $V_3 = f(t)$ when the control voltage is applied to the amplidyne input (control winding).

The amplidyne response is generally determined by the time constants of

(1) control winding

$$\tau_1 = L_1/R_1$$

(2) quadrature-axis circuit

$$\tau_2 = L_2/R_2$$

(3) direct-axis circuit that must be taken into account when the machine operates into a load

$$\tau_3 = \frac{L_3}{R_3 + R_{load}}$$

where L_3 is the inductance of the armature winding direct-axis loop;

(4) compensating loop

$$\tau_c = L_c/R_c$$

However, with regard to the fact that actually $R_{load} \gg \gg R_3$, τ_3 is much shorter than the remaining three time constants and may be disregarded. The amplidyne response is influenced by the mutual coupling between the stator fields and the armature winding, as well as between the stator fields themselves, in particular the coupling between the control and quadrature windings due to the reaction of commutation currents in the quadrature-axis circuit. Shifting of brushes also changes the mutual coupling between the control winding and the quadrature-axis circuit and the character of transients.

Solving the transient equations with due account of all the couplings is rather a complicated problem and their effect on the transient process is negligible in most cases.

Let us consider how the emf of the output circuit rises as a function of time under no-load conditions with due regard for basic couplings in the amplidyne. Assume that

(1) the amplidyne magnetic system in the direct and quadrature axes is not saturated;

(2) the inductance of the control, compensating, and commutating windings is in zero relation with that of the quadrature-circuit windings.

For the case when the brushes are set to the correct neutral, the law of rise of the output circuit emf e_3 as a function of time can be derived by solving the following four equations of emf balance:

(1) For the control winding

$$V_1 = R_1 i_1 + L_1 \frac{di_1}{dt} + M_{1c} \frac{di_c}{dt} \tag{1.31}$$

where M_{1c} is mutual inductance between the control winding and the compensating winding; i_c is the compensating winding current.

(2) For the compensating loop

$$0 = R_c i_c + L_c \frac{di_c}{dt} + M_{c1} \frac{di_1}{dt} \tag{1.32}$$

where R_c and L_c are, respectively, resistance and inductance of the compensating loop; $M_{c1} = M_{1c}$.

(3) For the quadrature-axis armature circuit

$$e_2 = a_1 i_1 + a_c i_c = R_2 i_2 + L_2 \frac{di_2}{dt} \tag{1.33}$$

where i_2 is the quadrature-axis circuit current; a_1 and a_c are proportionality factors.

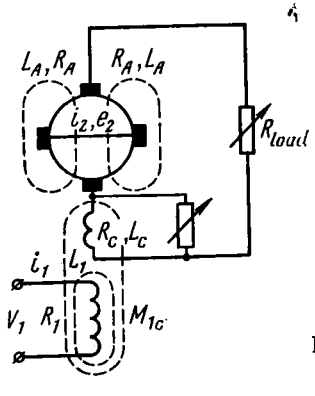

Fig. 1.10. Electromagnetic couplings in amplidyne

(4) For the direct-axis armature circuit

$$e_3 = a_2 i_2 \tag{1.34}$$

where a_2 is proportionality factor.

The a_1, a_2, and a_c factors are determined by design characteristics of the armature, the armature speed, and by the inductance of the respective windings.

Figure 1.10 presents a diagram showing the inductive coupling between the amplidyne fields during transients for the case under consideration.

If we assume that the factor of inductive coupling between the control and compensating fields is unity, equations (1.31) through (1.34) may be reduced to the second-order operator equation:

$$k_V V_1 = (\tau_1 + \tau_c)\,\tau_2 p^2 e_3 + (\tau_1 + \tau_2 + \tau_c)\,p e_3 + e_3 \tag{1.35}$$

where $k_V = a_1 a_2 / R_1 R_2$ is voltage gain.

Solving equation (1.35) shows a change in the output emf e_3 as a function of time with the signal applied in steps to the amplidyne input:

$$e_3 = k_V V_1 \left(1 + \frac{\tau_1 + \tau_c}{\tau_2 - \tau_1 - \tau_c} e^{-\frac{t}{\tau_1 + \tau_c}} - \frac{\tau_2}{\tau_2 - \tau_1 - \tau_c} e^{-\frac{t}{\tau_2}}\right) \tag{1.36}$$

Fig. 1.11. Amplidyne dynamic characteristics

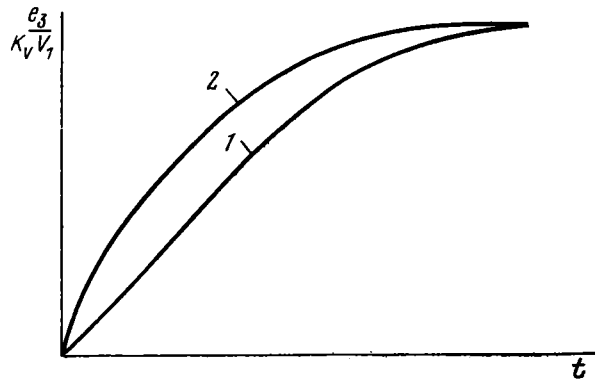

Equation (1.36) can be simplified. Since $\tau_2 > \tau_1 + \tau_c$, the transient equation can be written as follows:

$$e_3 = k_V V_1 (1 - e^{-\frac{t}{\tau_2}}) \tag{1.37}$$

As can be understood from equations (1.36) and (1.37), the amplidyne essentially comprises two series aperiodic components in the former case and one aperiodic component in the latter case.

Figure 1.11 illustrates the amplidyne dynamic characteristics. Curve *1* has been plotted according to equation (1.36) and curve *2* according to equation (1.37).

The amplidyne transfer function is found on the basis of equation (1.35):

$$W(p) = \frac{e_3}{V_1} = \frac{k_V}{1 + (\tau_1 + \tau_2 + \tau_c) p + (\tau_1 + \tau_c) \tau_2 p^2} \tag{1.38}$$

1.5. Application of Rotary Amplifiers

The rotary amplifiers are machines of serial production widely used in automatic control systems and automated electric drives. In variable-voltage systems the generator and often the exciter are essentially separate concatenated rotary amplifiers. The most popular of them are amplidynes which are noted for the following advantages:

(1) high power gain (up to 0.5×10^4 for amplidynes rated below 750 W and up to 10^5 for amplidynes of higher output ratings);

(2) low input power which makes it possible to feed the control windings from electronic valve and semiconductor amplifiers;

(3) rather fast response, that is, short time constants of the amplidyne circuits. The equivalent electromagnetic time constant is of the order of 0.1 to 0.2 s;

(4) sufficiently high reliability, long service life, and wide range of power control;

(5) provision for varying the amplidyne characteristics by adjusting the degree of its compensation.

The amplidyne, however, has a number of disadvantages:

(1) relatively large dimensions and mass as compared with d.c. generators of the same output rating as an unsaturated magnetic circuit is used to obtain high amplification;

(2) presence of residual voltage due to hysteresis.

The emf induced in the armature due to the residual magnetism flux distorts the linear characteristic of output voltage as a function of input signal in the region of low signals; reversal of the input signal polarity disturbs the unambiguity of the amplidyne output characteristics as a function of its input parameters, because the residual magnetism flux increases the control flux at one polarity and decreases it at the reverse polarity.

Besides, under the effect of residual emf, the amplidyne running overcompensated may get self-excited and lose control at a low load resistance and a zero input signal.

This can be explained by the fact that any increase in the direct-axis flux of the machine due to the effect of the compensating field is uncontrollable when this flux is equal to the residual magnetism flux.

To nullify the effect of residual magnetism flux, the amplidynes incorporate an a.c. demagnetizing arrangement and run in the system slightly undercompensated.

It should be noted that the trend today is to supersede the amplidynes in Ward-Leonard systems by magnetic amplifiers. The amplidynes, however, are finding increasing favour in the amplidyne motor-generator systems where the amplidyne functions as a generator that feeds the motor. The amplidyne motor-generator systems incorporating intermediate semiconductor amplifiers are recognized as high-speed electric drives with a wide range of control. These drive systems are used in a great variety of applications and their production is ever growing. As compared with other types of drives, the amplidyne motor-generator sets of up to 10 kW output rating are in a greater favour in radio electronic machines and installations.

Given below are a few examples of the amplidyne application in automatic-control systems.

Figure 1.12 illustrates a contactless sine-voltage amplitude automatic-control system. This system is employed in radio factories for tuning TV sets and radio receivers where the sine voltage is to be maintained constant in amplitude and varying in shape as a function of time. Ferroresonance stabilizers are not suitable for the purpose as they considerably distort the waveform while maintaining the

amplitude at the desired level. That is why use is made of automatic voltage stabilization systems with an induction regulator functioning as a control element.

As is seen from the diagram of Fig. 1.12, unstabilized three-phase voltage is applied to the rotor and to the input terminals of the stator of the induction regulator *IR*. The stabilized output voltage is picked off the output terminals of the stator, applied to the receivers and, at the same time, to the comparison element *CE* where it is compared with reference voltage. The error signal amplified by the electronic amplifier *EA* arrives at one of the amplidyne control windings CW_1 or CW_2. The amplidyne yields at its output a voltage, of a forward or reverse polarity depending on the polarity of the error signal, and the servo motor *SM* turns the induction regulator rotor either towards voltage decrease or increase.

Figure 1.13 shows the schematic diagram of a semiautomatic welder used for welding a glass bottom to a metal cone of cathode-ray tubes. Welding is made at a temperature of 1,100 to 1,200°C with high-frequency currents afforded by a high-frequency synchronous generator *SG* that supplies with power an inductor unit *IU*. The generator field winding *FW* is supplied with power from an amplidyne so as to obtain a stabilized voltage at its output. In this circuit the amplidyne functions as a power amplifier and a com-

Fig. 1.12. Contactless sine-voltage automatic-control system

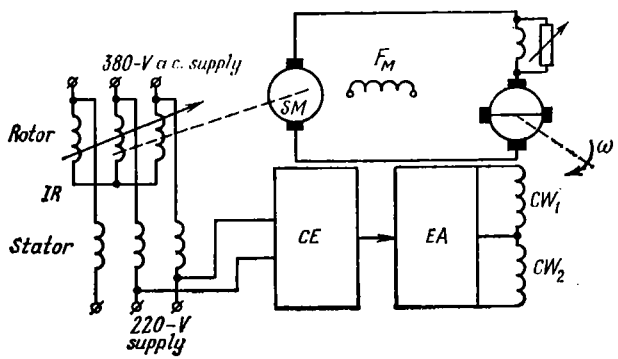

parison element. The voltage V_1 across the terminals of the amplidyne control winding CW_1 determines the output voltage level and, accordingly, the generator operating conditions. The negative voltage feedback signal arrives at the amplidyne control winding CW_2 from the a.c. output winding terminals of the generator G. An increase (or decrease) in the output voltage of the generator SG causes a decrease (or increase) in the resultant control flux of the amplidyne due to the windings CW_1 and CW_2 and, respectively, a decrease (or increase) in the generator field current. In this way, the generator output voltage is maintained at the desired level.

The diagrams illustrated by Figs. 1.12 and 1.13 relate to amplidynes used in radio electronic industry. Similar circuit arrangements are employed in a great variety of automatic control systems where the amplidynes function as power amplifiers. To perform this function, several control fields are provided to afford comparison of signals and to employ feedback circuits.

Fig. 1.13. Semiautomatic welder for welding a glass bottom to a metal cone of a cathode-ray tube

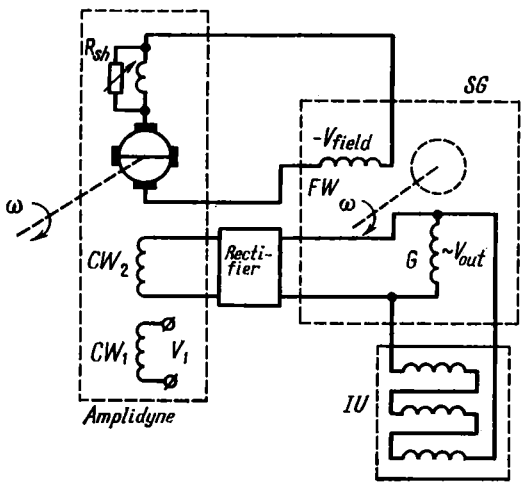

Chapter

2 FRACTIONAL-HORSEPOWER ELECTRIC MOTORS

2.1. General Information and Classification

Fractional-horsepower motors used in automatic control, remote-control, computing and other systems are rated from fractions of a watt to about 750 watts.

According to their mechanical design and principle of operation, these machines are classified as *commutator*, *induction* and *synchronous* motors.

The commutator motors include:

(a) direct-current motors,

(b) alternating-current motors,

(c) universal motors suitable for operation on both d.c. and a.c. supply.

The fractional-horsepower d.c. commutator motors are available of the types distinguished by the construction of the armature: with a *cylinder armature*, a *hollow nonmagnetic armature*, and a *disk armature*.

Along with sliding-contact motors incorporating a commutator and brushes there are contactless d.c. motors.

The fractional-horsepower induction motors employed in automatic-control systems are available of three types according to their mechanical design: with a *squirrel-cage rotor*, with a *hollow nonmagnetic rotor*, and with a *hollow magnetic rotor*.

The fractional-horsepower synchronous motors used in automatic-control systems where accurate speed control is important are available of the following basic types: *reluctance*, *hysteresis*, and *active-rotor*.

Most fractional-horsepower motors used in automatic-control systems and units function as servo power elements.

Servo motors are those machines that convert an electric signal applied to them (control voltage) into an angular velocity or movement of the shaft. These motors are meant to afford various functional conversions. They can operate either in a continuous-running duty or in a step duty depending on construction. Used as servo motors are d.c. independently excited motors, Ferraris motors, amplidyne motor-generator sets, and synchronous stepper motors.

The application of each servo motor depends on the characteristics of automatic-control systems, the purpose of these systems, operating conditions, and requirements to the motors that are to be used as component parts of these systems.

The servo motors are to meet the following basic requirements:

(1) steady-state stability and linearity of mechanical characteristics throughout the entire speed range;

(2) linear relationship between the rotor speed and the electric control signal, along with wide range of speed control;

(3) no inertia (the motor must stop running without delay as soon as the control signal is removed);

(4) fast response;

(5) light control power at a heavy mechanical power on the shaft, that is, a high power gain (this requirement is essential because of a limited power of control signal sources which are, in most cases, electronic devices).

Auxiliary drive motors of various types mentioned above function as auxiliary components of automatic-control systems or units and are meant to drive separate parts and mechanisms, etc.

Requirements to fractional-horsepower motors according to their application are to be found in Section 0.2.

2.2. Fractional-Horsepower D.C. Servo Motors. Mechanical Design and Principle of Operation

As has been already mentioned, used as **d.c. servo motors** are *sliding-contact* motors incorporating a *commutator and brushes* as well as *contactless* motors with *transistor commutators.*

Servo motors with a cylinder armature do not appreciably differ from a typical d.c. machine and therefore their mechanical design is not given attention in this book.

2.2.1. Low-Inertia Fractional-Horsepower Motors with Hollow Nonmagnetic and Disk Armatures

Figure 2.1*a* illustrates a fractional-horsepower electromagnetic-field d.c. motor with a nonmagnetic hollow armature. This motor is characterized in that its moment of inertia is reduced by using an armature of a unique design. It is divided into two parts, one of which is a wound commutator and the other a core. The core, which is a heavier part, is motionless. It is called an inner stator *3* and functions as a magnetic circuit. The armature *2* is a hollow plastic cylinder accommodating a copper winding or carrying on its surface a printed winding. The outer stator *1* carries a concentrated field winding. The hollow armature rotates in an air gap between the inner and the outer stator. Voltage is applied to the armature via brushes *5* and commutator *4*. As a result, the moment of inertia of such an armature is much lower than that of a cylinder armature.

Permanent-magnet motors of a similar type are also available. Figure 2.1*b* shows the type ЗДПРС motor whose inner stator *3* is a cylindrical radially magnetized permanent magnet that creates a field flux. The outer stator *1* made of non-retentive material functions as a magnetic circuit.

The disk-armature d.c. motors are made with a flat and not a cylindrical air gap. The armature (Fig. 2.2) is a thin slotless nonmagnetic disk *1* made of ceramic, textolite, or aluminium and carrying a printed winding. The printed winding conductors *2* are arranged radially on both sides of the disk and connected through holes *3* within the disk. Connections are obtained automatically while the winding is printed. The motor is excited by permanent magnets *1* (Fig. 2.3) with pole tips *4* made of non-retentive steel and shaped as circular blocks. The magnetic flux due to the permanent magnets cuts two air gaps and the nonmagnetic disk *5* carrying the printed winding, whereupon it

Fig. 2.1. General arrangement of low-inertia fractional-horsepower electromagnetic-field d.c. motor with a hollow non-magnetic armature (*a*) and exploded view of permanent-magnet motor ЗДПРС (*b*)

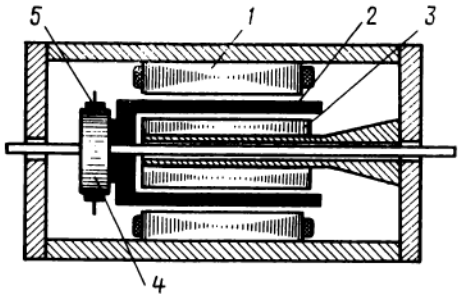

(*a*)

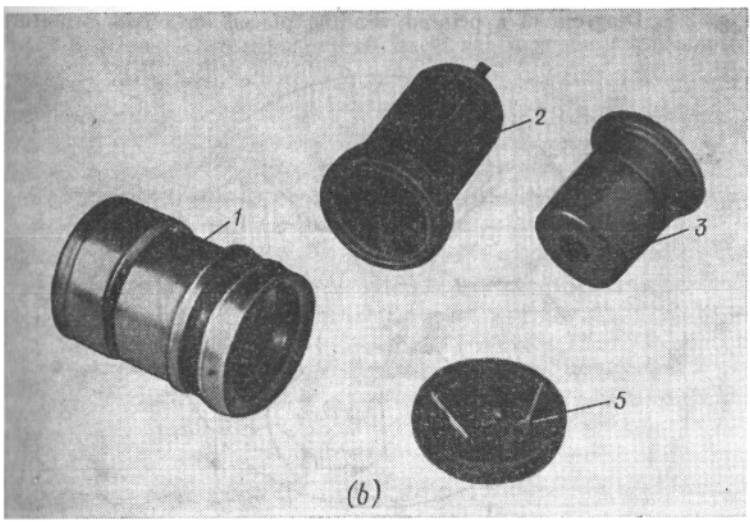

(*b*)

closes through rings *2*, *3* made of non-retentive steel and used as a yoke. The function of a commutator may be performed by bare portions of conductors on the surface of the disk over which brushes *6* are sliding. The current flowing through the armature winding produces the torque on the motor shaft in the direction of the armature disk plane.

The moment of inertia of the disk armature is much lower than that of the cylinder armature, which is one of major advantages of these motors. The printed winding can be made on an aluminium disk so as to ensure self-braking of the motor armature upon switching off. Eddy currents circulating in the disk will create a braking torque (so-called inherent damping). The efficiency of such a motor is reduced due to eddy-current losses in the disk.

There are still more advantages, in addition to low inertia, of the motors with hollow and disk armatures as compared to the motors with a cylinder armature.

1. The effect of armature reaction is negligible as the armature is free of ferromagnetic sections and the armature flux closes primarily through the air gap.

Fig. 2.2. Diagram of a printed winding placed on a disk armature

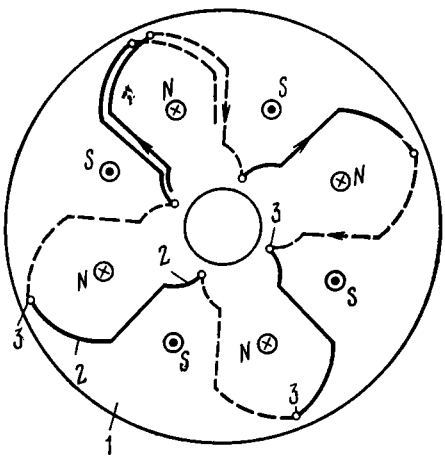

Self-inductance of the armature winding is low and all transients in the armature circuit proceed rapidly. Hysteresis and eddy-current losses in the armature are negligible.

2. The motor armature is a toothless structure, therefore, the flux is uniformly distributed in the air gap, ripple losses are eliminated, and noise is greatly reduced.

3. The friction torque in bearings is reduced along with windage and friction losses and breakaway voltage due to a lighter mass of the armature and absence of its radial attraction to the stator.

When such motors are made with a printed armature winding, the conductors of the winding are placed under better cooling conditions than those accommodated in the slots of a cylinder armature with the result that the current density within the armature conductors is raised to 30 or 40 A/mm^2. Hence, the motor mass and overall dimensions are reduced. An advent of a printed armature winding has become possible due to a high level of mechanization.

A high current density in the armature winding conductors, however, may affect the basic power characteristic of the motor, its efficiency, due to an increase in the armature

Fig. 2.3. General arrangement of fractional-horsepower d.c. motor with a disk armature

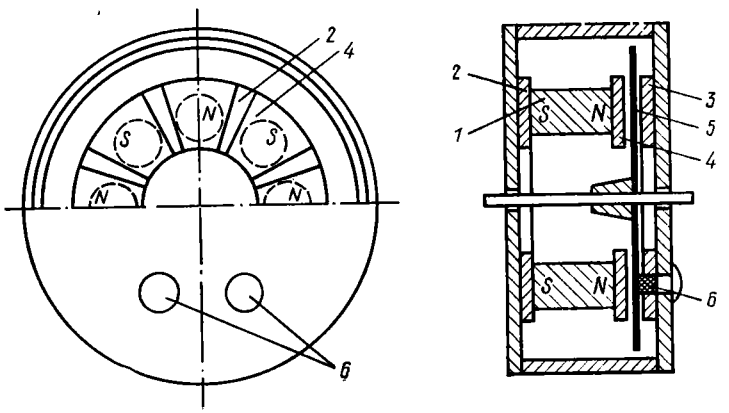

winding resistance since the cross-sectional area of conductors is reduced with an increase in the allowable current density. As a matter of fact, the efficiency, mass, and overall dimensions of the permanent-magnet motors with a hollow nonmagnetic or a disk armature are almost the same as, or sometimes better than, those of the motors with a cylinder armature because an increase in power losses is compensated for by a decrease in windage and friction losses and also in iron losses.

Losses in the field circuit are higher in electromagnetic-field motors with a hollow or a disk armature, as their nonmagnetic gap composed of an air gap and a nonmagnetic barrier of the armature body is larger. As a consequence, a higher exciting mmf is required to create the desired magnetic flux.

The service life of the disk-armature motors is shorter due to a rapid wear of printed conductors at the point where they come in contact with the brushes.

The motors with a hollow nonmagnetic or a disk armature are less dependable at higher temperatures, vibrations and shocks as they are more liable to deformation than the cylinder-armature motors.

2.2.2. Fractional-Horsepower Contactless Motors with Transistor Commutators

With the development of semiconductor technology it has become possible to create d.c. motors dispensing with a commutator and brushes. The function of these parts is fulfilled by transistor commutators controlled by position detectors.

A d.c. motor, in which a mechanical commutator and brushes are superseded by a semiconductor commutator, is more reliable and has a longer service life with added advantage of lower interference, particularly at high speeds when rapid wear of brushes causes serious sparking and heavy radio interference. The motor with a semiconductor commutator is recognized as a *contactless* fractional-horsepower d.c. motor.

The contactless fractional-horsepower d.c. motors incorporate the following features;

(1) the armature power winding is placed on the stator and consists of one or more coils spaced apart (one coil corresponds to the phase winding of a synchronous machine). The rotor is a permanent-magnet structure;

(2) contactless position detectors are incorporated in the form of transformers, induction or photoelectric transducers, etc. to indicate the position of the rotor flux axis relative to the axes of the stator winding coils so as to determine the moment of current commutation in these coils;

(3) a still another feature is a contactless commutator, most frequently a transistor commutator, that switches over the stator power winding coils upon the arrival of signals from the position detectors.

These three features make it possible to retain the peculiar property of the d.c. machine distinguishing it from the a.c. motor; the commutation frequency of the armature coils depends on the rotor speed, that is, it is controlled by the machine proper. With such an arrangement, the contactless d.c. motor generally retains characteristics of an independently excited commutator motor.

Described below is the general arrangement of a simple contactless motor (Fig. 2.4) that consists of a stator *1* with a single-coil winding *2* and a permanent-magnet rotor *3* with a single pair of poles. As soon as a d.c. voltage is applied to the stator winding terminals, the winding starts passing current which interacts with the rotor flux and creates a torque. Two transformer detectors D_1 and D_2 mounted on the flange of the motor frame and a ferromagnetic disk *4* fitted on the rotor shaft function as position detectors of the rotor, that is, of the flux axis. The disk is provided with a recess along its circumference. Since the output windings of the detectors are connected into a differential circuit, the signal is generated by each detector when two of the three transformer legs are engaged, that is, when the detector is set against a recess of the disk. In the position shown by Fig. 2.4, the signal controlling the transistor commutator *5* is picked off the detector D_1 and the commutator supplies voltage of the indicated polarity to the stator winding. When the control signal is taken off the detector D_2, the commutator supplies voltage of the reverse polarity to the stator winding.

A coordinated operation of the detectors and the commutating circuit is provided when the detectors D_1 and D_2 are arranged along the stator winding axis and the disk's lines of symmetry CC are normal to the rotor pole axis. In the action, the commutator reverses polarity of the stator winding voltage at the moment the rotor flux axis cuts the stator winding axis, that is, the current in the stator winding and the stator magnetic flux change their direction at the approach of the axis of the rotor poles of the reverse polarity (Fig. 2.5). So, the motor torque T is maintained unidirectional within a full revolution of the rotor. In other words, the transistor commutator functions as a usual commutator of a d.c. machine.

Since the torque of such a motor is created as a result of interaction between the stator flux Φ_s and the rotor flux Φ_r, its magnitude can be calculated as a product of vectors of the fluxes:

$$T = k\Phi_s\Phi_r \sin\theta$$

where $\theta = 0 - 180°$ is the angle between the axes of the fluxes; k is a design factor.

Fig. 2.4. Circuit schematic of contactless fractional-horsepower d.c. motor with a transistor commutator

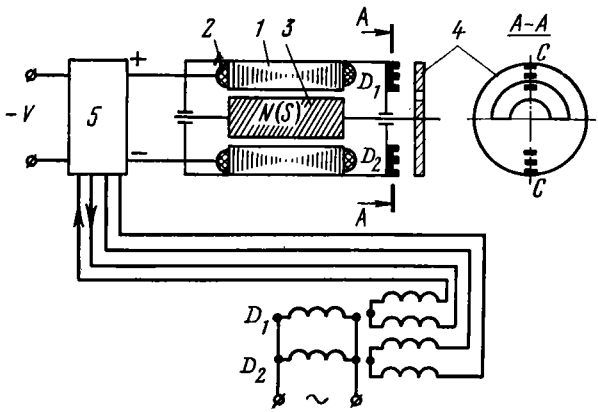

The rotor flux Φ_r is permanent and the stator flux Φ_s is proportional to the stator winding current I_s when the magnetic circuit is not saturated. So, the torque equation can be transformed as follows:

$$T = k_m I_s \sin \theta$$

where k_m is a factor depending on the rotor flux and the stator design characteristics.

As can be understood from the discussion of the motor operating principle and from the above torque equation, the motor rotor will fail to start when voltage is applied if the initial position of the rotor corresponds to an angle θ at which the torque T is less than the static torque on the shaft. Another drawback is considerable fluctuation of the torque within one revolution of the rotor and, hence, fluctuation of the rotor instantaneous speed.

All these drawbacks can be eliminated by using a multicoil power winding with the coils spaced apart at a certain angle. In this case, a decrease in the interaction moment between the rotor and one of the coils is compensated for by an increase in this moment between the rotor and another coil. The multicoil power windings of contactless motor stators may be connected as follows:

(a) delta connection (Fig. 2.6*a*);
(b) parallel connection with the power source (Fig. 2.6*b*);
(c) series connection with the power source (Fig. 2.6*c*);
(d) star connection of the coils (Fig. 2.6*d*).

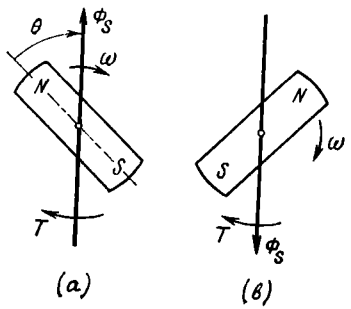

Fig. 2.5. Maintaining the direction of contactless motor torque
(a) signal from detector D_1;
(b) signal from detector D_2

In such a case, the internal torque equation can be written as follows:

$$T = k_m I_s \frac{\theta_c/2}{\sin \frac{\theta_c}{2}} \cos\left(\theta - \frac{\theta_c}{2}\right)$$

where θ_c is an intercommutating interval; $0 \leqslant \theta \leqslant \theta_c$. The interval 0_c tends to zero with increasing number of coils and the torque T tends to a constant value that is characteristic of standard commutator machines.

Instability of the rotor speed is determined as a ratio of the maximum speed variation within one revolution of the rotor to its average value:

$$N = \frac{\omega_{max} - \omega_{min}}{\omega}$$

Fig. 2.6. Connection of stator winding coils in contactless fractional-horsepower d.c. motors

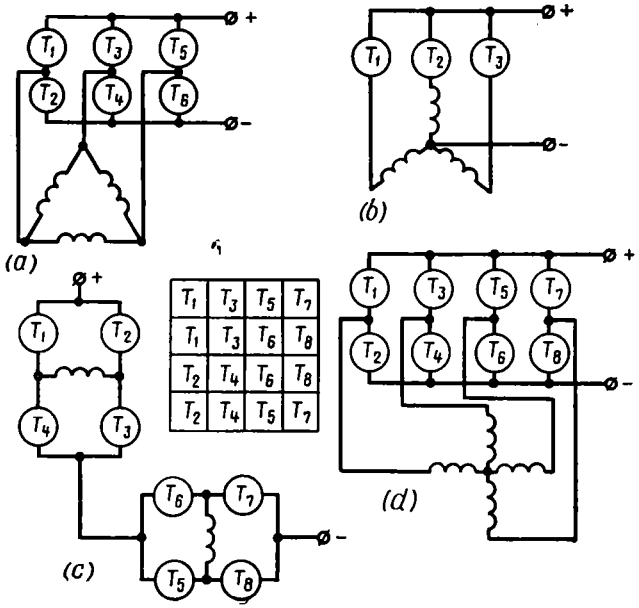

The degree of instability depends on the number of stator winding coils and their connection; it is much higher at low speeds ω and is inversely proportional to the rotor moment of inertia.

Figure 2.7 illustrates speed instability curves for a three-coil motor with the winding coils connected in delta (curve *1*) and in parallel (curve *2*).

Special modulation circuits for the stator coil voltage or current are used to improve the torque and speed stability.

From the comparison of fractional-horsepower contactless motors using different types of connection of winding coils we see that:

(1) delta-connected windings afford highest efficiency, lightest mass, most efficient utilization of active materials, and the least instability of speed because the coils of these windings take part in the electromagnetic interaction with the rotor at every moment of time; approaching them in these respects are windings with coils connected in series with the power source and those with star-connected coils;

(2) windings with coils connected in parallel with the power source are used with the motor commutator of the most simple construction.

The greater the number of coils in the armature power winding placed on the stator of a contactless motor, the

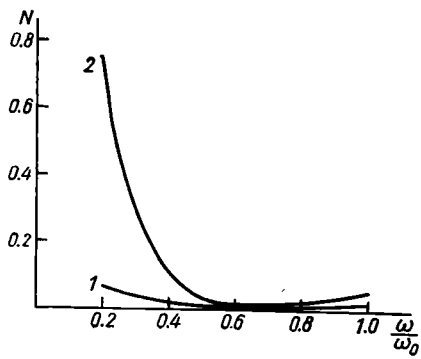

Fig. 2.7. Characteristics of contactless motor speed instability (ω_0 is ideal no-load speed)

closer will be the motor characteristics to those of a standard d.c. commutator motor. An increase in the number of coils, however, causes a proportional increase in the required number of position detectors and commutator transistors and complicates the design of signal elements in the position detectors and commutator. Therefore, a reasonable number for actual contactless motors is not to exceed three or four coils.

The mass and overall dimensions of the fractional-horsepower contactless motors may be somewhat greater than those of other fractional-horsepower d.c. motors, which is primarily because of the mass and dimensions of the commutator.

Used as servo motors are fractional-horsepower d.c. motors *excited by permanent magnets* (permanent-magnet motors) or by an *independent electromagnetic field.* Basic characteristics of these motors are almost the same because in either case the magnetic flux is independent of the operating conditions of the machine.

The advantage of the permanent-magnet machines is that they dispense with a power source for the field winding and their flux depends but slightly on the motor temperature, while a change in the temperature of electromagnetic-field motors causes a change in the resistance and current through the field coils and, hence, a change in the main flux. The efficiency of the permanent-magnet servo motors is higher due to the absence of field losses. Therefore, they afford a higher power output at the same dimensions and temperature limitations.

The disadvantage of the permanent-magnet motors is that magnets deteriorate with time. This drawback can be eliminated by using new high-grade magnetic materials. Another disadvantage of these machines is high cost of retentive materials required for the manufacture of magnetic poles.

The fractional-horsepower d.c. servo motors have a comparatively high efficiency amounting to 40 or 50 per cent for motors rated tenths fractions of a watt and several watts and, correspondingly, to 70 or 75 per cent for those having ratings of tens and hundreds of watts. A lower efficiency of motors having a lighter power rating is primarily

Fig. 2.8. Efficiency (*a*) and mass (*b*) per unit power output versus rated output of fractional-horsepower d.c. servo motors

СЛ—with cylinder armature and electromagnetic field; ДПМ—with cylinder armature and permanent-magnet field; ДПР—with hollow nonmagnetic armature and permanent-magnet field; ПЯ—with disk armature and permanent-magnet field (about 3,000 r/min); МБ—contactless with permanent-magnet field; (*L*)—rated speed about 2,500 r/min; (*H*)—rated speed about 9,000 r/min

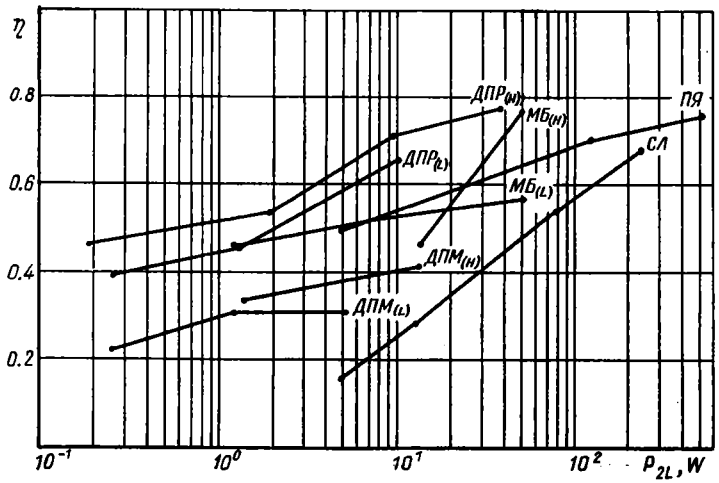

(*a*)

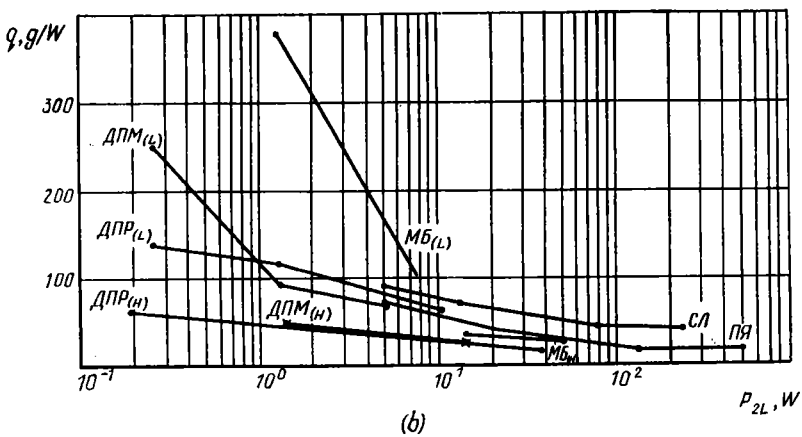

(*b*)

due to a relative grow of the armature winding resistance and I^2R losses. The size and mass of these motors are, in the average, two to four times smaller than those of induction servo motors of the same power ratings. Figure 2.8 shows efficiency η and mass per unit power output q for some serial-production fractional-horsepower d.c. servo motors.

The fractional-horsepower d.c. motors incorporating a mechanical commutator and brushes, when running, produce radio noise caused by sparking at the brushes that creates a spectrum of radio-frequency electromagnetic oscillations. When such a motor is supplied with power from a separate source, ripple voltages and currents in the armature cause higher harmonics of the current and voltage to appear in the circuit, which impairs the operation of other power consumers connected to the same power source.

These drawbacks are usually eliminated by using two methods, *viz.*, by shielding and by installing electric filters.

Shielding is more suitable for suppressing radio interference caused by sparking at the brushes. The motor frame with a metal cover plate over the commutator and brushes

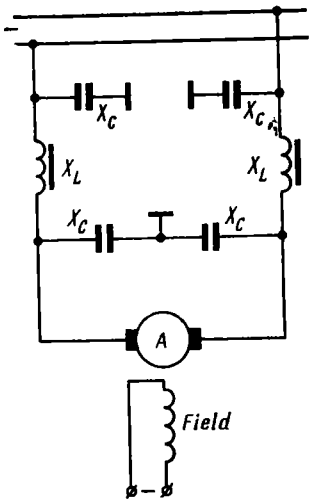

Fig. 2.9. Circuit diagram of U-section anti-interference filter

usually functions as a shield. All the winding leads are made of shielded wire whose outer brading is electrically connected to the machine frame.

Electric filters inserted in the armature circuit suppress most harmful higher harmonics of current and voltage in the supply circuit, at the same time passing the d.c. component. L- and U-section filters (Fig. 2.9) are employed for suppressing radio interference in the fractional-horsepower d.c. servo motors. Most important circuits incorporate combined multisection filters.

2.3. Methods of Control of Fractional-Horsepower D.C. Servo Motors

The rotor speed is usually controlled by one of the two methods:

(1) *continuous control* by a signal that is continuous in time and varying in magnitude. The signal can be applied in the form of an armature voltage (armature control) or a field-coil voltage (field control);

(2) *pulsed control* by varying the time within which the rated voltage is applied to the motor.

2.3.1. Armature Control

The field flux Φ (Wb) is created due to the current flowing in the field coils of the main poles (Fig. 2.10*a*) or due

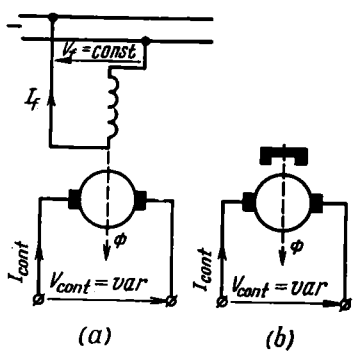

Fig. 2.10. Connection of fractional-horsepower d.c. servo motors using armature control

to permanent magnets (Fig. 2.10*b*). In the former case, the field winding is permanently connected to an independent power source delivering a voltage V_f (volts) equal to the motor rated voltage (that is, $\Phi = \text{const}$). The rotor speed ω (rad/s) is controlled by varying the control voltage V_{cont} across the armature terminals.

The analysis has been made on the assumption that the magnetic circuit saturation and the armature reaction may be disregarded.

The armature control analysis is started from deriving the equations of speed-torque and control characteristics. These equations are usually discussed in terms of relative units: $\alpha = V_{cont}/V_f$ is the signal ratio (for permanent-magnet motors, $\alpha = V_{cont}/V_r$, where V_r is the motor rated voltage). The α signal ratio may vary in the course of control between 0 and 1.25; $\omega^\partial = \omega/\omega_0$ is the motor speed, where ω_0 is an ideal no-load speed at $\alpha = 1$; $T^\partial = T/T_{start}$ is the motor torque, where T_{start} is the starting torque at $\alpha = 1$.

The speed-torque characteristic of a shunt-wound motor (that is, at $\alpha = 1$) is known from the general theory of d.c. commutator machines:

$$\omega = \omega_0 - \frac{R_A}{(k\Phi)^2} T \tag{2.1}$$

where the ideal no-load speed

$$\omega_0 = \frac{V_r}{k\Phi} \tag{2.2}$$

In equations (2.1) and (2.2) T is the motor torque, N·m; R_A is armature winding resistance, Ohm; k is design factor depending on the number of armature conductors, N, number of parallel circuits, a, and number of pole pairs, p, of the machine

$$k = \frac{Np}{2\pi a} \tag{2.3}$$

For an arbitrary value of α, equation (2.1), with due account of equation (2.2), takes the form

$$\omega = \frac{\alpha V_r}{k\Phi} - \frac{R_A}{(k\Phi)^2} T = \alpha\omega_0 - \frac{R_A}{(k\Phi)^2} T \tag{2.4}$$

Upon the division of the left-hand and right-hand parts of equation (2.4) by ω_0 we obtain

$$\frac{\omega}{\omega_0} = \omega^\partial = \alpha - \frac{R_A}{(k\Phi)^2 \omega_0} T \qquad (2.5)$$

The starting torque at $\alpha = 1$ is to be found from equation (2.4) by equating ω to zero:

$$T_{start} = \frac{(k\Phi)^2 \omega_0}{R_A} \qquad (2.6)$$

Upon substitution of Eq. (2.6) into (2.5) and appropriate transformations we obtain the following:

$$\omega^\partial = \alpha - T^\partial \qquad (2.7)$$

At a constant signal ratio α equation (2.7) presents a speed-torque characteristic $\omega^\partial = f(T^\partial)$ of a servo motor with armature control. At a constant motor torque T^∂, this equation shows a control characteristic $\omega^\partial = f(\alpha)$. It follows from equation (2.7) that with the armature control the motor has linear speed-torque and control characteristics. These characteristics are illustrated by Fig. 2.11.

The speed-torque characteristics (Fig. 2.11*a*) ensure a steady-state stability of the motor with armature control throughout the entire speed control range $\omega^\partial = 0$ to 1. The speed-torque characteristics (torque-to-speed increment ratio) are maintained flat at any signal ratio.

Fig. 2.11. Speed-torque (*a*) and control (*b*), (*c*) characteristics of fractional-horsepower servo motor using armature control

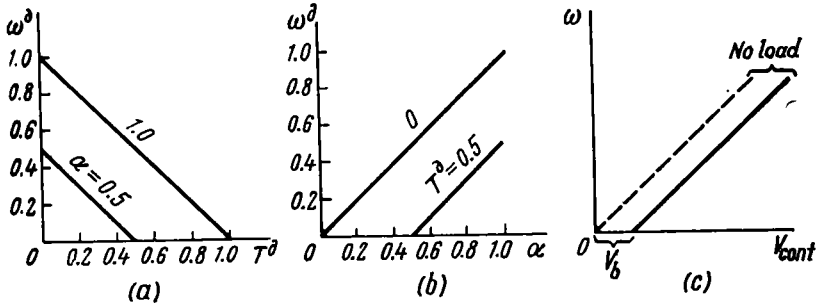

The motor develops its maximum torque at starting. The starting torque in terms of relative units is equal to the signal ratio (as is understood from equation 2.7):

$$T^{\theta}_{start} = \alpha \tag{2.8}$$

that is, the starting torque is directly proportional to the control voltage.

The armature control method provides for a linear rotor voltage versus control voltage curve at any static load torque on the shaft (Fig. 2.11*b*).

It should be noted that the control characteristic of a fractional-horsepower motor running at no load starts from zero in an ideal case only (dashed line) when windage and friction losses are equal to zero. Under real no-load conditions (Fig. 2.11*c*), the rotor starts rotating at a certain control voltage other than zero (solid line) that is referred to as a breakaway voltage V_b. This voltage depends on the frictional moment of the motor and determines the dead zone. The breakaway voltage of both d.c. and a.c. fractional-horsepower servo motors must never exceed 5 per cent of V_r. The speed control range is about (1/10) to (1/20) of the rated value.

In the discussion of fractional-horsepower servo motors as component parts of a particular system use is made of a number of factors.

Inherent damping factor k_d characterizing the magnitude and polarity of the inherent damping torque developed by the motor as a result of variation in the rotor speed equals the derivative with respect to the torque as a function of speed at a given point or the tangent of the characteristic's slope angle, $T = f(\omega)$:

$$k_d = dT/d\omega \tag{2.9}$$

The value of the k_d factor determines the flatness of the speed-torque characteristic portion under discussion.

The inherent damping factor is always negative on the steady portion of the speed-torque characteristic. This means that the damping torque opposes the speed increment and tends to suppress the latter. The closer the k_d factor to the positive region, the worse is the steady-state stability of the motor. The k_d factor is independent of the

rotor speed at linear speed-torque characteristics, and does not depend on the control voltage at an invariable flatness of the speed-torque characteristics.

For fractional-horsepower servo motors with armature control of speed, the k_d factor is found from equation (2.7)

$$k_d = \frac{dT^{\partial}}{d\omega^{\partial}} = -1 \tag{2.10}$$

As is seen from equation (2.10), the magnitude and sign of the k_d factor are independent of the speed and signal ratio.

Factor of proportionality between the starting torque and the control voltage

$$k_p = dT_{start}/dV_{cont} \tag{2.11a}$$

For armature control, it is found from equation (2.8)

$$k_p = dT_{start}/d\alpha = 1 \tag{2.11b}$$

and does not depend on the signal ratio.

Steady-state gain factor for fractional-horsepower servo motors

$$k_g = d\omega/dV_{cont} \tag{2.12a}$$

This factor is constant and equal to the tangent of the characteristic slope angle in the case of a linear control characteristic.

For armature control, using equation (2.7), we obtain

$$k_g = d\omega^{\partial}/d\alpha = 1 \tag{2.12b}$$

Here, the steady-state gain is independent of the motor output torque.

The mechanical output P_2 (W) of the fractional-horsepower servo motor is

$$P_2 = T_2\omega \tag{2.13}$$

where T_2 is the output torque that is lower than the torque T by the value of the no-load torque corresponding to the friction and iron losses.

It is a well-known fact that P_2 of a.c. motors is obtained due to the electric power input of the armature. In the case

of armature control, this output is the control power and amounts to 80-95 per cent of the total power input P_1 (the lower outputs refer to smaller motors). The control power

$$P_{cont} = V_{cont} I_{cont} \tag{2.14}$$

rises with the signal ratio and the load torque on the shaft. A heavy control power is the disadvantage of the armature control method since it involves high-power control-signal sources (valve and magnetic amplifiers, etc.).

In the case of armature control, the input power of the field coils is the exciting power

$$P_f = V_f^2 / R_f \tag{2.15}$$

where R_f is the resistance of the field coils.

This power is constant at any signal ratio. It is independent of the load and is fully dissipated in the form of heat losses. Since the resistance of the field coils is much higher than that of the armature, the exciting power accounts for a negligible portion of the total power input P_1:

$$P_1 = P_{cont} + P_f \tag{2.16}$$

The armature control method used for fractional-horsepower d.c. servo motors makes it possible to eliminate inertial running. As soon as the control signal is removed, the armature current and hence the torque drop to zero and the rotor stops running.

2.3.2. Field Control

When the field control method is used for fractional-horsepower servo motors, the field coils function as a control winding and the armature winding is continuously supplied with the rated voltage from an independent power source (Fig. 2.12). This voltage functions as an exciting voltage V_f. The armature speed is controlled by varying the control voltage V_{cont} across the field winding terminals.

The following assumptions shall be taken in the analysis of the motor characteristics: the motor magnetic system is not saturated and armature reaction is disregarded.

The machine flux Φ varies with the control voltage. For an arbitrary signal ratio, the flux $\Phi_\alpha = \alpha\Phi$, where Φ is the value of flux at $\alpha = 1$.

Using equations (2.1) and (2.2), we obtain the speed-torque characteristics in terms of absolute units:

$$\omega = \frac{V_r}{\alpha k\Phi} - \frac{R_A}{(\alpha k\Phi)^2} T = \frac{\omega_0}{\alpha} - \frac{R_A}{(\alpha k\Phi)^2} T \qquad (2.17)$$

Upon the division of the right-hand and left-hand portions of equation (2.17) by ω_0 and appropriate transformations with due account of equation (2.6) we obtain

$$\omega^\partial = \frac{\omega}{\omega_0} = \frac{\alpha - T^\partial}{\alpha^2} \qquad (2.18)$$

At a constant signal ratio α equation (2.18) is the speed-torque characteristic equation, while at a constant motor torque T^∂, it is the equation of the control characteristic of a fractional-horsepower servo motor using the field control method. The speed-torque and control characteristics of these motors plotted in accordance with equation (2.18) are illustrated by Fig. 2.13.

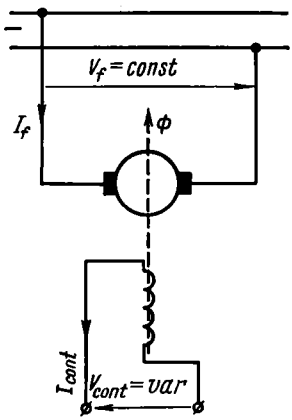

Fig. 2.12. Connection of fractional-horsepower d.c. servo motor using field control

It can be understood from equation (2.18) that speed-torque characteristics (Fig. 2.13*a*) are linear in the case of field control. The inherent damping factor, according to equations (2.10) and (2.18)

$$k_d = -\alpha^2 \qquad (2.19)$$

and is negative at any signal ratio (Fig. 2.14*a*). So, a steady-state stability of the motor is ensured at any control voltage throughout the entire speed range. The motor stability reduces with the signal ratio and so does the flatness of the speed-torque characteristics.

The starting torque in terms of relative units is equal to the signal ratio, as is the case with armature control, that is, it is directly proportional to the control voltage. The proportionality factor of the starting torque $k_p = 1$.

The control characteristics (Fig. 2.13*b*) in the case of field control are nonlinear. At small load torques they are ambiguous, that is, one speed corresponds to two values of the signal ratio. The ambiguity disappears and the characteristics become more linear at the motor torque $T^\partial \geqslant 0.5$.

The steady-state gain in the case of field control is a nonlinear function of the signal ratio (Fig. 2.14*b*) since

Fig. 2.13. Speed-torque (*a*) and control (*b*) characteristics of fractional-horsepower servo motor using field control

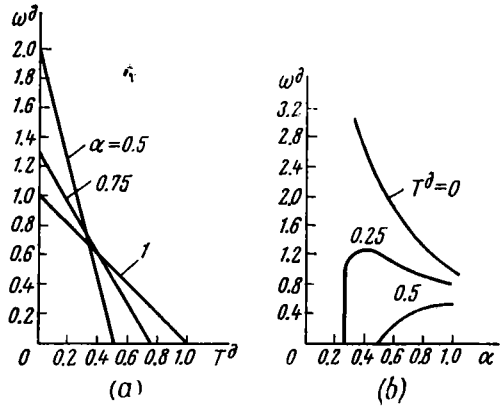

its expression according to Eqs. (2.12) and (2.18) is as follows:

$$k_g = \frac{2T^\partial - \alpha}{\alpha^3} \tag{2.20}$$

The control characteristics of fractional-horsepower motors using the field control method are also characterized in that the ideal no-load speed ($T^\partial = 0$) tends to infinity while the signal ratio tends to zero. In an actual motor this speed is limited as the shaft always suffers moments caused by the friction of brushes against the commutator and the friction of the bearings and the rotor against the air. At a low value of these frictional moments, however, the speed may appreciably exceed the permissible value with the result that the motor may run away. At a zero control voltage, the torque is produced here due to the interaction between the residual magnetism flux of the poles and the armature current. Hence, theoretically in the case of field control, inertial running may occur. If the static torque on the shaft is greater than the torque due to residual magnetism flux, the rotor will stop running.

The power P_{cont} (W) consumed by the field coils functions as a control power:

$$P_{cont} = V_{cont}^2 / R_f \tag{2.21}$$

Fig. 2.14. Inherent damping factor (*a*) and gain factor (*b*) of a fractional-horsepower servo motor using field control method

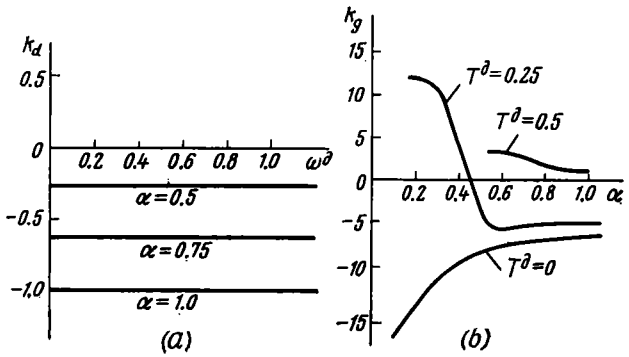

which usually does not exceed 5 to 20 per cent of the full power input of the motor.

By analysing the wiring diagrams and characteristic curves illustrated above we can compare both the methods of continuous control of the fractional-horsepower d.c. servo motors.

The advantages of the armature control method are as follows:

(1) linear and unambiguous control characteristics irrespective of the torque value;

(2) constant steady-state gain;

(3) constant flatness of the speed-torque characteristics maintained at all values of the control signal;

(4) higher inherent damping factor at an arbitrary control voltage which reduces the time of transient electromechanical processes, such as, acceleration, reversal, etc.;

(5) flow of current through the brush contact only when the rotor is running, which prevents burning of the commutator due to local heating at a motionless armature;

(6) much lower inductance of the armature winding as compared with that of the field coils due to a lower number of turns that ensures a faster rate of electromagnetic transient processes;

(7) no danger of inertial running.

The field control method requires a much lower control power than the armature control method.

The armature control method is more widely used in automatic-control systems as it has much more points in its favour.

As has been already pointed out, the equations of speed-torque and control characteristics for fractional-horsepower d.c. servo motors were obtained disregarding armature reaction. In practice, however, the linearity of these characteristics is disturbed due to a demagnetizing effect of armature reaction.

Flatness of the speed-torque characteristics of fractional-horsepower d.c. servo motors reduces with their power as a result of a relative increase in the armature winding resistance.

The speed-torque and control characteristics of contactless servo motors using armature control are distinguished by

some unique features. The commutating coil of the armature winding has a much greater number of turns than that of sliding-contact machines. In deriving speed-torque and control characteristics of contactless servo motors it would be necessary to make allowances for the self-inductance internal voltage in the commutating circuit if electromagnetic excitation were used. Most contactless motors, however, employ permanent-magnet excitation. The permanent-magnet rotor has a low permeability, and therefore the inductance of the armature coils is negligible. As a result, the speed-torque and mechanical characteristics of the contactless motors are maintained practically linear, as in the case of sliding-contact commutator motors.

When electromagnetic excitation is used for these motors, the linearity of the motor characteristics may be seriously disturbed due to the self-inductance internal voltage of the commutating coil.

2.3.3. Pulsed Control

Low-power automatic-control systems widely use the pulsed control method for fractional-horsepower servo motors. This method consists in that the rotor speed is controlled by varying the interval of rated voltage application rather than the control voltage continuously supplied to the motor armature. Generally speaking, the motor is supplied with pulses of a constant-amplitude control voltage V_{cont}, with the result that it runs with alternating periods of acceleration and braking. When these periods are short as compared with the total acceleration and stopping time, the rotor speed cannot reach the steady-state value by the end of each period, and a certain average speed ω_{av} is set. With the load torque and the field voltage being constant, the average speed ω_{av} is unambiguously defined by the relative duty factor

$$\tau = t_p/T_p$$

where t_p is pulse duration; T_p is pulse period (Fig. 2.15).

The armature speed rises with the relative pulse duration.

The instantaneous speed of the rotor is continuously varying within a definite range in the case of pulsed control.

The amplitude of these variations is inversely proportional to the ratio of the electromechanical time constant (time-lag characteristics) to the pulse repetition period. It decreases with an increase in the frequency of control pulses and the electromechanical time constant, the average speed being maintained constant.

In order that the rotor speed can be unambiguously determined by the relative duty factor, the rotor must be braked for the turn-off period (interval t_i). Both mechanical and electric braking may be employed.

The rotor speed will continuously rise at any value of τ and reach the no-load value unless the above condition is satisfied, because, while the pulse is functioning, the speed will rise and during the turn-off period it will remain practically constant.

At a constant relative duty factor τ the average speed will depend on the load torque and the field voltage, because the steady-state value of the rotor speed varies with the load torque and the field voltage. Hence, the pulsed control method makes it possible to control the rotor speed within a wide range by varying the relative pulse duration.

The main pulsed-control circuit arrangements are those in which the control contacts of electromagnetic relays (Fig. 2.16*a*) or contactless relays (transistor on Fig. 2.16*c*) connect the armature directly to the power source within one half-cycle, thereby affording a positive torque (accele-

Fig. 2.15. Speed curves at pulsed control

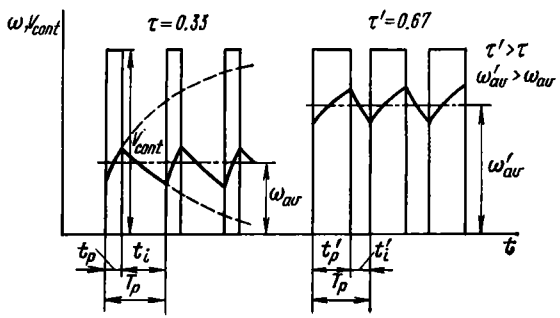

ration), and disconnect the armature from power supply (in the case of mechanical braking) or change it over to the resistor R_{db} (in the case of electric dynamic braking, Fig. 2.16*b*) within the other half-cycle.

Discussed below are speed-torque and control characteristics of a fractional-horsepower d.c. servo motor using pulsed control with reference to Fig. 2.16*a* illustrating the circuit arrangement of this motor where braking is afforded due to the static torque T_{st} on the shaft. The speed-torque characteristic of this motor is a curve showing the steady-state average speed versus static torque at a constant relative duty factor τ. The control characteristic is a curve showing the steady-state average speed versus relative duty factor τ at a constant static torque on the motor shaft.

At a low amplitude of instantaneous speed fluctuations in the course of regulation, variations in the motor torque within the time interval t_i may be disregarded. In such a case, during the acceleration period $\Delta\omega_a^\partial$ and the braking period $\Delta\omega_b^\partial$ the rotor speed varies linearly and is defined by the following equations:

$$\Delta\omega_a^\partial = \frac{T_{av}^\partial - T_{st}^\partial}{J} t_i c_m$$

$$\Delta\omega_b^\partial = -\frac{T_{st}^\partial}{J} t_i c_m$$

Fig. 2.16. Connection of fractional-horsepower d.c. servo motors at pulsed control

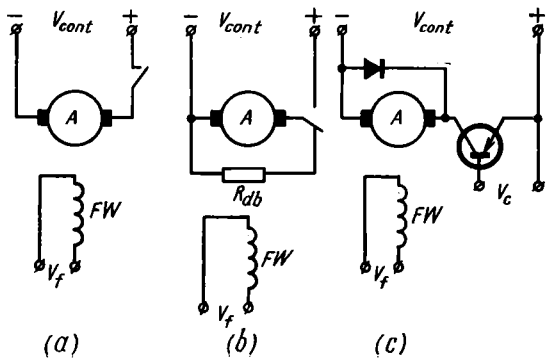

where T^{∂}_{av} is the average motor torque within the time interval t_i, expressed in relative units; T^{∂}_{st} is the static torque on the shaft, expressed in relative units; J is the armature moment of inertia; $c_m = T_{start}/\omega_0$ is the machine constant.

Under steady-state conditions

$$\Delta\omega^{\partial}_a = -\Delta\omega^{\partial}_b$$

or

$$c_m \frac{T^{\partial}_{av} - T^{\partial}_{st}}{J} t_i = c_m \frac{T^{\partial}_{st}}{J} t_t \qquad (2.22)$$

The value of T^{∂}_{av} corresponding to the steady-state average speed ω^{∂}_{av} can be found from equation (2.7) at $\alpha = 1$ since the pulse amplitude equals the rated control voltage:

$$T^{\partial}_{av} = 1 - \omega^{\partial}_{av}$$

Upon substituting this expression in equation (2.22) and making appropriate transformations we obtain

$$\omega^{\partial}_{av} = 1 - \frac{T^{\partial}_{st}}{\tau} \qquad (2.23)$$

Fig. 2.17. Speed-torque (*a*) and control (*b*) characteristics of a fractional-horsepower d.c. servo motor at pulsed control

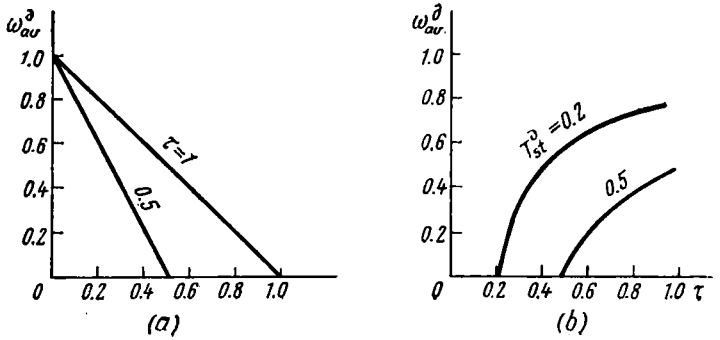

Equation (2.23) defines the speed-torque characteristic at $\tau = \text{const}$, and the control characteristic at $T_{st}^{\partial} = \text{const}$. The following conclusions can be made from the analysis of equation (2.23).

1. The speed-torque characteristics (Fig. 2.17*a*) are linear and originate from one common no-load point ($\omega_{av}^{\partial} = 1$, $T_{st}^{\partial} = 0$). The speed-torque characteristic stability is impaired with τ.

2. The control characteristics (Fig. 2.17*b*) are nonlinear. Control is possible only at $T_{st}^{\partial} > 0$ since at $T_{st}^{\partial} = 0$ the steady-state average speed $\omega_{av}^{\partial} = 1$ at any τ.

3. The motor starting conditions ($\omega_{av}^{\partial} > 0$) are defined by the inequality $\tau > T_{st}^{\partial}$.

A similar study of speed-torque and control characteristics can be made with reference to any other pulsed-control circuit arrangement. It should be noted that more linear control characteristics can be obtained for motors with electric braking.

The main advantage of the pulsed control method is a lower average control power requirement at the expense of a lower average-in-time control current. The control gear, however, is usually more complicated than that required for continuous control because most of automatic-control systems deal with continuous signals that must be converted into pulse trains for pulsed control. The pulsed control method is preferable for the control of contactless d.c. motors furnished with a transistor commutator.

2.4. Dynamic Characteristics of Fractional-Horsepower D.C. Servo Motors

Electromagnetic transient processes occur in fractional-horsepower d.c. servo motors at a higher rate than electromechanical processes. Therefore, the dynamic properties of these motors at transients can be studied with the aid of the torque equilibrium equation

$$T = T_{st} + J \frac{d\omega}{dt} \tag{2.24}$$

where T is motor running torque, T_{st} is static torque on the shaft; J is armature moment of inertia.

To simplify the analysis, we assume that $T_{st} = 0$. Then

$$T = J \frac{d\omega}{dt} \tag{2.25}$$

As can be understood from equation (2.25), variation in the rotor speed ω as a function of time obeys the law of the speed-dependent torque variation, that is, it is defined by the speed-torque characteristic.

Discussed below is the speed-torque characteristic of a fractional-horsepower d.c. servo motor at an arbitrary value of the signal ratio α (Fig. 2.18). The present point C on this characteristic is taken with the following coordinate rates: torque T and speed ω. As the triangles ABC and $AB'C'$ are similar, we have

$$\frac{T}{\omega_{0\alpha} - \omega} = \frac{T_{start\alpha}}{\omega_{0\alpha}} \tag{2.26}$$

where $\omega_{0\alpha}$ and $T_{start\,\alpha}$ are no-load speed and starting torque at a signal ratio α.

Solve equation (2.26) with respect to T, substitute it in equation (2.25) and obtain the differential equation of the rotor motion:

$$J \frac{\omega_{0\alpha}}{T_{start\alpha}} \cdot \frac{d\omega}{dt} + \omega = \omega_{0\alpha} \tag{2.27}$$

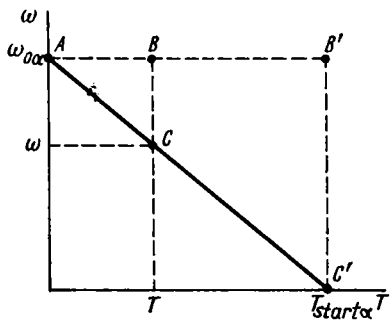

Fig. 2.18. Speed-torque characteristic of a fractional-horsepower d.c. servo motor at arbitrary value of signal ratio α

In the case of armature control, according to equation (2.7)

$$\omega_{0\alpha} = \alpha\omega_0 \tag{2.28}$$

$$T_{start\alpha} = \alpha T_{start} \tag{2.29}$$

Now equation (2.27) takes the form

$$J \frac{\omega_0}{T_{start}} \cdot \frac{d\omega}{dt} + \omega = \alpha\omega_0 \tag{2.30}$$

In the case of field control, $T_{start\alpha}$ can also be found from equation (2.29), and $\omega_{0\alpha}$ from equation (2.18):

$$\omega_{0\alpha} = \frac{1}{\alpha}\omega_0 \tag{2.31}$$

Substituting equations (2.29) and (2.31) in (2.27) gives

$$J \frac{\omega_0}{T_{start}\alpha^2} \cdot \frac{d\omega}{dt} + \omega = \alpha \frac{\omega_0}{\alpha^2} \tag{2.32}$$

As is seen from equations (2.30) and (2.32), the d.c. servo motor is an aperiodic component of the first order if the signal ratio α is taken as an input variable and the rotor speed ω as an output value. The speed derivative factor in these equations is the time constant that determines the motor response. Since this constant depends primarily on the mechanical characteristics, it is called an electromechanical time constant of the motor τ_m. The electromechanical time constant is a time period required for the rotor of a motor running at no load with a moment of inertia J to gain ideal no-load speed when started from standstill at a constant torque equal to the starting torque. For armature control, τ_m is defined by

$$\tau_m = J \frac{\omega_0}{T_{start}} \tag{2.33}$$

and for field control

$$\tau_m = J \frac{\omega_0}{T_{start}\alpha^2} \tag{2.34}$$

where

$$\frac{\omega_0}{T_{start}} = \frac{1}{k_d} = \frac{R_A}{(k\Phi)^2}$$

Now it is understood from equations (2.33) and (2.34) that the electromechanical time constant is directly pro-

portional to the rotor moment of inertia and no-load speed, and inversely proportional to the starting torque. In the case of armature control, τ_m is independent of the signal ratio and in the case of field control it rises with a decrease in the signal. This can be explained by less flat speed-torque characteristics. The τ_m is independent of the load torque on the motor shaft.

The ω_0 and ω_0/α^2 factors at a control signal ratio α in the right-hand portions of equations (2.30) and (2.32) are steady-state gain factors of the motor using, respectively, armature and field control methods. If the speed is expressed in the equations in terms of relative units, the gain factors are found from equations (2.12*b*) and (2.20) at $T^{\partial} = 0$, because equations (2.30) and (2.32) are derived for no-load conditions.

On solving equations (2.30) and (2.32) we have

$$\omega = \omega_0 \left[1 - \exp\left(-\frac{t}{\tau_m} \right) \right] \tag{2.35}$$

Equation (2.35) is the equation of a transient characteristic showing variations in the output value ω as a function of time with a certain constant signal α_s applied to the input (Fig. 2.19*a*). The transfer function corresponding to equations (2.30) and (2.32) is

$$W(p) = \frac{k_g}{\tau_m p + 1} \tag{2.36}$$

that is, it corresponds to the aperiodic component.

If the rotor angle of turn, θ ($d\theta/dt = \omega$), and not the rotor speed, is taken as the output value of a d.c. servo motor, the latter will function as an inertial integrating component, that is, the value of θ will be proportional to the integral with respect to the input variable (signal ratio α) as a function of time. This is evident from the equation derived from Eqs. (2.30) and (2.32) with due account of Eqs. (2.33) and (2.34):

$$\tau_m \cdot \frac{d^2\theta}{dt^2} + \frac{d\theta}{dt} = k_g \alpha \tag{2.37}$$

The τ_m and k_g values in Eq. (2.37) are taken in accordance with the method of control used. In this case, the equation

of the transient characteristic illustrated in Fig. 2.19*b* is derived upon the solution of differential equation (2.37):

$$\theta = k_g \alpha_s [t - \tau_m (1 - e^{-t/\tau_m})] \qquad (2.38)$$

The transfer function of the d.c. servo motor, corresponding to equation (2.37)

$$W(p) = \frac{k_g}{p(\tau_m p + 1)} \qquad (2.39)$$

As is seen from equations (2.30), (2.32), and (2.37), the dynamic properties of a fractional-horsepower d.c. servo motor greatly depend on the electromechanical time constant. The lower the τ_m value, the closer are the motor properties to an ideal inertialess component. The motor response increases at a decrease in τ_m, in which case the period between a change in the signal across the control winding and the moment of obtaining the desired speed or angle of turn of the rotor is reduced.

The following measures can be taken to reduce τ_m:

(1) the moment of inertia of the rotor can be reduced by proper selection of the rotor construction. While τ_m of

Fig. 2.19. Transient characteristics of a fractional-horsepower d.c. servo motor at armature control

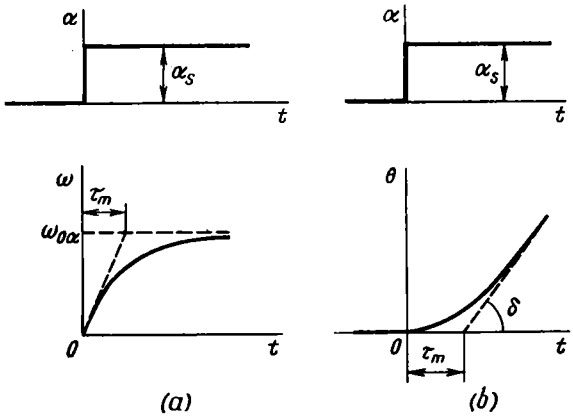

motors with a cylinder rotor is within the range of 0.035 to 0.15 s, that of motors with a nonmagnetic hollow rotor is as low as 0.015 to 0.02 s (such as, in series ДПР motors) and τ_m of motors with a disk rotor is still lower and ranges from 0.005 to 0.02 s (such as, in series ПЯ motors);

(2) the starting torque can be increased by improving the mechanical design of the motor, using better retentive materials, and increasing the current density in windings.

The analysis of dynamic properties of a fractional-horsepower d.c. servo motor has been made disregarding the electromagnetic time constant that defines the rate of electromagnetic transients in the control winding. However, when the electromagnetic time constant is comparable with the electromechanical time constant (such as, in contactless electromagnetic-field motors with a small number of coils, in low-inertia servo motors with field control, etc.), it must be taken into account in the analysis of the motor dynamic properties.

2.5. Universal Fractional-Horsepower Commutator Motors

Universal fractional-horsepower commutator motors (Fig. 2.20) are the machines suitable for operation on both d.c. and single-phase a.c. supply. According to construction, the universal commutator motor is a fractional-horsepower d.c. commutator motor with a laminated field structure (stator and rotor) and a sectionalized field winding. The laminated construction of the stator and rotor is necessary because when running on a.c. supply, they are affected by variable magnetic fluxes causing appreciable magnetic losses. Sectionalized field windings make it possible to obtain almost similar performance characteristics of the motor on d.c. and a.c. supply by varying the number of field turns connected.

A universal fractional-horsepower commutator motor may be designed as a series- or shunt-wound, or independently excited machine.

Nowadays, these motors are designed as series-wound machines only. The field winding consists of two parts connected at different ends of the armature. Such a connection

or balancing of the windings is necessary to reduce radio interference.

When connected to a d.c. supply, the motor operates just in the same way as a normal fractional-horsepower series-wound d.c. commutator motor. When running on a.c. supply, the motor displays a number of the following features.

1. When connected to an a.c. voltage source, the armature current and the field flux vary according to the law of sine waves:

$$I' = I_{max} \sin(\omega_1 t + \beta)$$
$$\varphi = \Phi_{max} \sin \omega_1 t$$

where I' and I_{max} are, respectively, instantaneous and maximum values of current; φ and Φ_{max} are, respectively, instantaneous and maximum values of flux; ω_1 is angular velocity.

The instantaneous value of torque T' is characterized by the equation

$$T' = k\varphi I' = k\frac{\Phi_{max} I_{max}}{2}[\cos\beta - \cos(2\omega_1 t + \beta)] \qquad (2.40)$$

where k is to be found from equation (2.3).

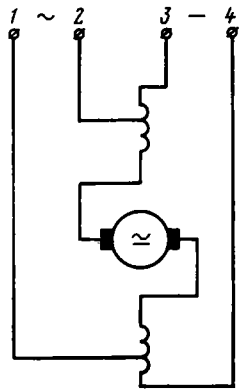

Fig. 2.20. Circuit diagram of a universal fractional-horsepower commutator motor

Figure 2.21 shows the instantaneous values of current i, flux φ, and torque T' as functions of time. As is seen from the illustration, the torque T' is unidirectional for the greatest portion of the period because the armature current changes its direction simultaneously with the field flux. At certain time intervals, however, when a phase shift occurs between the armature current and the field flux, the torque becomes negative and the rotor slows down.

The instability of the motor torque does not actually affect the motor operation since it fluctuates at a high rate and the rotating parts have a high moment of inertia.

The average value of the torque is to be found by integrating equation (2.40):

$$T = \frac{2}{\tau} \int_0^{\tau/2} T' \, dt = k\Phi I \cos\beta \qquad (2.41)$$

where I and Φ are rms values of current and flux; τ is the period of current.

Hence, the torque developed by a universal fractional-horsepower commutator motor operating on a.c. supply depends not only on the value of field flux and current, as is the case with the same motor connected to d.c. supply, but also on the phase shift between them. The highest

Fig. 2.21. Curves showing the current, flux, and torque of a fractional-horsepower universal commutator motor

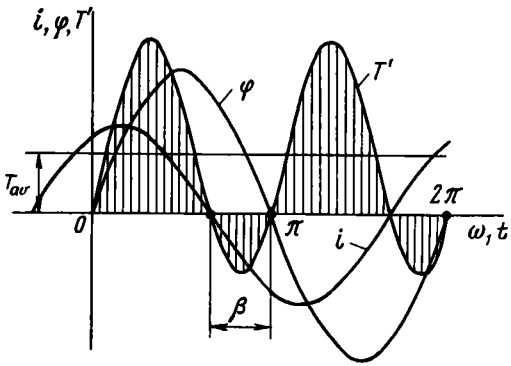

torque is obtained when the field flux and the armature current are in phase, that is, when $\beta = 0$ and $\cos \beta = 1$.

Therefore, to create a sufficient torque in the shunt-wound and independently excited motor, special phase-shifting networks are required so that the $\beta \approx 0$ condition is satisfied.

2. The performance characteristics of a universal commutator motor powered from a.c. supply are worse than those of the same motor connected to a d.c. source. This is because of the effect of the inductive reactance produced by the armature and field windings on the magnitude and phase of the current when the machine operates on a.c. supply. This effect manifests itself, in particular, in that the speed-torque characteristic of a motor operating on a.c. supply is not sufficiently flat, especially at heavy loads (solid lines on Fig. 2.22).

As has been already indicated, this drawback is partially eliminated by using a sectionalized field winding (see Fig. 2.20), which makes it possible to connect a less number of field turns (terminals *1-2*) on a.c. supply than on d.c. supply (terminals *3-4*), with the result that the magnetic flux reduces and the rotor speed increases. The speed-torque characteristic slightly rises but retains its steepness (dash

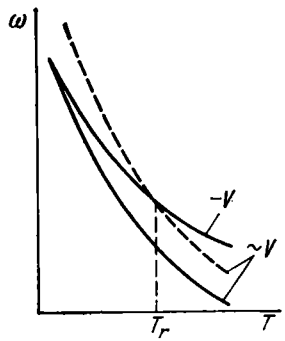

Fig. 2.22. Speed-torque characteristics of a universal fractional-horsepower commutator motor

line on Fig. 2.22). The number of turns connected on a.c. and d.c. should be selected so as to obtain the maximum similarity of characteristics at a rated torque T_r or at a torque approaching the rated value.

For the same power output, the current of the universal fractional-horsepower commutator motor operating on a.c. supply rises with a decrease in the number of field turns and is higher than that of the motor running on d.c. supply by the value of reactive component of the current. The power loss is also higher because iron loss is added and copper loss rises due to an increase in the input current.

3. When a universal fractional-horsepower d.c. motor operates on a.c. supply, its commutation is much worse and sparking at brushes is much heavier. This can be explained by the fact that the commutating coil is cut by a pulsating field flux that induces a transformer emf in this coil

$$E_{tr} = 4.44 f_1 w_c \Phi_{max} \qquad (2.42)$$

where w_c is number of turns in the commutating coils; f_1 is current frequency.

This noncompensated transformer emf causes poor commutation and, hence, serious radio interference. To reduce radio interference, the universal commutator motors incorporate anti-interference filters, but this measure does not make it possible to fully eliminate radio noise. That is why the use of universal commutator motors in automatic-control and computing equipment is restricted.

The universal commutator motors, however, have found a rather wide application due to the following features:

(1) they can operate both on a.c. and d.c. supply;

(2) the rotor speed can be easily and steplessly controlled within a wide range with the motor running on either supply by varying the input voltage and shorting out the armature or field winding through a shunt resistor;

(3) a rather high speed of up to 2000 rad/s can be obtained at a commercial frequency, which cannot be attained with commercial-frequency synchronous or induction motors unless a step-up reduction unit is furnished.

The universal fractional-horsepower commutator motors are used as auxiliary drives in automatic-control systems, computing machines and devices.

2.6. Fractional-Horsepower Induction Servo Motors. Mechanical Design and Principle of Operation

Ferraris motors (Fig. 2.23*a*) are usually employed as *fractional-horsepower induction servo motors.* The stator of these motors carries two phase windings that are spaced apart; one is a field winding *FW* and the other is a control winding *CW*. The control voltage magnitude and phase, as well as the space angle between the windings, determine the motor speed and output power.

As compared to general-purpose fractional-horsepower induction motors, the servo motors possess a higher rotor resistance. This is required to afford a steady-state stability of the motor speed-torque characteristic throughout the entire speed range (at a slip $s = 0$ to 1). As is known from the theory of induction motors, the steady-state stability of these motors can be ensured only on the portion from $s = 0$ to $s = s_{cr}$ (s_{cr} is critical slip). Hence, the rotor resistance of a fractional-horsepower induction servo motor must be of a value at which the $s_{cr} \geqslant 1$ condition is satisfied. The critical slip of actual fractional-horsepower induction motors is usually selected within the range of 3 to 4.

Figure 2.23*b* illustrates torque versus slip curves for a general-purpose fractional-horsepower induction motor

Fig. 2.23. Circuit diagram and speed-torque characteristics of a Ferraris motor

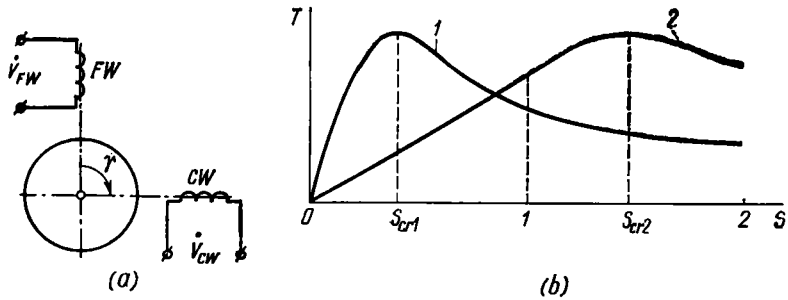

(curve *1*) and a fractional-horsepower induction servo motor (curve *2*).

The fractional-horsepower induction servo motors are available of the following three types distinguished by the rotor construction: *squirrel-cage*, with a *hollow nonmagnetic rotor*, and with a *hollow ferromagnetic rotor.*

The fractional-horsepower squirrel-cage induction servo motors are similar in design to three-phase squirrel-cage induction motors, the only difference being that they are being manufactured of the so-called "through" construction. With such a construction (Fig. 2.24), the stator bore equals the outer diameter of the bearings, so that the former and the bearing seats in the end shields can be machined integral. Moreover, the rotor runout in the stator bore is reduced to a minimum which makes it possible to diminish the air gap to 0.03 or 0.05 mm. A reduction in the air gap, at the same size and flux, reduces the magnetizing current and, consequently, stator I^2R loss, thereby increasing the efficiency and power factor cos φ_1. On the other hand, a reduction in the air gap at the same size, magnetizing component of stator mmf, and the same stator I^2R loss, that is, at the same temperature conditions of the motor, makes it possible

Fig. 2.24. Fractional-horsepower squirrel-cage induction servo motor of a "through" type of construction

1—stator core; *2*—stator winding; *3*—rotor; *4*—frame; *5*—end shield; *6*—bearing; *7*—shaft

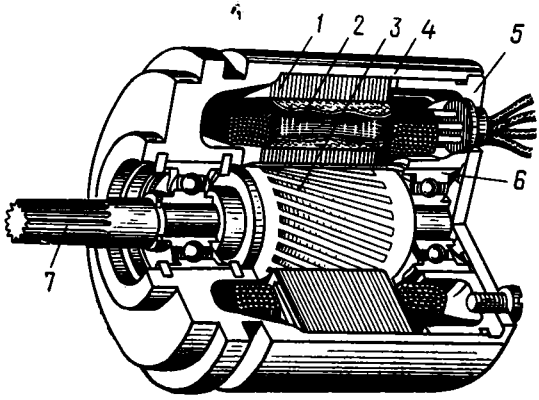

to increase the main flux (in the absence of saturation) and, hence, to raise the torque.

Low-inertia fractional-horsepower induction servo motors with a hollow nonmagnetic rotor are widely used in automatic-control circuits to reduce the electromechanical time constant. The general arrangement of such a motor is shown on Fig. 2.25.

The external stator *1* is similar to that of a normal fractional-horsepower induction motor. It is built up of electric steel stampings that are insulated from each other. The stator slots accommodate two windings *2* (a field winding and a control winding) spaced 90 electrical degrees apart. The internal stator *4* stacked of electric steel stampings of a cylindrical projection *5* of one of the end shields serves to reduce the reluctance on the path of the main flux cutting the air gap.

A hollow rotor *3* in the form of a thin-walled sleeve made of a nonmagnetic material, such as an aluminium alloy, is placed in the air gap between the external and the internal stator. The bottom of the rotor is rigidly fixed on the shaft that rotates in bearings mounted in end shields. The rotor walls are from 0.2 to 1 mm thick.

The hollow rotor mass is very small, so its moment of inertia is negligible. In this way, a fast response of the motor is ensured.

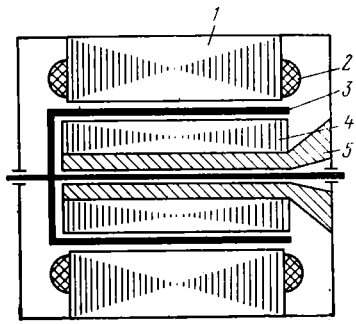

Fig. 2.25. General arrangement of a fractional-horsepower induction servo motor with a hollow nonmagnetic rotor

The motors rated some watts or lower still have their field and control windings placed in the slots of the internal stator. When this is the case, the external stator only serves to reduce the reluctance. With such a construction, the stator is wound more easily and the torque is slightly increased, but the rotor diameter becomes larger due to an increase in the winding space on the internal stator with a consequent increase in the rotor moment of inertia. To avoid this drawback, one of the windings is usually placed on the external and the other on the internal stator.

Figure 2.26 illustrates a type АДП-123 fractional-horsepower servo motor with a hollow nonmagnetic rotor and field windings placed on the external stator.

As distinct from the rotors of other types, the hollow nonmagnetic rotor of the fractional-horsepower induction

Fig. 2.26. Fractional-horsepower induction servo motor with a hollow nonmagnetic rotor, Type АДП-123
1—external stator; *2*—internal stator; *3*—hollow nonmagnetic rotor

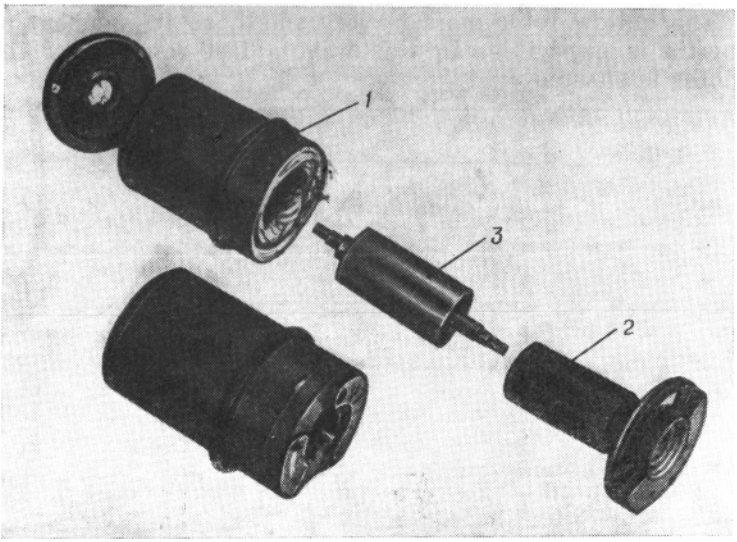

servo motor has a negligible inductive reactance. That is why the motor has more linear speed-torque and control characteristics.

The smooth cylindrical surface of the hollow nonmagnetic rotor aids in reducing the noise level of the motor. A low frictional moment and hence a low breakaway signal are afforded due to a light mass of the hollow nonmagnetic rotor and absence of the radial pull to the stator.

The disadvantage of the fractional-horsepower motor with a hollow nonmagnetic rotor is a large nonmagnetic gap composed of two air gaps, *viz.*, a gap between the external stator and the rotor and that between the rotor and the internal stator (each up to 0.25 mm), plus the nonmagnetic wall of the rotor.

Because of a large nonmagnetic gap, that amounts to 0.5-1.5 mm between the internal and the external stator, the motors have a high magnetizing current (0.8 to 0.9 of the rated value) and a low power factor. The latter drawback can be partially eliminated by using capacitor control, but heavy magnetizing currents cause appreciable I^2R loss in the motor windings and reduce the motor efficiency. A fractional-horsepower servo motor with a hollow nonmagnetic rotor rated several tens of watts has an efficiency as low as 20-35 per cent as compared with 40 or 50 per cent of a squirrel-cage motor of the same rating, while the size and mass of the former are 1.2 or 2 times as large. At a rated supply frequency as high as 400 to 1000 Hz, the size and mass per unit power output decrease to a certain extent so that these characteristics of the both types of motors are more identical due to a relative reduction in the stator winding resistance (as compared with the inductive reactance) and in I^2R loss.

Figure 2.27 shows efficiency η and mass per unit power output q versus rated power of some serial-production fractional-horsepower induction servo motors.

The fractional-horsepower motors with a hollow nonmagnetic rotor are less dependable at high temperatures, vibrations, and shocks as the probability of deformation under such conditions is higher with a hollow nonmagnetic rotor than with a squirrel-cage rotor.

Fig. 2.27. Efficiency (*a*) and mass per unit power (*b*) versus rated power of fractional-horsepower induction servo motors

АДП—with hollow nonmagnetic rotor; (*LF*)—50-Hz frequency; (*HF*)—400-Hz frequency; ЭМ-М—with hollow nonmagnetic rotor (400 Hz); ДИД—with hollow nonmagnetic rotor (400 Hz); ДКМ—with squirrel-cage rotor (400 Hz)

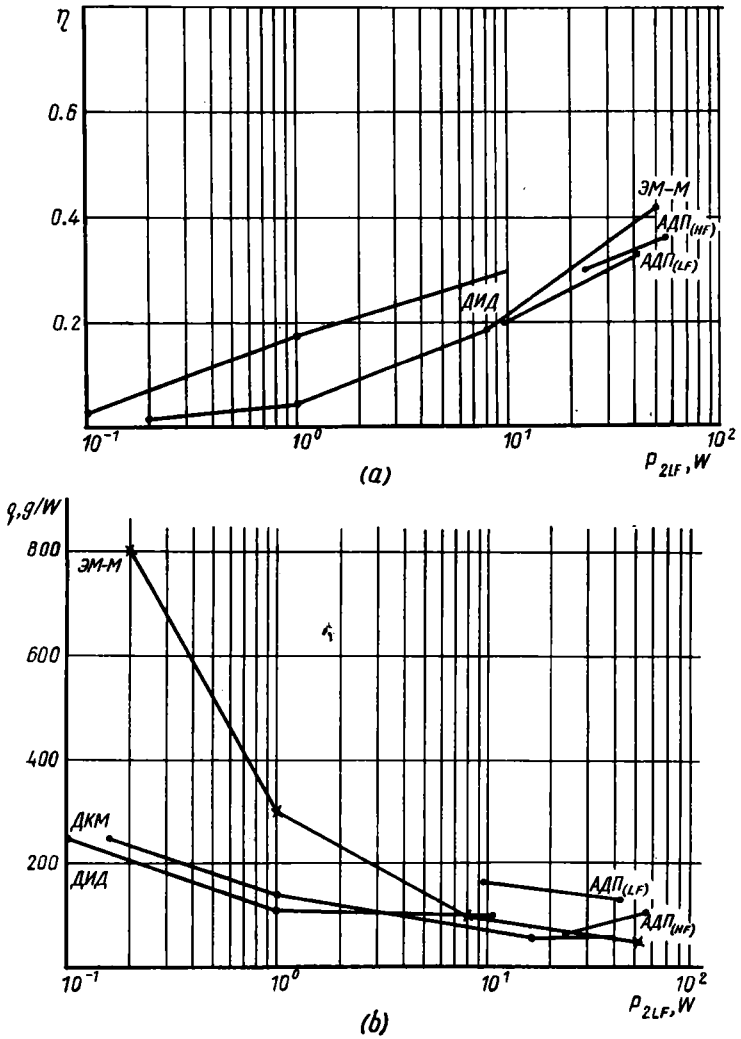

The nonmagnetic gap can be reduced by using a hollow ferromagnetic rotor. Such a construction can dispense with an internal stator as the magnetic flux closes directly through the rotor. The rotor sleeve walls are made thicker to prevent saturation and excessive resistance of the rotor material. As a result, the rotor mass increases and the motor response decreases. The resistance of some such motors is reduced by plating the rotor surface with a thin layer of copper.

The fractional-horsepower induction servo motor depends for its operation on the same principle as a fractional-horsepower three-phase induction motor. The rotating stator field is created due to the interaction between the mmfs of windings *FW* and *CW* provided there is a space shift between them and a time shift between the voltages applied to these windings. As is known from the theory of electrical machines, the magnetic field vector remains constant in magnitude, that is, the field remains circular under the following conditions:

(1) the stator windings are spaced apart through an angle $\gamma = 90$ electrical degrees;

(2) the currents through the stator windings are shifted in time by an angle $\beta = 90$ degrees;

(3) the field and control windings have equal mmfs:

$$I_{CW} w_{CW} k_{w,\,CW} = I_{FW} w_{FW} k_{w,\,FW}$$

where w is number of turns of the respective winding; k_w is winding factor.

If at least one of these conditions is not satisfied, the field takes an elliptical form, that is, the magnetic flux vector describes an ellipse and not a circle. When this is the case, the total field $\dot{\Phi}$ does not remain constant while rotating and varies in magnitude. The instantaneous speed of rotation of the field $\dot{\Phi}$ vector varies too within each revolution at a constant average value.

The elliptical field causes a lower torque than the circular field of the same amplitude. This field can be presented as a sum of two unequal circular fields rotating synchronously in opposite directions (Fig. 2.28*a*). The circular

field $\dot{\Phi}_1$ rotating in the same direction as the elliptical field is referred to as a forward-rotating field and the other $\dot{\Phi}_2$ is a backward-rotating field.

The forward-rotating field causes the running torque and the backward-rotating field, the drag torque. The more elliptical becomes the field due to a change in the angles β and γ or due to a decrease in the mmf of one of the stator phases, the smaller will be the forward component of the field and torque and the greater the backward component. The rotor speed decreases with the resultant torque at a constant load torque. The backward-rotating field causes additional losses and a decrease in the motor output and efficiency.

It should be pointed out that an increase in the mmf of one of the stator phases in excess of the value corresponding to the circular field results in an elliptical field of an amplitude exceeding that of the circular field. In the action, both the components of the field rise and within a certain range the resultant torque may rise in respect to the original circular field. Such a boosting of the stator mmf, however, may occur as a result of too high phase voltages and currents exceeding the rated values corresponding to the circular field. This cannot always be admitted since it causes additional losses and heating of the motor, saturation of the field structure and breakdown of insulation.

Fig. 2.28. Elliptical (*a*) and pulsating (*b*) fields and their components

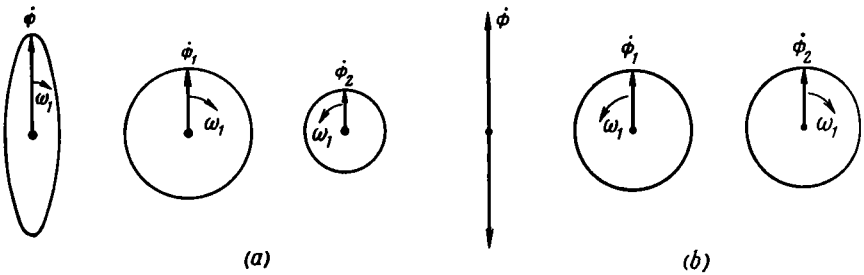

When at least one of the circular-field conditions such as $\beta = 0$ or $\gamma = 0$, or $I_{FW} = 0$ or $I_{CW} = 0$, is not complied with, the stator field starts pulsating and the motor fails to develop torque with a stalled rotor. In order to illustrate this phenomenon, replace the pulsating field $\dot{\Phi}$ (Fig. 2.28*b*) by two fields $\dot{\Phi}_1$ and $\dot{\Phi}_2$ rotating in opposite directions at a synchronous speed ω_1, the amplitudes of these fields being equal to half the pulsating field amplitude.

With the rotor stalled, both the fields rotate at a synchronous speed with respect to the rotor. Each field induces equal currents in the rotor winding since the fields and relative speeds are equal. Like the fields the torques produced are equal in magnitude and opposite in direction. The resultant torque is zero and the rotor cannot be set in motion.

It is all quite different when a pulsating stator field is set up with the rotor revolving in either direction. In this case, the motor under certain conditions may keep developing the running torque since its rotor slips unequally relative to the forward- and backward-rotating fields. The stator field in a fractional-horsepower induction servo motor starts pulsating as soon as a control signal is cancelled. So, the rotor may keep running with the control signal removed, which is inadmissible for servo motors. This phenomenon referred to as inertial running will be discussed in detail under Section 2.7.

From the physical point of view, the appearance of an internal torque at a pulsating stator field and at a slip $s \neq 1$ can be explained as follows. In addition to the transformer emf, a rotating emf shifted in phase from the former is induced in the revolving rotor due to the pulsating field of the stator. The rotor currents due to the rotating emf set up a magnetic flux of the rotor that is shifted in space and in time relative to the stator flux. The resultant magnetic field of the motor built up due to the interaction of these two fluxes is an elliptical rotating field. The direction of this rotating field depends on the motor performance characteristics.

The internal torque for a fractional-horsepower induction servo motor is to be derived as follows. In a general case,

the magnetic field of the motor is of an elliptical form due to an unbalance of the mmfs of the windings *FW* and *CW*, that is, due to the violation of at least one of the circular-field conditions. Since the windings of most motors are spaced at an angle $\gamma = 90$ deg., the unbalance of the mmfs may be expressed through the asymmetry of corrected currents in the stator windings *CW* and *FW*. It means that the time shift angle β of vectors $\dot{I}_{CW}$ and $\dot{I}_{FW}$ is other than 90 deg. and the modules referred to the number of turns of the field winding, w_{FW}, are not equal:

$$I'_{CW} = I_{CW}/k_{tr} \neq I_{FW}$$

where $k_{tr} = \frac{W_{FW}k_{w.FW}}{W_{CW}k_{w.CW}}$ is the transformation ratio of the windings *FW* and *CW*.

The currents and running torques of fractional-horsepower induction servo motors can be determined by using the calculation methods for fractional-horsepower induction motors with balanced supply (refer to the general course of electrical machines). To this end, the method of symmetric components applied to two-phase systems should be employed.

According to this method, the two-phase asymmetric system of vectors of currents $\dot{I}_{FW}$ and $\dot{I}_{CW}$ (Fig. 2.29) having unequal magnitudes and spaced apart by an arbitrary angle can be resolved into two symmetric systems, each composed of two vectors equal in magnitude and spaced

Fig. 2.29. Asymmetric system of current vectors and its symmetric components

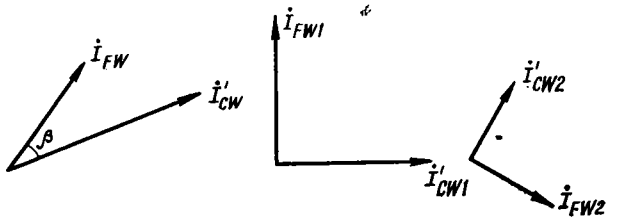

90 deg. apart. The forward-sequence system of vectors ($\dot{I}_{FW1}$, $\dot{I}'_{CW1}$) has the same phase sequence as the original system. The backward-sequence system of vectors ($\dot{I}_{FW2}$, $\dot{I}'_{CW2}$) has a backward phase sequence. With this,

$$\dot{I}'_{CW1} = -j\dot{I}_{FW1};\ \dot{I}'_{CW2} = j\dot{I}_{FW2} \qquad (2.43)$$

The original and derived systems are equivalent when

$$\dot{I}_{FW1} + \dot{I}_{FW2} = \dot{I}_{FW}$$

$$\dot{I}'_{CW1} + \dot{I}'_{CW2} = \dot{I}'_{CW} \qquad (2.44)$$

Set up equivalent circuits required to determine currents flowing in the stator and rotor windings. With the windings connected in the same way, the characteristics of the equivalent circuits for phases *FW* and *CW* in the equivalent form are equal; so, it will be sufficient to set up an equivalent circuit for phase *FW* only.

The equivalent circuits are to be set up separately for the forward (Fig. 2.30*a*) and backward (Fig. 2.30*b*) sequences, since the forward- and backward-sequence fields revolve at a different speed with respect to the rotor; this fact determines expressions for slip and impedances of the equivalent circuits. The rotor slip relative to the backward-sequence field,

$$\frac{-\omega_1 - \omega_2}{-\omega_1} = \frac{\omega_1 + (1-s)\,\omega_1}{\omega_1} = 2 - s \qquad (2.45)$$

where ω_2 is rotor speed; ω_1 is synchronous speed;
s is rotor slip relative to forward-sequence field.

The rotor sections of the equivalent circuits use s or $2-s$, respectively.

The impedances of the equivalent circuits illustrated by Fig. 2.30 can be determined either by calculations or experimentally.

When a phase-shifting element is series-connected in the motor field circuit, its impedance Z_{ph} must be inserted in the stator portion of the phase FW equivalent circuit, that is, in series with Z_{FWs}. With this, the currents and torque are calculated by using the same methods, but the calculation equations are more complicated.

The voltage V_1 across the field terminals and the voltage across the control winding terminals $V'_{CW} = k_{tr}V_{CW}$ are balanced by the voltage drop across the impedances of the respective equivalent circuits due to the currents of both sequences. In other words,

$$\left.\begin{aligned} \dot{V}_1 &= \dot{I}_{FW1}(Z_{FW1} + Z_{ph}) + \dot{I}_{FW2}(Z_{FW2} + Z_{ph}) \\ \dot{V}'_{CW} &= \dot{I}'_{CW1}Z_{FW1} + \dot{I}'_{CW2}Z_{FW2} \end{aligned}\right\} \quad (2.46)$$

Upon the solution of the set of equations (2.46) with due account of equation (2.43) we obtain the equations of sym-

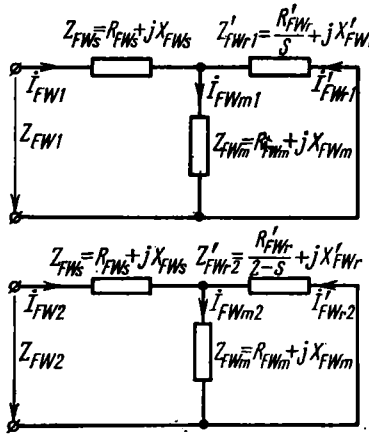

Fig. 2.30.
Equivalent circuits of fractional-horsepower induction servo motor
R_{FWs}, X_{FWs}—resistance and inductive reactance of stator winding FW; R_{FWr}, X'_{FWr}—resistance and inductive reactance of rotor referred to the number of stator phases and the number of FW turns; R_{FWm}, X_{FWm}—resistance and inductive reactance of FW phase corresponding to the mutual inductance flux of the stator and rotor; Z_{FW_1}, Z_{FW_2}—forward and backward impedances of the equivalent circuit

metric phase current components:

$$\dot{I}_{FW1} = \frac{\dot{V}_1 Z_{FW2} + j\dot{V}'_{CW}(Z_{FW2} + Z_{ph})}{Z_{FW2}(Z_{FW1} + Z_{ph}) + Z_{FW1}(Z_{FW2} + Z_{ph})}$$
$$\dot{I}_{FW2} = \frac{\dot{V}'_1 Z_{FW1} - j\dot{V}'_{CW}(Z_{FW1} + Z_{ph})}{Z_{FW2}(Z_{FW1} + Z_{ph}) + Z_{FW1}(Z_{FW2} + Z_{ph})} \quad (2.47)$$

The symmetric components of the rotor current are to be found from the equivalent circuits of Fig. 2.30:

$$I'_{FWr1} = I_{FW1}\left|\frac{Z_{FWm}}{Z_{FWm} + Z'_{FWr1}}\right|$$
$$I'_{FWr2} = I_{FW2}\left|\frac{Z_{FWm}}{Z_{FWm} + Z'_{FWr2}}\right| \quad (2.48)$$

The internal torque T (N·m) of a balanced multiphase induction motor supplied with power from a symmetric system of voltages can be found from the equation

$$T = \frac{m_s (I'_r)^2 R'_r}{\omega_1 s} \quad (2.49)$$

where m_s is number of stator phases; I'_r is rotor current referred to the number of phases and the stator winding turns, A; R'_r is rotor resistance referred to the number of phases and stator winding turns, Ohm.

Equation (2.49) can likewise be used to determine the forward- and backward-sequence torques of fractional-horsepower induction servo motors as the forward- and backward-rotating magnetic fields are set up due to symmetric systems of currents.

According to the equivalent circuits of Fig. 2.30 and equation (2.48), the equations for the forward- and backward-sequence torques can be written as follows:

$$T_1 = \frac{2(I'_{FWr1})^2 R'_{FWr}}{\omega_1 s} = \frac{2I^2_{FW1} R'_{FWr}}{\omega_1 s}\left|\frac{Z_{FWm}}{Z_{FWm} + Z'_{FWr1}}\right|^2$$
$$T_2 = \frac{2(I'_{FWr2})^2 R'_{FWr}}{\omega_1 (2-s)} = \frac{2I^2_{FW2} R'_{FWr}}{\omega_1 (2-s)}\left|\frac{Z_{FWm}}{Z_{FWm} + Z'_{FWr2}}\right|^2 \quad (2.50)$$

The resultant torque is the difference of the forward- and backward-sequence torques:

$$T = T_1 - T_2 = \frac{2I_{FW1}^2 R'_{FWr}}{\omega_1 s}\left|\frac{Z_{FWm}}{Z_{FWm}+Z'_{FWr1}}\right|^2 - \frac{2I_{FW2}^2 R'_{FWr}}{\omega_1 (2-s)}\left|\frac{Z_{FWm}}{Z_{FWm}+Z'_{FWr2}}\right|^2 \quad (2.51)$$

The torque developed by a circular-field motor where $I_{FW2} = 0$ and $I_{FW1} = I_{FW}$, with equation (2.47) taken into account,

$$T_0 = \frac{2(V'_{CW})^2 R'_{FWr}}{\omega_1 s}\left|\frac{Z_{FWm}}{Z_{FW1}(Z_{FWm}+Z'_{FWr1})}\right|^2 \quad (2.52)$$

For a circular field, the starting torque $T_{start\ 0}$ is found from equation (2.52) at $s = 1$.

From the analysis of equation (2.51) it follows:

(1) at a pulsating stator field ($I_{FW1} = I_{FW2}$) and a slip $s = 1$, the minuend and subtrahend in the right-hand portion of equation (2.51) are equal, that is, under these conditions the starting torque is zero;

(2) at a pulsating stator field and $s \neq 1$, the minuend and subtrahend in the right-hand portion of equation (2.51) are not equal ($s \neq 2 - s$; $Z_{FW1} \neq Z_{FW2}$; $Z'_{FWr1} \neq Z'_{FWr2}$) and the motor develops a forward or a backward torque;

(3) as the stator field changes from a pulsating to a circular form, the torque T_2 reduces and T_1 increases at the same time, hence, the resultant torque T rises correspondingly.

2.7 Methods of Control of Fractional-Horsepower Induction Servo Motors

The rotor speed of a fractional-horsepower induction servo motor is regulated and the motor as a whole is controlled by methods defined by the theory of the form of rotating magnetic fields (see Section 2.6). The stator field can be

changed by varying the control voltage V_{CW} and the angles β and γ either separately or at a time, thereby varying the rotor speed.

Amplitude control (Fig. 2.31). The field winding *FW* is connected to an a.c. network with a rated voltage $\dot{V}_{FW} = \dot{V}_1$. A signal in the form of a control voltage $\dot{V}_{CW1}$, that is in phase quadrature with the field voltage $\dot{V}_{FW}$, is impressed on the control winding *CW*. The rotor speed is controlled by varying the amplitude of the control voltage with its phase maintained constant.

The given control and field voltages being equal ($V'_{CW} = V_{FW}$), the rms signal ratio

$$\alpha_e = k_{tr}\alpha = 1 \tag{2.53}$$

and the stator field is circular ($\alpha = V_{CW}/V_{FW}$ is the signal ratio for amplitude control).

Any variation in the control voltage causes an rms signal ratio other than unity and a rotating field of the elliptical form. With $\alpha_e = 0$, that is, with the control signal removed, the stator field proves pulsating.

Fig. 2.31. Amplitude control circuit arrangement

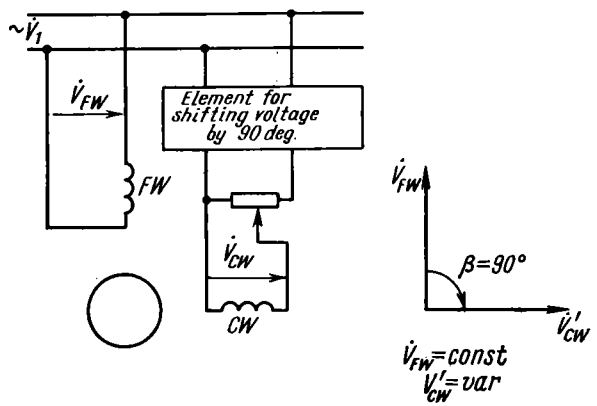

Phase control (Fig. 2.32). The field winding *FW* is connected to an a.c. network with a rated voltage $\dot{V}_{FW} = \dot{V}_1$. The control winding *CW* is supplied with a voltage that is equal to the rated value in magnitude and varying in phase relative to the field voltage. The rated voltage is a control voltage obeying the equality $V'_{CW} = V_{FW}$. The rotor speed is controlled by varying the control voltage phase (angle β). The signal ratio is $\sin \beta$. At $\sin \beta = 1$ the stator rotating field becomes circular; at $1 > \sin \beta > 0$ it is elliptical, and at $\sin \beta = 0$ it is pulsating.

Space control (Fig. 2.33). The field winding *FW* is connected to an a.c. supply with a rated voltage $\dot{V}_{FW} = \dot{V}_1$. The control winding *CW* is supplied with a rated voltage that is in phase quadrature with the field voltage. The rotor field is controlled by varying the angle γ by which the field and control windings (*FW* and *CW*, respectively) are spaced apart. The signal ratio is $\sin \gamma$. At $\sin \gamma = 1$, the rotating field of the stator is circular; at $1 > \sin \gamma > 0$ it is elliptical and at $\sin \gamma = 0$ it is pulsating.

Amplitude-and-phase control with field circuit incorporating a capacitor (capacitor control, Fig. 2.34*a*). The control winding *CW* is connected to an a.c. supply via a voltage

Fig. 2.32. Phase control circuit arrangement

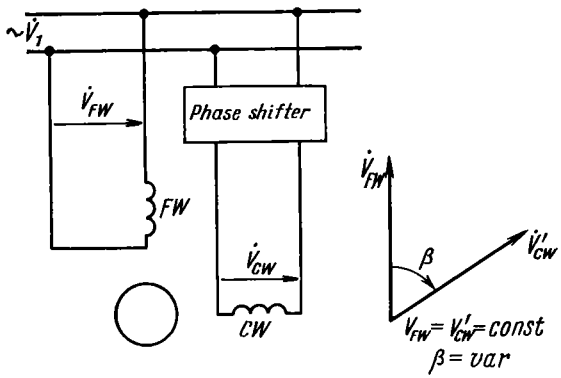

regulator; the control voltage $\dot{V}_{CW}$ is in phase with the supply voltage $\dot{V}_1$. The field current and consequently the field voltage are shifted in phase with respect to the control winding by means of a capacitor connected in series with the field winding. The motor control is afforded by varying the control voltage magnitude.

It should be noted that in spite of the fact that the control voltage phase is constant and coincides with the supply voltage phase, the field voltage $\dot{V}_{FW}$ varies both in magnitude and in phase upon a change in the control voltage. The same takes place when the rotor speed is varied by changing the load torque at a constant control voltage. This can be explained by the fact that the field voltage $\dot{V}_{FW}$ equals the geometric difference between the supply voltage $\dot{V}_1$ and that across the capacitor $\dot{V}_C$ (Fig. 2.34*b*).

$$\dot{V}_{FW} = \dot{V}_1 - \dot{V}_C \tag{2.54}$$

The capacitor voltage $\dot{V}_C$ varies with the control voltage and rotor speed due to variations in the field current that

Fig. 2.33. Space control circuit arrangement

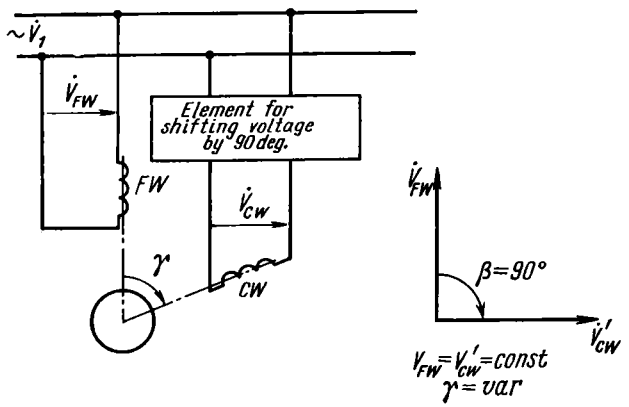

is a function of the slip and signal ratio [see the values of symmetric components of $\dot{I}_{FW}$, equation (2.47)]:

$$\dot{V}_C = -j\dot{I}_{FW}X_C \tag{2.55}$$

Hence, the field voltage $\dot{V}_{FW}$ changes its magnitude and phase.

Since a circular field exists only as long as the $\dot{V}_{FW} = j\dot{V}'_{CW}$ condition is satisfied, it can be retained so, for a given capacitance in the field circuit, only at a definite signal ratio $\alpha_0 = V_{CW0}/V_1$ and a definite slip s.

When a circular field is set up during the starting period ($s = 1$), the signal ratio α_0 and the capacitive reactance X_{C0} are determined by the formulas obtained through the analysis of symmetric current components:

$$\alpha_0 = \frac{X_{FW\,start}}{k_{tr}R_{FW\,start}} \tag{2.56}$$

$$X_{C0} = \frac{X^2_{FW\,start} + R^2_{FW\,start}}{X_{FW\,start}} \tag{2.57}$$

Fig. 2.34. Circuit arrangement for amplitude-and-phase control using a capacitor in the field circuit

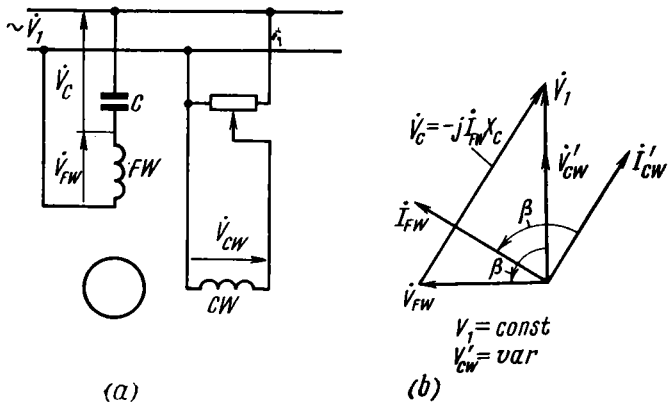

where $X_{FW\ start}$ and $R_{FW\ start}$ are, respectively, inductive reactance and resistance of phase FW equivalent circuit (see Fig. 2.30) at starting ($s = 1$).

The motor field will not retain its circular form at other control voltages and under other operating conditions. Motor starting at a circular field will ensure the desired starting torque at minimum input power.

By increasing the capacitance C within certain limits relative to C_0 it is possible to raise the starting torque. The maximum starting torque is attained at $X_C = X_{Cm}$, with the elliptical form of field and an increased input power, which is essential in analysing the motor thermal conditions.

The capacitive reactance X_{Cm} at $\alpha = \alpha_0$ and $s = 1$ is found from the formula

$$X_{Cm} = \sqrt{X^2_{FW\ start} + R^2_{FW\ start}} \qquad (2.57a)$$

From the comparison of equations for X_{C_0} and X_{Cm} it can be easily understood that $X_{Cm} < X_{C0}$; that is, $C_m > C_0$. The maximum torque is n times higher than the starting torque at a circular field:

$$n = 0.5\left(1 + \sqrt{1 + \frac{1}{\alpha^2_{e0}}}\right)$$

where $\alpha_{e0} = \alpha_0 k_{tr}$ is the rms signal ratio at a circular field.

According to the above discussion, there are two basic starting methods for fractional-horsepower induction motors, *viz.*, (a) at a circular field and (b) at a maximum starting torque. Using the capacitance C_m during the starting period at a predetermined starting torque $T_{start} = T_{start\ 0}$, makes it possible to reduce n times the starting control signal. The total input power will rise in this case $(n^4 + 1)/2n^2$ times.

The methods of control discussed above provide for a rather wide range of rotor speed regulation and amounts to (1 : 100)-(1 : 200) for fractional-horsepower servo motors with a hollow nonmagnetic rotor.

The most popular in the automatic-control systems are the amplitude, phase, and amplitude-and-phase control methods. The speed-torque and control characteristics of

the fractional-horsepower induction servo motors in terms of relative units at $s_{cr} \geqslant 1$ for all the above methods of control are illustrated by Figs. 2.35 and 2.36 ($\omega_2^\partial = \omega_2/\omega_1 = 1 - s$; $T^\partial = T/T_{start\ 0}$).

From the analysis of the speed-torque characteristics with reference to torque equation (2.51), it is evident that the control characteristics are nonlinear irrespective of the control method used and their flatness reduces with the control signal. The degree of nonlinearity of the speed-torque characteristics is a ratio of the maximum difference for the torque ΔT^∂_{max} between the actual characteristic and the straight line connecting the no-load speed and starting torque points to the starting torque value, that is, $\Delta T^\partial_{max}/T^\partial_{start}$ (Fig. 2.35*a*). A more linear speed-torque characteristic can be attained by increasing the rotor resistance and, to a certain extent, by decreasing the inductive leakage reactance of the stator and rotor windings. On the other hand, the motor power factor and efficiency will decrease with an increase in the rotor resistance. Therefore, a nonlinearity of the order of 10 per cent is allowed for the fractional-horsepower induction servo motors operating in automatic-control systems.

As can be seen from Figs. 2.35 and 2.37, most linear characteristics are obtained in the case of phase control, the

Fig. 2.35. Speed-torque characteristics of fractional-horsepower induction servo motor using (*a*) amplitude, (*b*) phase, and (*c*) amplitude-and-phase control method

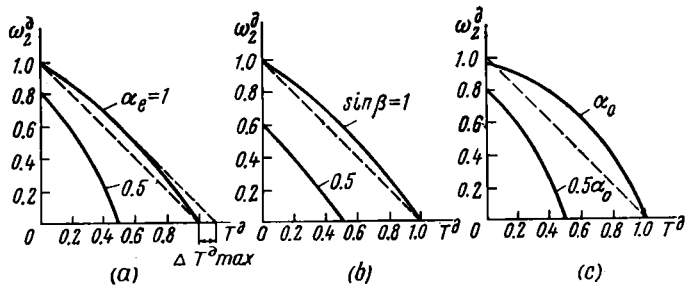

flatness of these characteristics being practically the same at any signal ratio. The least linear are the speed-torque characteristics obtained at amplitude-and-phase control. Whatever method of control is used, the speed-torque characteristics remain stable throughout the entire speed range of the motor, and their shift with the reduction of the signal ratio is towards lower torques and speeds. The motor running torque and output are higher in the case of the amplitude-and-phase control method, because the field voltage and flux slightly increase with an increase in the rotor speed of the fractional-horsepower capacitor motor; hence, a higher motor running torque is obtained as compared to the case of amplitude or phase control. A disadvantage of the amplitude-and-phase control is a certain loss of stability at low speeds.

The analysis of the control characteristics (see Fig. 2.36) shows that whatever method of control is used, these characteristics are generally nonlinear. The degree of nonlinearity is greater under no-load conditions and primarily depends on the same parameters of the motor as those affecting the speed-torque characteristics. Most linear characteristics are attained at phase control, less linear at amplitude control, and the least linear at amplitude-and-phase control (Fig. 2.38). In the case of amplitude-and-phase (capacitor) control, the degree of nonlinearity can be adjusted within

Fig. 2.36. Control characteristics of fractional-horsepower induction servo motor using (*a*) amplitude, (*b*) phase, and (*c*) amplitude-and-phase control methods

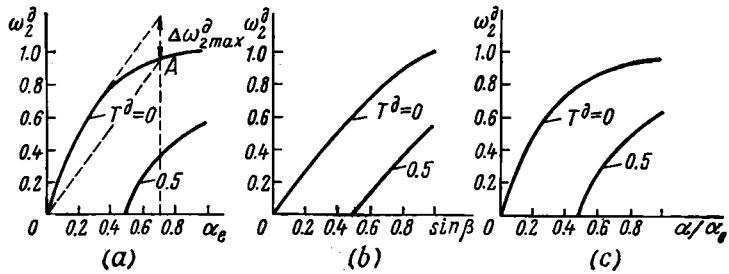

a certain range by varying the capacitance inserted, that is, by changing the elliptical form of the magnetic field. The more elliptical the field, the more linear are the control characteristics. That is why the characteristics are most linear and steep at their origin. To attain more linear control characteristics, the motor must run at low signals and relative speeds. The relative speeds are reduced most efficiently by raising the motor supply frequency that causes a proportional increase in the synchronous speed.

The quantitative estimate of the degree of nonlinearity of the control characteristic is made as follows (see Fig. 2.36*a*). The straight line connecting the characteristic points $\omega_2^\partial = 0$ and $\omega_2^\partial = \omega_{2A}^\partial$ (where ω_{2A}^∂ is the speed corresponding to the maximum signal value) determines the linear control law. The degree of the control characteristic nonlinearity is the ratio of the maximum difference for the speed $\Delta\omega_{2\max}^\partial$ between the actual and the linear control characteristic to the speed at point A under consideration, that is, $\Delta\omega_{2\max}^\partial / \omega_{2A}^\partial$. With speed-torque characteristics nonlinearity below 10 per cent, the degree of nonlinearity of the no-load control characteristic is not over 20 per cent within the signal ratio variation range of 0 to 0.7.

Under all methods of control, the starting torque is directly proportional to the control signal, and in terms of relative units it is equal to the rms signal ratio.

Fig. 2.37. Inherent damping factor k_d versus speed and signal ratio with different control methods
(*a*) amplitude; (*b*) phase; (*c*) amplitude-and-phase

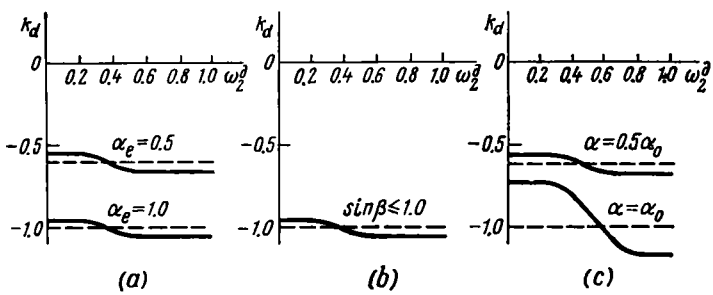

The exciting power is the power consumed by the motor field circuit:

$$P_{FW} = V_1 I_{FW} \cos \varphi_{FW} \tag{2.58}$$

where φ_{FW} is angle of shift between the supply voltage and the field current.

The control power is the power consumed by the motor control winding:

$$P_{CW} = V_{CW} I_{CW} \cos \varphi_{CW} \tag{2.59}$$

where φ_{CW} is angle of shift between the voltage and current in the control winding.

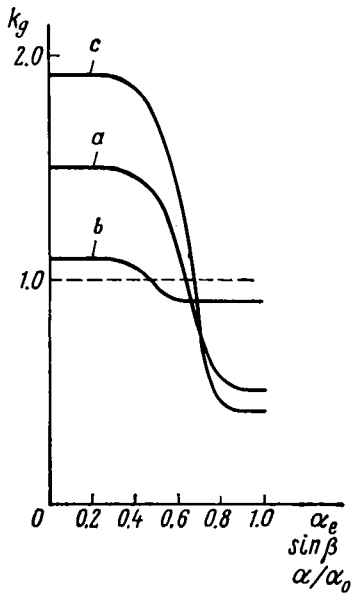

Fig. 2.38. Gain factor versus signal ratio with different methods of control
(*a*) amplitude; (*b*) phase; (*c*) amplitude-and-phase

As is seen from the analysis of equation (2.59), the control power of fractional-horsepower induction servo motors is almost the same with amplitude and amplitude-and-phase control methods and its dependence on the signal ratio is equally strong while with phase control this power remains practically constant with a decrease in the signal ratio (Fig. 2.39). In this respect, the amplitude and amplitude-and-phase control methods are fairly more advantageous than the phase control method.

The efficiency of the fractional-horsepower induction servo motors is lower than that of the general-purpose induction motors of the same power rating as they have a higher rotor resistance. The highest efficiency of the former is obtained with amplitude control, a lower efficiency is with amplitude-and-phase (capacitor) control and the lowest is with phase control (because a high control power is required). The efficiency of the capacitor-controlled motors can be raised by varying the capacitance inserted in the field circuit ($\cos \varphi = 0.8$ to 0.95).

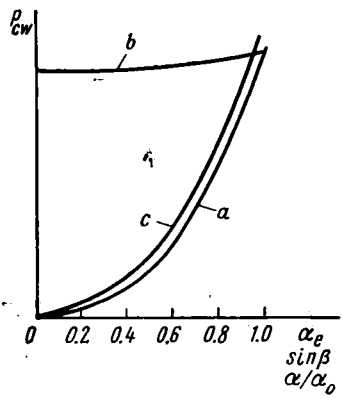

Fig. 2.39. Control power versus signal ratio with different control methods
(*a*) amplitude; (*b*) phase; (*c*) amplitude-and-phase

The simplest supply circuit among those used for fractional-horsepower induction servo motors is that of a capacitor motor as it has no complicated devices for phase shifting between the control and field voltages.

Hence, the amplitude-and-phase control method involving a capacitor in the field circuit has a number of advantages, which accounts for its wide use in automatic-control systems and computing units. However, each time the desired control method must be selected with due consideration given to operating conditions of the system incorporating the motor and the requirements to this motor as a component part of the system.

An important requirement to fractional-horsepower induction servo motors operating in automatic-control systems is absence of inertial running.

Let us discuss the phenomenon called inertia of induction servo motors with reference to the functions $T = f(s)$ for the forward- and backward-sequence torque (T_1 and T_2, respectively) with a pulsating stator field and at different values of critical slip s_{cr} (Fig. 2.40*a*, *b*).

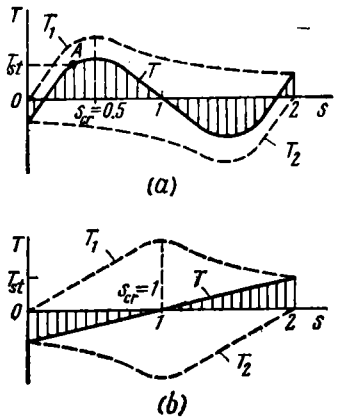

Fig. 2.40. Torque versus slip at different values of slip

Figure 2.40 illustrates the curve of the resultant torque T obtained for a pulsating stator field as a geometric sum of the forward- and backward-sequence torques.

In the case illustrated by Fig. 2.40*a*, the critical slip s_{cr}, as referred to the forward-sequence field, equals 0.5, and the resultant torque within the motor duty conditions ($s = 0$ to 1) is unidirectional with the forward-sequence torque and, hence, with the rotor sense of rotation. Therefore, the rotor will not stop upon the removal of the control signal unless the static torque T_{st} is lower than the maximum resultant torque (for instance, the duty condition of point A).

In the case illustrated by Fig. 2.40*b*, the critical slip s_{cr}, as referred to forward-sequence torque equals unity. Here, the resultant torque curve intersects the axis of slip at one point only, $s = 1$, and within the motor duty condition the torque T is negative, that is, it is a drag torque opposing the motor rotation. Therefore, the rotor will stop for sure as soon as the control signal is removed. The same will take place at $s_{cr} > 1$.

It should be pointed out that the value of s_{cr} (with the $s_{cr} > 1$ condition satisfied) required to ensure elimination of inertial running depends on the connection of the control winding. So a higher critical slip is required when the control signal is removed upon opening the control winding than when the signal can be removed without doing this.

Reversal of the fractional-horsepower induction servo motors is afforded by inverting the control voltage phase (as by changing over the leads of the control winding CW). In the action, the stator field starts revolving in the opposite direction thereby reversing the rotor.

2.8. Dynamic Characteristics of Fractional-Horsepower Induction Servo Motors

It should be borne in mind when analyzing the transient processes occurring in the fractional-horsepower induction servo motors that the time of electromagnetic transients is much shorter than that of electromechanical transients, and so in most cases the former may be neglected.

Accurate analytical expressions for the transient characteristic and transfer function of a fractional-horsepower

induction servo motors are rather complicated due to nonlinearity of speed-torque and control characteristics. In actual calculations, these characteristics or their portions are assumed to be linear. The dynamic properties of a fractional-horsepower induction servo motor on a linear portion of the speed-torque characteristic are described by equations similar to Eqs. (2.35), (2.36), and (2.39) for a fractional-horsepower d.c. servo motor. This means that the induction servo motor is an aperiodic component of the first order in case the rotor speed functions as an output value, and an integrating delay component when the output value is the rotor angle of turn.

The induction servo motor response is recognized by the electromechanical time constant τ_m.

The time constant τ_m is a time taken by the rotor of a motor running at no load with a moment of inertia J to accelerate from standstill to the ideal no-load speed ω_0 at a constant running torque equal to starting torque T_{start}, that is,

$$\tau_m = J \frac{\omega_0}{T_{start}} \tag{2.60}$$

For a linearized portion of the speed-torque characteristic equation (2.60) is written as follows:

$$\tau_m = J/k_d \tag{2.61}$$

The value of τ_m for the fractional-horsepower induction servo motors generally depends on the signal ratio. In the case of amplitude and amplitude-and-phase (capacitor) control, the speed-torque characteristic is flattened with the control signal applied, that is, the ω_0/T_{start} ratio rises and the inherent damping factor k_d decreases (see Fig. 2.37), thereby causing τ_m to grow. With these methods of control, τ_m can be found to a first approximation (at $0 < \alpha_e \leqslant 1$) by using the equation

$$\tau_m = J \frac{\omega_1}{T_{start\,0}} \left(\frac{2}{1+\alpha_e^2} \right) \tag{2.62}$$

In the case of phase control, the speed-torque characteristic flatness is independent of the signal and the value

of τ_m can be found from the equation

$$\tau_m = J \frac{\omega_1}{T_{start\ 0}} \tag{2.63}$$

The electromechanical time constant τ_m of actual fractional-horsepower motors appears to be somewhat shorter than that obtained from equations (2.62) and (2.63) due to the nonlinearity of their speed-torque characteristics. With such a characteristic, the running torque at the same speed is higher than with a linear characteristic.

The time constant τ_m rises with an increase in supply frequency f and a decrease in the number of pole pairs p since the synchronous speed varies according to the following law:

$$\omega_1 = 2\pi \frac{f}{p}$$

The time constant τ_m can be reduced and the motor response increased by taking the following measures:

(1) reducing the moment of inertia of the rotor, for example, through the use of a hollow nonmagnetic rotor;

(2) raising the starting torque through modifying the construction and reducing the air gap; for example, by using a "through" type of construction.

The response of the fractional-horsepower induction servo motors with a hollow nonmagnetic rotor should be compared with that of the motors having a squirrel cage rotor at equal output power, total loss per unit area of the frame surface characterizing the motor heating, equal degree of nonlinearity of the motor characteristics and equal supply frequency.

As can be seen from equation (2.60), the relation between the time constants τ_m of the motors running at the same speed is directly proportional to the ratio of the rotor moments of inertia and inversely proportional to the ratio of the starting torques.

The moment of inertia of a hollow nonmagnetic rotor is much lower than that of a squirrel-cage rotor of the same diameter and length.

On the other hand, the squirrel-cage rotors have a higher mechanically allowable length-to-diameter ratio than the

thin-walled hollow nonmagnetic rotors hanging on the shaft. It means that the diameter and the moment of inertia of the squirrel-cage rotor can be reduced by increasing its length without changing the surface area required for passing the main flux.

With the field structure unsaturated and with other conditions being equal, a higher starting torque can be obtained in the case of a squirrel-cage motor by reducing the air gap (see Section 2.6).

All these factors determine the response characteristics of the fractional-horsepower induction servo motors. At power ratings as low as some watts or fractions of a watt and with a relatively small size and mass of the rotor, a lower time constant τ_m can be obtained with a squirrel-cage motor of a "through"-type construction than with a motor having a hollow nonmagnetic rotor. Among the motors of higher power ratings, those having a hollow nonmagnetic rotor are distinguished by a higher response. The time constant τ_m of a circular-field motor with a hollow nonmagnetic rotor at a frequency of 400 Hz is within the

Fig. 2.41. Time constant τ_m versus rated power for fractional-horsepower induction servo motors

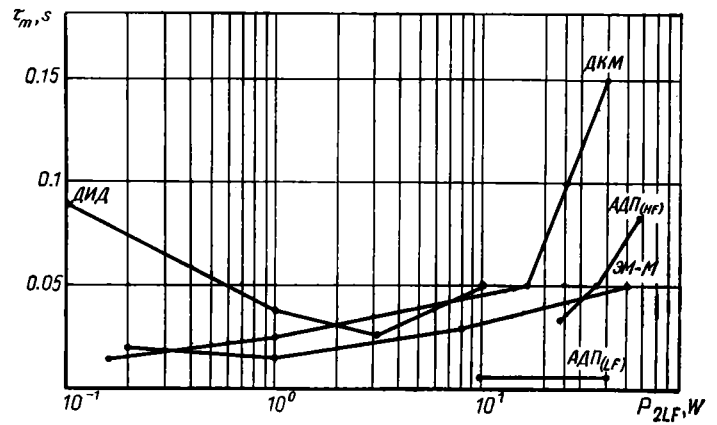

range of 0.015 to 0.15 s while that of a squirrel-cage motor is between 0.05 and 1.5 s.

Figure 2.41 illustrates the response characteristics of some serial-production fractional-horsepower induction servo motors (for designations, refer to Fig. 2.27).

2.9. Continuous-Running Fractional-Horsepower Synchronous Motors

The *fractional-horsepower synchronous motors* built to the classical standard of an electromagnetic-field synchronous machine with a squirrel-cage starting winding have optimum starting and working characteristics. However, these motors are usually not favoured for low-power automatic-control units and devices where efficiency and power factor are not of primary importance, because:

(1) the motor requires two power sources, one a.c. and the other d.c.;

(2) the sliding contact between the slip rings and brushes reduces the motor dependability and makes its construction more complicated;

(3) a special starting circuit arrangement is required to disconnect the rotor field from the d.c. source while the motor gains speed and to connect it to an external resistor.

Fig. 2.42. Connection of fractional-horsepower motors
(*a*) three-phase permanent-magnet motor; (*b*) single-phase hysteresis motor

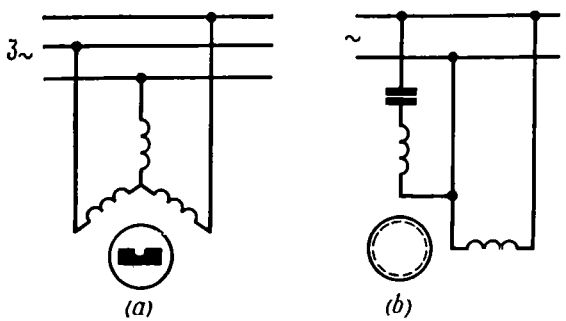

Most widely used in low-power automatic-control systems, units, and domestic appliances are fractional-horsepower contactless synchronous motors in which these drawbacks are eliminated. These fractional-horsepower motors are classified according to the rotor mechanical design and construction, and also the rotor material which greatly influences the internal torque characteristics and the motor performance. The following three types are available:

(1) permanent-magnet (active type);
(2) reluctance;
(3) hysteresis.

The stator of these motors is of a standard construction used for normal synchronous and induction machines. It is stacked up of electric steel stampings. The stator slots accommodate a three-phase or two-phase distributed winding that sets up a rotating magnetic field (Fig. 2.42).

The fractional-horsepower motors discussed in this section have one feature in common: during synchronous running the rotor revolves at the same speed as the fundamental component of the stator magnetic field.

2.9.1. Permanent-Magnet Motors (active type)

The rotor of a permanent-magnet motor is built up of two basic parts:

(a) permanent magnets that set up a magnetic field flux of the rotor and afford the electromagnetic torque at synchronous running;

(b) a squirrel-cage winding placed in an electric steel stack that affords an internal torque in the course of asynchronous starting.

Most popular are rotors with permanent magnets and a squirrel-cage winding arranged radially (Fig. 2.43*a*) or axially (Fig. 2.43*b*).

The internal torque is created due to the interaction between the rotating stator field and the rotor field.

Under synchronous running conditions, in the case of a balanced magnetic circuit and a negligible resistance of the stator winding, the internal torque of a fractional-horsepower synchronous motor is found from the equation

known from the general theory of active-type synchronous machines:

$$T_s = \frac{m_1 V_1 E_0}{\omega_1 X_s} \sin \theta_V \qquad (2.64)$$

where m_1 is number of stator winding phase belts; V_1 is phase voltage across the stator winding terminals; E_0 is emf induced in the stator winding phase belt due to the magnetic flux of the rotor; X_s is synchronous inductive reactance of the stator winding; $\omega_1 = 2\pi (f/p)$ is angular synchronous speed; f is supply frequency; p is number of stator winding pole pairs; θ_V is time angle between the $\dot{V}_1$ and E_0 vectors.

Angle θ_V is numerically equal to the space angle (in electrical degrees) between the space wave of the stator voltage and the rotor quadrature axis q.

Under synchronous running conditions, the angle θ_V is dependent on the static torque on the motor shaft. The angular characteristic corresponding to equation (2.64) is illustrated on Fig. 2.44 (solid line).

The actual fractional-horsepower permanent-magnet synchronous motors have an unbalanced magnetic system. The direct-axis inductive reactance of the stator winding X_d

Fig. 2.43. General arrangement of rotors of fractional-horsepower permanent-magnet synchronous motors
1—permanent magnets; *2*—electric steel core; *3*—squirrel-cage rotor bars

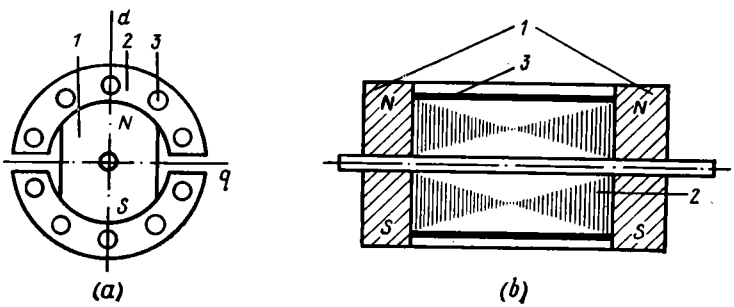

(a) (b)

is not the same as the quadrature-axis inductive reactance X_q. The illustrative example is a fractional-horsepower motor of a radial construction (Fig. 2.43*a*) in which the rotor reluctance along the direct axis *d* is higher than that along the quadrature axis *q* due to a low permeability of the permanent-magnet material *1* as compared to that of the electric steel *2*.

The stator winding resistance R_1 of fractional-horsepower synchronous motors is commensurable with the inductive reactances X_d and X_q, which is not the case with large synchronous motors. That is why a great portion of the input power is lost in the resistance R_1.

Both these factors are responsible for variations in the internal torque T_s as a function of angle θ_V.

The main component of the torque is that corresponding to the interaction between the stator and rotor fields:

$$T_{main} = \frac{m_1 V_1 E_0}{\omega_1} \left[\frac{X_q (2R_1 X_d - R_1 X_q + X_q X_d)}{(X_q X_d + R_1^2)^2} \sin \theta_V + \right.$$
$$\left. + \frac{R_1 (2X_q^2 - X_q X_d + R_1^2)}{(X_q X_d + R_1^2)^2} \cos \theta_V \right]$$

Fig. 2.44. Angular characteristic of fractional-horsepower permanent-magnet synchronous motor

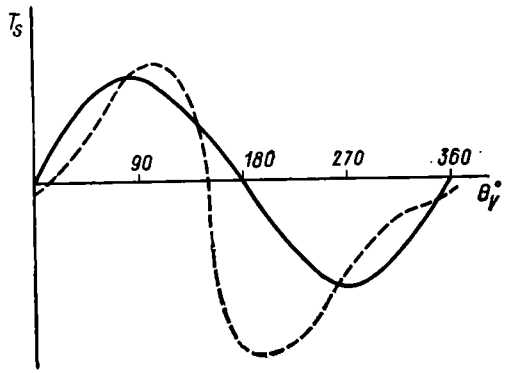

At $R_1 = 0$ the equation for the torque T_{main} is to be transformed into equation (2.64).

The result is a d.c. component of the torque:

$$T_{d.c.R_1} = -\frac{m_1 E_0^2}{\omega_1} \cdot \frac{R_1 (X_q^2 + R_1^2)}{(X_q X_d + R_1^2)^2}$$

that is proportional to power loss in the stator winding due to currents induced in this winding by the rotor flux.

The inequality of direct- and quadrature-axis inductive reactances causes a d.c. component of the torque

$$T_{r,d.c.} = -\frac{m_1 V_1^2}{2\omega_1} \cdot \frac{R_1 (X_d - X_q)^2}{(X_q X_d + R_1^2)^2} \qquad (2.65a)$$

and an a.c. component of the torque

$$T_{r,a.c.} = \frac{m_1 V_1^2}{2\omega_1} \cdot \frac{(X_d - X_q)}{(X_q X_d + R_1^2)^2} \times$$
$$\times [(X_q X_d - R_1^2) \sin 2\theta_V + R_1 (X_q + X_d) \cos 2\theta_V] \qquad (2.65b)$$

which are referred to as reactive components. At $X_q = X_d$ these components equal zero.

The d.c. components of the torque, $T_{d.c.R_1}$ and $T_{r,d.c.}$, are negative and function as drag components.

The resultant electromagnetic flux of the fractional-horsepower permanent-magnet synchronous motor is generally a sum of all these components:

$$T_s = T_{main} + T_{d.c.R_1} + T_{r,d.c.} + T_{r,a.c.} \qquad (2.66)$$

Figure 2.44 (dash line) illustrates the angular characteristic of a radial fractional-horsepower synchronous motor, corresponding to equation (2.66).

When these motors are incorporated in a synchro tie system, it is often important to know the synchronous torque T_s as a function of angle γ between the mmf (or flux) axis of the stator and the direct axis of the rotor. It should be noted that the angular characteristic $T_s = f(\gamma_{el})$ is also nonsinusoidal, but at angles $\gamma_{el} = 0$ and 180 deg. the torque $T_s = 0$ (γ_{el} is angle γ in electrical degrees).

Other conditions being equal, the torque T_s rises with the emf E_0, that is, with the intensity of the rotor magnetic flux.

During the starting period, while the rotor has not yet gained synchronous speed, the permanent-magnet fractional-horsepower synchronous motor runs as an induction machine. The rotating magnetic field of the stator interacts with the currents induced by this field in the squirrel-cage winding and, in the action, sets up an induction torque T_i (Fig. 2.45). This method of starting is distinguished from that used for the electromagnetic-field motors by the fact that the rotor field flux takes part in starting the motor. This flux induces in the stator winding of the running machine an emf of a frequency other than the supply frequency. This emf causes currents to flow in the stator winding circuit, which interact with the rotor flux, the result being a drag torque T_d opposing the induction torque T_i. Under such conditions, dips will appear on the resultant speed-torque characteristic $T_{res} = f(s)$ which will impair starting conditions. For example, at a static drag torque on the shaft $T_{st\ A}$ (Fig. 2.45) the rotor will revolve at a speed corresponding to a slip s_A. This speed is far from being the synchronous speed and the rotor will never be pulled in step with the stator field.

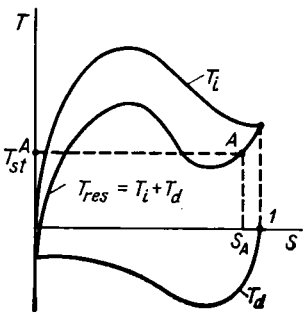

Fig. 2.45. Speed-torque characteristic of fractional-horsepower permanent-magnet synchronous motor running as induction motor (s—slip)

It should be noted that during synchronous running conditions ($s = 0$) the torque T_d is the component of the electromagnetic torque $T_{d.c.R1}$ that has been discussed above. In order to reduce the drag torque T_d, the excitation of the rotor permanent magnets, that is, the E_0/V_1 ratio, should be reduced.

Excitation of the permanent magnets may be considered properly selected when the best characteristics are ensured for a synchronously running machine at desired speed-torque characteristics.

2.9.2. Reluctance Motors

The fractional-horsepower synchronous reluctance motors are machines that run with an unexcited rotor and with the reluctance varying over the air gap. The rotating field of such motors is set up only due to the stator mmf. The electromagnetic torque appears as a result of a change in the energy of the magnetic field in the air gap in the event of a mismatch between the field and rotor axes.

Variation of the reluctance in the motor air gap is afforded by a proper selection of the rotor shape and material.

The rotors depicted in Fig. 2.46*a* and *b* differ from a normal squirrel-cage rotor of an induction motor by provision of external open slots (in the case of a salient-pole construction, Fig. 2.46*a*) or internal slots (in the case of a nonsalient-pole construction, Fig. 2.46*b*) that ensure variation of the

Fig. 2.46. General arrangement of rotors for fractional-horsepower synchronous reluctance motors
1—electric steel core; *2*—squirrel-cage rotor bars

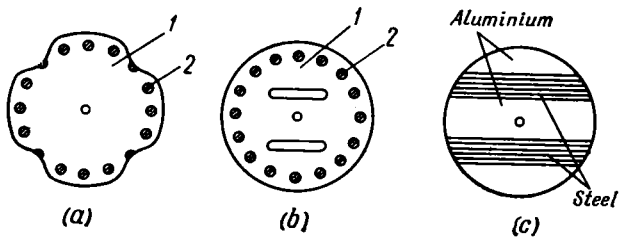

reluctance along the motor periphery. As for the rotor illustrated in Fig. 2.46*c*, this variation is provided due to the use of two materials having different magnetic properties.

Figure 2.47 shows a fractional-horsepower synchronous reluctance motor, type СД-09М, with a rotor construction illustrated by Fig. 2.46*a*.

The operating principle of a reluctance motor can be understood by studying a static model of Fig. 2.48. The rotating stator field is replaced here by a permanent magnet. The stator mmf axis and the rotor direct axis *d* are spaced apart at an angle γ. The stator mmf and magnetic flux Φ_1 are assumed to be unidirectional.

Figure 2.48*a* shows the rotor position when the angle γ (mismatch angle) is zero. The magnetic lines of force take the path of the lowest reluctance and are not deformed. The reluctance torque $T_r = 0$. The rotor is in a stable equilibrium position. Turning the rotor by force through

Fig. 2.47. Fractional-horsepower synchronous reluctance motor СД-09М
1—stator with a two-phase winding; *2*—rotor; *3*—end shield

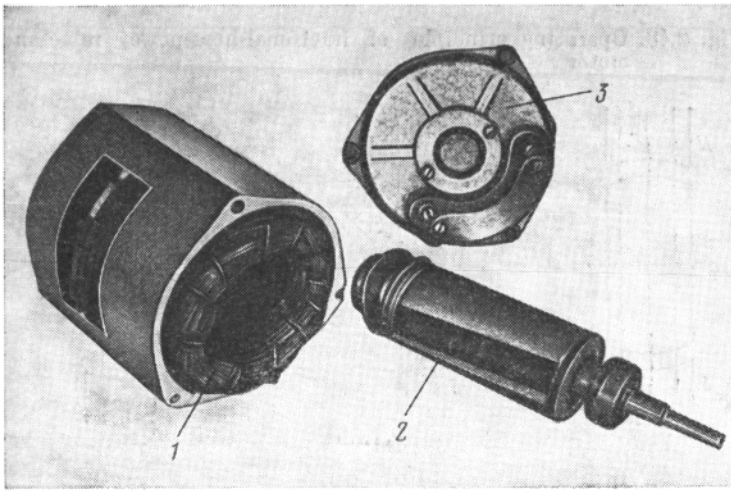

angle γ in the clockwise direction will bend the magnetic lines of force (Fig. 2.48*b*). As a result of resilient properties of the magnetic lines of force, the deformed magnetic field will set up a reluctance torque that will tend to turn the rotor in the counter-clockwise direction. The rotor will obviously settle at such an angle γ to the stator flux axis that the external torque will be balanced by the motor reluctance torque. Upon the removal of the external torque the rotor will return to the stable equilibrium position in which $\gamma = 0$. With the rotor turned through 90 deg. (Fig. 2.48*c*), the magnetic lines of force will follow a rectilinear path again and will not bend, but the reluctance in this event will be higher than at $\gamma = 0$.

The reluctance torque $T_r = 0$, that is, the rotor is in the equilibrium state. There is, however, an essential difference between the equilibrium positions at $\gamma = 0$ and at $\gamma = 90$ deg. In the former case, the equilibrium position is stable as any deviation from this position will cause the rotor to tend to its original position, while in the latter case the equilibrium state is unstable and a slight disturbance is sufficient to return the rotor to the stable state of

Fig. 2.48. Operating principle of fractional-horsepower reluctance motor

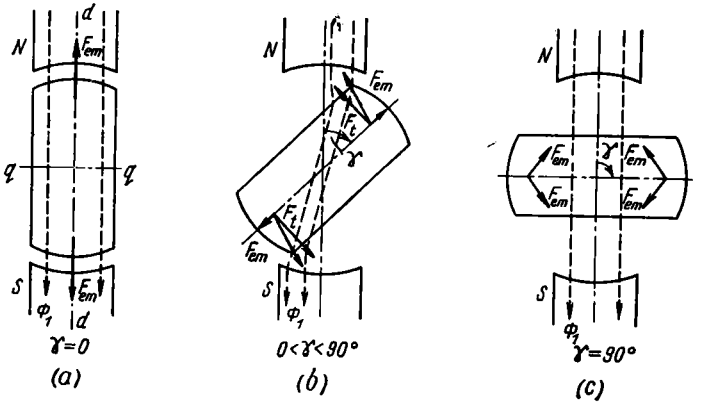

maximum permeance illustrated in Fig. 2.48*a* or to a position shifted 180 deg. from the former.

Thus, the reluctance torque always tends to place the rotor in a position of minimum reluctance on the path of the motor flux. A stable equilibrium position of the rotor is attained at $\gamma = 0$ or 180 deg., and an unstable equilibrium position at $\gamma = 90$ or 270 electrical degrees.

Discussed above is a physical process of creating a reluctance torque under steady state conditions that takes place when the rotor axis is displaced relative to the centre line of the permanent-magnet poles. In actual fractional-horsepower reluctance synchronous motors, the magnetic field rotating in space at a constant or a varying speed is set up due to the stator windings *1*, and the rotor *2* is forced to revolve along with the rotating field at the same speed due to the reluctance torque (Fig. 2.49).

Analytical expressions of the reluctance torque through angle γ are rather complicated. To simplify them, angle θ_V between the space wave of the stator voltage and the rotor quadrature axis is used in calculations, this angle being dependent on the load torque.

The angular characteristic of the reluctance motor obeys the law of magnetic reluctance variation along the stator

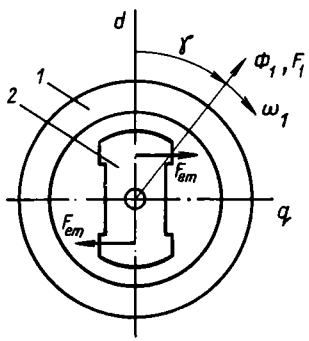

Fig. 2.49. Model of a fractional-horsepower synchronous reluctance motor

periphery. The torque corresponding to the fundamental (quadratic) harmonic of the a.c. component of magnetic reluctance, disregarding the stator winding resistance, can be found from the formula known from the general theory of salient-pole machines:

$$T_r = \frac{m_1 V_1^2}{2\omega_1}\left(\frac{1}{X_q} - \frac{1}{X_d}\right)\sin 2\theta_V \qquad (2.67a)$$

where X_d and X_q are, respectively, direct and quadrature inductive reactances of the synchronous machine.

The reluctance torque T_r, as distinct from the active torque, varies as a function of angle θ_V according to the $\sin 2\theta_V$ law (solid line on Fig. 2.50). The steady-state condition of the motor is attained at a certain angle θ_V at which $T_r = T_{st}$, where T_{st} is static drag torque on the motor shaft.

Actual fractional-horsepower synchronous motors have a rather high stator winding resistance R_1 that is commensurable with X_d and X_q. That is why, more precise formulas (2.65*a*) and (2.65*b*) must be used in the calculations of

Fig. 2.50. Angular characteristic of fractional-horsepower synchronous reluctance motor

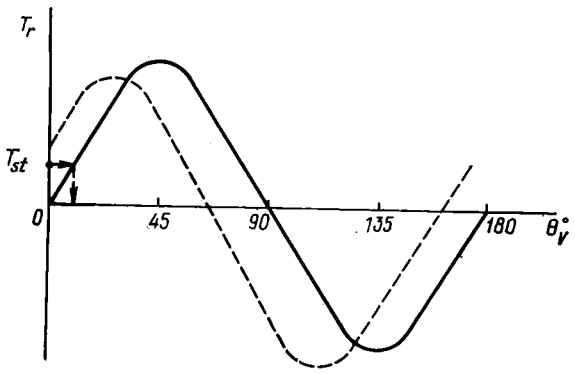

the reluctance torque

$$T_r = T_{r,\,d.c.} + T_{r,\,a.c.} = \frac{m_1 V_1^2}{2\omega_1} \cdot \frac{X_d - X_q}{(X_q X_d + R_1^2)^2} \times$$
$$\times [(X_q X_d - R_1^2) \sin 2\theta_V + R_1 (X_q + X_d) \times$$
$$\times \cos 2\theta_V - R_1 (X_d - X_q)] \quad (2.67b)$$

At $R_1 = 0$, equation (2.67*b*) is transformed into equation (2.67*a*). As can be understood from equation (2.67*b*), resistance R_1 produces an effect on the torque T_r. The torque maximum is displaced from 45 deg. towards lower angles θ_V = (30 to 40 deg.) as is shown by the dash line on Fig. 2.50.

The angular characteristic $T_r = f(\theta_V)$ can be transformed to the argument of γ by using the equation

$$\theta_V = \arctan \frac{X_q \sin \gamma_{el} - R_1 \cos \gamma_{el}}{X_d \cos \gamma_{el} + R_1 \sin \gamma_{el}}$$

where $\gamma_{el} = p\gamma$ is angle γ in electrical degrees.

The angular characteristics $T_r = f(\gamma_{el})$ are nonsinusoidal, but at angles $\gamma_{el} = 0$, 90, 180, and 270 deg. the reluctance torque $T_r = 0$.

If the rotor and the rotating field revolve at different speeds, the angle θ_V becomes a periodic function of time and the average value of reluctance torque is zero. That is why, during the starting period the reluctance motors run as induction machines. A squirrel-cage winding (see Fig. 2.46*a* and *b*) or aluminium parts of the rotor (see Fig. 2.46*c*) may function as a starting winding. Starting characteristics, and in particular the pull-in torque, of motors furnished with a rotor illustrated by Fig. 2.46*b* are the best when a complete set of the rotor bars is retained.

In the course of starting the reluctance motors, an a.c. component of magnetic flux appears due to the change in the magnetic reluctance R_m. This component induces an additional emf in the stator winding. As in the case of permanent-magnet motors, a drag torque T_d builds up, but its effect on the starting characteristics of the reluctance motor is not that great as the motor runs underexcited.

Under synchronous running conditions $T_d = T_{r.d.c.}$.

The efficiency and power factor of the reluctance motors are low. A low power factor is explained by the fact that the magnetic flux of a reluctance motor is set up only due to the magnetizing current induced in the stator. A heavy magnetizing current is the result of a high reluctance of the magnetic circuit due to dips on the rotor ($R_{mq} > R_{md}$). Correspondingly, the efficiency of the reluctance motors is low because of heavy power loss in the stator winding.

Hence, the greater the unequality of magnetic reluctances and inductive reactances along axes q and d, the higher will be the reluctance torque T_r [see equation (2.67*a*)] and the lower the motor power factor and efficiency. In actual fractional-horsepower synchronous reluctance motors, the rotor pole arc to pole pitch ratio is approximately 0.5 to 0.6 and the maximum-to-minimum air gap ratio is about 10 to 12.

2.9.3. Fractional-Horsepower Hysteresis Motors

A *fractional-horsepower hysteresis motor* (Fig. 2.51) is a *synchronous machine* with its torque produced due to the effect of hysteresis at the reversal of the rotor polarity.

The rotor of a hysteresis motor is made of a retentive material (cobalt-vanadium alloy, alni) having a wide hysteresis loop. To save expensive retentive materials, the rotor is assembled of different materials (Fig. 2.52).

Best utilization of the retentive material properties, highest possible power factor and efficiency are attained by a proper selection of the thickness of the retentive ring *1* and the rotor diameter.

What the hysteresis torque is can be understood from the analysis of physical processes occurring in the rotor of the above-described design when it rotates asynchronously, that is, when the rotor material continuously reverses its polarity (Fig. 2.53). Assume that the axes of the stator and rotor mmfs and those of the fluxes coincide. At the moment when the vector of the stator rotating flux Φ_1 assumes

position A (Fig. 2.53*a*), the elementary magnets of the rotor orient themselves along this flux. The forces due to interaction of the elementary magnets, say T_1 and T_2, with the stator flux act along this flux and do not produce a torque. As soon as the stator flux assumes position B, the elementary magnets will turn in the same direction (Fig. 2.53*b*). However, the magnets T_1 and T_2 will not instantly turn through the same angle as the flux Φ_1 due to magnetic lag, with the result that a mismatch angle γ_h (magnetic lag angle) will appear between them. Thereupon, interaction forces F_{em} will have tangential components F_t that will cause the hysteresis torque T_{ha} with asynchronous running. This hysteresis torque is proportional to the vector product of the space vectors of rotor magnetic flux $\overline{\Phi}_2$ due to the elementary magnets and stator magnetic flux $\overline{\Phi}_1$. These

Fig. 2.51. Fractional-horsepower synchronous hysteresis motor
1—stator with a two-phase winding; *2*—rotor; *3*—end shield

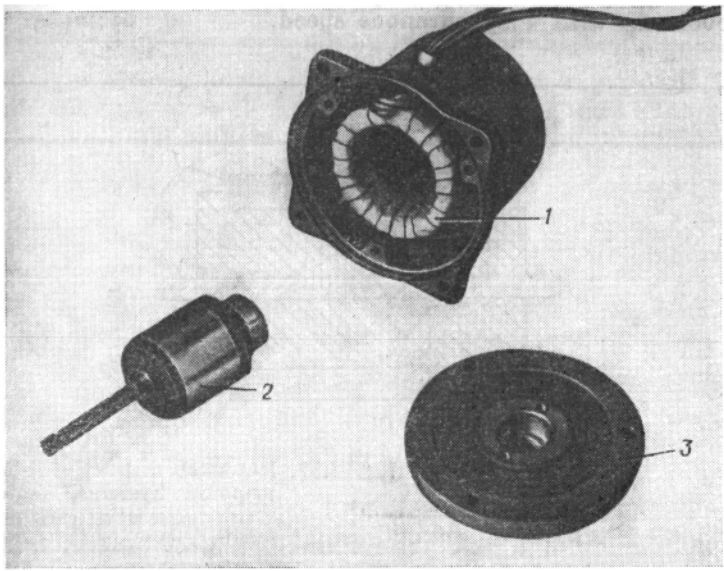

fluxes rotate at an equal speed and are shifted in phase by an angle γ_h:

$$T_{ha} = k\,[\overline{\Phi}_1\overline{\Phi}_2] = k\Phi_1\Phi_2 \sin\gamma_h \qquad (2.68a)$$

where k is factor depending on the motor characteristics.

Fluxes Φ_1 and Φ_2 do not depend on the rotor speed in the case of a balanced supply, such as three-phase supply. The space angle γ_h by which the rotor flux lags behind the stator flux is also independent of the rotor speed and is determined by the coercive force H_c at which the field of the elementary magnets starts reversing its polarity, that is, the space angle depends on the shape of the rotor material hysteresis loop. The hysteresis torque T_{ha} is also independent of the rotor speed.

Figure 2.54*a* (solid line) shows an ideal speed-torque characteristic of a fractional-horsepower hysteresis motor. As can be seen from this characteristic, the synchronous hysteresis motor, as distinct from fractional-horsepower synchronous motors of the other types, possesses its own hysteresis torque that is equal to the torque on a rotor revolving with a synchronous speed.

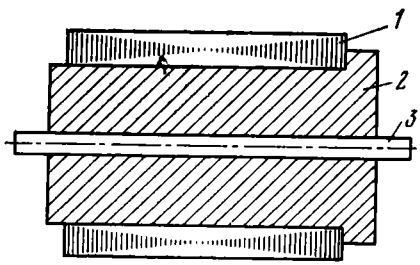

Fig. 2.52. Rotor of a fractional-horsepower hysteresis motor
1—ring made of retentive material; *2*—bush made of nonmagnetic or nonretentive material; *3*—shaft

The hysteresis torque magnitude is determined from the power balance in the rotor. The hysteresis loss power in a motionless rotor

$$P_{hl} = P_{sl} f_1 V$$

where P_{sl} is specific hysteresis loss per unit volume within one reversal cycle, the hysteresis loss being proportional to the hysteresis loop area; V is volume of the rotor retentive material; f_1 is supply frequency.

When the rotor runs with a slip s, its reversal frequency f_s is equal to sf_1 and the hysteresis loss in the rotor

$$P_{hs} = sP_{hl}$$

The difference between P_{hl} and P_{hs} corresponds to a full mechanical power developed by the motor:

$$P_{mech} = P_{hl} - P_{hs} = P_{hl}(1 - s)$$

Now the hysteresis torque

$$T_{ha} = \frac{P_{mech}}{\omega_2} = \frac{P_{hl}}{\omega_1} = \frac{P_{sl} f_1 V}{\omega_1} \qquad (2.68b)$$

where ω_2 and ω_1 are the rotor and field speeds.

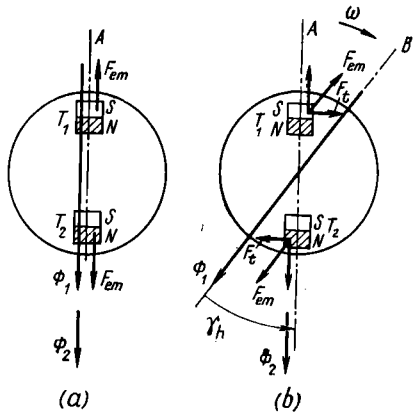

Fig. 2.53. Operating principle of fractional-horsepower hysteresis motor

It follows from equation (2.68*b*) that the hysteresis torque can be increased by selecting a rotor material having the highest possible coercive force H_c, residual flux density B_h, and most prominent shape of the hysteresis loop (Fig. 2.55). An ideal material would be that having a rectangular hysteresis loop *1*. Materials of the cobalt-vanadium and alni types having a hysteresis loop shown by curve *2* approach the ideal material. Standard electric steels have a hysteresis loop as is shown by curve *3* and cannot afford the desired hysteresis torque.

Actual hysteresis motors may have a speed-torque characteristic that is not absolutely flat. A change in the hysteresis torque as a function of the rotor speed (slip) can be primarily attributed to the following three factors.

(1) When the rotor and the stator field revolve at different speeds, eddy currents are induced in the rotor. These currents interact with the field Φ_1 and build up a torque T_{ec} which is essentially an induction motor torque (dash line on Fig. 2.54*b*).

(2) When a two-phase hysteresis motor (Fig. 2.42*b*) is connected to a single-phase network through a capacitor, the shape of the rotating field and hence the value of the torque T_{ha} (dash-and-dot line on Fig. 2.54*b*) depend on the rotor speed. A change in the rotor speed causes a change in the polarity-reversal frequency along with the rotor loss and the current in the stator windings. Voltages are divided

Fig. 2.54. Speed-torque characteristics of hysteresis motor

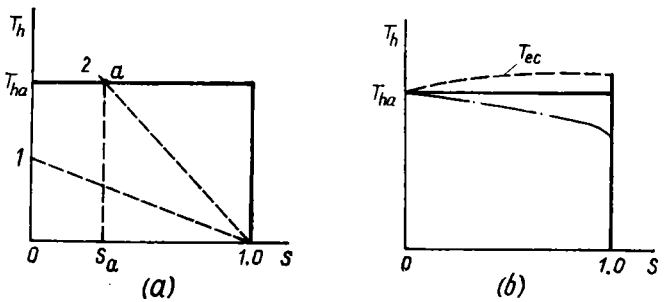

between the capacitor and the phase winding in a quite different proportion, and the field, that has been circular at one speed (say, at $s = 0$), becomes elliptical at another speed, just as is the case with fractional-horsepower induction motors (see Section 2.6).

(3) Effect of the torques due to upper harmonics of the field is still another factor causing a change of the hysteresis torque as a function of the rotor speed.

When the rotor runs in step with the stator field, the speed of the both is equal, and no reversal of polarity takes place in the rotor material. The rotor magnetic flux Φ_2 is retained due to residual magnetism. This flux revolves in step with the rotor. The higher the residual flux density B_h, the greater is the flux. The fractional-horsepower motor runs as a standard permanent-magnet synchronous motor, the only difference being that the rotor field axis taken as a direct axis of the hysteresis motor lags behind the stator field axis by angle γ that will never exceed the magnetic

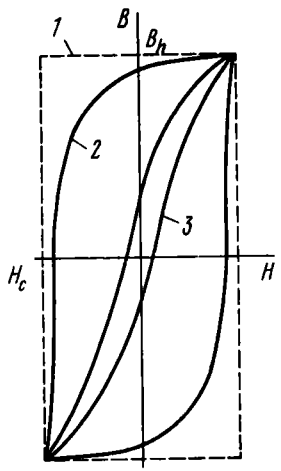

Fig. 2.55. Hysteresis loop for different materials

lag angle γ_h since otherwise the rotor would start reversing its polarity. Hence, the highest torque T_{hs} developed by the hysteresis motor during synchronous running is that equal to T_{ha}. At a static torque on the shaft exceeding T_{ha} the rotor is pulled out of step. The angle γ_h of fractional-horsepower hysteresis motors usually does not exceed 20 or 25 deg.

It follows from the above discussion that a synchronous hysteresis motor develops a running torque both at a synchronous and an asynchronous speed of the rotor. Its operating conditions depend on the magnitude and type of the static torque on the shaft T_{st} (Fig. 2.54*a*). When the static torque (straight line *1*) is lower than the hysteresis torque throughout the entire slip range from 1 to 0, the motor runs as a synchronous machine. The rotor field axis lags behind the stator field axis by an angle γ at which $T_{hs} = T_{st}$, that is, the torques are balanced. When the static torque varies as is illustrated by straight line *2*, the torques will be balanced at a slip s_a corresponding to point *a*, that is, the motor will run as an induction machine ($T_{ha} = T_{st}$). However, it is not feasible to use hysteresis motors as induction machines because of heavy hysteresis losses in the rotor, especially at high slips.

Synchronous hysteresis motors possess rather valuable properties. They develop a high starting torque and can pull in step at a high moment of the load inertia. The rotor of the hysteresis motor runs in step smoothly, without jerks, due to a practically constant hysteresis torque throughout the entire starting period from $s = 1$ to $s = 0$. The input current of the hysteresis motor varies negligibly (by 20 to 30 per cent) within the period from short-circuit starting to no-load running. That is why these motors are most suitable for intermittent running. The hysteresis motors are simple in design and reliable in operation.

The efficiency and power factor of the hysteresis motors are not very high as the rotor flux is set up due to the working flux of the stator, and such motors operate as underexcited synchronous machines. However, in the course of synchronous running the magnetizing current of these machines can be varied thereby causing variations in their efficiency and power factor.

This can be understood by analyzing the characteristic of Fig. 2.56 showing current I_1 of a synchronous hysteresis motor versus field voltage V_1 as the latter drops to the starting voltage $V_{1\,start}$.

The rotor mmf depends on the starting voltage $V_{1\,start}$ and the resultant flux of the motor reduces with V_1. So, with a decrease of $V_1/V_{1\,start}$ the rotor mmf takes a greater part in building up a resultant field that causes a change in the magnitude and type of the stator current. The inductive magnetizing component of the stator current ($\varphi > 0$) gradually drops to zero ($\varphi = 0$) and then a capacitive demagnetizing component appears ($\varphi < 0$). From the physical point of view, the characteristic described above is identical to the U-shaped characteristic of an electromagnetic-field synchronous motor.

Under working conditions, the efficiency and power factor of a hysteresis motor running as a synchronous machine can be raised by magnetizing the rotor through a short-time increase (within two or three cycles) of the stator flux, which can be attained by applying a higher voltage to the stator. The additionally magnetized rotor, like the permanent-magnet rotor of a usual synchronous motor, will take a greater part in setting up the main working flux, thereby reducing the reactive magnetizing current in the stator winding. This corresponds to a displacement of the working point on the motor characteristic from A to B (Fig. 2.56).

Synchronous motors are available for operation both on constant-frequency and varying-frequency supply.

The former are used where a constant speed is required at a static torque varying within a certain range, such

Fig. 2.56. U-shaped characteristic of fractional-horsepower hysteresis motor

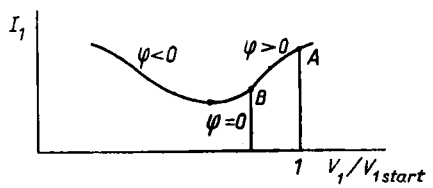

as in sound-recording and TV sets, etc. The synchronous speed of such motors can be varied only upon changing the stator windings over to a different number of pole pairs. It should be noted that among the synchronous machines only the hysteresis motors can operate at a different number of the stator winding poles. The number of pole belts on the rotors of these motors is always the same as the number of poles on the stators. As for all the other synchronous motors, the number of poles on the rotor is determined at the design stage.

The latter motors are meant for a stepless or stepped control of the rotor synchronous speed by varying the supply frequency. The motors using a stepless control of frequency are generally used in synchro tie systems.

The important feature required from synchronous motors intended for use in sound-recording, sound-reproducing and the like systems is low radio noise. The discussion of the main causes of radio noise given below will be useful in comparing different synchronous motors with respect to this characteristic.

Mechanical noise due to vibrations caused by a dynamically unbalanced rotor, by running bearings and sliding contacts.

Aerodynamic noise due to windage of a revolving rotor.

Magnetic noise due to vibrations in the magnetic circuit under the effect of alternating electromagnetic forces caused by variations in the reluctance along the rotor periphery.

According to the above-mentioned, the least level of radio noise can be attained with hysteresis motors having a mechanically and magnetically symmetrical rotor with a smooth surface. The highest level of noise is characteristic of reluctance motors with a salient-pole rotor (Fig. 2.46*a*).

Fractional-horsepower permanent-magnet motors of the active type have the highest efficiency η and power factor $\cos \varphi$ and the lightest mass q per unit power output. At a supply frequency of 50 Hz and a power output ranging from 10 to 100 W, $\eta = 40$ to 80 per cent (lower values refer to motors of a lighter power rating). The next machines in this respect are hysteresis motors which run, as has been stated above, like underexcited synchronous motors. Under the same conditions, their efficiency $\eta = 30$ to 50 per cent.

Reluctance motors, where the rotor field flux is absent, have the lowest efficiency and power factor. Under the above-specified conditions, their efficiency $\eta = 20$ to 40 per cent.

The power factor cos φ of the motor greatly depends on the method of its connection: three-phase or single-phase through a capacitor. A rather low power factor inherent in reluctance and hysteresis motors (about 0.3 to 0.5 in the case of a three-phase connection) is higher in the case of connection through a capacitor and is almost the same as that in permanent-magnet motors (approximately 0.6 to 0.9).

Synchronous motors designed for operation at a high frequency (400 and 1,000 Hz) may have higher efficiency and power-to-mass ratio than those running at 50 Hz.

Figure 2.57 illustrates efficiency and mass per unit power output of some serial-production synchronous motors.

Fig. 2.57. Efficiency (*a*) and mass per unit power output (*b*) versus rated output of synchronous motors

СДПМ—active-type permanent-magnet; Г, ГТ—hysteresis; (*L*)—50-Hz frequency; (*H*)—400-Hz frequency; (*3*)—three-phase supply; (*1*) single-phase supply; *P*—reluctance

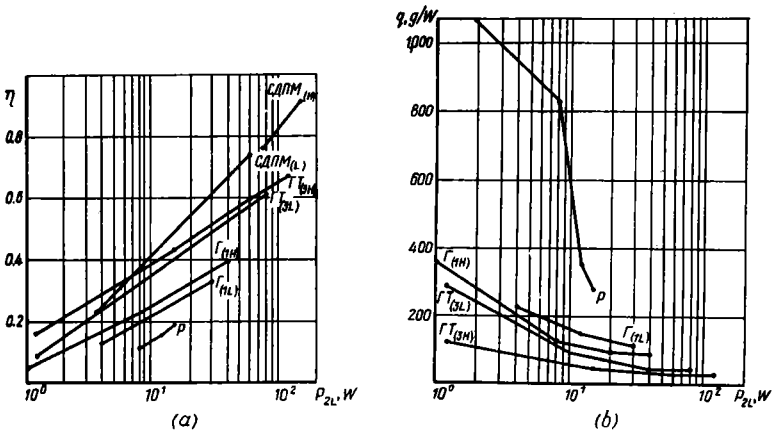

The fractional-horsepower synchronous motors are often used in auxiliary equipment and domestic appliances as general-purpose motors. The most simple in design and manufacturing technique of all the above-discussed fractional-horsepower synchronous motors are reluctance motors that are made of cheap nonretentive materials.

2.10. Stability of Fractional-Horsepower Synchronous Motor Speed

Very often the requirement placed on fractional-horsepower synchronous motors used for high accuracy devices is stability of not only average, but also instantaneous rotor speed.

The average rotor speed ω_{2av} of synchronous motors at a known supply frequency is a constant quantity and equals to, or is a multiple of, the average speed of the rotating field ω_1. The instantaneous speed ω_2 may vary within one revolution relative to the average speed (Fig. 2.58*a*).

Since the rotor does not revolve uniformly, the angular position of the output shaft extension, α, at time t differs from the design value $\alpha_d = \omega_{2av}t$ (Fig. 2.58*b*). The angular error $\Delta\alpha$ is most dangerous when the motors operate in angular displacement transmission or conversion systems.

Variations in the instantaneous speed are sometimes called hunting of a synchronous motor rotor. To understand

Fig. 2.58. Fluctuations of instantaneous speed and angle of rotor turns as function of time

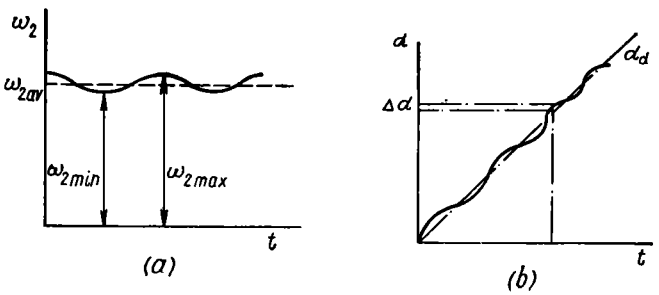

this process, let us see how a fractional-horsepower synchronous motor operates when its rotor revolves at a constant speed equal to the field speed ($\omega_{2av} = \omega_1$), with the static torque varying in steps (Fig. 2.59).

The electromagnetic synchronizing torque T_s of all the synchronous motors developed during synchronous running is a function of the angle between the stator flux axis and the rotor direct axis.

At a static torque $T_{st\,1}$ on the shaft, the rotor direct axis is offset in respect to that of the stator flux Φ_1 through a certain angle γ_1 at which the torque T_s developed by the motor is equal to the static torque ($T_s = T_{st\,1}$). If the static torque decreases ($T_{st\,2} < T_{st\,1}$), the motor running torque will exceed the static torque, the instantaneous speed of the rotor will rise ($+\Delta\omega_2$) and the rotor direct axis will approach the stator flux axis, that is, angle γ will become smaller. A new angular position of the rotor, γ_2, will correspond to the static torque $T_{st\,2}$ at which $T_s = T_{st\,2}$. Howe-

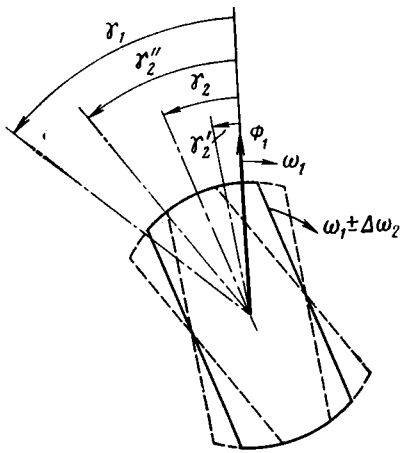

Fig. 2.59. Illustration of rotor hunting in synchronous motors

ver, the rotor will not assume position γ_2 at once and rather pass it by inertia, with the result that the rotor direct axis will approach the stator flux axis by an angle $\gamma_2' < \gamma_2$. With this, the motor torque will be lower than the static torque ($T_s < T_{st\,2}$). The instantaneous speed will start slightly decreasing ($-\Delta\omega_2$) and the angle γ will increase till γ_2'' becomes greater than γ_2. This means that the rotor will oscillate about angular position γ_2 for a certain period of time and its instantaneous speed will vary.

Generally speaking, there are three causes of unstable rotor speed of synchronous machines, *viz.*, (a) alternating electromagnetic forces in the motor, (b) alternating mechanical forces in the motor, (c) external factors.

Alternating electromagnetic forces are usually set up due to an elliptical rotating field, nonsinusoidal distribution of flux density over the air-gap circumference, and nonuniform permeance overdifferent axes of an actual motor.

An elliptical field may be caused by unbalanced supply voltage, connection of a capacitor in one of phases in the case of a single-phase supply, and unbalanced phase mmfs of the stator winding due to unequal resistances or turns

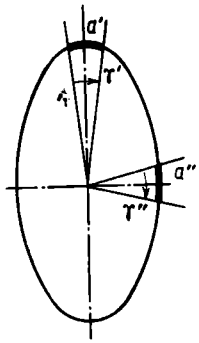

Fig. 2.60. Variations in instantaneous angular speed of elliptical field ($t' = t''$; $a' = a''$; $\gamma' < \gamma''$; $\omega_1' < \omega_1''$; $\omega_2' < \omega_1''$)

in phases. The linear speed of the field vector end being constant, the angular speed of the elliptical field and, hence, the instantaneous speed of the rotor within one revolution will be other than constant (Fig. 2.60).

Nonsinusoidal distribution of the flux density over the air-gap circumference may be the result of a nonsinusoidal law of distribution of mmf and saturation, nonuniform air gap (elliptical stator or rotor, runout, surface slots, etc.), or heterogeneous magnetic material. Upper space harmonics of the stator and rotor are set up in the air gap.

The upper harmonic fields rotate at a speed determined by the order of these harmonics. Synchronous torques are built up due to the interaction of the upper harmonics of the stator and rotor fields revolving at different speeds. The average value of these torques is zero and the instantaneous torques are pulsating in accordance with the sinusoidal law at a rate equal to the difference of the speeds of the interacting fields (as is the case with a synchronous machine pulling out of step). As a result, the instantaneous rotor speed fluctuates at a corresponding rate.

Teeth on the stator and rotor surfaces cause tooth reluctance torques because reluctance R_m on the path of the flux is a function of the angular position of the rotor in respect to the stator (Fig. 2.61).

Pulsations of the tooth reluctance torques cause corresponding fluctuations of the instantaneous speed of a running rotor.

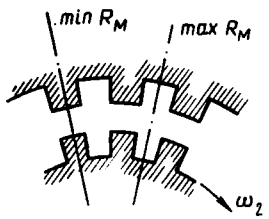

Fig. 2.61. Effect of stator and rotor teeth on reluctance

Alternating mechanical forces in the motor are caused by design, manufacturing, and operational factors. So, a poorly balanced rotor sets up alternating dynamic forces. Incorrectly fitted bearings on the shaft bring about local strains and drag torques. Temperature fluctuations cause nonuniform deformation of separate motor parts, rotor unbalance, etc.

The main *external factors* causing unstable rotation of the synchronous motor rotor are fluctuations of supply voltage and load, and deviation of supply voltage from the sinusoidal waveform.

Fluctuations in the amplitude of supply voltage cause a change in the stator flux and, as a consequence, a change in the torque developed by the motor. An equilibrium of the motor running and static torques is disturbed as the rotor starts hunting. The same occurs in the event of variations in the load torque on the motor shaft.

Any deviation of supply voltage from the sinusoidal waveform causes upper time harmonics in the rotating field. Their speed of rotation is other than that of the rotor, hence, pulsating torques result. These pulsating torques, like the torques built up due to upper space harmonics, disturb the stable rotation of the rotor.

A more stable rotation of fractional-horsepower synchronous motors can be attained in the following two ways:

(1) by improving the mechanical design and manufacturing technique of the motors so as to eliminate causes of variations in the instantaneous speed of the rotor;

(2) by using electronic circuits to stabilize the instantaneous speed.

The degree of stability of the synchronous motor rotation greatly depends on the value of specific synchronizing torque, characteristics of the squirrel-cage rotor (if such is incorporated), and the moment of inertia of the rotor.

The specific synchronizing torque T_{sp} of a fractional-horsepower synchronous motor is a torque per geometrical degree of the mismatch angle between the stator field and rotor axes at angle γ approaching zero:

$$T_{sp} = \left(\frac{\Delta T_s}{\Delta \gamma}\right)_{\gamma \approx 0} \tag{2.69}$$

Other conditions being the same, the specific torque T_{sp} is evidently greater at a lower amplitude of angular rotor os-

cillations $\Delta\gamma$, torque increments ΔT being equal (Fig. 2.62*a*; $T_{sp\,1} > T_{sp\,2}$).

A higher specific torque, for example, can be attained by using a greater number of pole pairs (Fig. 2.62*b*).

The squirrel-cage starting winding mounted on the rotor of an active or reluctance synchronous machine functions as an electric damper when the machine runs in step. Variations in the instantaneous speed of the rotor cause currents in the squirrel-cage winding that set up a damping induction torque as a result of their interaction with the field that has induced these currents. The rotor speed can be appreciably stabilized by a proper selection of the squirrel-cage winding characteristics.

The moment of inertia of the rotor and that of the load should be selected so as to provide for a resonance frequency of the motor shifted in respect to the frequency of most dangerous variable forces.

A quantitative estimate of the rotor speed stability can be made through the use of the so-called instability of instantaneous rotor speed that is the ratio of the maximum speed gradient to the average speed (see Fig. 2.58*a*):

$$N = \frac{\omega_{2\,max} - \omega_{2\,min}}{\omega_{2\,av}} \qquad (2.70)$$

Variations in angle γ and speed ω_2 generally take place without obeying the law of harmonics. For the fundamental harmonic of the rotor hunting the relation between the

Fig. 2.62. Angular characteristics of fractional-horsepower synchronous motors

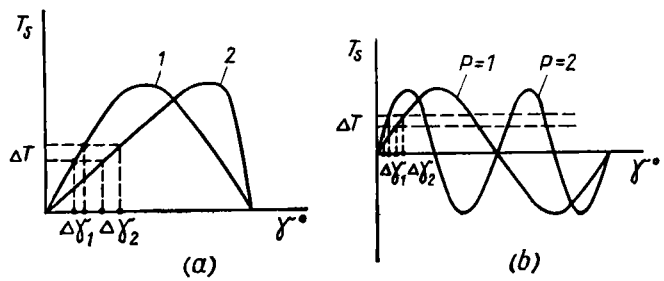

instantaneous speed instability and the amplitude of angular oscillations is described through a rather simple equation:

$$N = \frac{2\pi\gamma_{1\,max}}{21,600k} \qquad (2.71)$$

where γ_{1max} is amplitude of angular oscillations in angular minutes:

$$k = \tau_0/\tau_r$$

where τ_0 is the period of the fundamental harmonic of oscillations; τ_r is the period of the rotor revolution.

Active-type permanent-magnet synchronous motors with the rotor carrying a squirrel-cage winding have a minimum speed instability, because a high specific synchronizing torque is provided due to the internal field flux of the rotor, and the squirrel-cage winding, if properly selected for its characteristics, affords a strong damping action. Hysteresis synchronous motors have a greater speed instability as their rotor does not carry a squirrel-cage winding.

The instability of instantaneous rotor speed of reluctance synchronous motors is also higher than that of permanent-magnet motors in spite of the fact that their rotor carries a squirrel-cage winding. A high instantaneous speed instability of these motors is due to the effect of torques built up by upper space harmonics of the magnetic field and tooth reluctance torques brought in because of specific design features of their rotor.

Table 2.1 gives approximate values of rotor speed instability for different types of fractional-horsepower synchronous motors within the range of power ratings from several watts to tens of watts.

Table 2.1

Synchronous motor type	Instability $N\times10^{-3}$	Amplitude $\gamma_{1\,max}$, min
Permanent-magnet, with a squirrel-cage winding	0.2-0.8	3.5-30
Hysteresis	1.8-6	6-23
Reluctance, with a squirrel-cage winding	6-12	8-18

2.11. Continuous-Running Low-Speed Synchronous Motors

It is sometimes desired to run a fractional-horsepower synchronous motor of a standard frequency at low rotor speeds without the use of intermediate mechanical reduction units. Ideal synchronous motors discussed under Section 2.9 operated at a standard supply frequency of 50, 400, and 1,000 Hz develop a rotor speed as high as 1,000 r/min and higher still. Automatic-control systems and devices often require a speed as low as some revolutions or tens of revolutions per minute. A mechanical reduction unit with such a high gear ratio would complicate the fractional-horsepower drive system, reduce its general reliability, increase noise level, overall dimensions and mass. Moreover, fractional-horsepower motors with bearings rotating at a high speed would be unreliable under specific conditions, such as, in vacuum or at high temperatures.

Synchronous motors discussed in this Section are designed so that the rotor speed is not equal to but somewhat lower than the speed of the stator field. The speed ratio of such a motor, when running in synchronism, is independent of external factors, such as, load torque, voltage, etc. Such a reduction of speed is attained either due to inherent design features of synchronous machines (reducing motors and steromotors) or by designing a synchronous machine as a harmonious combination of an electrical machine and a reduction unit (harmonic-drive motors).

According to the excitation system, the low-speed synchronous motors are classified as two basic types:

(a) *inductor* motors with the rotor magnetized by a permanent flux on the stator side;

(b) *reluctance* motors with an underexcited rotor.

2.11.1. Reducing Motors

Reducing motors are synchronous machines in which the rotor speed is reduced electromagnetically in respect to the speed of the stator field fundamental. This is achieved by using upper tooth harmonics, and not the fundamental, as working harmonics which are amplified due to a specific

configuration of the stator and rotor surfaces. As is known, the pole number of the upper space harmonic field is proportional, and the speed is inversely proportional, to its order. Machines of this type are called reducing machines.

The mechanical design and the principle of operation of fractional-horsepower synchronous reducing motors can be understood from the analysis of a reluctance machine (Fig. 2.63).

The stator and the rotor are built up of electric steel stampings. The stator S is made in the form of a ring with semicircular slots on the inner surface; the rotor R is a disk provided with similar slots on the outer surface. The number of stator teeth Z_s and that of rotor teeth Z_r is different; usually, $Z_r > Z_s$. The stator slots accommodate a winding designed for three-phase or single-phase power supply. This winding sets up a rotating magnetic field Φ_s.

Fig. 2.63. General arrangement of synchronous reluctance-type reducing motors

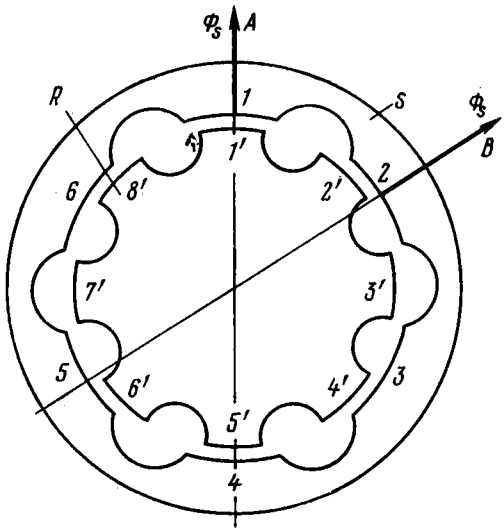

From Section 2.9 we know how the running torque is produced in reluctance motors. If the flux Φ_s is in position *A* at a given moment, the reluctance torque will force the rotor to turn in the direction of the highest permeance, that is, the rotor teeth *1'* and *5'* will be against the stator teeth *1* and *4*. As the flux Φ_s moves to position *B*, that is, turns through an angle of 360 deg/Z_s, the rotor will turn through the same angle under the action of the reluctance torque so as to afford maximum permeance again. This will be obtained after the rotor teeth *2'* and *6'* are settled against the stator teeth *2* and *5*, that is, after the rotor turns through the angle

$$\frac{360 \text{ deg}}{Z_s} - \frac{360 \text{ deg}}{Z_r}$$

Hence, the angular speed of the rotor, ω_2, will be lower than that of the stator field, ω_1,

$$\frac{360 \text{ deg}}{Z_s} \Big/ \left(\frac{360 \text{ deg}}{Z_s} - \frac{360 \text{ deg}}{Z_r} \right) = Z_r/(Z_r - Z_s) \text{ times}$$

It means that

$$\omega_2 = \frac{Z_r - Z_s}{Z_r} \omega_1 \tag{2.72}$$

where $\omega_1 = 2\pi (f/p_s)$; f is supply frequency; and p_s is number of stator winding pole pairs.

In our case (Fig. 2.63),

$$\omega_2 = \frac{8-6}{8} \omega_1 = \frac{1}{4} \omega_1$$

If we choose $Z_r = 100$ and $Z_s = 98$, then

$$\omega_2 = \frac{1}{50} \omega_1$$

It should be borne in mind that the number of teeth that can be arranged over the circumference of a definite diameter is limited by the minimum possible tooth thickness according to manufacturing considerations.

As is seen from equation (2.72), for a given value of Z_r the rotor speed will be lower at a smaller difference of $Z_r - Z_s$. The best reduction is attained at $Z_r - Z_s = 1$. In this case, however, only one rotor tooth can be accurately

positioned against one stator tooth, which would reduce permeance in the gap and impair the motor utilization factor. Therefore, to reduce the reluctance to a minimum, the difference $Z_r - Z_s$ must be chosen as an even number equal to $2p_s k$, where $k = 1, 2, 3, \ldots$.

Although simple in construction, the reluctance reducing motors have some drawbacks inherent in all the reluctance synchronous motors as compared to the active types, *viz.*, low efficiency, power factor, and power-to-mass ratio. Inductor-type reducing motors (Fig. 2.64) are better in these respects; their stator and rotor do not appreciably differ in construction from those of reluctance reducing motors, but the stator end carries an axially magnetized toroidal permanent magnet. The permanent magnetizing flux Φ_m closes through the rotor in the axial direction and through the air gap between the stator and rotor in the radial direction. It is a unipolar flux, that is, unidirectional over the entire rotor circumference, but the flux density B_m is different at different points in the air gap and depends on magnetic reluctance. Figure 2.65 shows how the flux density varies under the effect of at least one toothed surface (that of a stator or rotor). The result is the appearance of upper harmonics of the rotor field, which interact with the upper harmonics of the rotating stator field Φ_s causing a torque at a low rotor speed (as compared to ω_1).

The inductor-type synchronous reluctance motors perform equally well with an even and an uneven difference of

Fig. 2.64. General arrangement of inductor-type synchronous reducing motor

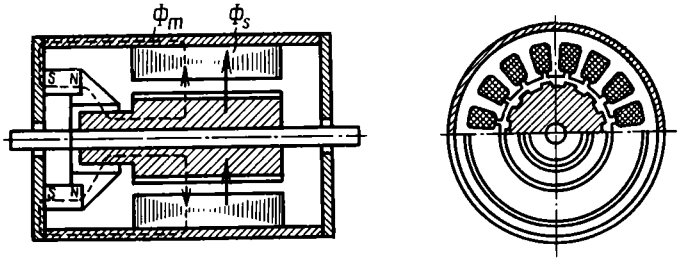

rotor and stator teeth, that is, we may select $Z_r - Z_s = p_s k$, where $k = 1, 2, 3, \ldots$. It means that these motors can afford twice as high speed reduction ratio for the same number of teeth and correspondingly the same rotor diameter as compared with the reluctance motors. The efficiency of such motors is lower than that of synchronous motors without speed reduction due to their performance on upper harmonics and not on the fundamental.

The angular hunting amplitude of the rotors of reducing motors is somewhat lower than that of the earlier-discussed continuous-running synchronous motors because they function as if multipole machines due to operation on upper space harmonics. At a rotor speed of 100 to 200 r/min the amplitude reaches 1-5 angular minutes. A great amount of upper harmonics, however, causes a high frequency of the rotor hunting. The hunting period-to-one revolution time ratio τ_h/τ_r decreases, with the result that the instantaneous rotor speed instability increases (equation 2.72, Section 2.10). The instability of reluctance reducing motors may reach $N = (40\text{-}80) \times 10^3$.

2.11.2. Steromotors

The rotor speed in synchronous steromotors is reduced in respect to the stator field speed due to an eccentric arrangement of the rotor in the stator bore, which makes it free to move along the stator circumference. The main internal torque is set up due to a unilateral magnetic pull between the rotor and the stator afforded by the asymmetric rotating field.

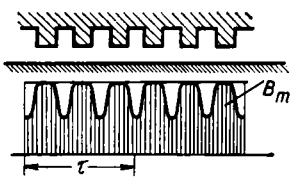

Fig. 2.65. Effect of stator or rotor teeth on flux density

The construction of actual steromotors greatly depends on the method by which an asymmetric field is obtained, on the arrangement of the rolling surfaces, and the mechanical design of the drive gear used for the eccentric rotor.

Figure 2.66 illustrates the general arrangement of an inductor-type steromotor. The frame *1* accommodates a stator core *2*, permanent magnets *4*, and stator tracks *9*. The stator is similar in design to that of an ideal synchronous machine, and its windings *3* function to set up a symmetric rotating flux Φ_s. The permanent magnets are radially magnetized and afford a unipolar magnetizing flux Φ_m. Sometimes, a d.c. winding is used for the purpose. The stator tracks have a smooth or a toothed surface.

The rotor is mounted on a hollow bush *7*, which serves at the same time as a magnetic circuit for the magnetizing flux. The main core *5* of the rotor, built up of electric steel laminations, is unwound. Toroidal cores *6* stacked up of electric steel laminations reduce magnetic reluctance on the path of the magnetizing flux. Rotor wheels *8* have a smooth or a toothed surface. Their outer diameter is made somewhat greater than the rotor diameter. This is necessary to prevent direct contact between the rotor and stator surfaces and premature wear. The hollow bush accommodates a drive mechanism of any suitable type for transmitting the eccentric rotation of the rotor.

Fig. 2.66. General arrangement of inductor-type synchronous steromotor

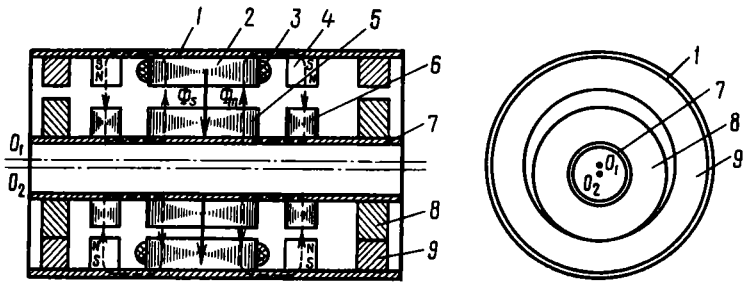

When the wheels run on the tracks, the stator axis A_1 is not aligned with the rotor axis A_2, that is, the axes are eccentric.

The unipolar magnetizing flux Φ_m in the air gap between the stator and rotor is superimposed on the rotating flux Φ_s that is distributed along the circumference following a law approaching that of sine waves (Fig. 2.67). The resultant rotating field Φ_δ in the air gap becomes asymmetric.

The electromagnetic pull acting on the rotor surface element can be found from the Maxwell equation

$$f_{em} = \frac{B_n^2}{2\mu_0} \tag{2.73}$$

where B_n is flux density vector component normal to the rotor surface; and μ_0 is air gap permeability.

Hence, the resultant magnetic pull between the rotor and stator acts along the wave maximum of flux density B_δ (Fig. 2.67), that is, along the axis of resultant rotating field Φ_δ.

How a synchronous steromotor operates can be best understood from the model illustrated by Fig. 2.68. A ferromagnetic rotor having a diameter D_2 is eccentrically mounted

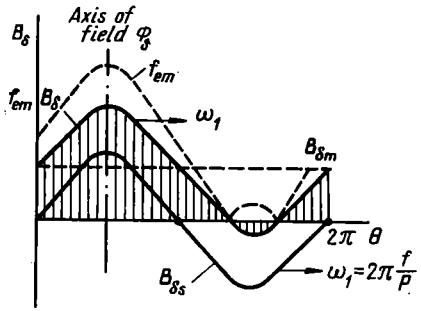

Fig. 2.67. Air-gap flux density distribution for the stator field ($B_{\delta s}$), magnetizing field ($B_{\delta m}$), and resultant field (B_δ)

in a stator bore D_1. In the qualitative analysis assume that the axes of the stator mmf F_s, stator flux Φ_s, and resultant flux Φ_δ are aligned. Let the coordinate axis intersecting the stator centre O_1 and the minimum-gap point be a direct axis d and that normal to the direct axis, a quadrature axis q.

In the original position (Fig. 2.68*a*), the axis of the flux Φ_δ intersects point A where the stator comes in contact with the rotor. The magnetic pull F_{em} between the stator and rotor acts along axis d, the component along axis q is zero, and the rotor is in equilibrium state.

As soon as the flux Φ_δ (Fig. 2.68*b*) is set off the contacting point A, the component along the axis q starts acting. The force F_q causes an internal torque

$$T_{in2} = 0.5 F_q D_2 \tag{2.74}$$

relative to point A as a torque relative to the instantaneous centre of rotation.

The rotor actuated by the torque T_{in2} moves along the stator surface till the point of its contact with the stator is displaced to A' and its centre O_2 is positioned on the axis of flux Φ_δ.

As the field completes the revolution $\alpha_1 = 2\pi$ (Fig. 2.68*c*), the rotor point coming in contact with the original point A_r on the stator will be displaced from original point A_r

Fig. 2.68. Principle of operation of synchronous steromotor

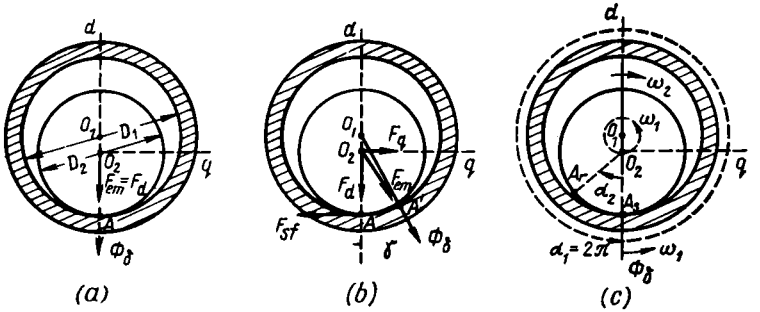

by a value corresponding to the difference between the circles described by the stator and rotor ($\pi D_1 = \pi D_2$). So, the rotor will turn about its centre O_2 against the direction of the field through an angle

$$\alpha_2 = 2\pi \frac{D_1 - D_2}{D_2} = \alpha_1 \frac{D_1 - D_2}{D_2} \tag{2.75}$$

With the field rotating continuously at synchronous speed ω_1, the rotor point contacting the stator revolves in step and unidirectionally with the field along with the rotor centre O_2 relative to the stator centre O_1. As follows from equation (2.75) the rotor revolves about its axis O_2 against the field with a speed

$$\omega_2 = \omega_1 \frac{D_1 - D_2}{D_2} \tag{2.76}$$

which is the output speed of the motor. If the stator bore and the rotor diameter are almost equal,

$$\frac{D_1 - D_2}{D_2} \ll 1 \text{ and } \omega_2 \ll \omega_1$$

that is, the motor speed is greatly reduced.

The reduction ratio of motors now in use is as high as 1,500.

In an actual motor, as has been already mentioned, the rotor proper does not move over the stator, but its wheels run on the stator tracks. Therefore, equation (2.76) must be written as follows:

$$\omega_2 = \omega_1 \frac{D_t - D_w}{D_w} \tag{2.77}$$

where D_t and D_w are, respectively, diameters of circles described by the tracks and wheels.

To determine the torque delivered by the motor to its shaft, find from equation (2.74)

$$F_q = \int_0^{2\pi} f_q \, ds \tag{2.78}$$

where f_q is projection of the pull f_{em} (2.73) onto axis q; and ds is rotor active surface element.

For the motor construction under discussion, the torque equation can be written in the following general form:

$$T_{in2} = k_e \Phi_m \Phi_s \sin \gamma \qquad (2.79)$$

where k_e is factor depending on design parameters and amount of eccentricity; in the absence of eccentricity $k_e = 0$; and γ is angle between the axis of the flux Φ_s and the rotor direct axis d.

As can be understood from the above-mentioned, the torque T_{in2} is zero in the absence of either the magnetizing flux Φ_m (the rotating field is symmetrical) or eccentricity of the rotor and stator.

The internal torque of synchronous steromotors of another design may have a reluctance component, in addition to the active component (2.79), that obeys the $\sin 2\gamma$ law.

As in the case of all the synchronous motors, the rotor will keep running at the same speed upon an increase in the static torque T_{st}, but the contacting point will lag behind the field axis by a greater angle. If the torque T_{st} exceeds the maximum of T_{in2}, the rotor will pull out of step.

One more case of pulling out of step may occur with steromotors having smooth wheels and tracks. The relationship between the speeds (2.77) is valid for the case of rolling without slipping. If the tracks and wheels have toothed surfaces, slipping is impossible. With a smooth surface there is no slipping when

$$F_q \leqslant F_{sf} \qquad (2.80)$$

where F_{sf} is slipping friction force at the contacting point (Fig. 2.68*b*).

Hence, when the static torque T_{st} is so high that the force F_q greater than F_{sf} is required to build up a torque $T_{in2} = T_{st}$, that is, the condition of equation (2.80) is not satisfied, the wheels start slipping on the tracks and the motor runs as an induction machine:

$$\omega_2 < \omega_1 \frac{D_t - D_w}{D_w}$$

The steromotors have good dynamic characteristics: on a frequency $f = 50$ Hz, the starting time is about 0.01 s, the reversal time is 0.015 to 0.025 s since the electromecha-

nical time constant of the motor proportional to the moment of inertia and speed of rotating parts is very small. This is because the rotor revolves about its centre at a very low speed ω_2. The rotor centre revolves about the stator centre at a high speed ω_1, but at a small eccentricity the rotation radius and consequently the moment of inertia are negligible.

Stopping the motor by switching off the stator a.c. supply causes rotor self-locking due to a heavy pull to the stator afforded by the magnetizing field at the contacting point.

Along with many advantages, the steromotors have a number of drawbacks. Hypocyclic rotation of the rotor results in a complex construction of the motor as a whole and of the drive mechanism in particular. Centrifugal forces due to the rotation of the rotor centre about the stator centre cause vibrations, noise, and instability of the instantaneous rotor speed.

2.11.3. Harmonic-Drive Motors

The fractional-horsepower synchronous harmonic-drive motors are, essentially, a combination of an electrical machine and a harmonic gear drive. These motors are distinguished by unique construction. The rotor is a flexible structure deforming in the radial direction that carries on its surface the toothed rim of a harmonic drive.

The electrical machine proper develops a torque and functions as an electromagnetic generator of mechanical waves of deformation for the harmonic drive.

As an example, we shall take a reluctance machine to study the mechanical design of a synchronous harmonic-drive motor.

Figure 2.69 illustrates the general arrangement of a synchronous harmonic-drive reluctance motor in which magnetic flux closes radially and axially. The frame *1* accommodates U-shaped ferromagnetic stator cores *2*. The cores carry concentrated coils *3* that make up a two-phase or three-phase winding used to afford a rotating field in the air gap. The fixed toothed rim *8* of the harmonic drive is secured on the inner surface of the stator. The rotor *4* is a thin-walled metallic or plastic flexible sleeve mounted on the

output shaft *9*. The outer surface of the rotor carries a flexible toothed rim *7* of the harmonic drive. The internal magnetic circuit consists of separate ferromagnetic blocks *5* that are free to move radially, thereby deforming the rotor. They are held tight against the inner surface of the rotor by means of flexible centering rings *6*.

Applying a.c. voltage to the stator windings causes a magnetic field Φ_s in the air gap, which rotates at a speed $\omega_1 = 2\pi \frac{f}{p}$. The fundamental of the flux density $B_{\delta s}$ of this field for a winding pole pair $p = 1$ is shown by Fig. 2.70*a*. The internal magnetic circuit blocks suffer in the field the action of magnetic pull to the stator. The waveform of this electromagnetic pull f_{em} plotted with regard to Eq. (2.79) is also illustrated by Fig. 2.70*a*. The blocks move in the radial direction and deform the rotor and, hence, the flexible toothed rim of the harmonic drive (Fig. 2.71). The teeth of the flexible rim come in mesh with those of the fixed rim mounted in the stator. The number of mechanical deformation waves v in reluctance motor rotors equals the number of poles ($v = 2p$).

The mechanical deformation waves rotate synchronously with the field at a speed ω_1 and the flexible rim moves over

Fig. 2.69. General arrangement of harmonic-drive synchronous reluctance motor with the flux closed radially and axially

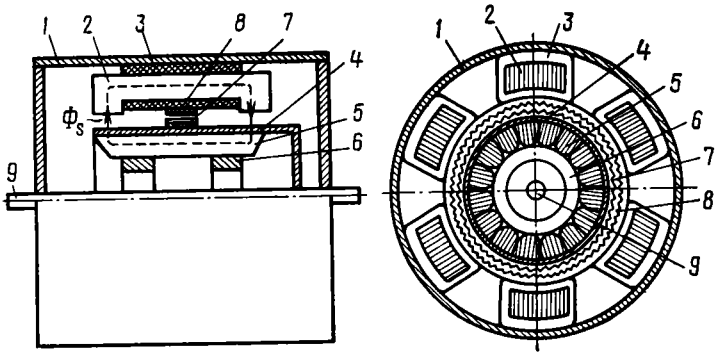

the fixed rim. The harmonic drive affords reduction of speed so that the flexible rim, together with the rotor, slowly rotates about its axis in the direction opposing that of the field at a constant speed

$$\omega_2 = \omega_1 / i_{hd} \tag{2.81}$$

where $i_{hd} = Z_{fl}/(Z_{fix} - Z_{fl})$ is the reduction ratio of the harmonic drive; Z_{fix} and Z_{fl} is number of teeth of the fixed and the flexible rim, respectively, with Z_{fix} being greater than Z_{fl}.

Rotor deformation (Fig. 2.71) causes unequal air gaps along the direct (d) and quadrature (q) axes, with the result that magnetic reluctances and inductive reactances along these axes become also unequal ($R_{md} \neq R_{mq}$ and $X_d \neq X_q$, respectively). As is known from the discussion under Section 2.9, such conditions cause a reluctance torque in the motor. Disregarding the stator winding resistance, the reluctance torque equation takes the form

$$T_r = T_{r\,max} \sin 2\theta_0 \tag{2.82}$$

Fig. 2.70. Distribution of flux density and air-gap pull along the rotor circumference of harmonic-drive motor

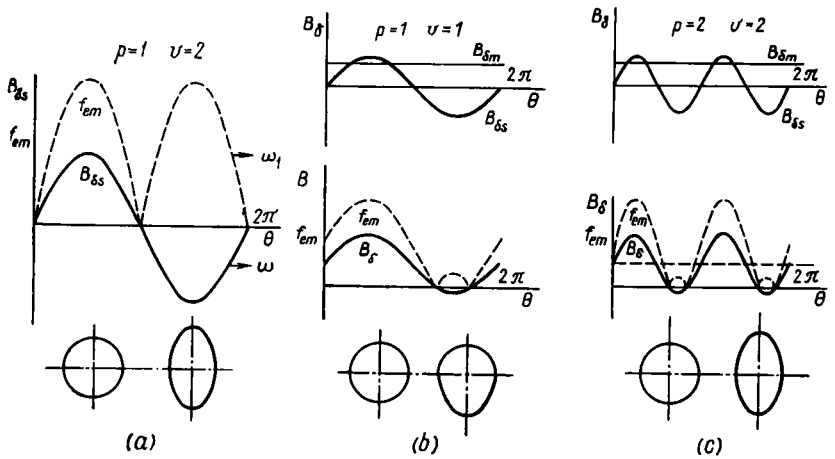

where θ_v is the angle between the axis of the spatial voltage wave of the stator and the quadrature axis q of the deformed rotor. This angle corresponds to that given in equation (2.67*a*).

The angle θ_v depends on static torque, as is the case with all the synchronous motors.

The reluctance torque equation that allows for the stator winding resistance agrees with equation (2.67*b*).

As follows from equation (2.67*a*), the maximum reluctance torque $T_{r\,max}$ is proportional to the difference of inductive reactances X_d and X_q. In a harmonic-drive motor this difference depends on the amount of rotor deformation

$$X_d - X_q = f(a/\delta) \tag{2.83}$$

where a is maximum radial deformation; and δ is average air gap.

In a harmonic drive the torque is reduced (or increased) so that the motor shaft torque

$$T_2 = T_r i_{hd} \eta_{hd} \tag{2.84}$$

where η_{hd} is efficiency of harmonic drive and bearings.

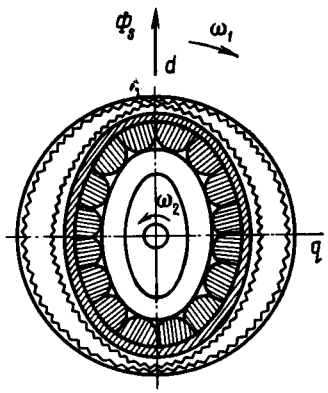

Fig. 2.71. Deformation of harmonic-drive motor rotor

An inductor-type harmonic-drive motor can be built using the same general arrangement as that of a reluctance motor (Fig. 2.69), the only difference being that cores *2* must carry in addition d.c. windings to set up a unipolar magnetizing flux. The inductor-type harmonic-drive motors develop a higher torque than the reluctance motors due to the interaction between the rotating and magnetizing fields. They have higher efficiency and power factor. As distinct from the reluctance motors, the number of waves of deformation in them equals the number of pole pairs ($v = p$). This fact is illustrated by the flux density and magnetic pull curves of Fig. 2.70*b*, *c*. Therefore, the inductor-type harmonic-drive motors must have $p \geqslant 2$ so as to keep them dynamically balanced.

Figure 2.72 shows the general arrangement of a synchronous harmonic-drive reluctance motor with the flux closed radially. The stator is of an ideal construction as far as

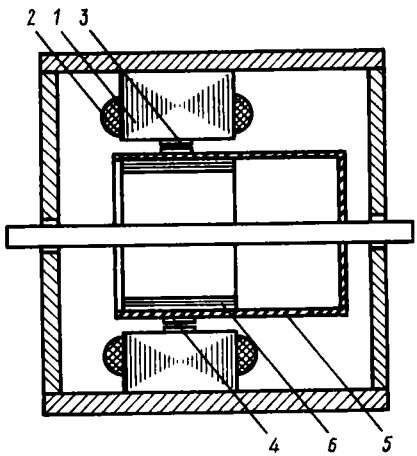

Fig. 2.72. General arrangement of reluctance-type synchronous harmonic-drive motor with flux closed radially

a.c. machines are concerned. It consists of a laminated cylindrical core *1* carrying a multiphase winding *2* which produces a rotating magnetic field Φ_s. The fixed toothed rim *3* is located on the stator surface. The flexible toothed rim *4* is mounted on the surface of a flexible deforming rotor *5*. The internal magnetic circuit *6* is a resilient elastic ring wound of permalloy ribbon. It functions to close the magnetic flux along the rotor circumference and to make the rotor deform under the action of magnetic pull to the stator.

The harmonic-drive motors are noted for good dynamic characteristics. The starting time at a rated frequency $f = 50$ Hz is as short as 3 or 4 ms. The rotor has a rather low inertia and revolves with a low speed. The motor response primarily depends on the kinetic energy of the deforming-rotor masses moving in the radial direction rather than on the rotational kinetic energy of the rotor. It means that the starting time is actually determined by the time of rotor deformation up to the moment of engagement of the harmonic drive toothed rims. The wave of deformation disappears equally fast upon the disconnection of supply voltage so that the rotor stops immediately and practically without rundown. Rotating masses of motors, where waves of deformation $v \geqslant 2$, are dynamically balanced, so the vibration level is much lower than that of steromotors.

These motors, however, are complex in design and difficult to manufacture, the main difficulty being to make the rotor sufficiently flexible. Another disadvantage of harmonic-drive motors consists in that they have rather low efficiency, power factor, and power-to-mass ratio. This concerns in particular reluctance motors as they have large nonmagnetic gaps on the path of the magnetic flux and a unique construction of the external and internal magnetic circuits.

Since all the above-discussed fractional-horsepower motors do not employ high-speed rotating parts and bearings, the units as such are remarkably trouble-free. For example, the guaranteed service life of reducing synchronous motors (type ДСР) is three or four times as long as that of synchronous motors with a mechanical reduction unit (series ДСД) providing the same speed of the output shaft.

The efficiency and power-to-mass ratio of motors under discussion greatly depend on the effective gear ratio and

go down with its increase. For example, the output power and efficiency of steromotors of the same size, running at the same frequency (f = 50 Hz, field velocity 3,000 r/min), vary from about 0.4 to 22 W and from 0.7 to 33 per cent, respectively, as the rotor speed changes from 2 to 200 r/min. The efficiency of inductor-type reducing synchronous motors rated at about 1 W with a frequency f = 50 Hz and gear ratio 10 to 30 is 5 to 8 per cent.

The power factor of inductor-type motors is as high as 0.7 to 0.85 and may reach 0.95 when a capacitor circuit arrangement is used.

Low speed, high torque, and excellent dynamic properties make the harmonic-drive motors and steromotors most suitable for use in miscellaneous precision mechanisms (verniers of duplicating machines, clock mechanisms, etc.) and also in electromechanical remote-control keying systems (vacuum and radiation sets, etc.).

2.12. Stepper Motors

Increasing requirements of digital computing technology have necessitated the development and modification of stepped-control servo elements, in particular, special-purpose fractional-horsepower electrical machines, the so-called stepper motors.

Stepper motors are fractional-horsepower synchronous motors whose normal operation consists in converting a command preset in the form of pulses into discrete angular motions of a shaft or into discrete motions without feedback transmitters.

Used as stepper motors are fractional-horsepower motors whose rotor has at least two stable angular positions within one revolution.

Stepper motors operate in conjunction with electronic switching devices. The switching device functions to switch over the stepper motor control windings with a frequency and sequence corresponding to the command issued.

A stepper motor and switching device assembly is essentially a synchronous-motor speed control system distinguished by a step-by-step supply of windings with rectangular voltage pulses and a discrete angular motion of the

rotor. The resultant angle of turn of the stepper motor rotor strictly follows the number of switchings of the control windings, the sense of rotation depends on the switching sequence, and the rotor speed varies according to the rate of switchings.

Stepper motors, like all the synchronous machines, are classified as *permanent-magnet* (*active-type*), *reluctance*, and *inductor-type machines.*

Stepper motors may be wound as machines of any number of phases, most popular being two-, three-, and four-phase stepper motors. The stator phase winding either functions as a nonsplit control winding or is split (centre-tapped) into two windings whose magnetic axes are spaced 180 deg. apart.

The control winding of a stepper motor is supplied with unipolar or heteropolar rectangular pulse trains delivered from the switching device.

2.12.1. Active-Type Motors

As distinct from continuous-running synchronous motors, the stator of stepped motors has salient poles carrying control windings. The number of pole pairs p of each control winding equals that of the rotor. The most popular stepper motors of the active type are permanent-magnet motors whose rotor is made in the form of a permanent-magnet spider cast integral or assembled of a number of permanent magnets (Fig. 2.73).

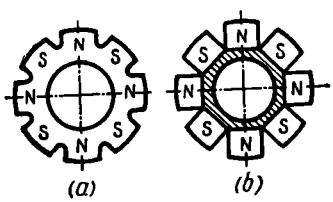

Fig. 2.73. Constructions of permanent-magnet stepper motor rotors
(*a*) cast integral; (*b*) assembled of separate magnets

The operating principle of such a stepper motor can be understood by studying the operation of a two-phase double-pole motor illustrated in Fig. 2.74. Assume that the mmfs and fluxes both in the rotor and in the stator are unidirectional. Each control pulse applied to the switching device input causes a stepped variation of the magnitude and polarity of voltage fed to the control windings *A* and *B*. The magnetic flux Φ_s due to the control windings moves over the stator circumference through a certain angle. The synchronizing torque produced in the action tends to turn the rotor to a position in which the mutual attraction between the stator and rotor magnetic fields is greatest. The rotor makes a step, that is, turns through a certain angle equal to the stator flux vector step (positions *a*, *b*, *c* on Fig. 2.74).

The separate-and-joint sequence of the control windings illustrated by Fig. 2.74 concerns asymmetric switching systems because odd and even steps correspond to energization of a different number of windings and to a different magnitude of the resultant stator flux.

The switching system is referred to as symmetric if an equal number of control windings is energized at all the steps (in one, two, three windings, etc.). As can be understood from Fig. 2.74, the step is twice as large with symmetric switching whilst the resultant stator flux at all the steps is the same.

The number of steps of the resultant stator flux and the number of increments by which the rotor is stepped through

Fig. 2.74. Operating principle of a stepper motor

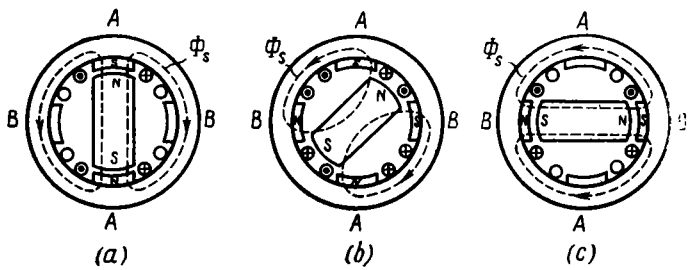

360 electrical degrees are generally proportional to the number of control windings, m_{cont}, and depend on the switching circuit arrangement.

Figure 2.75 shows circuit diagram of control windings, time diagram of voltage pulses across the windings, and space diagram of positions occupied by the resultant stator flux Φ_s for the following types of switching circuits:

(a) heteropolar symmetric switching circuit of a stepper motor with a two-phase nonsplit stator winding ($m_{cont} = 2$);

(b) unipolar symmetric switching circuit of a stepper motor with a two-phase split stator winding ($m_{cont} = 4$).

From the comparison of these two types it becomes evident that heteropolar switching used for motors with nonsplit-phase stator windings produces the same effect on the increment as splitting of the phase winding, that is, doubling the number of control windings, with unipolar switching (Table 2.2).

Fig. 2.75. Switching charts and diagrams of a stepper motor

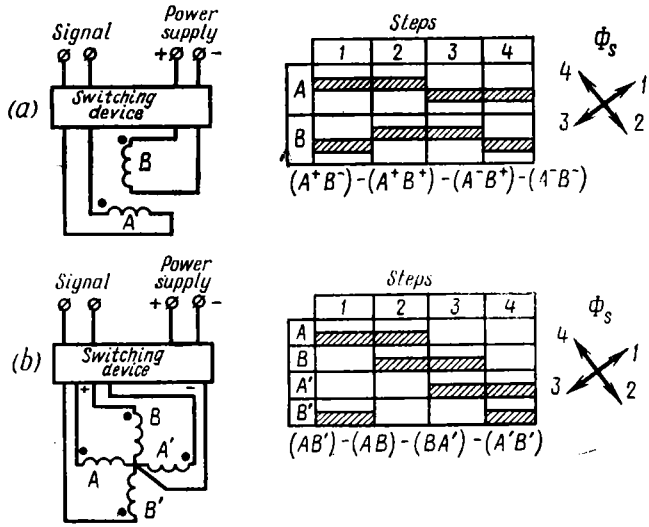

Table 2.2

Number of control windings, m_{cont}	2	3	4	5	6	7	8
Positions of stator flux vector within 360 electrical degrees in the case of unipolar switching	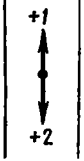		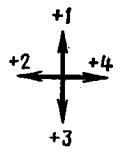	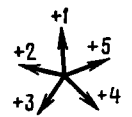	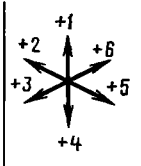	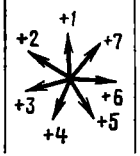	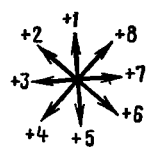
Number of control windings m_{cont}	1	—	2	—	3	—	4
Positions of stator flux vector within 360 electrical degrees in the case of heteropolar switching	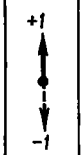		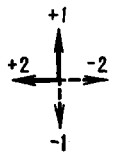		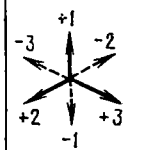		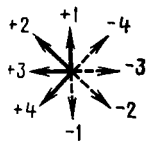
Number of switching steps k_{step}	2	3	4	5	6	7	8

Let the number of the switch states ensuring a new angular position of the resultant stator flux within 360 electrical degrees be step number k_{step} of the control circuit. It follows from the above discussion that the step number of a control circuit

$$k_{step} = m_{cont}\, n_1\, n_2 \tag{2.85}$$

where n_1 is a factor equal to 1 for a symmetric switching circuit and to 2 for an asymmetric switching circuit; n_2 is a factor equal to 1 for unipolar switching and to 2 for heteropolar switching.

The use of heteropolar switching for motors with split-phase stator windings is not reasonable.

In most control circuits the vector of Φ_s follows all the possible k_{step} numbers within one revolution (in electrical degrees), the rotor increment being (in electrical degrees)

$$\gamma_{el.inc} = \frac{360 \text{ deg}}{k_{step}} \tag{2.86}$$

Actual stepper motors are multipole machines ($p > 1$) and the mechanical step angle or increment, that is, the angle of turn of the rotor per switching step

$$\gamma_{inc} = \frac{\gamma_{el.inc}}{p} = \frac{360 \text{ deg}}{k_{step}\, p} \tag{2.87}$$

The number of pole pairs in actual stepper motors is usually kept within $p = 4$ to 6, for a greater number is limited by the rotor diameter and by interpole flux leakage. The number of control windings is usually $m_{cont} = 2$ to 4, for a greater number of these windings will require a more complicated switching device. Therefore, the rotor of active-type stepper motors steps in increments γ_{inc} of about ten degrees.

2.12.2. Reluctance and Inductor-Type Motors

The rotor increment in reluctance and inductor-type stepper motors is reduced by using the principle of electromagnetic speed reduction discussed under Section 2.11.

The following discussion and the illustration of Fig. 2.76 are concerned with the mechanical design and operating

principle of a three-phase reluctance stepper motor. The stator and the rotor are stacked of electric steel stampings. The rotor and the stator pole shoes have a toothed surface. The tooth pitch is equal for the stator and the rotor. The rotor teeth are aligned with the teeth of one pair of diametrically opposite pole shoes on the stator and are displaced one third the tooth pitch in respect to the other two pairs of pole shoes in the clockwise and the counter-clockwise direction, respectively. With the control windings receiving unipolar supply in sequence, the stator magnetic flux turns through 120 deg., and the synchronizing reluctance torque forces the rotor to turn through one third the tooth pitch towards the position of minimum reluctance in respect to the energized pole pair. If the number of rotor teeth, Z_r, is great, its angle of turn will be much smaller than that of the stator field.

The stator and rotor tooth axes are generally displaced by an angle of 360 deg/$m_{cont}Z_r$. Within a full switching

Fig. 2.76. General arrangement of a reducing reluctance-type stepper motor

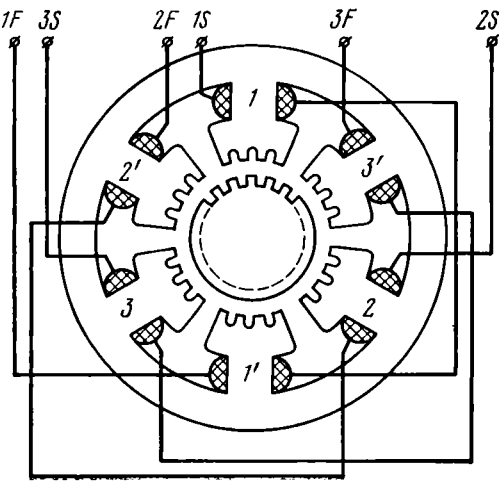

cycle the rotor will swing through one tooth pitch 360 deg/Z_r, and the increment will be found from the equation

$$\gamma_{inc} = \frac{360 \text{ deg}}{k_{step} Z_r} \tag{2.88}$$

It should be borne in mind that with a reluctance motor displacement of the field by 180 electrical degrees will not produce any effect on the state of the rotor, so in calculating the step number k_{step} from equation (2.85) the n_2 factor must be taken as unity both for unipolar and heteropolar switching.

In a reluctance stepper motor the full variation cycle of the reluctance and the magnetic field in the air gap corresponds to the rotor turn through one tooth pitch relative to the stator. It means that the rotor tooth and slot are equivalent to the pole pair and occupy 360 electrical degrees, that is, $Z_r = p$, and the rotor increment can be determined in electrical degrees from equation (2.86).

Comparison of equations (2.87) and (2.88) shows that for the same number of pole shoes the rotor increment of a reluctance stepper motor is half as large as that of an active-type motor. Besides, for the same rotor diameter, a much greater number of teeth can be made on a reluctance motor rotor than the number of poles on a permanent-magnet rotor. That is why, the rotor of reluctance stepper motors can be designed to step in increments as small as some degrees and even fractions of a degree.

Inductor-type stepper motors differ from the above-discussed reluctance motors in that they use a permanent stator flux for magnetizing the rotor, just as is the case with inductor-type reducing synchronous motors. With such an arrangement, the synchronizing torque is raised to a certain extent and the power and dynamic characteristics are improved.

Along with stepper motors discussed herein, harmonic-drive stepper motors, steromotors, disk-rotor, and printed-winding stepper motors are coming into use with a view of decreasing the rotor step or increment and improving the dynamic characteristics. There are also linear stepper motors that function to convert a command issued in the form of pulses into a linear motion.

2.12.3. Operating Conditions and Characteristics of Stepper Motors

A stepper motor is said to operate steadily when its rotor steps in all the stable positions corresponding to those of the resultant stator mmf vector for each step of the mmf vector.

The operating conditions of stepper motors are primarily classified according to the rate of control pulses, f.

Static condition ($f = 0$). The control windings carry direct current and set up a stationary magnetic field. Under this condition the static synchronizing torque T_s varies as a function of mismatch angle γ_{el} (electrical degrees) between the direct axis of the rotor and the axis of the stator mmf (Fig. 2.77, solid line). The rotor direct axis of a permanent-magnet stepper motor coincides with the direction of the rotor flux, and that of a reluctance or an inductor motor coincides with the direction of the lowest reluctance. As is known from the theory of fractional-horsepower synchronous motors (Section 2.9), the synchronizing torque is a periodic function of the mismatch angle $T_s = f(\gamma_{el})$. The synchronizing torque fundamental

$$T_s = T_{s\,max} \sin \gamma_{el} = T_{s\,max} \sin (\theta_{1\,el} - \theta_{2\,el}) \qquad (2.89)$$

Fig. 2.77. Angular characteristics of a stepper motor with symmetric teeth

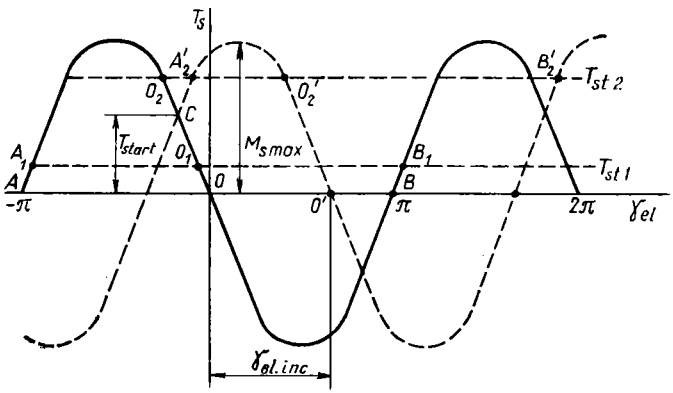

where $T_{s\,max}$ is maximum synchronizing torque; $\theta_{1\,el}$, $\theta_{2\,el}$ are angles of turn of stator mmf and rotor axes in electrical degrees, respectively.

The static stability region, γ_{ss}, is about the stable equilibrium point on the angular characteristic, from any point of which the rotor will return to the original point of stable equilibrium upon the removal of a disturbance action. At a static torque $T_{st} = 0$ the stable equilibrium point is at O and unstable equilibrium points are at A and B, that is, the stable equilibrium region AOB is symmetrical:

$$\gamma_{ss} = (-\pi) \text{ to } (+\pi)$$

At a torque $T_{st} \neq 0$, the stable equilibrium region becomes asymmetrical, as $A_1O_1B_1$ at $T_{st\,1} > 0$.

The maximum static torque T_{start} at which a stepper motor may start in the desired direction, that is, stepping angle generation, is determined by point C where the original angular characteristic intersects the characteristic shifted through one step (dash line on Fig. 2.77):

$$T_{start} = T_{s\,max} \cos \frac{\pi}{k_{step}} (k_{step} \geqslant 2) \qquad (2.90)$$

When $T_{st} = T_{st\,2} > T_{start}$, the rotor (point O_2), at the stator field step, will be carried past the new static stability region $A_2'O_2'B_2'$ and the motor will not start. The stepping angle will be generated from standstill on condition that

$$\gamma_{stab} > \gamma_{unstab} + \gamma_{el.inc} \qquad (2.91)$$

where γ_{stab} and γ_{unstab} are, respectively, positions of stable and unstable equilibrium points on the original angular characteristic.

As is seen from equation (2.90), $T_{start} = 0$, at $k_{step} = 2$. Hence, the minimum number of switching steps required to ensure starting conditions (at $T_{st} = 0$) is $k_{step} > 2$, that is, an active-type stepper motor, where heteropolar switching is possible, must have at least two control windings, while reluctance and inductor stepper motors must have at least three control windings. This is a characteristic feature of all synchronous motors where $T_s = 0$ at $\gamma_{el} = 180$ and 360 deg.

Stepper motors can be made as single-phase machines with $k_{step} = 2$. The reluctance stepper motors of this type have their stator and rotor made with asymmetric teeth (Fig. 2.78*a*). The angular characteristic of such a stepper motor has half-waves of different shapes (Fig. 2.78*b*) as a result of changes in magnetic reluctance over the air gap of the machine. Now we see that $T_{min} \neq 0$ at $\gamma_{el.\,inc} = \pm\pi$.

The static error of a stepper motor, that is, the mismatch between the angles of turn of the rotor and the stator mmf under static conditions (position of point O_1 on Fig. 2.77) depends on the magnitude and sign of the static torque and on the steepness of the original section of the angular characteristic, that is, on the specific torque.

Single-step angle generation condition. This condition corresponds to a rate of control pulses at which transients, more often of oscillatory nature, occurring at each step cease by the beginning of the next step, that is, the angular velocity $\dot{\theta}_2$ of the rotor is zero at the beginning of each step (Fig. 2.79).

By the instant of time t_γ the rotor has made one step, but it continues to move at a maximum speed $\dot{\theta}_{2\,max}$ and possesses a kinetic energy large enough to keep swinging against the field forces. As a result, the rotor starts hunting about a stable equilibrium point, just as is the case with

Fig. 2.78. Angular characteristics of a reluctance stepper motor with asymmetric teeth

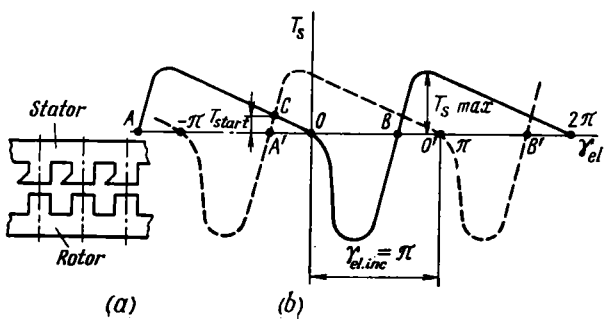

all the fractional-horsepower synchronous motors (see Section 2.10). Oscillations decay as soon as all the kinetic energy is wasted on electric, magnetic, windage and friction losses caused by this process. The greater these losses, the lower is the amplitude and the shorter the decay time of these oscillations.

The main factors determining the single-step angle generation condition are as follows:

(a) transient overshoot, $\Delta\theta_{to}$, that is, maximum deviation of the rotor from the new stable equilibrium position at transients;

(b) maximum instantaneous speed of the rotor, $\dot{\theta}_{2max}$, as it makes a step;

(c) rotor oscillation decay time per step, t_{decay}.

It will be good practice to minimize $\Delta\theta_{to}$ and t_{decay} of stepper motors at the same time keeping the instantaneous rotor speed $\dot{\theta}_2$ within the desired limits.

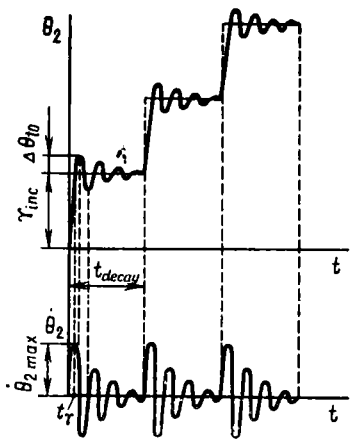

Fig. 2.79. Single-step angle generation condition for stepper motor

The average speed (rad/s) of a stepper motor rotor is to be found from the equation

$$\omega_2 = \frac{\pi}{180} f \gamma_{tne} \tag{2.92}$$

Steady state condition of a stepper motor corresponds to a constant rate of control pulses at t_{decay} exceeding the time of one switching step.

Under a steady state condition the rotor motion with a certain average speed ω_2 is accompanied by forced oscillations about an instantaneous point of stable equilibrium. The amplitude of these oscillations reaches its maximum at a rate of control pulses equal to the resonance frequency which is the inherent frequency of the rotor.

For a range of frequencies within which electromagnetic transients occur at a much higher rate than mechanical transients, the rotor motion of an unloaded stepper motor can be mathematically expressed through the torque equilibrium equation

$$T_s = T_{dyn} + T_{damp} \pm T_f \tag{2.93}$$

where T_{dyn} is dynamic torque; T_{damp} is internal damping torque; T_f is frictional torque.

The dynamic torque depends on the rotor moment of inertia and on acceleration:

$$T_{dyn} = J \frac{d^2\theta_2}{dt^2} = \frac{J}{p} \cdot \frac{d^2\theta_{2\,el}}{dt^2} \tag{2.94}$$

Internal electromagnetic damping of rotor oscillations is provided due to a rotating emf induced in the control windings. The rotating emf is induced in active-type stepper motors by the rotor field flux and in reluctance and inductor motors by the a.c. component of the field flux set up as a result of changes in reluctance in the course of the rotor motion. The rotating emf causes additional currents in the control winding circuit, which interact with the flux built up due to these currents, with the result that a damping torque appears and maintains constant the rotor speed.

The damping torque is proportional to the rotor speed

$$T_{damp} = D \frac{d\theta_{2\,el}}{dt} \tag{2.95}$$

where D is damping factor.

The damping factor depends primarily on the a.c. component of mutual attraction between the rotor flux and the stator field. Other conditions being equal, this factor is greatest with active-type stepper motors. Disregarding the frictional torque T_f, and taking a stepper motor that runs at small mismatch angles between the rotor axis and the stator mmf axis ($\sin \gamma \approx \gamma$), substitute Eq. (2.89), (2.94) and (2.95) in Eq. (2.93) to obtain a differential equation of the rotor motion:

$$\frac{d^2 \theta_{2\,el}}{dt^2} + \frac{Dp}{J} \cdot \frac{d\theta_{2\,el}}{dt} + \frac{T_{s\,max}\, p}{J} \theta_{2\,el} = \frac{T_{s\,max}\, p}{J} \theta_{1\,el} \tag{2.96}$$

From Eq. (2.96), the factor to $\theta_{2\,el}$ is a square of angular velocity of the rotor oscillations (in radians)

$$\omega_0 = \sqrt{\frac{T_{s\,max}\, p}{J}} \tag{2.97}$$

The rate of control pulses, f_0, corresponding to the main resonance, is $f_0 = \omega_0/2\pi$. In actual stepper motors, where the torque/pulse rate curves are not linear, the main resonance frequency is slightly lower than f_0. Frequency resonance occurs at a rate of control pulses lower than f_0 by an integer number.

The factor to $\dot{\theta}_{2\,el}$ in Eq. (2.96) characterizes the relative oscillation damping factor λ:

$$2\lambda = \frac{Dp}{J} \tag{2.98}$$

An important characteristic of the steady state condition is the threshold torque/pulse rate curve (rate of control pulses *versus* static torque) at which the rotor pulls out of step (solid line on Fig. 2.80). This curve defines the threshold past which further stepless loading of the stepper motor

shaft will pull the motor out of step at a given rate of control pulses. The threshold torque/pulse rate characteristic is usually studied at $f > f_0$.

The torque of the stepper motor reduces with an increase in frequency, which can be attributed to the following two factors: (a) the action of the damping torque set up due to rotating emf; (b) the inductance voltage in the control windings becomes commensurable with supply voltage, and current through the control windings has no time to reach the steady state value within a step period, which reduces the resultant stator flux. A marked drop of the synchronizing torque occurs at a longer electromagnetic time constant of the control windings.

The dynamic error of a stepper motor, that is, the instantaneous mismatch angle between the moving axes of the rotor and the stator mmf, may exceed the static error due to a stepped motion of the stator mmf and an oscillatory motion of the rotor.

Transient conditions, that is, starting, braking, frequency change-over, involve transient processes occurring in stepper motors due to variations in the rate of control pulses and in the rotor speed.

An important characteristic of the starting condition is the rate of response, that is, the maximum rate of control

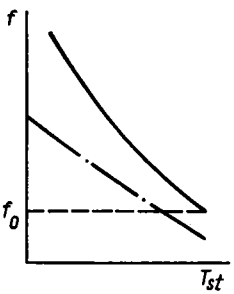

Fig. 2.80. Threshold torque/pulse rate curve and acceleration curve of a stepper motor

pulses at which the rotor is still reliably pulled in step. A stepped rise of the rate of control pulses, when the motor is started from standstill and accelerated to full speed, causes the rotor to lag for the first period behind the stator mmf due to inertia of rotating parts. As the motor further accelerates, it reaches the stator mmf speed and may appear to be ahead of the mmf at the expense of stored kinetic energy. The rotor oscillations gradually decay and the motor attains a steady state condition. Hence, during the starting period the rotor may lag behind the stator mmf by a step or more and may pull out of step. The rate of response grows with the synchronizing torque and with the decrease of the step value, the moment of inertia of rotating parts, and the static torque (dash-and-dot line on Fig. 2.80).

Frequency drops occurring during braking and reversal of stepper motors, which ensure transients without loss of a step, are one more limiting consideration. The maximum braking frequency under steady state conditions of rotation is equal to the rate of response. The maximum braking frequency at transients and the maximum frequency of reversals are 30 to 40 per cent lower than the rate of response.

2.13. Auxiliary Fractional-Horsepower Single-Phase Motors

Noncontrolled light-power drive systems employ *split-and-shaded-pole motors* and *induction motors with starting elements* as auxiliary drives. These motors operate on single-phase supply, therefore, they are referred to as single-phase motors.

2.13.1. Split-and-Shaded-Pole Motors

Most simple single-phase a.c. motors are split-and-shaded-pole motors (Fig. 2.81*a*) that can be built as synchronous or induction machines. The salient-pole stator *1* of such a motor consists of two electric steel stacks. The stator accommodates a single-phase field winding *2*. Each of the poles *3* has a longitudinal slot accommodating one of the ends of pole shaders *4* that embrace and shield some portion of the

pole (one-fifth to half of the pole arc). The motor rotor *5* is placed in the stator bore. The rotor construction depends on the type of motor. Induction motors are furnished with a squirrel-cage, hollow nonmagnetic or ferromagnetic rotor. Synchronous motors may have a permanent-magnet (active-type), hysteresis (made of a retentive material), or reluctance (with reluctance varying along the air gap) rotor.

Applying single-phase a.c. voltage to the field winding terminals sets up a pulsating magnetic flux $\dot{\Phi}$ in the stator magnetic circuit. This flux, while cutting the stator poles, is split at the longitudinal slots into two fluxes $\dot{\Phi}'$ and $\dot{\Phi}''$ that are spaced apart by angle γ. The flux $\dot{\Phi}'$ closes through the shaded portion of the poles and induces a transformer emf in the pole shaders. The pole shaders carry a current that lags behind the emf due to the inductive reactance of the pole shaders. The mmf of pole shaders builds up a flux $\dot{\Phi}_{ps}$ that closes through the shielded portion of the poles. This flux and flux $\dot{\Phi}'$ make up a resultant flux $\dot{\Phi}_{sh}$ of the shielded portion of the poles. The resultant flux is in time shift with respect to the flux $\dot{\Phi}''$ of the nonshielded portion of the poles:

$$\dot{\Phi}_{sh} = \dot{\Phi}' + \dot{\Phi}_{ps} \qquad (2.99)$$

The vector diagram of the motor is shown on Fig. 2.81*b*.

Magnetic fluxes $\dot{\Phi}''$ and $\dot{\Phi}_{sh}$ that are in space and time shift relative to one another build up a resultant rotating field. Since these fluxes are shifted in space and in time by an angle smaller than 90 deg., and their magnitudes are not equal, the resultant field will be of an elliptical rather than of a circular shape. The rotating field interacts with the rotor and builds up a torque that is determined by the type of the rotor.

An essential advantage of split-pole single-phase motors, apart from their simple construction and low cost, is reliable operation at frequent starts and stops under voltage, because the main losses occurring in these motors are electric losses in pole shaders. Hence, the total loss in the motor remains the same throughout the entire period from no-load running

to a short-circuit condition (rotor stalling under voltage across the field winding terminals), with the result that the field winding does not run hot.

One of the main disadvantages of these motors is a rather low starting torque which is the result of appreciable ellipticity of the magnetic field. This can be understood from the following discussion taking as an example an induction motor. The motor fluxes $\dot{\Phi}_{sh}$ and $\dot{\Phi}''$ are generally asymmetric and form a rotating field (see Sections 2.6 and 2.7):

$$\alpha_{el} = \frac{\Phi_{sh}}{\Phi''} < 1; \quad \sin\beta < 1; \quad \sin\gamma < 1 \qquad (2.100)$$

The starting torque of induction motors in terms of relative units equals the rms value of the signal ratio. Taking the starting torque $T_{start\,0}$ developed by a circular field with the amplitude of Φ'' as unity, the starting torque of an actual shaded-pole motor, T_{start}, will be

$$T_{start} = T_{start\,0}\,\alpha_{el}\sin\beta\sin\gamma \qquad (2.101)$$

Fig. 2.81. General arrangement (*a*) and vector diagram (*b*) of a single-phase split-and-shaded-pole motor

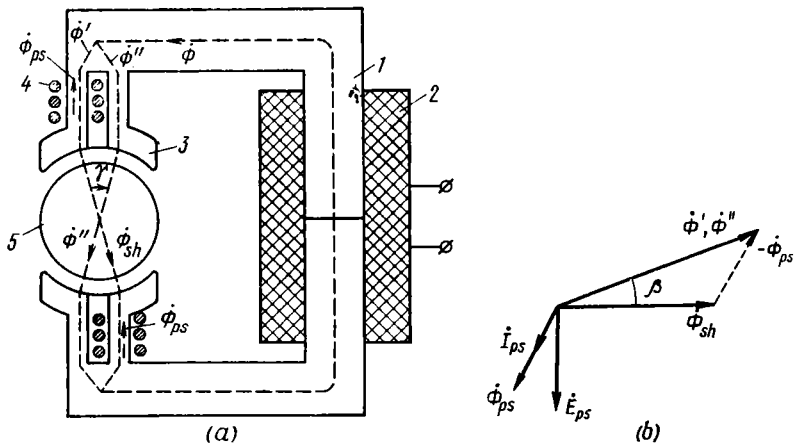

With regard for unequality (2.100) we obtain $T_{start} \ll \ll T_{start\ 0}$. The starting torque of shaded-pole induction motors is usually 20 to 60 per cent of rated value.

In the same manner we can show that due to a high degree of ellipticity of the field the motor develops a rather low mechanical speed at a high level of losses. The efficiency of these motors of different power ratings does not exceed 0.1 to 0.4. The power factor is from 0.4 to 0.6.

A uniform air gap may slightly improve efficiency, power factor, and starting characteristics of the motor. An example is a composite-stator motor illustrated by Fig. 2.82. The stator consists of a cylinder *1* and a spider *2*. The spider forms the motor poles and magnetic shunts *MS* in-between. The magnetic shunts have a small cross-sectional area, and the main portion of magnetic flux due to the poles reaches the rotor through the air gap. With such a construction, the flux density is distributed within the gap by following an almost sinusoidal law with added advantage

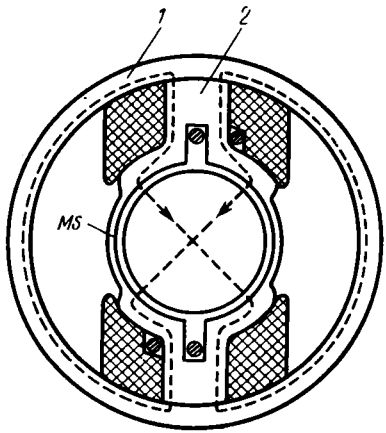

Fig. 2.82. General arrangement of fractional-horsepower motor with a composite stator

of the reduction of losses and stray moments due to upper harmonics of the field.

The above-discussed motors are non-reversible machines. Figure 2.83 illustrates a single-phase split-and-shaded-pole motor that may be reversed and controlled within a certain range of the running torque.

The only difference between the motor illustrated on Fig. 2.83 and that shown on Fig. 2.81*a* is that the former has coils with brought-out leads instead of pole shaders. Four coils *A*, *B*, *C*, and *D* are mounted on both the halves of each pole and arranged so that each half can be shaded by closing the respective pair of coils (*A*, *D* or *B*, *C*), thereby reversing the sense of rotation of the magnetic field and the rotor. When these coils are connected via a potentiometer *R*, their shielding action at a neutral position of the potentiometer wiper will be similar and a pulsating magnetic field will result. Shifting the wiper from the neutral position changes the shading coil fluxes Φ_{ps} on both the poles along with the phase shift (sin β) and the amplitude ratio (α_{el}) of fluxes Φ'_{sh} and Φ''_{sh}. The ellipticity of the rotating field and the torque change too.

A single-phase split-and-shaded-pole motor may be theoretically treated as a two-phase motor whose phase windings are shifted by an angle other than 90 deg. and the terminals of one of the windings are shorted out.

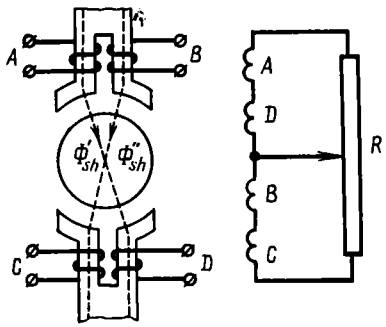

Fig. 2.83. General arrangement of reversible split-and-shaded-pole motors

2.13.2. Induction Motors with Starting Elements

Fractional-horsepower single-phase induction motors are manufactured by using an ideal circuit arrangement of a squirrel-cage induction machine (see Fig. 2.24). The stator carries two single-phase windings, one being a running winding and the other an auxiliary winding. These windings are usually spaced 90 electrical degrees apart. The rotor winding has a low resistance that ensures a critical slip $s_{cr} \ll 1$, thereby affording good characteristics under rated duty conditions.

There is a great variety of design and circuit arrangements for single-phase induction motors. The general classification offers two main groups:

(1) motors with a stator field rotating under working conditions;

(2) motors with a stator field pulsating under working conditions.

Group (1) includes fractional-horsepower motors (Fig. 2.84*a*) with capacitors permanently inserted in the auxiliary winding (capacitor motors). The running and auxiliary windings of these motors occupy an equal number of slots. The motors depend for their operation on the same principle as induction servo motors using the amplitude-and-phase control method and incorporating capacitors

Fig. 2.84. Connection diagram and slip/torque characteristics of a single-phase capacitor motor

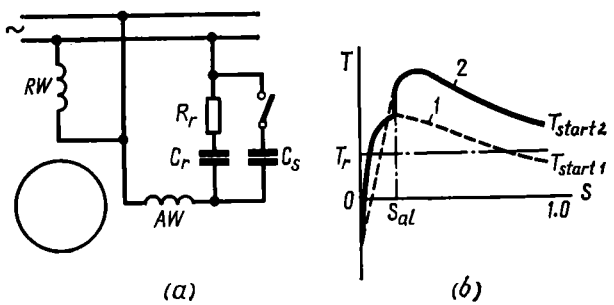

in the field circuit (see Sections 2.6 and 2.7). Basic equations relating to the latter concern likewise the motors under discussion.

It is general practice to use two capacitors in the motor circuit, one being a running capacitor, C_r, and the other a starting capacitor, C_s. The capacitance of the running capacitor C_r is selected so as to ensure a circular rotating field and, hence, a minimum rated slip. In this way, high efficiency and power factor are obtained under rated duty conditions.

Equations (2.47) of symmetric current components are valid for capacitor motors. From the analysis of these equations we can derive inductive reactances and resistances (in ohms) of phase-shifting elements affording a circular field at a certain slip s:

$$X_{c0} = X_{AW} + \frac{R_{AW}}{k_{tr}} \tag{2.102}$$

$$R_0 = \frac{X_{AW}}{k_{tr}} - R_{AW} \tag{2.103}$$

where X_{AW} and R_{AW} are, respectively, inductive reactance and resistance of auxiliary winding AW at a slip s and with a circular field (see Fig. 2.30*a*); $k_{tr} = w_{AW\ eff}/w_{RW\ eff}$ is transformation ratio of the stator windings; w_{eff} is effective number of turns in the respective windings.

The series resistor R_0 is inserted only when k_{tr} is lower than X_{AW}/R_{AW}.

By substituting in equations (2.102) and (2.103) the X_{AW} and R_{AW} quantities corresponding to a rated slip s_r, we can obtain the capacitance of running capacitor C_r and the resistance of R_r. The slip/torque curve of a motor with a running capacitor is shown on Fig. 2.84*b* (curve *1*).

Substituting in equation (2.102) the X_{AW} and R_{AW} quantities corresponding to a slip $s = 1$ (X_{AWs} and R_{AWs}), we can determine the total capacitance $C_0 = C_r + C_s$ required to ensure an almost circular field at starting.

The value of capacitor C_T required to provide for a maximum starting torque T_{start} is to be found from Eq. (2.57*a*).

The starting-to-rated torque ratio

$$k_T = T_{start}/T_r \tag{2.104}$$

can be raised from $k_T < 1$ to $k_T = 1.5$ or 2 by inserting capacitor C_s. A motor incorporating a starting capacitor may gain a slip s_{al} (Fig. 2.84*b*, curve *2*). As soon as this takes place, the capacitor C_s is cut out and the motor runs according to curve *1*.

A disadvantage of capacitor-start motors is large size of the starting capacitor which is usually larger than the running capacitor.

The Group (2) motors (Fig. 2.85*a*) have a pulsating field when running. This field is set up due to the running winding occupying two thirds of the stator slots. The auxiliary winding is accommodated in the remaining slots. In order to gain better understanding of the operating principle of these motors, let us resolve the pulsating field into two fields—one rotating in the forward sequence and the other in the backward sequence (see Section 2.6). Figure 2.85*b* illustrates torque curves for the forward and backward sequences and the curve of the resultant torque T_{res} which is the geometric sum of the torques T_1 and T_2. So, at a static torque $T_{st} < T_{res\,max}$ the motor may operate steadily with a pulsating field. As has been already noted (Section 2.6), at $s \neq 1$ the resultant field of the motor is a field revolving due to a rotating emf induced in the rotor rather than a pulsating field.

Fig. 2.85. Operating principle of a single-phase induction motor

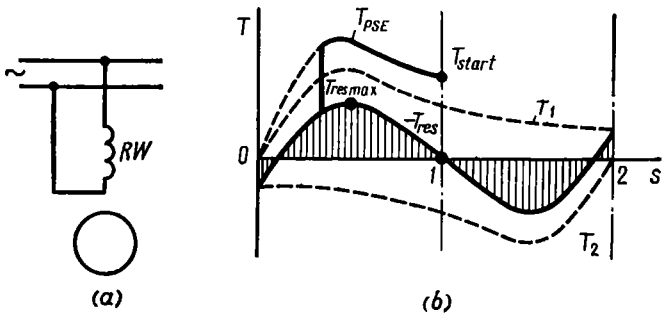

At $s = 1$, however, the starting torque is zero. So, to provide for a starting torque, a rotating field is set up for the period of motor starting. To this end, during starting the auxiliary stator winding is connected to power supply through phase-shifting elements *PSE* (Fig. 2.86*a*). The function of a *PSE* can be theoretically performed by a resistor, a capacitor, or an inductance coil. In practice, however, use is made only of capacitors and resistors. Figure 2.86*b* shows a vector diagram of currents and voltages with a resistor R used as a phase-shifting element. Since the windings possess active resistance and inductive reactance, currents in the running and auxiliary windings are shifted in phase by an angle

$$\beta = \varphi_{RW} - \varphi_{AW} < 90 \text{ deg}$$

When this is the case, a circular field cannot be obtained. The starting-to-rated torque ratio k_T is not over 1 or 1.5.

Some single-phase motors using this method of starting do not incorporate a series resistor R in the auxiliary winding circuit. Since the auxiliary winding AW functions for a short period of time, it is wound of wire having a smaller

Fig. 2.86. Starting circuit arrangement and vector diagrams of a single-phase induction motor using phase-shifting elements

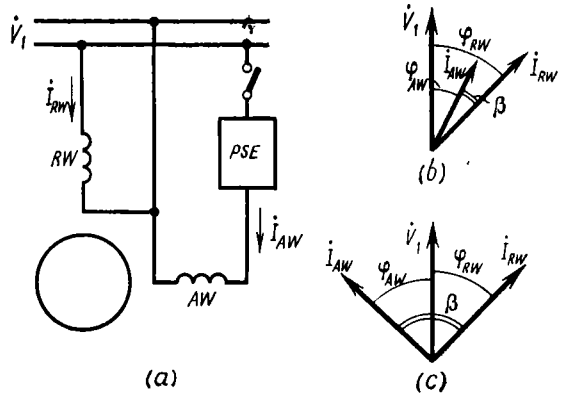

cross-sectional area than that used for the running winding RW, and it offers a higher resistance R_{AW}. Besides, some portion of this winding is bifilar wound, which reduces its inductive reactance X_{AW}.

Hence,

$$\frac{X_{AW}}{R_{AW}} < \frac{X_{RW}}{R_{RW}}, \quad \varphi_{AW} < \varphi_{RW} \text{ and } \beta \neq 0$$

A circular starting field can be obtained only by using a capacitor for phase shifting purposes. The vector diagram of currents and voltages for this case is shown by Fig. 2.86*c*. The currents through the windings are shifted in phase by an angle

$$\beta = \varphi_{AW} + \varphi_{RW}$$

and at a certain capacitance it may reach 90 deg. With such a starting circuit arrangement, the starting-to-rated torque ratio k_T may reach 1.5 or even 2. A disadvantage of this method is the large size of the starting capacitor.

The torque/slip curves of a single-phase motor for the starting period (curve T_{PSE}) and for the running period (curve T_r) are shown by Fig. 2.85*b*.

Currents and torques for both the duty conditions can be found from equations (2.44) through (2.51).

Fractional-horsepower induction motors are also available with a three-phase stator winding. These motors can operate both on three-phase and single-phase supply. When operated

Fig. 2.87. Circuit arrangement for connecting three-phase induction motors to single-phase supply

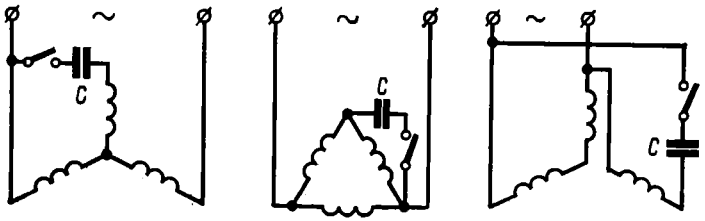

on a single-phase supply, the three-phase induction motor is treated as one of the modifications of a single-phase motor. Such motors may run both with a rotating and a pulsating stator field. Figure 2.87 shows some circuit arrangements for connecting a three-phase motor to a single-phase supply, with starting capacitor C used as a phase-shifting element.

The starting capacitor is to be selected by solving the equations similar to Eqs. (2.57*a*) and (2.102), taking into account the stator arc occupied by the auxiliary winding.

2.14. A.C. Motor Sets

The speed control systems of fractional-horsepower a.c. motors often use control units incorporating magnetic amplifiers and transformers. These units and induction motors are in most cases built integral as a single set to obtain better power output, power-to-mass ratio, and reliability.

2.14.1. Induction Motor-Amplifier Sets

An induction motor-amplifier set is essentially a three-phase or two-phase induction motor built integral with a magnetic amplifier. Servo motor-amplifier sets are generally two-phase machines with a squirrel-cage or hollow non-magnetic rotor. The magnetic amplifier core is part of the motor magnetic circuit.

The general arrangement of a two-phase reversible squirrel-cage motor-amplifier set incorporating two magnetic amplifiers is shown on Fig. 2.88. The stator core *1* is divided over its length into four stacks. Each stack functions as a toroidal core of the magnetic amplifier. The power windings *2* of the magnetic amplifier are wound on each stack, while each bias and control winding *3* is placed on two stacks. The two-phase distributed winding *4* of the motor stator is placed in the slots already accommodating the magnetic amplifier windings. The rotor *5* construction is typical of induction machines.

The magnetic amplifier windings are arranged and connected so that the magnetic flux Φ_0 closes through the

stator core without by piercing the rotor through the air gap (Fig. 2.89). The motor flux Φ_m is superimposed on the amplifier flux in the stator core.

When the stator core is not saturated, the motor flux is equally distributed in either direction from the AA axis, the demagnetizing effect of the amplifier flux in one half of the core is the same as in the other half, so the magnetic systems of the motor and amplifier may be considered independent. It means that the motor-amplifier set has the same characteristics as a corresponding motor with an external magnetic amplifier.

These characteristics are somewhat distorted when the stator core is saturated. In this case, the magnetizing effect of the flux Φ_a on the flux Φ_m is not the same as the demagnetizing action, and an inductive coupling between the motor and amplifier windings results.

The rotor speed of the set is controlled in the same way as that of induction servo motors using amplitude or amplitude-and-phase control method (see Section 2.7).

Fig. 2.88. General arrangement of two-phase reversible motor-amplifier set

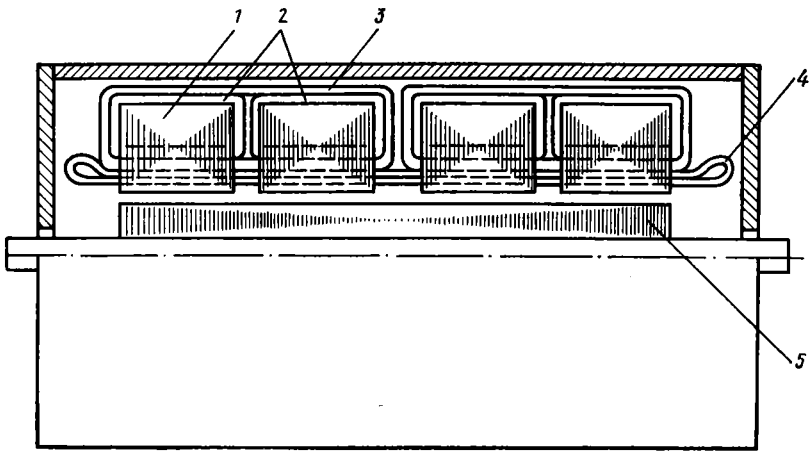

Figure 2.90 illustrates a reversing amplitude-and-phase control circuit of a motor-amplifier set. The motor control winding CW_m does not actually carry current and the rotor is motionless as long as no signal is applied to the amplifier control winding CW_a.

With an increase in the current through the control winding of the first amplifier MA_1, the permeability of its core decreases thereby reducing the inductance and inductive reactance of the amplifier power windings P_A connected in series with the motor control winding CW_m. The amplitude of current and voltage in the CW_m winding rises, thereby causing a change in the shape of the elliptical stator field, and the rotor starts running.

As soon as a control signal arrives at the control winding of the second amplifier MA_2, the current in the motor control winding starts flowing in the reverse direction thereby reversing the motor.

The speed-torque characteristics of a motor-amplifier set for different currents in the amplifier control winding, I_{ACW}, are shown by Fig. 2.91. These characteristics slightly differ from those illustrated by Fig. 2.35 where the effect of the signal source output resistance is disregarded ($I_{ACW3} < I_{ACW2} < I_{ACW1}$).

Fig. 2.89. Distribution of magnetic fluxes in a motor-amplifier set

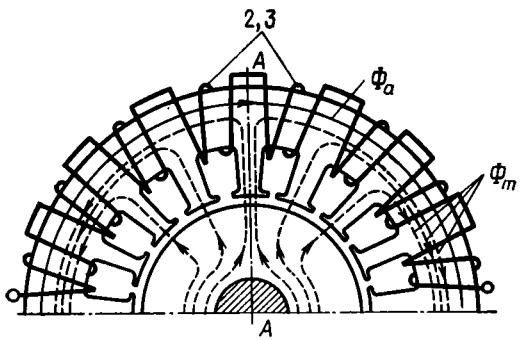

As is seen from Fig. 2.91, critical slip appreciably decreases with the amplifier control current (ω_{2cr} rises), and an unstable section (I_{ACW3} curve) may appear on the speed-torque characteristic. This can be attributed to the fact that the inductive reactance of the magnetic amplifier power winding, X_a, in the control circuit incorporating a magnetic amplifier is connected in series with the inductive reactance of the motor stator, X_s. When this is the case, the critical slip of the motor is determined by the equation

$$s_{sr} \approx \frac{R'_r}{X_a + \frac{X_s}{\sigma} + X'_r} \qquad (2.105)$$

where $\sigma = 1 + \frac{X_s}{X_m}$; R'_r and X'_r are, respectively, active resistance and inductive reactance of the rotor; X_m is mutual inductive reactance.

As has been already stated, X_a increases with the decrease of the amplifier control current I_{ACW}, and, hence, the critical slip s_{cr} diminishes.

Fig. 2.90. Reversing amplitude-and-phase control circuit of a motor-amplifier set

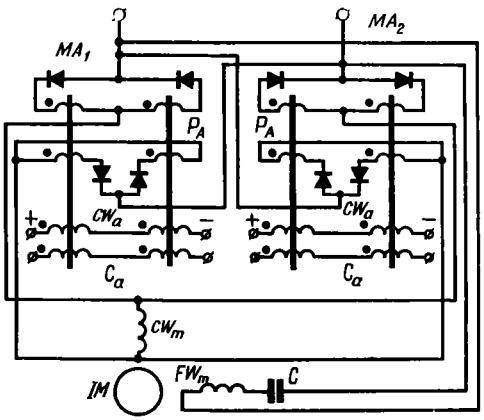

2.14.2. Synchronous Motor-Transformer Sets

A synchronous motor-transformer set is essentially a two-phase synchronous motor built integral with a transformer.

The stator circuit of a synchronous motor-transformer set is generally similar to that of an induction motor-amplifier set (Fig. 2.88), the only difference being that the stator core carries primary and secondary windings of two single-phase transformers and not amplifier windings. The transformer and motor windings are arranged so that the resultant inductive coupling between them is eliminated as long as the magnetic circuit is not saturated.

The rotor construction depends on the type of synchronous motor used (permanent-magnet, reluctance, or hysteresis motor).

Synchronous motor-transformer sets are usually employed in adjustable-frequency speed control systems of fractional-horsepower synchronous drives. In these systems, the transformer is incorporated in the static frequency changer that is supplied with power from a self-contained d.c. source, such as, a storage battery, a sun battery, etc.

Figure 2.92 shows an adjustable-frequency speed control system of a fractional-horsepower motor-transformer set. A semiconductor switch TS is built around transistors T_1 through T_4. Transistors T_1 and T_2 alternately close and open the circuits so that the d.c. voltage picked off the

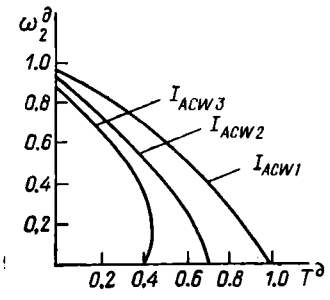

Fig. 2.91. Speed-torque characteristic of a motor-amplifier set

power source, $V_{d.c.}$, is applied to different halves of the Tr_1 transformer primary. The transformer yields an alternating voltage whose fundamental functions as a working voltage of the synchronous motor *SM*. The switching moments of transistors T_3 and T_4 are shifted half the switching time step in respect to those of transistors T_1 and T_2. The voltage supplied from transformer Tr_2 to the motor winding FW_2 is in phase quadrature with that across winding FW_1. In this way, one of circular field conditions is satisfied.

Varying the switching frequency of transistors changes the frequency and speed of the rotating stator field and, hence, the rotor speed.

Performance characteristics of a synchronous motor-transformer set are actually the same as those of a synchronous motor of a corresponding type supplied with power from an external light-power transformer.

It should be noted that induction motor-transformer sets depending for their operation on the same principle can be built for adjustable-frequency speed control systems.

Induction motor-amplifier sets and synchronous motor-transformer sets are more complicated in design and more difficult to manufacture than the respective motors. These drawbacks however are compensated for by small size, light mass, and high reliability of the sets when used for

Fig. 2.92. Amplitude-frequency speed control system of a synchronous motor-transformer set

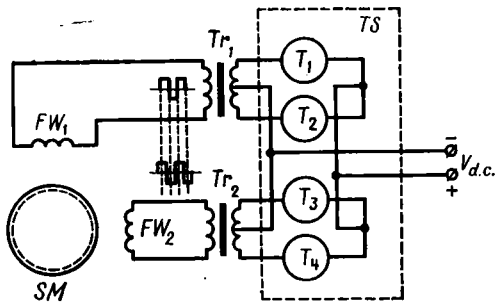

special-purpose applications. The mass of an induction motor-amplifier set may be 1.5 times as small as that of a corresponding drive built up of a separate motor and an amplifier and twice as light as that of a d.c. drive.

2.15. Application of Servo Motors

Fractional-horsepower servo motors are widely used in automatic control systems, measuring and monitoring equipment where they function as controlling and converting elements (integrators and differentiators), in program-control systems and computers.

2.15.1. D.C. Armature-Control Motors Incorporated in a Servo System

Ever increasing applications of the spark-discharge method for machining metals has brought in need electromechanical servo systems incorporating servo motors. A spark-discharge machine usually contains an electromechanical servo system meant for maintaining optimum electrode gaps (spark gaps). Figure 2.93 illustrates the diagram of such a machine. The spark gap between the part being machined, *MP*, and the tool electrode, *TE*, is usually controlled by an independently excited d.c. servo motor *SM* (type CJI121 or CJI161). The motor armature winding is connected across

Fig. 2.93. Spark-discharge machine

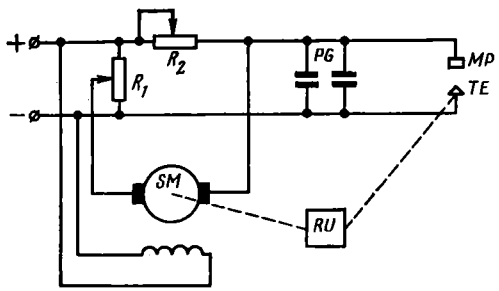

the diagonal of a bridge whose arms are resistors R_1 and R_2 and the resistance of the spark gap.

The armature speed and sense of rotation depend on the amount and direction of current flowing in the bridge diagonal. The armature is coupled via the reduction unit *RU* with the tool electrode and functions to move the latter in respect to the part being machined. Current pulses are afforded by the capacitor-type pulse generator *PG*. The breakdown voltage and, hence, the amount of spark gap, is preset by appropriately positioning the wiper of the rheostat R_1.

When a spark does not jump the gap between the electrodes, (the spark-gap resistance is infinitely large), the bridge diagonal current flows in a direction causing the motor armature to force the tool electrode towards the part being machined. The *PG* capacitors start charging. The electric strength of the spark gap reduces and a breakdown occurs. The part is machined due to the spark discharge. In the action, the spark-gap resistance abruptly drops, the bridge diagonal current reverses its flow, and the servo motor starts rapidly carrying the tool electrode away from the part. The electric strength of the spark gap is restored and the above-described cycle is resumed.

2.15.2. Integrator Incorporating an Induction Servo Motor

An important problem in the automation of production processes is to maintain at the desired level or to vary in accordance with a preset program one or more controlled variables, such as the temperature, pressure, level or amount of a substance, etc. To this end, use is made of integral or proportional/integral controllers. An essential part of these controllers is a motor-driven servo element that functions to integrate the desired value.

This electromechanical integrator (Fig. 2.94) consists of an electronic amplifier *EA*, an induction servo motor *SM* using amplitude-and-phase control with the aid of a capacitor *C* inserted in the field circuit *F*, a step-down reduction unit *RU*, and an inductive position detector *PD* whose plunger *Pl* is coupled with the servo motor shaft via the

reduction unit RU. The output voltage V_{out} of the inductive position detector is proportional to the motion of the plunger and, hence, to the angle of turn of the servo motor shaft, θ:

$$V_{out} \sim \theta \tag{2.106}$$

A voltage V_{in} applied to the EA amplifier input has an amplitude modulated over the controlled variable. Any variation in V_{in} causes a corresponding change in the voltage across the servo motor control field, and, consequently, in the motor speed. The plunger position changes in proportion as does the output voltage V_{out} of the position detector PD.

To determine the correlation between the input and output voltages of the integrator, integrate differential equation (2,37) relating to the servo motor:

$$\tau_m \frac{d\theta}{dt} + \theta = k_g \int_0^t \alpha dt \tag{2.107}$$

Taking into account equation (2.106) and the fact that the signal ratio α is directly proportional to the motor control voltage and consequently to V_{in}, we obtain

$$\tau_m \frac{dV_{out}}{dt} + V_{out} = k_g \int_0^t V_{in}\, dt \tag{2.108}$$

From equation (2.108) we can see that the output voltage V_{out} varies in accordance with the integral of a function

Fig. 2.94. Electromechanical integrator. Circuit diagram

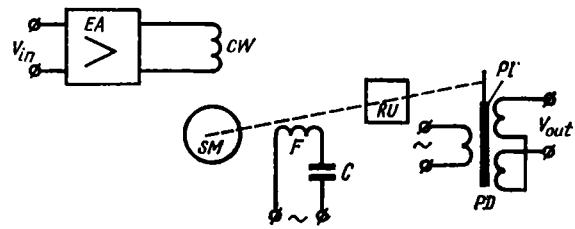

determined by the input voltage V_{in}. The value of τ_m determines the integrator time lag. An ideal integrator must have most linear control characteristics of the servo motor, and the lowest possible rate of change of the controlled variable, that is, the highest possible ratio of the controlled process time constant to the electromechanical time constant of the servo motor and of the integrator as a whole. When this is the case,

$$V_{out} = k_g \int_0^t V_{in}\, dt \qquad (2.109)$$

2.15.3. Stepper Motor as Part of a Machine Tool Program-Control System

Stepper motors are used as feed drives of metal-working machine tools furnished with a magnetic or punched tape programmed digital control system. In the process, it is often required to convert a digital or pulse code into a modulated signal.

The system operation is illustrated by Fig. 2.95. The system comprises a stepper motor *StM* with a transistor

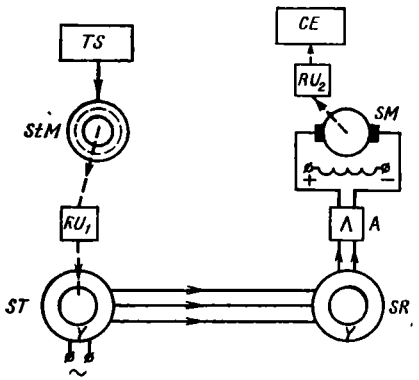

Fig. 2.95. Pulse code-to-modulated signal conversion by means of a stepper motor

switch TS, a synchro transmitter ST, a synchro receiver SR, an amplifier A, and a d.c. servo motor SM. The rotors of the stepper motor and synchro transmitter are coupled via a step-down reduction unit RU_1 that makes it possible to reduce the motor increment. The synchro transmitter and synchro receiver (ST and SR) are connected into a transformer circuit where the output voltage of the synchro receiver is the function of the angle of turn of the synchro transmitter (see Section 4.4). The servo motor moves the equipment under control, CE, via the reduction unit RU_2 at a program-specified speed.

The system operates as follows. The program is read out of the tape, information arrives at the transistor switch and the latter switches over the stepper motor control windings in accordance with the information received. The stepper motor steps in an appropriate number of increments and turns the synchro transmitter rotor. The synchro receiver output voltage, that is proportional to the angle of turn of the stepper motor, passes through the amplifier to the armature winding of the servo motor. The latter starts running and drives the equipment under control at a speed proportional to the applied voltage, that is, in accordance with the preset program.

2.15.4. Semiautomatic Program-Controlled Gear for Selecting Micromodule Resistances

Figure 2.96 illustrates the block-diagram of a semiautomatic control gear incorporating stepper motors and used to select resistances by searing the conducting carbon paste with a laser beam. The micromodules are arranged on a coordinate desk CD which moves along the X and Y coordinates with the aid of two stepper motors.

The program-control system consists of the following basic units: program panel PP, analyzer An, control gear CG, stepper motor control unit $SMCU$ (transistor switch), position detectors PD, laser control gear LCG, laser L, and information decoder ID.

The program according to which the stepper motors position the coordinate desk relative to the centre line of the laser L is set on the program panel PP. Information arrives

at the stepper motor control unit via the analyzer and the control gear. The stepper motor control unit changes over the control windings of the stepper motors in accordance with the specified program, whereupon the stepper motors start running and move the coordinate desk via the step-down reduction unit. Meanwhile, the position detectors of the coordinate desk turn and yield a signal that arrives at the analyzer via the information decoder. The analyzer compares the present coordinates of the coordinate desk with those preset by the program and corrects the motor motion. The coordinate desk stops moving as soon as it reaches the desired point.

As this takes place, the control gear issues a command to the laser control gear and the latter turns on the laser. Thereupon searing of the micromodule carbon paste commences.

Fig. 2.96. Block-diagram of a semiautomatic gear for selecting resistances incorporating a stepper motor

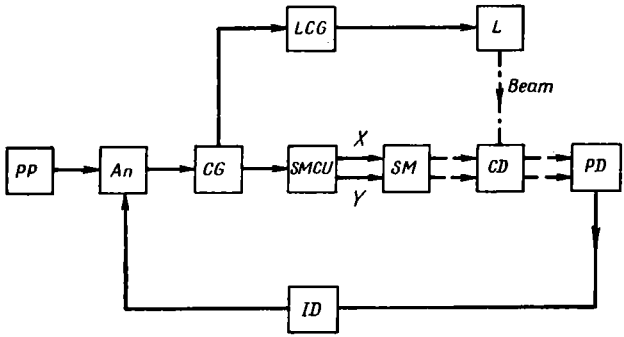

Chapter

3 TACHOGENERATORS

3.1. General Information and Classification

Tachogenerators are fractional-horsepower electrical machines running as generators that function to convert a rotational speed into a proportional electric signal. In this case, the conversion law depends on the output characteristic of the tachogenerator, that is, on the input variable (shaft speed ω) versus output value (voltage V_{out} across the output winding) curve.

A general output characteristic equation for an ideal tachogenerator is as follows:

$$V_{out} = k_g \omega = k_g \frac{d\theta}{dt} \tag{3.1}$$

where θ is angle of turn of the tachogenerator rotor; k_g is steady-state gain (steepness of output characteristic).

Equation (3.1) shows that the tachogenerator can be used for electromechanical differentiation if the reference variable is the rotor angle of turn.

The tachogenerator is similar in design to the respective fractional-horsepower motor.

According to design and principle of operation, the tachogenerators are classified as *direct-current*, *induction* and *synchronous alternating-current machines.*

Basic requirements to tachogenerators are as follows:

(1) minimum amplitude error, that is, deviation of the output characteristic from the linear curve;

(2) minimum phase error, that is, variation in the output voltage phase due to a change in the operating conditions;

(3) maximum amplification (gain);

(4) low inertia of the rotor;

(5) low electromagnetic time constant.

Requirements to tachogenerators according to their application are set forth in Section 3.2.

The amplitude error ΔV is determined as a difference between the output voltage corresponding to the given speed with an ideal output characteristic and the actual output voltage.

The phase error $\Delta\beta$ is defined as a difference between the angle β by which the field voltage vector is shifted in respect to the output voltage vector of an ideal tachogenerator, whose β angle is independent of speed, and the actual angle of shift between these vectors.

3.2. Direct-Current Tachogenerators

According to operating principle and mechanical design, the direct-current tachogenerators are essentially direct-current commutator machines with independent electromagnetic-field or permanent-magnet excitation (see Fig. 3.1*a*).

The output characteristic of a d.c. tachogenerator is a voltage V across the armature terminals versus armature speed ω curve plotted at a constant field flux Φ and a constant load resistance R_{load}. As is known from the theory of electrical machines, the armature emf E_A is directly

Fig. 3.1. Circuit diagram and output characteristics of a d.c. tachogenerator

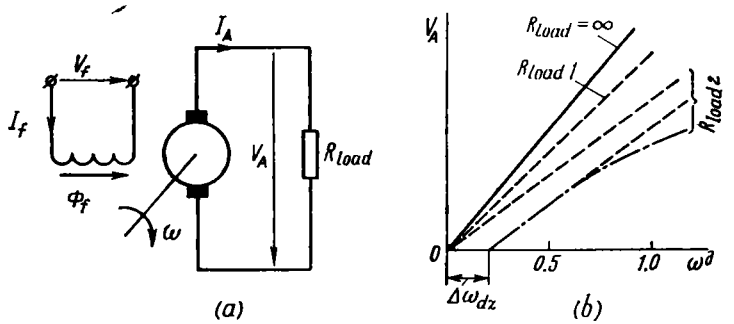

proportional to the field flux and the armature speed. So, for the constant flux the following equation will be true:

$$E_A = k_E \omega = k_E \frac{d\theta}{dt} \tag{3.2}$$

where θ is angle of turn of the tachogenerator armature; k_E is machine constant equal to $k\Phi$; k is design factor according to Eq. (2.3).

Equation (3.2) is an output characteristic equation of a d.c. tachogenerator running at no load, that is, at an open armature circuit. This linear characteristic is shown on Fig. 3.1*b* (for $R_{load} = \infty$). The speed ω^θ is taken in terms of relative units as has been done in Section 2.3.

When the armature winding is connected to the terminals of a device whose input resistance is a final value, the field flux being constant, the output voltage will be lower than the armature emf by the voltage drop across the armature circuit:

$$V_A = E_A - I_A R_{AC} \tag{3.3}$$

where I_A is armature current; R_{AC} is armature circuit resistance equal to the sum of armature winding resistance R_A and the brush contact resistance.

Since the current is found from Ohm's law

$$I_A = V_A / R_{load} \tag{3.4}$$

then

$$V_A = \frac{E_A}{1 + (R_{AC}/R_{load})} = \frac{k_E \omega}{1 + (R_{AC}/R_{load})} \tag{3.5}$$

Equation (3.5) shows that the direct-current tachogenerator will have a linear output characteristic at a constant field flux and a constant brush contact resistance.

Figure 3.1*b* shows output characteristics corresponding to Eq. (3.5) for two final values of load resistance, $R_{load\ 1}$ and $R_{load\ 2}$, with $R_{load\ 1}$ being higher than $R_{load\ 2}$.

The output characteristic of an actual d.c. tachogenerator, however, may deviate from the linear relationship determined by Eq. (3.5), that is, an amplitude error of speed may appear due to the following two factors:

(a) armature reaction of a loaded tachogenerator weakens the field flux. The resultant flux of a loaded machine will be

$$\Phi_{load} = \Phi - \Delta\Phi_r \tag{3.6}$$

where $\Delta\Phi_r$ is variation of the flux due to the demagnetizing effect of armature reaction that is proportional to the armature current; Φ is magnetic flux of a tachogenerator running at no load.

Hence, the armature emf of a loaded tachogenerator, $E_{A\ load}$, is not a constant value for the given armature speed, rather it varies with load in accordance with the following equation:

$$E_{A\ load} = k\omega\Phi_{load} \tag{3.7}$$

(b) with the tachogenerator connected to a load, voltage drop across the brush contact, rather than the contact resistance V_{brush} shall be considered as a constant value. This characteristic complies with the resistance versus current density curve of the brush material (graphite). Now it is evident that with the tachogenerator running under load the voltage across its armature terminals will be determined by the equation

$$V_A = E_{A\ load} - V_{brush} - I_A R_A \tag{3.8}$$

Transform this equation taking into account Eq. (3.4), (3.6), and (3.7):

$$V_A = \frac{k_E\,\omega - V_{brush}}{1 + (kk_r\,\omega + R_A)/R_{load}} \tag{3.9}$$

where $k_r = \Delta\Phi_r/I_A$ is factor of pr oportionality between the armature current and flux $\Delta\Phi_r$.

Equation (3.9) expresses the output characteristic of a d.c. tachogenerator with due regard for demagnetizing effect of armature reaction and constant voltage drop across the brush contact. Upon the analysis of Eq. (3.9) we come to the conclusion that

(a) the output characteristic is not linear (ω stands in the denominator);

(b) the output characteristic originates at a point other than zero because when the armature rotates at a low speed,

the emf is lower than the voltage drop across the brush-to-commutator contact ($k_E\omega < V_{brush}$). It means that the tachogenerator has a dead zone $\Delta\omega_{dz}$ within which the output voltage is zero.

The output characteristic plotted in accordance with Eq. (3.9) for the load resistance $R_{load\ 2}$ is illustrated by Fig. 3.1*b* (dash-and-dot line).

If we assume that the linear output characteristic expressed by Eq. (3.5) is ideal, $V_{A\ i}$, the amplitude error due to armature reaction can be written as a difference of equations (3.5) and (3.9) at $V_{brush} = 0$, as referred to $V_{A\ i}$:

$$\Delta V = \frac{V_{A\ i} - V_A}{V_{A\ i}} = \frac{1}{1 + (R_A + R_{load})/kk_r\omega} \qquad (3.10)$$

The error found from Eq. (3.10) is referred to as a design error.

In order to obtain a more linear output characteristic, it is good practice to load the tachogenerator with maximum possible external resistance R_{load} and to employ a narrow speed range ($\omega^\delta < 0.5$) so as to minimize armature reaction. Tachogenerators built around a hollow- or disk-armature d.c. machine have most linear output characteristics as the effect of armature reaction in such a machine is very low (lower than k_r).

The dead zone can be greatly reduced by using metal brushes with silver built up at the points where they come in contact with the commutator, because silver possesses a linear current-voltage characteristic. The dead zone can likewise be reduced by increasing amplification:

$$\Delta\omega_{dz} = V_{brush}/k_g \qquad (3.11)$$

The tachogenerator steady-state gain that characterizes the relationship between the armature winding terminal voltage and the armature speed can be found from Eq. (3.9):

$$k_g = \frac{dV_A}{d\omega} = \frac{(1 + R_A/R_{load})\, k_E + V_{brush} k k_r / R_{load}}{[1 + (R_A + k k_r \omega)/R_{load}]^2} \qquad (3.12)$$

As is seen from Eq. (3.12), k_g is generally a nonlinear function of the armature speed. Disregarding the demagnetizing effect of armature reaction, that is, assuming that

$k_r = 0$, we can transform Eq. (3.12) as follows:

$$k_g = \frac{k_E}{1 + (R_A/R_{load})} \tag{3.13}$$

In view of this assumption, k_g is independent of armature speed, depends on the design characteristics, is proportional to the field voltage of the machine (as referred to the k_E factor) and rises with the load resistance R_{load}. At $R_{load} \gg \gg R_A$, the d.c. tachogenerator gain $k_g = 3$ to 100 mV per r/min.

Electromagnetic-field d.c. tachogenerators may have a temperature error brought in due to heating of the field coils, excessive resistance of the field coils and too low field current, which results in a reduction of the field flux and output voltage. A similar error may occur at field supply voltage fluctuations. In order to maintain the field flux at the desired level under varying conditions mentioned above, the tachogenerator is provided with a heavily saturated magnetic system, that is, the working point on the *B-H* curve is selected above the kink of the curve where even serious variations in the field current will not cause appreciable variations in the magnetic flux.

A heavily saturated magnetic system, however, may be sometimes undesirable when the steady-state gain k_g of a tachogenerator is to be varied by adjusting the field flux at the expense of field current. If this is the case, the magnetic system is made unsaturated, and to eliminate temperature error use is made of magnetic shunts *MSh* (Fig. 3.2) whose reluctance rises with temperature. Upon heating the field resistance increases and flux Φ decreases, but reluctance to the leakage flux Φ_σ through the shunts rises. The leakage flux tends to close through the armature more and more, thereby bringing the armature emf to the initial value.

The permanent-magnet tachogenerator has no error brought in as a result of variations in the field flux caused by the above conditions. However, its steady-state gain cannot be controlled. An essential advantage of this tachogenerator is that it does not need a power source. A proper selection of the permanent magnet material may bring to a minimum errors due to deterioration of magnetic properties with time.

One more type of error characteristic of d.c. tachogenerators is output voltage unbalance. This error consists in that when a tachogenerator armature closed through a load rotates at an equal speed and in different directions, the output voltage may be different. This unbalance is in most cases the result of improper setting of the tachogenerator brushes on the correct neutral.

To illustrate this phenomenon, refer to Fig. 3.3. When the armature rotates clockwise at a speed ω_{cw}, it carries current $I_{A\ cw}$, with the result that a flux due to armature reaction, $\Phi_{A\ cw}$, is set up, the direct component of this flux being cumulative with the field flux Φ, which increases the resultant flux. When the armature rotates counterclockwise at a speed $\omega_{ccw} = \omega_{cw}$, the armature emf and current are reversed. This sets up a flux due to armature reaction, $\Phi_{A\ ccw}$, whose direct component is differential to the field flux Φ, which reduces the resultant flux. Hence, output voltage unbalance is caused by inequality of resultant fluxes at different senses of rotation. This unbalance U can be found from the equation

$$U = \frac{V_{A\ cw} - V_{A\ ccw}}{0.5\,(V_{A\ cw} + V_{A\ ccw})} \times 100\,\% \qquad (3.14)$$

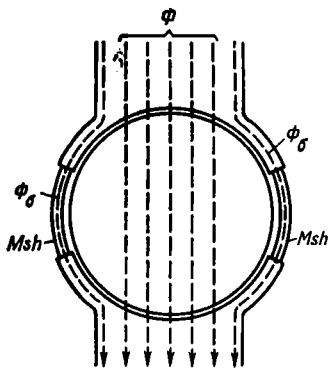

Fig. 3.2. Magnetic system with heat-sensitive magnetic shunts

Output voltage ripples also bring in some error that is not constant in time. There may be distinguished three types of ripples, *viz.*, *armature*, *tooth*, and *commutator ripples.*

Armature ripples are the result of changes in the reluctance and, consequently, a change in the magnetic flux within one revolution of the armature. This may be caused by ovality or runout of the armature, or by magnetic anisotropy of its material. The frequency of armature ripples in a two-pole machine

$$f_A = \omega/\pi \tag{3.15}$$

The amplitude of armature ripples can be reduced by making a relatively large air gap, by fanning out the armature stack, and by finishing the armature with higher accuracy.

Tooth ripples are the result of a change in the amount of flux and its unequal distribution at a pole due to a toothed surface of the armature. The frequency of tooth ripples

$$f_t = \frac{Z\omega}{2\pi} \tag{3.16}$$

where Z is number of teeth on the armature surface.

The amplitude of tooth ripples can be reduced by skewing the armature teeth with respect to the barrel generatrix,

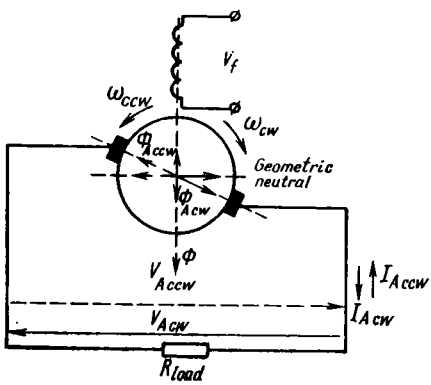

Fig. 3.3. Output voltage unbalance in d.c. tachogenerators

by a proper selection of the width of pole shoes, and by using ferromagnetic wedges to hold the winding in the slots.

The armature and tooth ripples can be eliminated by using a machine with a hollow nonmagnetic or a disk armature (Section 2.2).

Commutator ripples are caused in most cases by a periodic variation of the number of coils in parallel circuits of the armature winding during commutation and by chattering of brushes on the commutator. The commutator ripple frequency

$$f_c = \frac{K\omega}{2\pi} \tag{3.17}$$

where K is number of commutator segments.

The commutator ripple amplitude can be reduced by the use of a less number of coils and commutator segments and by more accurate finish of the commutator surface and better fitting of the brushes.

Tooth and commutator ripples of output voltage occur at a high frequency and are easily smoothed down by an LC filter. Armature ripples are of a lower frequency. Their adverse effect is most evident when the tachogenerator operates as part of an automatic control system in the range of low speeds (when the system approaches a steady-state position), in which case the ripple cycle becomes commensurable with the time constant of a servo element. The ripple amplitude of precision tachogenerators may reach 0.1 to 1 per cent of average voltage.

The advantages of d.c. tachogenerators are easily obtainable linearity of the output characteristic and absence of phase error, which makes them suitable for use in many automatic control systems.

Their utilization, however, is restricted because of a number of disadvantages, such as a sliding contact between the commutator and brushes involving mechanical wear problems, need of anti-interference and output voltage ripple filters, complicated mechanical design and relatively high cost.

The accuracy of operation of a d.c. tachogenerator is evaluated by two parameters, *viz.*, *nonlinearity of the output characteristic* and *unbalance of output voltage*.

The output characteristic nonlinearity is defined as a ratio of the difference between the output voltage measured at a given speed and the voltage calculated with reference to the standard linear characteristic to the voltage measured at a normal speed. The standard linear characteristic is a straight line intersecting the origin of coordinates and the point of rated speed on an experimental curve.

The output voltage unbalance is calculated as a ratio of the difference of output voltages measured while the tachogenerator rotates clockwise and counter-clockwise at a rated speed to the half-sum of these voltages.

The accuracy class of a tachogenerator is determined by the worst of the parameters obtained at speeds ranging from 0.1 of rated value to the rated speed. The output characteristic nonlinearity depends on the accuracy class and ranges between 0.05 and 1.0 per cent, the output voltage unbalance is between 0.2 and 2.0 per cent.

A d.c. tachogenerator can function as an accelerometer for measuring angular velocities. For this purpose, an *RC* network is to be connected in series to the armature terminals and the output voltage is to be picked off the terminals of resistor *R* (Fig. 3.4).

It is evident that at a uniform armature speed, capacitor *C* is charged: $v_C = v_A$, resistor *R* does not carry current and, hence, output voltage $v_R = 0$. The armature terminal

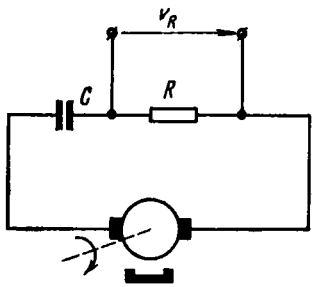

Fig. 3.4. D. c. tachogenerator operating as an accelerometer

voltage V_A starts changing in proportion to speed as soon as angular velocity appears,

$$\frac{dV_A}{dt} = k_g \frac{d\omega}{dt} \tag{3.18}$$

The capacitor C charges and discharges and resistor R starts carrying current i_R that is proportional to the rate of change of the capacitor terminal voltage. Hence,

$$i_R = \frac{k_R dV_A}{dt} \tag{3.19}$$

where k_R is proportionality factor.

Substituting Eq. (3.18) in Eq. (3.19) we obtain the equation for the voltage across resistor R:

$$v_R = i_R R = \frac{d\omega}{dt} k_g k_R R \tag{3.20}$$

As can be understood from Eq. (3.20), the output voltage v_R is proportional to the angular acceleration of the tachometer armature.

3.3. A.C. Induction Tachogenerators

Automatic-control systems and computing machines often incorporate induction tachogenerators which are similar in design to induction servo motors with a hollow nonmagnetic rotor (see Fig. 2.25).

The circuit diagram of an induction tachogenerator is shown on Fig. 3.5*a*. A field voltage $\dot{V}_{FW}$ constant in amplitude and frequency is applied to the stator winding FW. The other stator winding GW is the generator winding from whose terminals an output signal $\dot{V}_{GW}$ is picked off. This winding is generally shorted out through an external load impedance Z_{load}.

The operating principle of an induction tachogenerator can be best understood upon studying the equivalent circuit diagram of Fig. 3.5*b*. To facilitate qualitative analysis, the hollow rotor on the diagram is replaced by a final number of turns short-circuited at the ends, and the external circuit of winding GW is open. While the rotor is motion-

less, the tachogenerator may be treated as a transformer whose primary is the stator winding *FW* and secondary is the rotor winding. Magnetic flux due to the mmf of the *FW* cuts the rotor and induces in its turns a transformer emf $\dot{E}_{tr}$ (arbitrarily shown on the internal circle of turns). Since the rotor is short-circuited, these turns will carry current $\dot{I}_{tr}$ and a magnetic flux will be set up. This flux will oppose the magnetic flux due to the *FW* winding according to the Lenz rule. Hence, a resultant flux $\dot{\Phi}_f$ pulsating at a field voltage frequency f will be set up along the *FW* axis. When this is the case, the emf $\dot{E}_g$ in the generator winding is zero since the vector of the flux $\dot{\Phi}_f$ is normal to the axis of this winding.

Rotating the tachogenerator rotor at an angular speed ω_2 will not bring any changes in the process and the transformer emf $\dot{E}_{tr}$ will be induced in the same way since the rotor is balanced. As in the former case, the magnetic flux $\dot{\Phi}_f$ will be pulsating along the *B* axis. This flux may be considered to a first approximation as independent of the rotor speed. The rotor winding turns revolve in the field set up by this flux and a rotating emf $\dot{E}_{rot}$ is induced in them (this emf is arbitrarily shown on the outer circle of turns). As is known from the theory of direct-current machines, the resultant rotating

Fig. 3.5. Induction tachogenerator. Circuit diagram

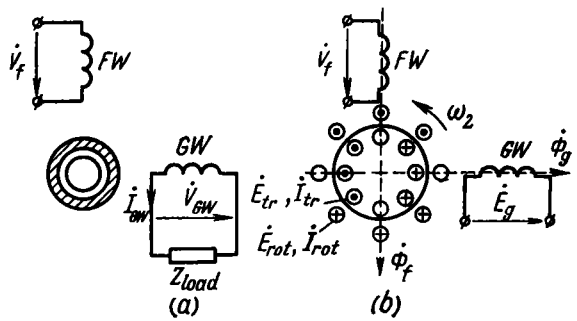

emf of the rotor winding

$$\dot{E}_{rot} = k\omega_2\dot{\Phi}_f \tag{3.21}$$

where k is factor depending on design characteristics of the machine.

From Eq. (3.21), at $\dot{\Phi}_f$ = const the emf E_{rot} is a linear function of the rotor speed and pulsates at a field voltage frequency f. The rotating emf causes a current $\dot{I}_{rot}$ to flow through the rotor winding. The direction of the flux $\dot{\Phi}_g$ produced by this current is along the axis of the generator winding GW in accordance with the right-hand screw rule. Since the magnitude of the current $\dot{I}_{rot}$ is directly proportional to that of the emf $\dot{E}_{rot}$, the flux $\dot{\Phi}_g$ produced by this current is directly proportional in magnitude to the rotor speed ω_2.

The flux $\dot{\Phi}_g$ pulsates at the same ripple frequency as the emf $\dot{E}_{rot}$ and the supply voltage. It induces in the generator winding of the stator a transformer emf $\dot{E}_g$ whose rms value can be found from the equation

$$\dot{E}_g = 4.44\, k_{GW} w_{GW} f \Phi_g \tag{3.22}$$

where w_{GW} is number of turns of the winding GW; k_{GW} is winding factor of the GW winding.

The output emf $\dot{E}_g$ pulsates at the same frequency f as the flux $\dot{\Phi}_g$ and the field voltage. This frequency is independent of the rotor speed ω_2, which makes it possible to use induction tachogenerators in systems operating at a constant frequency.

Since the $\dot{\Phi}_g$ is proportional to the rotor speed

$$\Phi_g = k_1\omega_2$$

equation (3.22) will be transformed as follows:

$$E_g = k_g\omega_2 = k_g \frac{d\theta}{dt} \tag{3.23}$$

where $k_g = 4.44 k_{GW} w_{GW} f k_1$; k_1 is factor depending on design characteristics and field voltage of the tachogenerator.

Upon the analysis of Eq. (3.23) we may come to the conclusion that the tachogenerator rotor output emf E_g is directly proportional to its rotor speed. On the assumption that the field flux Φ_f is independent of the rotor speed ω_2, we can state that the $E_g = f(\omega_2)$ relationship is a linear function.

In actual tachogenerators, however, the flux $\dot{\Phi}_f$ slightly reduces at an increase in the rotor speed ω_2 due to an additional rotating emf $\dot{E}_{rot\ add}$ induced in the revolving turns of the rotor winding by the flux $\dot{\Phi}_g$. The additional emf is cumulative with the transformer emf $\dot{E}_{tr}$. Since the flux $\dot{\Phi}_g$ is proportional in magnitude to the rotor speed ω_2, the $\dot{E}_{rot\ add}$ will be proportional to the square of ω_2. Hence, the current and flux produced by this emf will reduce the flux $\dot{\Phi}_f$ at a higher speed in a nonlinear manner. The no-load output characteristic of an induction tachogenerator $\dot{E}_g = f(\omega_2)$ deviates from the linear shape, causing an amplitude velocity error. (The quantitative analysis of this error is given in deriving the general output characteristic equation for an induction tachogenerator.)

When the stator winding *GW* is closed to an external load impedance Z_{load}, it carries a current $\dot{I}_{GW}$. The flux $\dot{\Phi}_g$ is produced by the vector sum of the mmfs of the rotor and the stator winding *GW*, which changes the magnitude of the emf $\dot{E}_g$. Besides, the output voltage $\dot{V}_g$ proper is determined by the vector difference of the emf $\dot{E}_g$ and the voltage drop across the winding impedance Z_{GWs}:

$$\dot{V}_{GW} = \dot{E}_g - \dot{I}_{GW} Z_{GWs} \qquad (3.24)$$

These physical processes determine the type of the tachogenerator on-load output characteristic.

From the analysis of the induction tachogenerator output characteristic we see that the output voltage $\dot{V}_{GW}$ can be found by using the procedure of Section 2.6 for a two-phase

induction motor since an induction tachogenerator is similar in design to an induction servo motor and the electrical machines are convertible.

The equivalent circuits of the *FW* phase of a servo motor (see Fig. 2.30) are valid for the *GW* phase of an induction tachogenerator, provided an impedance Z_{load} is inserted in the stator circuit of the latter and the input terminals are short-circuited. The equivalent circuits of the *FW* phase of a tachogenerator are similar to those of the motor *FW* phase. All the characteristics of the tachogenerator *GW* phase are referred to the number of turns of the stator field winding *FW*.

The tachogenerator output voltage is the voltage across the impedance Z_{load} in the *GW* phase:

$$\dot{V}_{GW} = \dot{I}_{GW} Z_{load} \tag{3.25}$$

The current $\dot{I}_{GW}$ can be expressed through symmetrical components $\dot{I}_{GW1}$ and $\dot{I}_{GW2}$. In the reduced form,

$$\dot{I}'_{GW} = \frac{1}{k_{tr}} \dot{I}_{GW} = \dot{I}'_{GW1} + \dot{I}'_{GW2} \tag{3.26}$$

where the transformation ratio of the *FW* and *GW*

$$k_{tr} = \frac{w_{FW} k_{FW}}{w_{GW} k_{GW}}$$

According to the method of symmetrical components, the forward and backward components of the tachogenerator field current can be defined as $\dot{I}'_{GW1}$ and $\dot{I}'_{GW2}$:

$$\dot{I}_{FW1} = j\dot{I}'_{GW1}; \quad \dot{I}_{FW2} = -j\dot{I}'_{GW2} \tag{3.27}$$

Since voltages applied to the *FW* and *GW* of the tachogenerator are balanced out by the voltage drops across the impedances of the respective equivalent circuits caused by the symmetrical current components, we have, in accordance with the Kirchhoff's second law and with due allowance for the zero voltage across the *GW*:

$$\begin{aligned} 0 &= \dot{I}'_{GW1} (Z'_{GW1} + Z_{load}) + \dot{I}'_{GW2} (Z'_{GW2} + Z'_{load}) \\ \dot{V}_{FW} &= \dot{I}_{FW1} Z_{FW1} + \dot{I}_{FW2} Z_{FW2} \end{aligned} \tag{3.28}$$

where Z'_{GW1} and Z'_{GW2} are equivalent impedances of the GW phase equivalent circuit for the forward and backward sequencies ($Z_{GW} = k_{tr}^2 Z_{GW}$); $Z'_{load} = k_{tr}^2 Z_{load}$ is equivalent load impedance. Solve the set of equations (3.28) with respect to $\dot{I}'_{GW1}$ and $\dot{I}_{GW2}$ taking into account Eq. (3.27). Substitute the symmetrical component expressions in Eq. (3.26) and then in Eq. (3.25) to define the expression for the output voltage $\dot{V}_{GW}$ of a tachogenerator through the rotor speed, equivalent circuit parameters, and field voltage:

$$\dot{V}_{GW} = \frac{j\dot{V}_{FW} k_{tr} \omega_2^{\partial}}{\dot{A} - (\omega_2^{\partial})\,\dot{B}} \qquad (3.29a)$$

where $\dot{A}$ and $\dot{B}$ are complex constants depending on the equivalent circuit parameters and on the load.

Disregarding the inductive reactance of the rotor, which is much lower than the resistance in induction tachogenerators, especially in those with a hollow nonmagnetic rotor, we shall have

$$\left.\begin{aligned} \dot{A} &= \frac{1}{Z'_{load}}\left(\frac{Z_{FWs}^2 C_{FWr}^2}{R'_{FWr}} + 2Z_{FWs}C_{FWr} + R'_{FWr}\right) + \\ &+ \frac{Z_{FWs}C_{FWr}^2}{R'_{FWr}} + C_{FWr}; \\ \dot{B} &= \frac{Z_{FWs}}{R'_{FWr}}\left(\frac{Z_{FWs}}{Z'_{load}} + 1\right) \end{aligned}\right\} \qquad (3.30)$$

where $C_{FWr} = \dfrac{Z_{FWm} + R'_{FWr}}{Z_{FWm}}$

(for designations refer to Fig. 2.30).

The relative rotor speed

$$\omega_2^{\partial} = \frac{\omega_2}{\omega_1} = 1 - s$$

where ω_1 is synchronous speed (for tachogenerators it is a conditional speed).

Equation (3.29a) relates to the output characteristic of an induction tachogenerator. The square of relative speed $(\omega_2^{\partial})^2$ in the denominator of this equation points to nonlinearity of the output characteristic and to tachogenerator phase error (velocity error).

For an ideal tachogenerator free from amplitude and phase errors, the output characteristic equation is derived from Eq. (3.29*a*) allowing for the fact that $(\omega_2^{\partial})^2 \times B = 0$:

$$\dot{V}_{GW\ id} = \frac{j\dot{V}_{FW} k_{tr} \omega_2^{\partial}}{\dot{A}} \qquad (3.29b)$$

The rated amplitude error of a tachogenerator is defined as the difference of voltage modules according to equations (3.29*a*) and (3.29*b*):

$$\Delta V = \frac{V_{GW\ id} - V_{GW}}{V_{GW\ id}} \approx - \left| \frac{\dot{B}}{\dot{A}} \right| (\omega_2^{\partial})^2 \qquad (3.31)$$

The phase error is defined as the difference of arguments of these voltages.

As can be understood from equations (3.30) and (3.31), the amplitude error reduces at an increase in the rotor resistance because $|\dot{A}|$ rises and $|\dot{B}|$ diminishes. That is why the tachogenerator rotors are usually manufactured from phosphor bronze whose resistivity is approximately twice as high as that of aluminium. It should be borne in mind, however, that an increase in the rotor resistance causes a decrease in the tachogenerator voltage gain because the $\dot{A}$ constant grows (see Eq. 3.29*a*).

Besides, the tachogenerator speed must be high enough to ensure that the relative value of speed being measured will not exceed 0.2 or 0.3. In our case, the $(\omega_2^{\partial})^2$ term is small and the output characteristic on the working portion $\omega_2^{\partial} =$ $= 0\text{-}0.3$ is almost linear. Therefore, tachogenerators are often made for operation on high-frequency supply. The synchronous speed rises with frequency thereby causing a reduction in the relative value of speed under measurement.

The curves of Fig. 3.6*a* are output characteristics plotted with referen e to Eq. (3.29*a*) in terms of relative units ($V_{GW}^{\partial} = V_{GW}/V_{FW}$).

The effect of external load on the amplitude and phase error of a tachogenerator depends on the type of load. A purely capacitive load brings in the least amplitude error ΔV, and an inductive load causes the least phase error $\Delta\beta$ (Fig. 3.7).

The tachogenerator steady-state gain can be found according to Eq. (3.29*a*):

$$k_g = \frac{dV_{GW}}{d\omega_2} = \frac{V_{FW} k_{tr}}{\omega_1} \left| \frac{\dot{A} + (\omega_2^\partial)^2 \dot{B}}{[\dot{A} - (\omega_2^\partial)^2 \dot{B}]^2} \right| \qquad (3.32)$$

Modern tachogenerators have a gain ranging between 1 and 10 mV per r/min at $Z_{load} \gg Z_{GWs}$.

The k_g value is practically constant at $\omega_2^\partial = 0$ to 0.3 and goes down nonlinearly at $\omega_2^\partial > 0.3$ (Fig. 3.6*b*).

A change in the output voltage and steady-state gain under the effect of variations in the magnitude and type of external load is determined by the variation in the $\dot{A}$ and $\dot{B}$ complex constants in equations (3.29*a*) and (3.32). Figure 3.8 exhibits this relationship.

A physical substantiation of the functions

$$V_{GW}^\partial,\ k_g = f(X_{C\,load},\ X_{L\,load},\ R_{load})$$

where $X_{C\,load}$, $X_{L\,load}$, and R_{load} are, respectively, capacitive and inductive reactances and resistance of the load, has been already given in the discussion of the tachogenerator operating principle. The only thing to be noted here is that voltage resonance occurs at a certain capacitive reactance in the case of a capacitive load.

Fig. 3.6. Output characteristics and steady-state gain of induction tachogenerator (ideal linear characteristics are shown by dash lines)

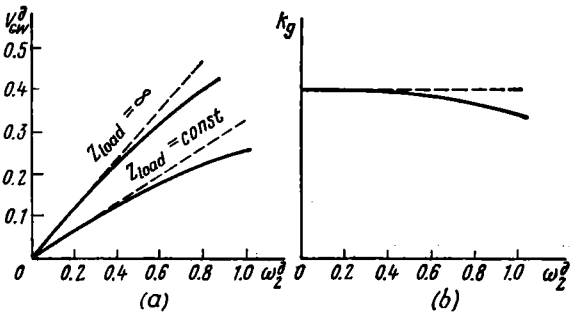

The analysis of Figs. 3.7*a* and 3.8 shows that a capacitive load should be added to an external resistive load in order to reduce the amplitude velocity error and the effect of load on the k_g value.

The resistive/capacitive load, however, will raise the tachogenerator phase error (Fig. 3.7*b*). At the same time, the effect of the load magnitude on phase error rises. Figure 3.9 shows the output voltage phase (angle β between the $\dot{V}_{FW}$ and $\dot{V}_{GW}$ vectors) as a function of the magnitude and type of load.

From the analysis of the curves illustrated by Figs. 3.7*b* and 3.9 it can be easily understood that the best way to reduce the phase velocity error and the effect of load magnitude on the output voltage phase is to insert an inductive reactance in the external resistive load. Thus, the conditions of load compounding for reducing amplitude and phase errors are conflicting. Therefore, in compounding an external load, it is reasonable to add the quantity whose constancy is essential for the given circuit.

The temperature of a running tachogenerator may appreciably affect the accuracy of the machine. This takes place as a result of variations in the machine resistances, particularly in the rotor resistance which is much higher than the stator resistance. An increase in the rotor resistance due

Fig. 3.7. Amplitude and phase errors versus speed at different types of load

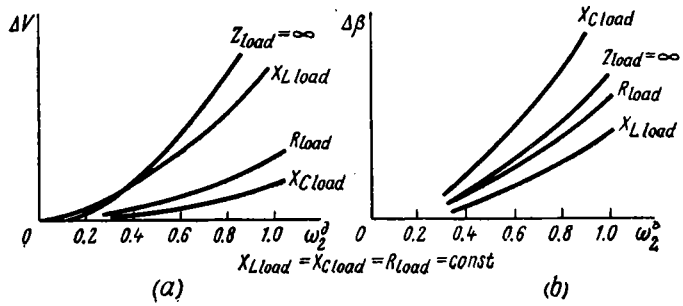

to heating causes a reduction of the output characteristic steepness, which brings in a temperature amplitude and phase error. To prevent this error, the material used for manufacturing the rotors of precision induction tachogenerators must have a low coefficient of temperature expansion, and, besides, expansion devices must be inserted.

A no-voltage signal is another error occurring in induction tachogenerators due to residual emf $\dot{E}_{GW\,0}$ in the generator winding with a stalled rotor. The residual emf is the result of improper processing of the tachogenerator; it comprises two components, *viz.*, a d.c. component independent of the angular position of the rotor and an a.c. component varying at a double frequency (in electrical degrees) as the rotor turns through a certain angle.

A transformer coupling may set up between the stator windings if they are spaced apart by an angle other than 90 deg. A rotating excitation field is built up due to unequal magnetic properties of the stator magnetic circuit components, which is caused by short-circuited turns and stampings, and unequal permeance of stampings in different directions, which still remains though the stacks are assembled in a fanned manner. In either case a d.c. component of residual emf is induced in the *GW* generator winding that is shifted in phase by a certain angle relative to the field voltage $\dot{V}_{FW}$.

Fig. 3.8. Output voltage and steady-state gain as functions of load magnitude and type

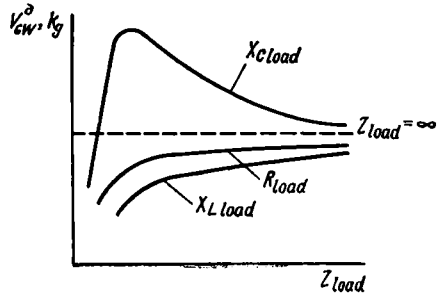

An electrical unbalance of the rotor caused by a nonuniform thickness of its walls or eccentricity causes an a.c. component of residual emf. An unbalanced rotor may be considered as a combination of a balanced rotor and a short-circuited turn outside the balanced system (Fig. 3.10*a*). The magnetic flux $\dot{\Phi}_f$ induces in the short-circuited turn a transformer emf and a current, with the result that a pulsating flux $\dot{\Phi}_{sc}$ of the short-circuited turn is set up. This flux is linked with the generator winding *GW* and induces in the latter an emf $\dot{E}_{GW\ 0}$. The maximum value of this emf is when the turn is positioned at an angle of 45 deg. to the stator winding axes and varies in accordance with the rotor angle of turn.

The residual emf causes a displacement of the output characteristic from the origin of coordinates. Hence, additional variable amplitude and phase errors appear, especially at low speeds. This is illustrated by the vector diagram of Fig. 3.10*b* where the resultant vector of the output emf $\dot{E}_{GW\,r}$ equals the vector sum of the emf $\dot{E}_{GW\ 0}$ that is independent of the rotor speed and the emf $\dot{E}_{GW}$ that varies in proportion to the rotor speed.

The residual voltage also causes asymmetry of output voltage. In the ideal case, the output emf must remain constant

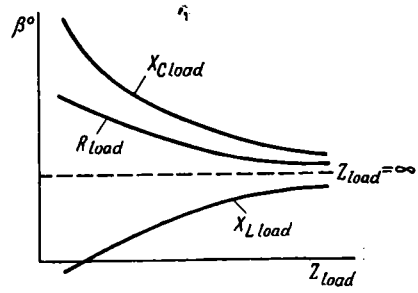

Fig. 3.9. Output voltage phase as function of load magnitude and type

in magnitude and opposite in phase when the rotor reverses its sense of rotation. The emf $\dot{E}_{GW\,0}$ violates both these conditions (vectors $\dot{E}_{GWr1}$ and $\dot{E}'_{GWr1}$ on Fig. 3.10*b*).

The d.c. component of residual emf can be considerably reduced by placing the *FW* and *GW* windings separately on an external and an internal stator. To this end, after the tachogenerator is manufactured, a voltage is applied to the *FW* winding while the rotor is motionless and the internal stator is turned relative to the external stator until a minimum no-voltage signal is obtained in the *GW*.

Whenever an a.c. component of residual emf is to be reduced, the rotor must be electrically balanced. For this, the rotor is additionally machined to remove unnecessary material from its respective surfaces. It should also be borne in mind that the effect of the stator and rotor unbalance in multipole machines is not so great.

An essential advantage of induction tachogenerators, as compared with d.c. tachogenerators, is the absence of sliding contacts, which makes these machines remarkably trouble-free. The machines are simple in design and do not

Fig. 3.10. Equivalent circuit diagram of unbalanced rotor and emf vector diagram of induction tachogenerator

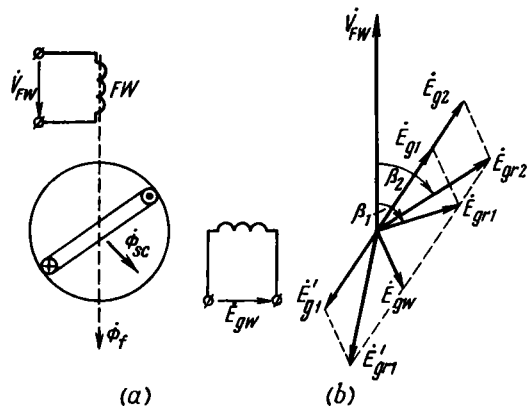

produce radio noise. The drawbacks of induction tachogenerators are worse linearity of the output characteristic, lower gain, phase error, and variation of output voltage depending on the type of load applied.

The tachogenerator accuracy is estimated by three parameters, *viz.*, output characteristic nonlinearity, residual emf, and phase error. The accuracy class is established by the worst values of these parameters within the speed range from 0.1 of rated to the rated value. Permissible nonlinearity of the output characteristic for different classes of tachogenerators ranges from 0.02 to 1 per cent (see Section 3.2).

An induction tachogenerator can be employed as an angular acceleration transmitter (accelerometer). Its field winding *FW* (Fig. 3.5*a* and *b*) must be connected to d.c. supply. The flux Φ_f will then be continuous and not pulsating. When the rotor revolves at a constant speed, the flux Φ_g will also be continuous. The emf in the generator winding *GW* will be zero. As soon as an angular acceleration appears, the rotor emf E_{rot} will start changing causing a change in the current I_{rot} and in the flux Φ_g. A change in the Φ_g with time will be more sudden at a higher acceleration of the rotor. The flux $\Phi_g(t)$ that varies with time will induce an emf in the generator winding as if it were a transformer secondary winding. As is known, the emf magnitude depends on the rate of change of magnetic flux:

$$e_g = \frac{d\Phi_g(t)}{dt} w_g k_{GW} \tag{3.33}$$

Since the rate of change of the flux is proportional to the rotor angular acceleration,

$$\frac{d\Phi_g(t)}{dt} = c\frac{d\omega_2}{dt} \tag{3.34}$$

where c is proportionality factor, then the generator winding emf is also proportional to the rotor acceleration

$$e_g = \frac{d\omega_2}{dt} c w_g k_{GW} \tag{3.35}$$

3.4. Alternating-Current Synchronous Tachogenerators

Alternating-current synchronous tachogenerators depending for their operation on the synchronous generator principle have not found application in a.c. constant-frequency automatic-control systems as their output emf frequency is the function of the rotor speed. They are mainly used to directly measure the speed of controlled equipment. When this is the case, the output winding of the tachogenerator is connected to a voltmeter calibrated in terms of angular velocity.

At present, inductor-type synchronous tachogenerators using a semiconductor rectifier at the output have found application. An inductor tachogenerator is similar in design to an inductor-type reducing synchronous motor (see Section 2.11, Fig. 2.64). The stator-to-rotor tooth ratio Z_s/Z_r usually equals the number of phases of the stator winding which functions as an a.c. output winding. With the rotor running at a speed ω, a unipolar magnetizing flux Φ_m is modulated due to a toothed surface of the stator and rotor (see Fig. 2.65). An a.c. component of the flux Φ_{ac} that depends on the tachogenerator design, induces in each phase of the stator winding a no-load emf

$$E_{out} = 4.44 f \Phi_{ac} w k_w \tag{3.36}$$

where wk_w is effective number of turns per phase; $f = Z_r\omega/2\pi$ is emf frequency.

Hence, the no-load emf is directly proportional to the rotor speed which is the main requirement for running an electrical machine as a tachogenerator. However, when such a tachogenerator is loaded with a terminal impedance, its output characteristic becomes nonlinear. The first reason is that

$$\dot{V}_{out} = \dot{E}_{out} - \dot{I}_{out} Z_{out} = \frac{\dot{E}_{out}}{1 + Z_{out}/Z_{load}} \tag{3.37}$$

where the reactive components of the winding impedance Z_{out} and load impedance Z_{load} vary as functions of frequency f and, consequently, as functions of speed ω. The

other reason is the effect of the armature reaction flux (output winding flux) on the emf $\dot{E}_{out}$ proper.

The output voltage of inductor-type synchronous tachogenerators is rectified by semiconductor rectifiers so as to make it possible to use these tachogenerators in d.c. servo systems. Since a great number of rotor teeth can be built, the output voltage ripple frequency will be sufficiently high. Now high-frequency ripples can be easily eliminated by means of *LC* filters.This is the main advantage of inductor tachogenerators distinguishing them from commutator d.c. tachogenerators, with added advantage of higher reliability due to the absence of commutator and brushes.

3.5. Dynamic Characteristics of Tachogenerators

In the study of the dynamic properties of d.c. tachogenerators at transients, armature reaction and voltage drop across the brush contact are disregarded. The equation of emf and armature circuit voltage balance that obeys Kirchhoff's second law (Fig. 3.1*a*) is as follows:

$$E_A = i_A (R_A + R_{load}) + L_A \frac{di_A}{dt} \tag{3.38}$$

where i_A is instantaneous value of armature current; L_A is armature winding inductance.

By solving Eq. (3.38) together with Eq. (3.2) we shall obtain a differential equation showing variation of the armature current with the rotor angle of turn θ

$$\frac{L_A}{R_A + R_{load}} \cdot \frac{di_A}{dt} + i_A = \frac{k_E}{R_A + R_{load}} \cdot \frac{d\theta}{dt} \tag{3.39}$$

Transform equation (3.39) taking into account that $v = i_A R_{load}$:

$$\tau_{em} \frac{dv}{dt} + v = k_g \frac{d\theta}{dt} \tag{3.40}$$

where $\tau_{em} = L_A / (R_A + R_{load})$ is electromagnetic time constant of the armature circuit; k_g is steady-state voltage gain (see Eq. 3.13).

Upon the solution of differential equation (3.40) we shall obtain a transient characteristic equation:

$$v = \frac{k_g \theta_c}{\tau_{em}} \exp\left(-\frac{t}{\tau_{em}}\right) \tag{3.41}$$

The transient characteristic is illustrated by Fig. 3.11*a* where θ_c is steady-state value of the rotor angle of turn.

The tachogenerator transfer function derived from Eq. (3.40)

$$W(p) = \frac{v}{\theta} = \frac{k_g p}{\tau_{em} p + 1} \tag{3.42}$$

As is seen from equations (3.42) and (3.40) and from Fig. 3.11*a*, the tachogenerator is an inertial differentiating element that performs differentiation with a certain degree of distortion determined by the value of the time constant τ_{em}. If a tachogenerator is meant for differentiating without distortions, its time constant must be minimized so as to make the tachogenerator an almost inertialess differentiating component. The function of such an ideal tachogenerator is defined by the following equation:

$$v = k_g \frac{d\theta}{dt} \tag{3.43}$$

Fig. 3.11. Tachogenerator transient characteristics

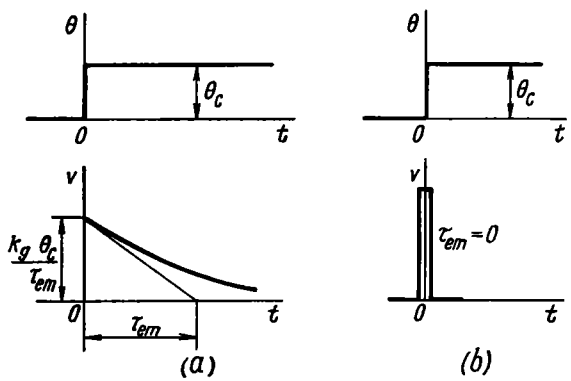

The transient characteristic of such a tachogenerator is shown by Fig. 3.11*b*. The electromagnetic time constant τ_{em} can be considerably reduced by using d.c. machines with a hollow nonmagnetic rotor (armature) or a disk rotor whose armature winding inductance is very low, as has been already pointed out.

If the rotor sped ($\omega = d\theta/dt$) is treated as an input signal of a tachogenerator, the transfer function will be

$$W(p) = \frac{v}{\omega} = \frac{k_g}{\tau_{em}p + 1} \tag{3.44}$$

When this is the case, the tachogenerator functions as an aperiodic first order component.

A similar study of dynamic characteristics can be carried out for an induction tachogenerator. The rotor resistance of this tachogenerator is much higher than the stator generator winding resistance at the machine output. The electromagnetic time constant of the rotor winding is much shorter than that of the stator generator winding and can be disregarded in the analysis of transient processes. The dynamic properties of a resistance-loaded induction tachogenerator will then be defined by equations (3.40) through (3.44) with due considerations given to electromagnetic transients occurring in a.c. circuits.

The rotating parts of the tachogenerator impart an additional moment of inertia to associated servo motors. So, to reduce the electromechanical time constant of the servo motor-tachogenerator shaft line, and hence to increase its response, tachogenerators should employ rotors in the form of a hollow sleeve or a disk having a low moment of inertia.

3.6. Application of Tachogenerators

The tachogenerators are classified according to their application as follows:

(1) tachogenerators functioning as speed counters. Used as such may be d.c. or a.c. tachogenerators of any accuracy class;

(2) tachogenerators function as feedback accelerating or retarding signal transmitters in automatic control systems and as speed regulation system elements. For this purpose

use can be made of d.c. and induction tachogenerator having an accuracy class of 0.5 to 1;

(3) tachogenerators functioning as automatic computer elements for differentiating and integrating different functions. For this purpose use shall be made of tachogenerators of the highest accuracy class of 0.05 to 0.2.

Some examples of the use of tachogenerators in radio equipment, automatic computers, and some other units and devices are given below.

3.6.1. Tachogenerator Functioning as a Speed Counter

Figure 3.12 illustrates a circuit arrangement of a machine for annealing spiralized tungsten wire used for spiral heaters of radio valves. The wire to be annealed is reeled off the brake and passed through a hydrogen furnace wherein it is heated to the desired temperature as electric current flows through it. The wire reeling and laying gear is driven by a d.c. motor, type П11. The wire speed is controlled by

Fig. 3.12. Wire annealing installation. Schematic diagram

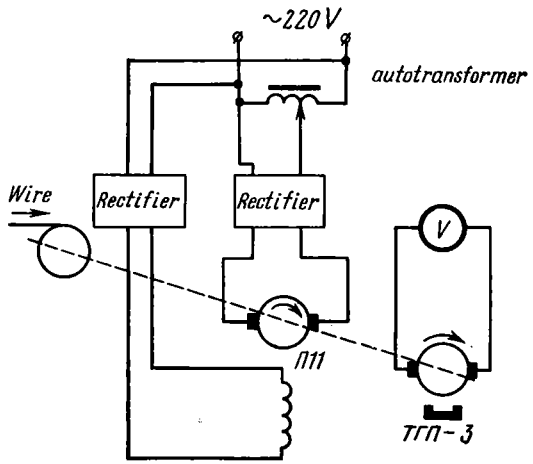

varying the armature terminal voltage of the drive motor П11 with the aid of a laboratory autotransformer.

One of the factors determining the quality of annealing is the wire speed in hydrogen. The machine incorporates a type ТГП-3 d.c. tachogenerator to provide for a continuous check of this speed. The tachogenerator armature is mechanically coupled with the shaft of the П11 drive motor. The tachogenerator output voltage is applied to a d.c. voltmeter V calibrated in terms of linear speed. The operator can always check the wire speed and adjust it whenever required.

3.6.2. Tachogenerator Functioning as a Speed Regulation System Element

Discussed below is the operation of a radar aerial spinning drive running at a constant speed. The drive system (Fig. 3.13) comprises a d.c. servo motor SM_{dc} using armature control and affording a spinning motion for the aerial A, an induction tachogenerator ITG mechanically coupled with the SM_{dc} shaft, an electronic amplifier EA, and an amplidyne. The driving element is a voltage divider R that is supplied with power from an a.c. source.

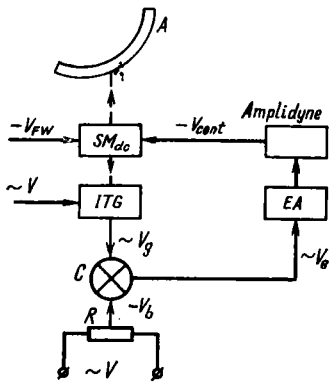

Fig. 3.13. Block-diagram of radar antenna drive

The drive system operates as follows. The desired speed is governed by the respective value of the reference voltage V_r which is delivered to the EA input via a comparison unit C. A control voltage V_{cont} passed through the EA and the amplidyne is applied to the control winding of the servo motor whose field winding is permanently connected to a voltage source V_f. The motor rotor starts running and turns the aerial A and the ITG rotor. The tachogenerator output voltage V_g is compared in the C with the reference voltage V_r and a constant value of V_{cont} determined by the error voltage V_e is set across the amplifier stage output. The SM_{dc} rotor and the aerial revolve continuously at a constant speed.

The reference and tachogenerator voltages (V_r and V_g, respectively) are phased out so that any increase in the tachogenerator voltage causes a decrease of the error voltage V_e. Hence, any variation in the SM_{dc} rotor and the aerial speed will cause such a change of the voltage V_g and V_e, and consequently V_{cont}, that the speed will tend to retain the original value. So, a tachogenerator inserted in a feedback circuit has made it possible to stabilize the aerial speed.

3.6.3. Tachogenerator Functioning as an Automatic Computer Element

Tachogenerators are used in differentiating, integrating, and smoothing electromechanical calculators. Such calculators are usually employed for transforming comparatively slow-varying functions when the inherent time constants of elements are negligible. The calculators of this class must incorporate a number of features that cannot be found in electric or electronic differentiators, integrators, and smoothing device built around RC or RL networks. These features are as follows:

(a) they must be capable of performing the required operation with high accuracy while the process goes on for a rather long period of time;

(b) angular displacements must be used directly as input signals;

(c) they must retain their characteristics at supply voltage fluctuations.

Figure 3.14 illustrates the block-diagram of a differentiator that meets the above-specified requirements. It consists of a driving element in the form of an induction tachogenerator *ITG*, a computing stage, a comparison unit *CU*, and a decoding servo system. The computing stage consists of a linear rotary transformer *LRT*, whose output voltage is directly proportional to the angle of turn of the rotor (for the *LRT* operating principle refer to Section 5.5), and a scaling element *SE* that matches the scales of the driving and computed rates. The servo system consists of an electronic amplifier *EA* and a servo motor *SM* with a reduction unit. The amplifier receives a signal from the comparison unit *CU* and the output voltage is fed to the *SM* control winding. The servo motor shaft is mechanically coupled with the *LRT* rotor.

When an independent variable X is introduced in the form of the angle of turn of the *ITG* rotor, the tachogenerator output yields a voltage $V_1 pX$ that is proportional to supply voltage and to the tachogenerator rotor speed pX. The out-

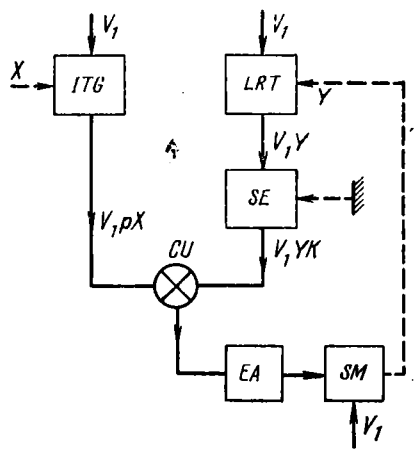

Fig. 3.14. Block-diagram of a differentiator incorporating induction tachogenerator

put voltage of the computing stage is V_1YK, where Y is angle of turn of the LRT rotor; K is the scale of the SE. When the voltages V_1pX and V_1YK are not equal, the comparison unit yields an error voltage that arrives at the amplifier input. The amplified voltage is applied to the servo motor input and the motor turns the LRT rotor until the following equality is satisfied

$$V_1pX = V_1YK \tag{3.45}$$

The error voltage drops to zero and the angle is not computed any longer. From Eq. (3.45) we obtain

$$Y = \frac{1}{K}\, pX \tag{3.46}$$

where $1/K$ is the derivative scale.

Equation (3.46) shows that the angle of turn of the LRT rotor is automatically computed in proportion to the derivative of X.

Chapter

4 SYNCHROS

4.1. General Information and Classification

Synchros or *selsyns* are self-synchronizing electrical machines used as synchro transmitters and synchro receivers in induction synchro tie systems.

Induction synchro units function to transmit an angular displacement or a linear motion converted into an angular displacement over a certain distance by virtue of electrical interconnection between the master (angle transmitting) synchro and the receiving synchro. This electrical connection betwen the synchro transmitter and the synchro receiver is referred to as a data transmission line. The angular displacement is duplicated by this system synchronously, cophasally, and steplessly.

Synchros used in induction synchro systems are classified as three-phase power synchros and single-phase synchros.

Three-phase synchros are employed in electric shaft systems where a synchronous and cophasal rotation of two remote motors must be maintained. The synchro operates in such systems both as a transmitter and as a receiver.

Single-phase synchros can operate in two basic modes, *viz.*:

(a) *indicating mode*, when the transmitter is turned by force and the receiver reproduces its motion under the action of its inherent synchronizing torque;

(b) *transformer mode*, when the transmitter is turned by force and the receiver generates a voltage varying as a function of the mismatch (error) angle.

Each of the modes may employ one of the following systems:

(a) synchro transmitter-receiver composed of one transmitter and one receiver;

(b) multiple system composed of a transmitter and more than one receiver;

(c) differential system composed of two transmitters and a receiver.

A single-phase synchro can operate both as a transmitter and a receiver in the indicating and transformer mode. However, the mode of operation is specified at the manufacturing stage so as to utilize the unique features required for the particular application.

All the single-phase synchros must incorporate the following features:

(1) high static and dynamic accuracy. Static accuracy is defined by an angle transmission error at a slow turn, and dynamic accuracy by the same error at continuous rotation;

(2) ability of self-synchronizing within one revolution, that is, ability of the synchro system to assume only one stable matched position within a revolution;

(3) ability of self-synchronizing at very high speeds of rotation.

In order to meet these requirements, the synchros must develop maximum specific and synchronizing torques and have a minimum damping time for the receiver rotor. Synchro transformers must possess maximum possible specific output voltage at a preset load resistance and a minimum output resistance of the receiver.

The synchro must also meet the requirements of Section 0.2 in compliance with their operating conditions.

4.2. Mechanical Design of Single-Phase Synchros

Single-phase synchros may be of a slip-ring and a magnetic slip type, the latter being usually referred to as magslips.

The *slip-ring synchros* (Fig. 4.1*a*) consist of a stator and a rotor. The stator (or the rotor) carries a single-phase field-winding (*FW*) and the rotor (or the stator) mounts a synchronizing winding *SW*. These synchros are identical to synchronous machines with electromagnetic excitation.

The synchronizing winding of single-phase synchros is made as a three-phase winding composed of three star-connected windings spaced 120 deg. apart, the emfs induced in

this winding and the currents through its separate coils being in the same time phase. That is why the correct term for the synchronizing winding would be a star winding.

The synchronizing winding is always of the distributed type. The field winding can be built as a distributed or a concentrated winding. Since the torque characteristic in the case of a distributed winding is less steep, a concentrated field winding is preferred for synchro indicators.

The number of pole pairs for synchros should be unity ($p = 1$) so as to provide self-synchronizing within one revolution.

The field winding builds up a pulsating flux which passes through the synchro magnetic circuit, cuts the synchronizing winding branches and induces in them an emf varying with the rotor angle of turn. Since mutual inductance between the field winding and the synchronizing winding varies steplessly obeying the cosine law as the rotor turns through a certain angle, the emfs induced in the synchronizing winding branches will be proportional to the cosine of the rotor angle of turn.

Some synchros are fitted with a damping winding *DW* arranged perpendicular to the field winding.

Fig. 4.1. Slip-ring synchro

(*a*) circuit diagram (*b*) general arrangement *1*—stator; *2*—synchronizing winding; *3*—rotor; *4*—field winding; *5*—damping winding; *6*—slip rings

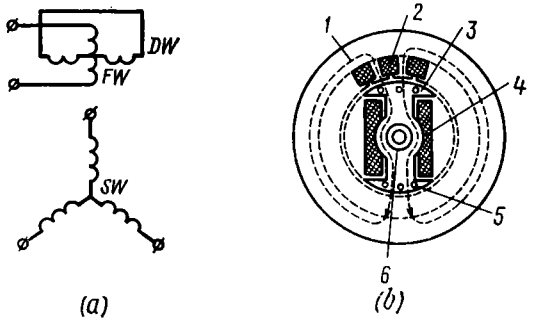

The synchro does not depend for its operation on whether a particular winding is placed on the stator or on the rotor. Most popular, however, are synchros having their field winding placed on the rotor and the synchronizing winding on the stator (Fig. 4.1*b*). These synchros require a less number of slip rings and brushes which makes them more reliable in operation, reduces their friction torque and size. The signal transmission circuit (data transmission line of the synchronizing winding) dispenses with sliding contacts. Such a construction facilitates mounting of a damping winding on the rotor.

Sliding contacts greatly reduce reliability of the slip-ring synchros. That is why magnetic-slip synchros (magslips) are more favoured today. Most popular among them are magslips with unipolar excitation of the rotor on the stator side and those with an intervening toroidal transformer.

In a *unipolar-excitation magslip* current is applied to the rotor through a magnetic flux and not through slip rings and brushes. Fig. 4.2 shows a general arrangement of such a magslip.

The stator carries a main stack *1* whose slots accommodate a three-phase synchronizing winding *2*. The field winding *3*

Fig. 4.2. General arrangement of a magslip with unipolar excitation

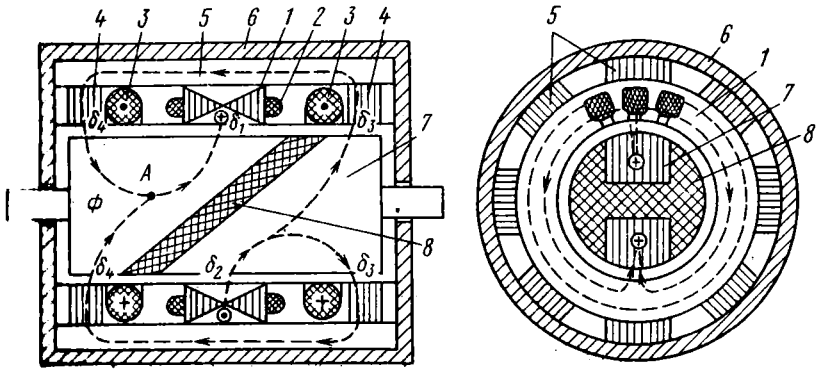

made in the form of two toroidal coils is also placed on the stator. Two toroidal cores *4* are arranged at the stator ends. Magnetic linkage betwen these cores is provided through the stacks of the external magnetic circuit *5*, which are press-fitted in a synchro barrel or frame *6*.

The main magnetic circuit and the toroidal cores are assembled of insulated electric steel stampings which are laminated along the transverse axis of the synchro. Each stamping has a radial cut to prevent it from forming a short-circuited turn on the path of the main field flux injected along the direct axis.

Uniform permeance in all directions is ensured by stacking the stampings in a fanning manner. The stacks of the external magnetic circuit are laminated along the direct axis of the synchro. The synchro rotor *7* consists of two stacks separated by a nonmagnetic barrier *8*. Each stack is built up of insulated electric steel stampings which are parallel to the direct axis of the synchro. The nonmagnetic barrier is usually made of a plastic material with the stampings of both the stacks press-fitted into it. The nonmagnetic barrier is sometimes made of silumin.

The operating principle of a magslip can be easily understood by following the path of the flux Φ.

Let the current flow through the field winding *3* as is shown on Fig. 4.2. Then the flux will be directed from left to right. Upon leaving point *A* it is stopped by the nonmagnetic barrier *8* which makes it change its direction and reach the stack of the magnetic circuit *1* through the air gap δ_1. Within this stack the flux covers a path of 180 deg. and passes to the right-hand stack of the rotor through the air gap δ_2. Then it goes through the air gap δ_3 and pierces the right-hand toroidal core *4*. Therefrom the flux passes over the stacks of the external magnetic circuit *5* to the left-hand toroidal core *4* and, having crossed the air gap δ_4, arrives at the left-hand stack of the rotor again, wherein it completes the loop at point *A*. While passing the main magnetic circuit *1*, the field flux comes in linkage with the synchronizing winding and induces an emf in this winding.

Turning the rotor also turns the flux, that is, the linkage between the synchronizing winding and the field flux obeys the same law as in slip-ring synchros. Hence, magslips func-

tion in synchro systems basically in the same way as slip-ring synchros.

From the comparison of the magnetic flux paths in magslips and slip-ring synchros (Figs. 4.1*b* and 4.2), it is evident that in a magslip the flux crosses twice as many air gaps as in a slip-ring synchro. A considerable portion of the field mmf is required to negotiate an air gap; so, for the same useful torque the field winding of magslips is made larger and heavier than that of slip-ring synchros. The magnetic circuit of magslips is also larger and heavier than that of slip-ring synchros.

Table 4.1

Parameter	БС-404	НС-404	БС-501	НС-501
Specific torque, N·m/deg	4×10^{-4}	10×10^{-4}	35×10^{-4}	50×10^{-4}
Mass per unit specific torque, kgf/(N·m/deg.) . .	3,000	800	1,140	570
Exciting power per unit specific torque, VA/(N × × m/deg.)	12.4×10^{4}	3.1×10^{4}	4.2×10^{4}	1.66×10^{4}

Table 4.1 gives some data on two types of magslips of the БС series and synchro receives of the НС series of comparable sizes wound for 50-Hz supply.

The exploded view of a type БС-404 magslip with unipolar excitation is shown on Fig. 4.3.

Magslips with intervening transformers consist of a rotating machine and a transformer, operating by virtue of electrical interconnection only (Fig. 4.4). The rotating machine is identical with a slip-ring synchro. The stator *1* carries a magnetizing winding *2*, and the rotor *3* accommodates a field winding *4* and sometimes a damping winding. The two-winding toroidal transformer incorporates a stator winding *5* wound on a ferromagnetic core *6* and a rotor winding *7* placed on a ferromagnetic core *8*. The windings are composed of concentrated coils whose magnetic axes coincide with the shaft rotation. The mutual inductance of the windings does not change with the rotor motion due to their concentric

arrangement. With a single-phase voltage applied to the stator winding terminals of the transformer, a secondary voltage constant in amplitude is picked off its rotor winding. This voltage is passed over conductors to the field winding of the rotating machine. In this way, sliding contacts are dispensed with.

A high exciting power of magslips, as compared to that of slip-ring synchros, is attained by virtue of a double transmission of energy through the air gap (in the transformer and in the rotating machine). The intervening transformer increases the magslip length.

Magslips are more complicated in design and more expensive, but their high reliability compensates these drawbacks.

Besides, magslips have a lower frictional torque on the shaft than slip-ring synchros.

Differential synchros are similar to single-phase slip-ring devices discussed above, the only difference being that they have star windings on the stator and rotor.

Fig. 4.3. Magslip with unipolar excitation. Exploded view
1—main stack; *2*—synchronizing winding; *3*—field winding; *4*—toroidal core; *5*—external magnetic circuit stacks; *6*—frame; *7*—rotor

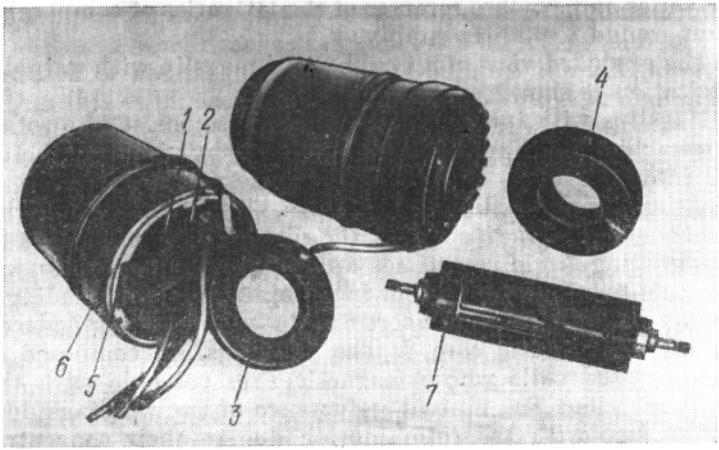

4.3. Synchro Indicators

Synchro indicators are most useful where information on the position of a control element, such as a valve, a throttle, etc., is to be transmitted over a certain distance, especially when control elements are located in dangerous-to-get-at places and their position is to be displayed on a control board. The synchro receiver of such a system must not develop a static torque on the shaft, and its rotor is connected only to the pointer indicating the angle being transmitted.

Synchro indicators usually comprise two synchros of the same type, one being a synchro transmitter (*ST*) and the other a synchro receiver (*SR*). Figure 4.5 illustrates the schematic diagram of single-phase synchros running as a synchro indicator. The field windings are connected to single-phase a.c. supply. The respective synchronizing windings are interconnected via a data transmission line.

The field windings of the synchro transmitter and synchro receiver set up identical pulsating fluxes $\dot{\Phi}_f$ in the magnetic systems of these synchros. When the magnetic circuit of the machine is not saturated and the flux density over the air gap follows the sine-wave law, the pulsating fluxes will cause emfs in the branches of the synchronizing windings. These

Fig. 4.4. Magslip with an intervening toroidal transfomer. General arrangement

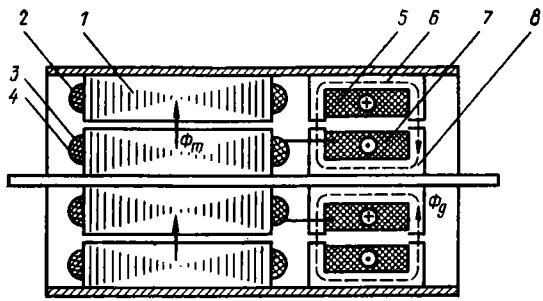

emfs vary depending on the cosine of the angle of turn of the rotors. For a synchro transmitter,

$$\left.\begin{aligned} \dot{E}_{t1} &= \dot{E}_{\max} \cos \theta_t \\ \dot{E}_{t2} &= \dot{E}_{\max} \cos (\theta_t - 120°) \\ \dot{E}_{t3} &= \dot{E}_{\max} \cos (\theta_t - 240°) \end{aligned}\right\} \qquad (4.1)$$

where θ_t is angle of turn of the synchro transmitter rotor from the matched position (the matched position is assumed to be that in which the synchro transmitter synchronizing winding branch, where emf $\dot{E}_{t1}$ is induced, is in alignment with the field winding); $\dot{E}_{\max}$ is maximum rms value of the emf in the synchronizing winding branch when the axis of the latter is aligned with the field winding axis; $\dot{E}_{t1}$, $\dot{E}_{t2}$, $\dot{E}_{t3}$ are the emfs of the respective branches of the synchro transmitter synchronizing winding.

In the same way, for a synchro receiver we have

$$\left.\begin{aligned} \dot{E}_{r1} &= \dot{E}_{\max} \cos \theta_r \\ \dot{E}_{r2} &= \dot{E}_{\max} \cos (\theta_r - 120°) \\ \dot{E}_{r3} &= \dot{E}_{\max} \cos (\theta_r - 240°) \end{aligned}\right\} \qquad (4.2)$$

Fig. 4.5. Single-phase synchro indicators. Schematic diagram

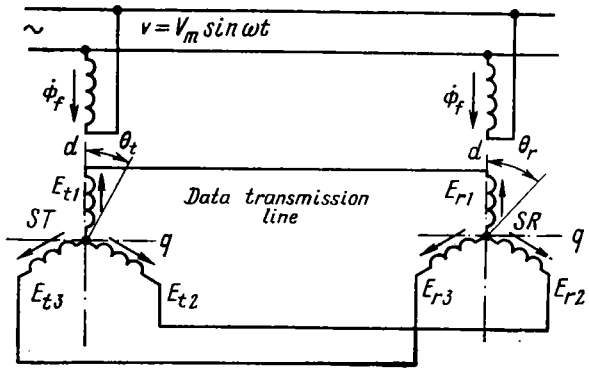

Since all the emfs of equations (4.1) and (4.2) have the same time phase (single-phase system) we shall further deal with scalar quantities instead of vectors.

The error angle is the difference between the angles of rotor turn of the synchro transmitter and synchro receiver:

$$\theta = \theta_t - \theta_r \tag{4.3}$$

When $\theta = 0$, that is, $\theta_t = \theta_r$,

$$E_{t1} = E_{r1}; \quad E_{t2} = E_{r2}; \quad E_{t3} = E_{r3}$$

The transmitter branch emf in the circuit is in opposition to the respective receiver branch emf, so the current through the data transmission line

$$I = \frac{E_t - E_r}{2Z} = 0 \tag{4.4}$$

where Z is branch impedance of one synchro.

In this case, the stator flux does not produce a torque on the rotor and the synchros are motionless.

At $\theta \neq 0$, emfs are produced between the respective branches of the synchro transmitter and receiver. These emfs are equal to the difference of the transmitter and receiver emfs. Let us designate these emfs through E_1, E_2, E_3, respectively. Then for $\theta_t \neq \theta_r$, taking into account equations (4.1) through (4.3), we shall have

$$\left.\begin{aligned} E_1 &= E_{t1} - E_{r1} = 2E_{\max} \sin\left(\theta_t - \frac{\theta}{2}\right) \sin\frac{\theta}{2} \\ E_2 &= E_{t2} - E_{r2} = 2E_{\max} \sin\left(\theta_t - 120° - \frac{\theta}{2}\right) \sin\frac{\theta}{2} \\ E_3 &= E_{t3} - E_{r3} = 2E_{\max} \sin\left(\theta_t + 120° - \frac{\theta}{2}\right) \sin\frac{\theta}{2} \end{aligned}\right\} \tag{4.5}$$

Find currents in the synchronizing windings and in the data transmission line disregarding the data transmission line impedances:

$$\left.\begin{aligned} I_1 &= \frac{E_1}{2Z} = I_{\max} \sin\left(\theta_t - \frac{\theta}{2}\right) \sin\frac{\theta}{2} \\ I_2 &= \frac{E_2}{2Z} = I_{\max} \sin\left(\theta_t - 120° - \frac{\theta}{2}\right) \sin\frac{\theta}{2} \\ I_3 &= \frac{E_3}{2Z} = I_{\max} \sin\left(\theta_t + 120° - \frac{\theta}{2}\right) \sin\frac{\theta}{2} \end{aligned}\right\} \tag{4.6}$$

where $I_{\max} = E_{\max}/Z$ is maximum rms current.

The currents carried by the synchronizing windings interact with the pulsating field fluxes and set up opposing torques on the transmitter and receiver. These torques tend to nullify the error angle θ.

Equations (4.6) confirm the self-synchronizing ability because currents in the synchronizing windings and torques caused by them are nullified simultaneously at $\theta = 0$.

In order to determine the synchronizing torque of synchro indicators, let us resolve the three-phase winding mmf into two components, one along the direct axis *d* coinciding with the field winding axis and the other along the quadrature axis *q* that is normal to the former.

The currents I_1, I_2, I_3 flowing in the synchronizing winding branches of the transmitter and receiver set up mmfs F_1, F_2, F_3 in the respective branches. The mmfs act along the axis of the respective windings. The direct component of the transmitter synchronizing winding mmf is

$$F_{td} = F_{t1}\cos\theta_t + F_{t2}\cos(\theta_t - 120°) + F_{t3}\cos(\theta_t + 120°) \tag{4.7}$$

The quadrature component of the transmitter synchronizing winding mmf is

$$F_{tq} = F_{t1}\sin\theta_t + F_{t2}\sin(\theta_t - 120°) + F_{t3}\sin(\theta_t + 120°) \tag{4.8}$$

The branch mmf of the transmitter or receiver synchronizing winding per two poles (double peak value of the mmf space wave fundamental) is

$$F = 1.8Iwk_w \tag{4.9}$$

where k_w is winding factor; w is number of turns in a synchronizing winding branch.

Substitute the mmf values of separate windings found from Eq. (4.9) in Eqs. (4.7) and (4.8), taking into account Eq. (4.6):

$$F_{td} = -\frac{3}{4}F_{\max}(1 - \cos\theta) \tag{4.10}$$

$$F_{tq} = \frac{3}{4}F_{\max}\sin\theta \tag{4.11}$$

where $F_{\max} = 1.8\ wk_wI_{\max}$.

For the receiver we have

$$F_{rd} = -\frac{3}{4} F_{\max} (1 - \cos\theta) \tag{4.12}$$

$$F_{rq} = -\frac{3}{4} F_{\max} \sin\theta \tag{4.13}$$

The direct component of the synchronizing winding mmf weakens the main field of the machine both in the transmitter and in the receiver, which is recognized by the minus sign in equations (4.10) and (4.12). The demagnetizing effect of the direct component is negligible, especially at small error angles. For example, at an error angle $\theta = 15$ deg., $F_{td} = F_{rd} = -\frac{3}{4} F_{\max} (1 - \cos 15°) = -0.026 F_{\max}$ that is, the demagnetizing effect of the direct component does not exceed 3% $F_{\max}$.

The total direct mmf of the synchro, $F_{\Sigma d}$, equals the sum of two mmfs, *viz.*, the field mmf F_f plus the synchronizing winding mmf F_d:

$$F_{\Sigma d} = F_f + F_d \tag{4.14}$$

The magnetic flux set up along the direct axis is

$$\Phi_d = F_{\Sigma d} \Lambda_d \tag{4.15}$$

where Λ_d is permeance along the d axis.

The quadrature component of the synchronizing winding mmf causes in the transmitter and in the receiver a quadrature reaction flux

$$\Phi_q = F_q \Lambda_q \tag{4.16}$$

where Λ_q is permeance along the q axis.

The synchronizing torque is mainly created due to the interaction between the flux Φ_d and the quadrature components of the synchronizing winding currents that produce the mmfs F_q.

Different signs in quadrature mmf equations (4.11) and (4.13) point to the fact that synchronizing torques of the transmitter and receiver oppose each other, which confirms the condition of self-synchronization within one revolution.

The instantaneous value of the synchronizing torque

$$T_s = c\varphi_d f_q = c\,[\Phi_d \sin \omega t F_{\max} \sin(\omega t - \psi) \sin\theta]$$
$$= \frac{1}{2} c\Phi_d F_{\max} \cos\psi \sin\theta$$
$$- \frac{1}{2} c\Phi_d F_{\max} \cos(2\omega t - \psi) \sin\theta \qquad (4.17)$$

where φ_d, f_q are instantaneous values of the flux Φ_d and mmf F_q; c is design factor; ψ is time shift angle between the vector of the flux Φ_d and that of the mmf $F_{\max}$.

Figure 4.6*a* exhibits the vector diagram of the synchronizing winding.

The average value of the synchronizing torque T_s equals the first term in the right-hand part of Eq. (4.17) as the average value of the second term within a period is zero.

Assuming that the time shift angle ψ, flux Φ_d, and mmf $F_{\max}$ are independent of the angle θ, we can write

$$T_s = T_{s\max} \sin\theta \qquad (4.18)$$

where

$$T_{s\max} = \frac{1}{2} c\Phi_d F_{\max} \cos\psi \qquad (4.19)$$

Fig. 4.6. Vector diagram of a synchronizing winding (*a*) and synchronizing torque curve (*b*)

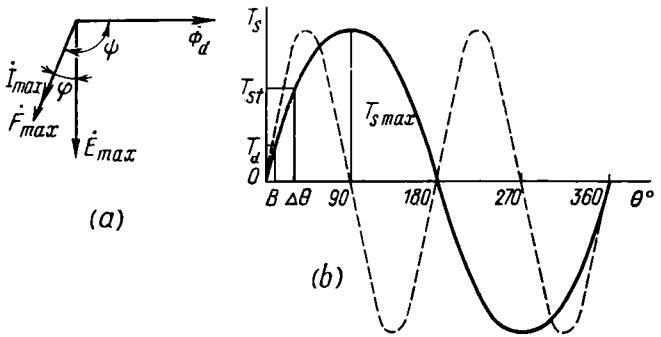

Figure 4.6*b* (solid line) exhibits the synchronizing torque T_s as a function of the error angle θ at $p = 1$.

As follows from Eq. (4.18), the $T_s = f(\theta)$ curve is a sinusoid. In actual synchros the $T_s = f(\theta)$ curve is not sinusoidal because the Φ_d and ψ quantities vary with θ, especially when error angles are great. The distortion of the curve is brought in by the demagnetizing action of the synchronizing winding mmf and by the dependence of the synchronizing winding parameters on the angle of turn. Moreover, an additional torque is set up due to the interaction between the flux Φ_q and the mmf F_d. It should be noted that the torque T_s is independent of the actual position of the transmitter and depends on the angle of turn only.

The synchronizing torque versus error angle curve shows that the synchro has two points of a matched position ($\theta = 0$; $\theta = 180$ deg.). In these points the torque is zero and this fact appears to be contradictory with the main property of synchros — their ability of self-synchronizing within one revolution. These positions, however, are not equivalent. One of them is a stable equilibrium position ($\theta = 0$) and the other is an unstable equilibrium position ($\theta = 180$ deg.). This fact can be exemplified by two magnets.

When a magnet is placed between the two poles of another magnet, the torque will be zero in two positions, *viz.*, (1) when one magnet faces the other by unlike poles (stable equilibrium) and (2) when one magnet faces the other by like poles (unstable equilibrium).

At a pole pair $p > 1$, the number of stable equilibrium points equals p (for example $\theta = 0$ and 180 deg. at $p = 2$; see the dash line on Fig. 4.6*b*) and angle transmission is ambiguous.

An important characteristic of synchros is specific synchronizing torque, that is a magnitude of synchronizing torque per degree of error angle at the origin of the characteristic. In other words, the specific synchronizing torque is the steepness of the initial portion of angular characteristic:

$$T_{sp} = \left(\frac{\Delta T_s}{\Delta\theta}\right)_{\theta \approx 0} \quad \text{or} \quad T_{sp} = \left(\frac{dT_s}{d\theta}\right)_{\theta=0} \qquad (4.20)$$

When transmitting and receiving units employ synchros of the same type, the specific synchronizing torque in

N·m/deg. can be found from the equation

$$T_{sp} = 20.8 \times 10^{-4} \frac{E_{\max} X_q}{f(X_q^2 + R_q^2)} \qquad (4.21)$$

where R_q and X_q are, respectively, quadrature-axis resistance and inductive reactance of the synchronizing winding; f is supply frequency.

Angle transmission in synchro indicators involves a certain amount of static angular error. Under no-load conditions, the error due to inherent friction torque T_f of the synchro receiver is the main error characterizing the receiver dead zone within which the receiver rotor is free to assume any position for the same position of the transmitter. The dead zone area in degrees is defined as a ratio of the synchro-receiver inherent-friction torque to the specific synchronizing torque (Fig. 4.6*b*):

$$B = T_f / T_{sp} \qquad (4.22)$$

and is inversely proportional to the specific torque magnitude.

When synchro indicators employ synchros of different sizes for the transmitting and receiving units, the synchronizing torque will be (1 to 50) $\times 10^{-4}$ N·m/deg.

Synchro indicators are available of four accuracy classes determined by the amount of static error $\Delta\theta$. The static error of the highest class synchros is not to exceed $\pm 30'$, that of the lowest class synchros amounts to $\pm 90'$.

The receiver error is much higher than the transmitter error for all the accuracy classes. The transmitter error is primarily brought in due to technological factors (asymmetry of windings, nonuniform distribution of permeance over the axes, etc.). The receiver error is influenced, in addition, by friction torques in the bearings and in the brush-to-slip ring contact, by the rotor static unbalance torque, by tooth reluctance torques, etc.

In the course of operation the synchro accuracy also depends on supply voltage and frequency fluctuations and data transmission line impedance. A decrease in supply voltage and an increase in frequency cause a reduction of the field flux Φ_d. The current through the synchronizing windings

and the mmf F_{max} are lower at a greater distance between the synchros and a higher resistance of the data transmission line. As is seen from Eq. (4.19), in either case the synchronizing torque and the accuracy of transmission are reduced. As soon as a load torque is applied to the receiver motor, the transmission accuracy abruptly decreases (Fig. 4.6*b*, $T_{st} = T_f + T_{load}$).

Sometimes synchro indicators are rated continuously, in which case the synchronizing torque, now referred to as a dynamic torque, is a function of speed because the rotating emf induced in the synchronizing windings reduces its magnitude. The dynamic synchronizing torque $T_{s\,dyn}$ developed by a synchro receiver can be found from the empirical equation

$$T_{s\,dyn} = T_{s\,max} \sin\theta \cos\frac{\omega_p}{4f} \qquad (4.23)$$

where ω is synchro receiver rotor speed; $T_{s\,max}$ is maximum static synchronizing torque.

At small error angles ($\theta < 5$ deg.) and a speed ranging from 0 to 0.2 of synchronous speed corresponding to a particular frequency, the dynamic synchronizing torque is practically the same as the static torque. A further increase in the speed causes an appreciable reduction of the dynamic synchronizing torque.

Sometimes an angular position must be transmitted to more than one point. For example, the position of a control element must be transmitted to the main control console and to local debugging boards, and the like. When this is the case, one transmitter is connected to several synchro receivers. Such a condition is called a multiplex reception (Fig. 4.7).

Let n receivers of the same type as the transmitter be connected to the latter. According to Eq. (4.19) the synchronizing torque is proportional to the mmf F_{max}, the latter, in turn, is proportional to the synchronizing winding current I_{max}. Since the receivers are connected in parallel to the transmitter, the synchonizing torque of the receiver will be n times as low as that of the transmitter, because

$$I_{r\,max} = I_{t\,max}/n$$

So, the transmission accuracy will be greatly reduced due to a decrease in the synchronizing torques of the synchro receivers.

In order to retain the desired synchronizing torque for the receivers, a synchro transmitter of a power n times higher than that of the synchro receivers is selected. Then the synchronizing winding impedance z_t will be n times lower than the synchronizing winding impedance z_r of each synchro receiver. In the general case

$$T_{sp} = T_{sp\,0} \frac{2}{1+nk} \tag{4.24}$$

where $T_{sp\,0}$ is specific torque for the case of one receiver connected to one transmitter of the same type; $k = z_t/z_r$.

In order to obtain a higher accuracy of angle transmission, synchro receivers should be selected of the same type and have equal static torques.

In the above-discussed systems, with a cophasal supply of the transmitters and receivers, the synchro transmitter develops a torque that tends to return the rotor to its original position. It may be sometimes required that an angular position should be synchronously transmitted at a low synchronizing torque on the synchro transmitter shaft. For example, when a synchro transmitter rotor is mechanically coupled with the sensing element of an instrument, its synchronizing torque may affect the instrument accuracy. To

Fig. 4.7. Synchros connected for multiplex reception

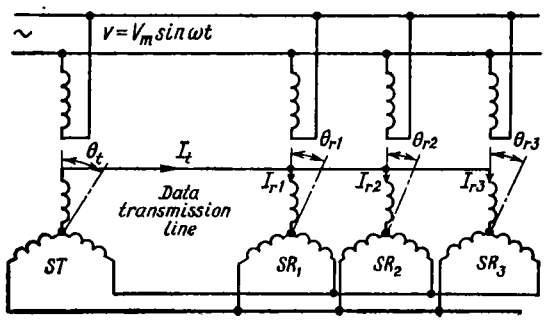

eliminate this torque, a phase-shifting capacitor C (Fig. 4.8*a*) is inserted in the field circuit. The transmitter torque is reduced because the phases of the ST and SR fluxes are shifted by an angle β (Fig. 4.8*b*).

4.4. Synchro Transformers

Synchro transformers are used when in transmitting an angular or rotational motion a high static torque must be defeated. In the action, a low-power signal is passed via the data transmission line, then this signal is amplified to a value sufficient to actuate a servo motor which drives the equipment under control and at the same time functions to reduce the error angle between the synchro transmitter and the synchro receiver.

Figure 4.9 exhibits the schematic diagram of synchro transformers. The field winding of the synchro transmitter, like that of a synchro indicator, is connected to supply mains and serves to afford a pulsating flux in the magnetic system of the machine. The synchronizing windings of the transmitter and receiver are appropriately interconnected with the data transmission line.

The synchro transmitter field winding functions to generate a signal (voltage) depending on the error angle $\theta = \theta_t - \theta_r$.

Fig. 4.8. Synchro indicator using compensated-torque transmitting unit

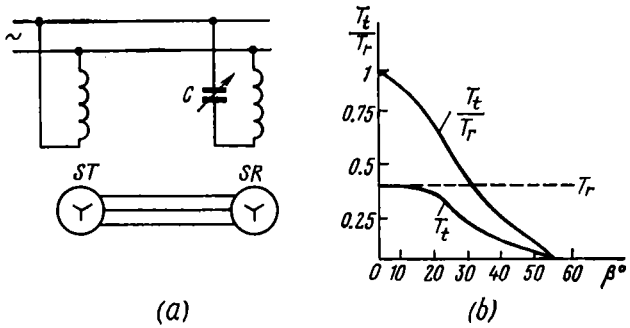

A synchro transformer system is considered to be in a matched condition when the field winding of the synchro receiver is shifted beforehand through 90 deg. relative to that of the synchro transmitter (Fig. 4.9 illustrates synchros in a matched condition). The angle of turn of the receiver rotor, θ_r, is counted off starting from this position.

The pulsating flux of the transmitter field winding, $\dot{\Phi}_f$, induces in the synchronizing winding branches emfs E_{t1}, E_{t2}, E_{t3}, which can be found from Eq. (4.1). With the data transmission line impedance assumed to be negligible and the impedances of both the synchros equal, that is, $Z_t = Z_r = Z$, the following currents will flow in the winding circuit and in the data transmission line due to these emfs:

$$\left.\begin{aligned} I_1 &= \frac{E_{\max}}{2Z}\cos\theta_t \\ I_2 &= \frac{E_{\max}}{2Z}\cos(\theta_t - 120°) \\ I_3 &= \frac{E_{\max}}{2Z}\cos(\theta_t + 120°) \end{aligned}\right\} \qquad (4.25)$$

Fig. 4.9. Synchro transformers. Schematic diagram

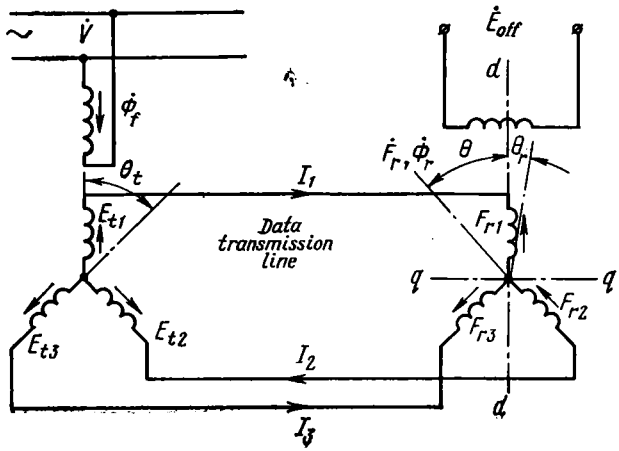

These currents, while flowing through the branches of the receiver synchronizing winding, set up in these branches mmfs F_{r1}, F_{r2}, F_{r3}. The mmf per pole pair is to be found from Eq. (4.9).

The resultant mmf can be obtained by virtue of finding two components. For this, determine the direct-axis component F_{rd} and the quadrature-axis component F_{rq} by projecting the mmfs F_{r1}, F_{r2}, F_{r3} on the direct and quadrature axes, d and q, respectively, after turning the synchro receiver rotor through an angle θ_r from the matched position and the synchro transmitter rotor through an angle θ_t.

The direct-axis component

$$F_{rd} = F_{r1} \cos \theta_r + F_{r2} \cos (\theta_r - 120°) + F_{r3} \cos (\theta_r + 120°)$$

or

$$F_{rd} = \frac{3}{2} F_{\max} \cos \theta \tag{4.26}$$

where $F_{\max} = 1.8 \frac{E_{\max}}{2Z} wk_w$.

The quadrature-axis component

$$F_{rq} = -\frac{3}{2} F_{\max} \sin \theta \tag{4.27}$$

The resultant emf

$$F_r = \sqrt{F_{rd}^2 + F_{rq}^2} = \frac{3}{2} F_{\max} \tag{4.28}$$

As is seen from equations (4.26) through (4.28), the resultant mmf of the receiver synchronizing winding is a permanent-length space vector $\frac{3}{2} F_{\max}$ that turns in space through an angle equal to the error angle θ.

The minus sign in Eq. (4.27) shows that the resultant mmf vector rotates in the direction opposite that of the transmitter rotor (Fig. 4.9).

The resultant mmf causes a flux Φ_r which interacts with the synchro receiver field winding and induces therein an output emf

$$E_{out} = E_{out\,max} \sin \theta \tag{4.29}$$

where $E_{out\ max}$ relates to the condition when the resultant mmf vector is unidirectional with the synchro receiver field axis. The output emf phase varies in steps of 180 deg. every 180 deg. of the rotor angle of turn. Figure 4.10 illustrates the output emf E_{out} of a synchro receiver as a function of the angle θ.

A sinusoidal $E_{out} = f(\theta)$ curve will be obtained if (a) the flux density in the air gap is distributed strictly according to the sine-wave law. This is achieved by appropriately selecting connections of the stator and rotor windings, air gaps, stator and rotor slots, along with thorough finish of the machine parts, (b) by selecting a distributed-field construction so as to avoid upper space harmonics.

Synchros used in synchro transformers are available of seven accuracy classes depending on the static error in transmitting the angular motion. The static error of the highest accuracy synchros is not to exceed $\pm 1'$ and that of the lowest accuracy synchros amounts to $\pm 30'$. Most popular are synchros whose maximum error ranges between $\pm 5'$ and $\pm 30'$.

A lower maximum error of synchro transformers as compared to that of synchro indicators may be attributed and the fact that the synchro transformer accuracy depends only on the magnetic or electric balance and not on stray shaft torques.

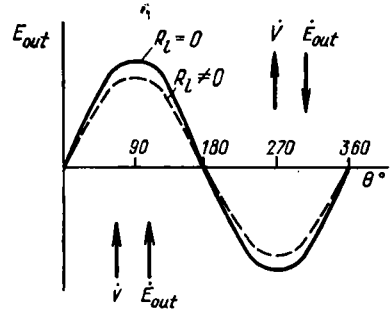

Fig. 4.10. Synchro transformer output emf curve

An essential characteristic of synchro transformers is a specific output voltage V_{sp}, at a preset load impedance Z_{load}, that is, the amount of output voltage per degree of the error angle near zero. The specific output voltage determines the output characteristic steepness at the origin of the coordinates:

$$V_{sp} = \left(\frac{\Delta V_{out}}{\Delta\theta}\right)_{\theta \approx 0}, \text{ or } V_{sp} = \left(\frac{dV_{out}}{d\theta}\right)_{\theta=0} \qquad (4.30)$$

where

$$\dot{V}_{out} = \dot{E}_{out} - \dot{I}_{out} Z_{out} = \frac{\dot{E}_{out}}{1 + Z_{out}/Z_{load}}$$

I_{out} is output circuit current; Z_{out} is receiver output winding impedance.

The synchro transformer sensitivity and accuracy increase with V_{sp}. This phenomenon can be explained as follows. Manufacturing errors and a difference in the transmitter and receiver characteristics cause an additional voltage $\Delta\dot{V}_{add}$ at the receiver output with the system being in the matched condition ($\theta = 0$). The voltage $\Delta\dot{V}_{add}$ generally has two components, one being an error voltage $\Delta\dot{V}_e$ which is in phase with the output voltage $\dot{V}_{out}$, and the other a residual voltage $\Delta\dot{V}_{res}$ which is in phase quadrature with the former. The error voltage can be compensated by the output voltage $\dot{V}_{out}$, for which purpose the receiver rotor should be turned through an angle at which $V_{out} = -\Delta V_e$. In the action, the servo motor will turn the equipment under control and the receiver rotor through an angle $\theta_r \neq \theta_t$, with the result that an angular error will appear:

$$\Delta\theta = \frac{\Delta V_e}{V_{sp}}$$

The synchronizing winding current and the E_{out} and V_{sp} will be reduced if the distance between the synchros and the data transmission line impedance are increased (see Fig. 4.10) A change in the load impedance of the receiver output winding circuit also changes the V_{sp} (see Fig. 3.8), as the inherent

voltage drop $I_{out}Z_{out}$ and the output winding response to the flux Φ_r change. Moreover, with a capacitive reactance load, voltage resonance in the output circuit may occur. Besides, the V_{sp} is directly proportional to the transmitter field voltage amplitude. The specific output voltage of modern synchros at $Z_{load} \gg Z_{out}$ is (0.5 to 2) V/deg.

4.5. Differential Synchros in Indicating Transmission Systems

In their solution, some problems involve an automatic addition and subtraction of angular quantities, or multiplication and division thereof if logarithms of these quantities are given as angles. This function is performed by a *differential synchro* which serves either as a receiver of two transmitters or as a second receiver.

Figure 4.11 shows an indicating transmission system incorporating a differential synchro DS (within a dash-line square). The field windings of synchro indicators ST_1 and ST_2 are connected to a single-phase supply. The synchronizing winding of the ST_1 is connected via a data transmission line to the stator winding of the DS; the synchronizing winding of the ST_2 is connected to the rotor winding of the DS via a data transmission line too.

Fig. 4.11. System incorporating a differential synchro

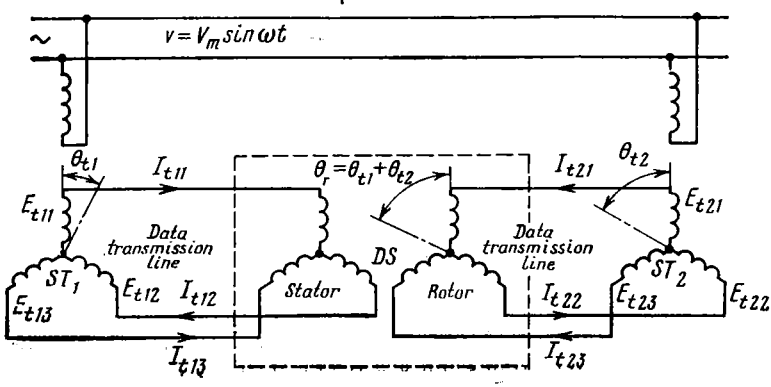

Let the system be in the matched condition, that is, $\theta_{t1} = \theta_{t2} = \theta_r = 0$. When this is the case, emfs E_{t11}, E_{t12}, E_{t13} will be induced in the synchronizing winding of the ST_1 due to the pulsating flux produced by the field winding of this synchro. Just as with synchro transformers, these emfs will cause currents I_{t11}, I_{t12}, I_{t13} to flow through the branches of the differential synchro stator winding. These currents build up a resultant stator emf $\dot{F}_s$ that is directed in our case along the ST_1 field axis.

A similar process occurs in the ST_2, and currents I_{t21}, I_{t22}, I_{t23}, while flowing through the branches of the differential synchro rotor windings, will produce a resultant rotor mmf $\dot{F}_r$. This mmf will be directed along the ST_2 field axis. Proceeding from the assumption that the axes of the ST_1 and ST_2 fields coincide, we may consider that the mmfs $\dot{F}_s$ and $\dot{F}_r$ are cumulative.

Magnetic fluxes $\dot{\Phi}_s$ and $\dot{\Phi}_r$ are built up in the differential synchro air gap under the effect of the mmfs $\dot{F}_s$ and $\dot{F}_r$. These fluxes are in aided relation with mmfs $\dot{F}_s$ and $\dot{F}_r$. The arrangement of fluxes $\dot{\Phi}_s$ and $\dot{\Phi}_r$ in space at $\theta_{t1} = \theta_{t2} = \theta_r = 0$ is shown by Fig. 4.12*a*.

The torque is proportional to the vector product of these fluxes. Since the angle between them is zero, the torque

Fig. 4.12. Space diagrams of magnetic fluxes

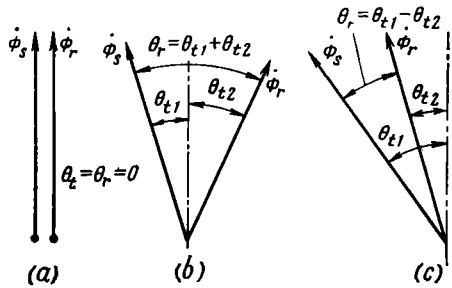

produced in the differential synchro will also be zero and the rotor will be motionless.

If the ST_1 rotor is now turned clockwise through an angle θ_{t1}, and the ST_2 rotor counter-clockwise through an angle θ_{t2}, the resultant fluxes $\dot{\Phi}_s$ and $\dot{\Phi}_r$ will turn through the same angles in differrent directions, like in the case of synchro transformers. The $\dot{\Phi}_s$ will turn through an angle θ_{t1} and the $\dot{\Phi}_r$ through an angle θ_{t2}. The arrangement of these fluxes in space is shown by Fig. 4.12*b*.

A synchronizing torque resulting from the interaction of fluxes $\dot{\Phi}_s$ and $\dot{\Phi}_r$ will force the DS rotor to turn through an angle $\theta_r = \theta_{t1} + \theta_{t2}$. The fluxes $\dot{\Phi}_s$ and $\dot{\Phi}_r$ will be again cumulative and the synchronizing torque will be nullified. Thus, the differential synchro rotor will follow up the sum of the ST_2 and ST_1 angles.

On the other hand, if both the synchro transmitters are turned in the same direction, the differential synchro rotor will turn through an angle equal to the difference of the angles of turn of the synchro transmitters (Fig. 4.12*c*).

4.6. High-Torque Indicating Transmission System

A remote-transmitting system incorporating synchro transformers and used for the remote transmission of angular positions to equipment under control at a high static torque is complicated because of servo system amplifiers. Special electrical machines (synchro-motor sets) make it possible to amplify the torque transmitted from the master synchro indicator to the receiving end.

The synchro-motor set is a combination of a slip-ring synchro or a magslip and an induction motor with a hollow nonmagnetic rotor.

Figure 4.13 illustrates the general arrangement of such a set composed of a slip-ring synchro and a motor. The hollow nonmagnetic rotor *1* is mounted in the bore between the external stator *2* carrying the synchronizing winding and the internal stator *3* carrying the field winding of the synchro. The hollow rotor *1* is coupled via a step-down reduc-

tion unit *4* with the synchro shaft *5* and through the latter with the equipment under control and with the internal stator.

The system (Fig. 4.14) functions as follows. A normal synchro is used as a synchro transmitter ST and a synchro-motor set as a synchro receiver SR. When in the matched condition, the field and synchronizing fluxes of the SR act along the direct axis. The resultant field of the synchro-motor set is pulsating, and the hollow rotor is motionless. When an angular motion is set on the synchro transmitter, a quadrature flux will appear in the synchros due to the quadrature components of mmf of the synchronizing winding *2* (see Synchro Indicators · Section 4.3). Now two fluxes $\dot{\Phi}_d$ and $\dot{\Phi}_q$ are produced in the synchro-motor set. These fluxes are shifted in space and in time (due to the capacitance C). The resultant field is rotating. The hollow rotor *1* starts spinning as in a normal induction motor and turns the controlled equipment through the preset angle. At the same

Fig. 4.13. Synchro-motor set. General arrangement

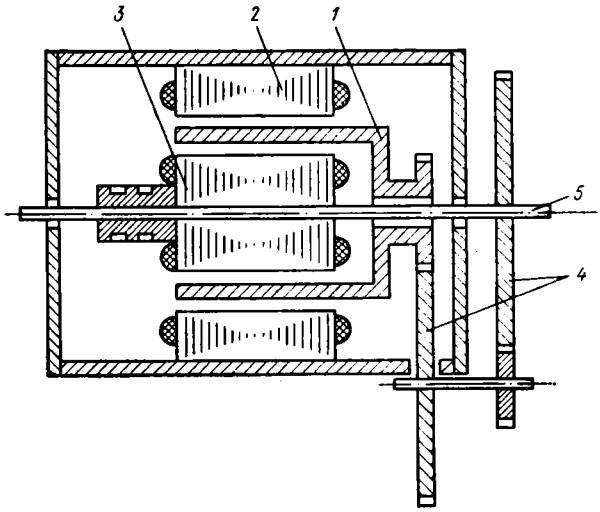

time, the internal stator *3* of the synchro-motor set is turned via the reduction unit so that the error angle is reduced. The angle follow-up is ceased as soon as the error angle between the synchros is eliminated, because the resultant field of the synchro receiver becomes pulsating again.

As follows from the above discussion, the speed of induction servo motors is controlled by synchro-motor sets using a space control method. Such a circuit arrangement has made it possible to obtain on the output shaft of the synchro receiver a specific synchronizing torque as high as 1 N·m/deg., which is much higher than that developed by usual synchros. The torque is amplified at the expense of power drawn by the field winding of the synchro-motor set from supply mains.

4.7. Dynamic Characteristics of Synchro Indicators

The receiving unit of a synchro indicator develops a reactionary torque on the shaft, which is composed of two components, one being a static component T_{st} and the other a dynamic component T_{dyn}. So,

$$T_{react} = T_{st} + T_{dyn} \tag{4.31}$$

The static reactionary torque comprises the frictional torque T_f proper (no-load torque) and the load torque T_{load}:

$$T_{st} = T_f + T_{load} \tag{4.32}$$

Fig. 4.14. Synchro system incorporating a synchro-motor set

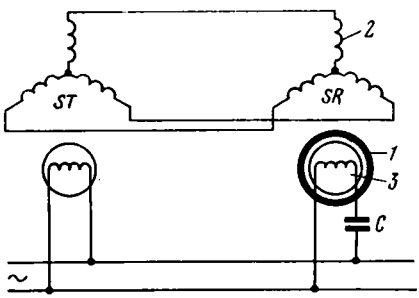

The dynamic torque is determined by the rotor moment of inertia J and by acceleration:

$$T_{dyn} = J \frac{d^2\theta}{dt^2} \tag{4.33}$$

where θ is angle of turn of the synchro receiver rotor.

In the event of a stepped variation of the synchro transmitter rotor angle of turn the synchro receiver rotor hunts for a certain period of time about the new stable equilibrium point. Under these conditions, when $T_{load} = 0$, the equation of torque equilibrium on the synchro receiver shaft takes the form

$$T_s = T_{dyn} + T_{damp} \pm T_f \tag{4.34}$$

where T_s is static synchronizing torque; T_{damp} is electromagnetic damping torque.

The sign at the frictional torque T_f in Eq. (4.34) depends on the sense of rotation.

The static synchronizing torque within the region of small error angles ($\sin\theta \approx \theta$) can be determined as follows, taking into account equations (4.18) and (4.20):

$$T_s = -T_{sp}\theta \tag{4.35}$$

The minus sign in Eq. (4.35) shows that the synchronizing torque always tends to reduce the error angle.

Electromagnetic damping oscillations occur due to rotating emfs in the synchronizing windings of the synchro receiver, which cause additional currents and a damping torque similar to an induction motor torque. The damping action of the synchronizing windings, however, is insufficient. To speed up the decay of rotor oscillations, the rotor is fitted with a short-circuited damping winding (except for that of magslips with unipolar excitation). The magnetic axis of this winding is normal to the field winding axis. During the hunting period of the rotor, the synchronizing winding flux induces a rotating emf in this winding. The interaction between currents flowing in the winding and the flux produced by them causes a damping torque. The resultant damping torque is proportional to the synchro receiver rotor speed:

$$T_{damp} = D \frac{d\theta}{dt} \tag{4.36}$$

where D is damping factor whose magnitude and sign depend on the synchro parameters.

Substitute in Eq. (4.34) equations (4.33), (4.35), and (4.36) to obtain the equation of the receiver rotor oscillations:

$$J\frac{d^2\theta}{dt^2}+D\frac{d\theta}{dt}+T_{sp}\theta=\pm T_f \qquad (4.37)$$

Equation (4.37) can be transformed by taking into account Eq. (4.22):

$$\frac{d^2\theta}{dt^2}+2\lambda\frac{d\theta}{dt}+\omega_0^2(\theta\pm B)=0 \qquad (4.38)$$

where B is dead zone; $\lambda = D/2J$ is oscillation decay factor; $\omega_0 = \sqrt{T_{sp}/J}$ is angular velocity of free oscillations of the rotor.

For a dead zone much smaller than the original amplitude of θ_0, that is, for $B \ll \theta_0$, equation (4.38) will take the form

$$T_{decay}=\frac{2.3}{\lambda}\log\left[1+\frac{\theta_0}{2B}(1-\delta)\right] \qquad (4.39)$$

where $\delta = \exp\left(-\pi\frac{\lambda}{\omega_0}\right)$ is decrement of decay; T_{decay} is receiver rotor oscillation decay time.

The characteristic equation derived from Eq. (4.38) upon the assumption that the frictional torque is negligible ($T_f = 0$, $B = 0$) can be written as

$$X^2+2\lambda X+\omega_0^2=0 \qquad (4.40)$$

The roots of this equation

$$X_{1,2}=-\lambda\pm\sqrt{\lambda^2-\omega_0^2} \qquad (4.41)$$

The transient process may be aperiodic if $\lambda>\omega_0$, critical aperiodic if $\lambda = \omega_0$, and oscillatory if $\lambda < \omega_0$, depending on the ratio of the angular velocity of free oscillations ω_0 to the decay factor λ.

The greater the damping factor D, the higher is the decay factor λ. The synchro can be transferred from a hunting condition to aperiodic operation by raising the damping factor. If electromagnetic damping is insufficient, the syn-

chro receivers are furnished with mechanical dampers mounted on the shaft.

The damping time of the synchro indicator receiving unit at an original error angle $\theta_0 = 180$ deg. is not to exceed 3 s.

4.8. Application of Synchros

All the above-described synchros incorporated in synchro systems are used for automatic-control equipment, telemechanics, etc. Some examples of application of synchros are given below.

As has been already mentioned, synchro indicators are used to transmit an angular or linear motion to a control console.

Figure 4.15 exhibits a circuit arrangement for transmitting the position of a nuclear reactor control rod. The control rod of the reactor is mechanically coupled with the rotor of a synchro transmitter ST via a rack-and-gear drive which transforms the linear motion into an angular turn. The synchro receiver SR is mounted on the reactor control console and its rotor shaft carries a rod position indicator pointer. The synchros are electrically interconnected. A high accuracy of the rod position indication can be attained by properly selecting the gearing drive.

The system discussed herein comprises one transmitter and one receiver. In practice there are multiplex systems where one transmitter operates in conjunction with several receivers. The example is a radioactive level gauge whose schematic diagram is shown by Fig. 4.16.

In this gauge one synchro transmitter ST is connected with two synchro receivers SR_1 and SR_2. The synchro receiver SR_1 is mechanically coupled with a radioactive radiation source, and the rotor of the synchro receiver SR_2 mounts a nuclear-particle counter. When the source and the counter are at the interface of two media (substance level), no signal is supplied to the amplifier and the system is motionless. When the substance level goes down, a great amount of radiation arrives at the counter and a signal of a definite phase reaches the amplifier A. The rotor of the induction servo motor SM starts running and turns the synchro transmitter rotor simultaneously with the secondary instrument

pointer indicating the substance level. The synchro receivers start turning in step with the synchro transmitter and force the source and the counter to follow the substance level. This follow-up will take place until the source-counter line reaches the interface of the two media again. The secondary instrument pointer will indicate the substance level.

Synchro indicators often operate with the transmitting and receiving units rotating continuously, such as in the systems of relative bearing data transmission from the aerial to the indicator of a radar.

The schematic diagram of such a system is shown on Fig. 4.17.

The shaft of the aerial A is driven by a motor SM and is coupled with the ST rotor via a speed-up reduction unit $RU1$ having a gear ratio $i = 30$.

The SR rotor is coupled with the deflecting coil rotator CR (the deflecting coil is designated DC) via a step-down reduction unit $RU2$ having a gear ratio $i = 30$. The field windings of the synchros are connected to 115 V, 427 Hz supply.

Fig. 4.15. Data transmission line for duplicating the position of a nuclear reactor control rod

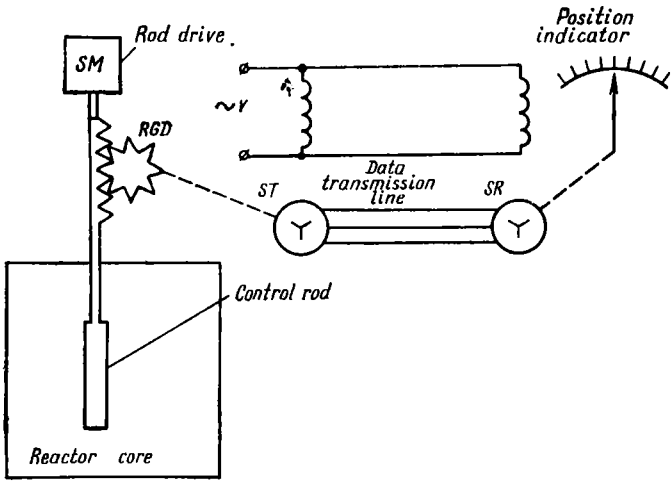

The synchro receiver rotates in step and in phase with the synchro transmitter, which ensures that the signal sweep line displayed on the indicator screen rotates synchronously and cophasally with the radar aerial.

In an ideal case, when the efficiency of the reduction units is unity and the angular displacement transmission error is zero, the system operates as follows.

An i-fold reduction of the reactionary torque caused by the deflecting coil rotator CR on the synchro receiver rotor axis (in our case a 30-fold reduction) and an i^2-fold reduction of the relative bearing transmission error brought in the reactionary torque produced by the CR could be attained through the use of a step-up reduction unit in the aerial and a step-down reduction unit in the indicator. This is possible due to the fact that the SR error brought in by the reactionary torque is reduced i times and the SR rotor position error referred to the aerial shaft is also reduced i times.

Such a gearing, however, makes the system lose its self-synchronizing property. Let the synchro transmitter ST be mismatched with the synchro receiver SR (say, upon removal of power supply). With power supply switched on, the CR shaft may assume one of its stable positions when the syn-

Fig. 4.16. Radioactive level gauge УР-4. Schematic diagram

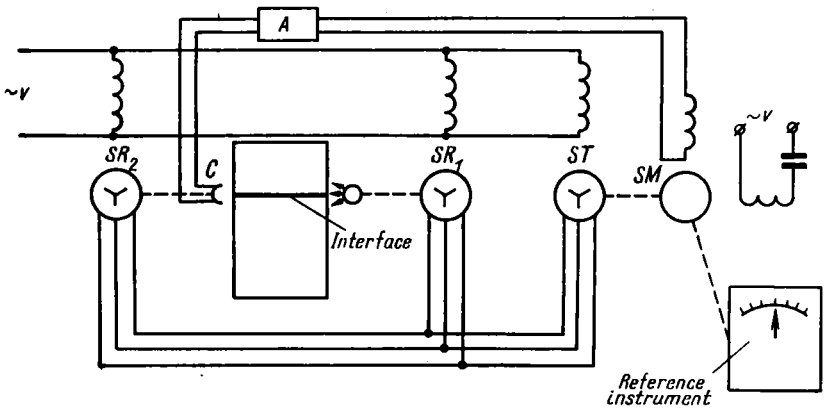

chro receiver torque is zero. For the adopted gear ratios, a definite position of the aerial A may correspond to 30 stable positions of the deflecting coil spaced at angles which are a multiple of 12 deg., because the synchro receiver rotor completes the revolution (turns through 360 deg.) and assumes a stable equilibrium position relative to the synchro transmitter again within every turn of the deflecting coil through an angle of 12 deg. To provide for self-synchronization, the system is fitted with an automatic self-synchroni-

Fig. 4.17. Radar relative bearing transmission system. Schematic diagram

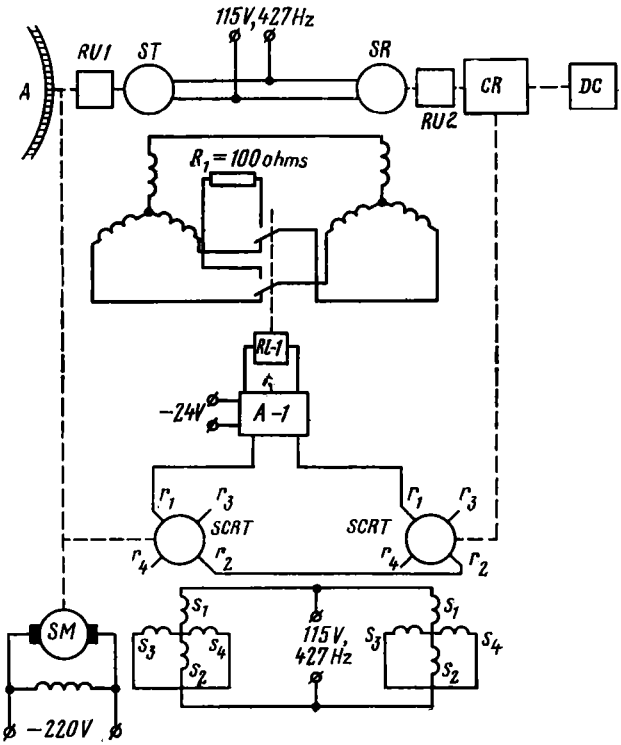

zing circuit composed of two sine-cosine rotary transformers *SCRT* (see Chapter V) that are mechanically coupled with the aerial and the deflecting coil; the circuit also comprises a relay *Rl-1* and a relay amplifier *A-1*.

The *SCRT* stator windings s_1s_2 are connected to 115-V, 427-Hz a.c. supply; the s_3s_4 windings are short-circuited for balancing the *SCRT*. The rotor windings r_1r_2 are connected into a signal comparison circuit. Voltage picked off these windings is delivered to the relay amplifier *A-1* which is loaded by the relay *Rl-1*.

When the aerial and the deflecting coil rotate in step and in phase, the output signal of the *SCRT* rotor coils is almost zero and the relay is open. If their rotation is not synchronous, an error angle $\theta \gg \pm 5$ deg. appears and causes an error signal. The relay *Rl-1* operates and closes with its contacts the synchro transmitter synchronizing winding through the resistor $R_1 = 100$ ohms (for immediate stopping). The synchro receiver will be motionless until the aerial arrives at the appropriate sector. When the radiation pattern of the aerial is in phase with the signal sweep line, the *Rl-1* gets deenergized, its contacts drop out, which restores the electrical connection between the synchronizing winding of the synchros, and the synchro receiver starts rotating the deflecting coil in step and in phase with the aerial.

Fig. 4.18. Light-power servo system

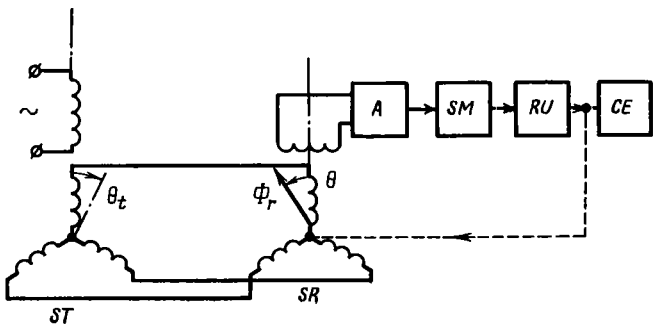

Some automatic-control systems require a high torque on the controlled shaft at a low torque on the controlling shaft. Such systems employ synchro transformers.

Figure 4.18 illustrates the block-diagram of a servo system incorporating synchro transformers. The output voltage of the synchro receiver is delivered to the servo motor *SM* via the amplifier *A*. The servo motor turns the equipment under control *CE* along with the synchro receiver rotor through an angle preset by the transmitter. As soon as the *CE* and the receiver rotor have turned through an angle $\theta_r = \theta_t$, the synchro receiver flux Φ_r positions itself perpendicular to the output winding axis again, the output voltage drops to zero, and the system assumes a new stable equilibrium position.

Chapter

5 ROTARY TRANSFORMERS

5.1. General Information and Classification

Rotary transformers are fractional-horsepower a.c. electrical machines used to transform an angle of turn θ into a voltage proportional to certain functions of the angle (such as, sin θ or cos θ) or to the angle of rotor turn θ proper. These machines are employed by computers for carrying out miscellaneous mathematical operations. They have found most wide application in automatic computers meant for solving geometrical and trigonometrical problems to construct triangles, convert coordinates, resolve and compute vectors.

Rotary transformers are also used in automatic-control systems where they function to measure and indicate a deviation of a system from a certain desired position.

Rotary transformers are manufactured of four basic types meant to perform different functions depending on the connection of their windings:

(1) sine-cosine rotary transformers whose windings are connected so that the output voltage of one of them is proportional to the sine of the rotor angle of turn, while that of the other winding is proportional to the cosine of the rotor angle of turn;

(2) vector-computing rotary transformers which function so that when voltages proportional to the vector components in rectangular coordinates (to the cathetus of a right-angled triangle) are applied to both the stator windings, the output voltage will be proportional to the vector module (hypotenuse) and the rotor angle of turn to its argument (the angle between the cathetus and the hypotenuse);

(3) linear rotary transformers whose output voltage is proportional to the rotor angle of turn. The function of these

transformers is most frequently performed by sine-cosine rotary transformers having a transformation ratio of 0.565;

(4) scale rotary transformers whose output voltage is proportional to the input voltage and the factor of proportionality (or scale) is determined by the angle of rotor turn.

Rotary transformers must meet the following basic requirements:

(1) minimum amplitude error in the reproduction of the desired function;

(2) minimum phase error, that is, minimum variation of the output voltage phase as a function of the angle of turn or voltage;

(3) high maximum permissible rotor speed.

For some applications the rotary transformers can be manufactured to meet the requirements of Section 0.2.

5.2. Mechanical Design of Rotary Transformers

According to their design, the rotary transformers may be classified as slip-ring and no-contact machines depending on whether they have a sliding contact or not.

A rotary transformer consists of two basic parts, *viz*, a fixed stator *1* and a movable rotor *2* (Fig. 5.1). The stator and rotor cores are stacked of electric steel or permalloy (low-reluctance material) stampings. Each stamping is covered on both sides with insulating varnish.

The material is selected depending on the application of the transformer and its position in the system employing it. Rotary transformers positioned at the input of a system and powered directly from supply mains, whose voltage is maintained constant, may be built with electric steel stampings for the stator and rotor cores. Those positioned in the middle or at the output of a system have permalloy cores because their input voltages may vary within a wide range.

Voltage variations cause a change in the magnetic circuit saturation and, hence, in the reluctance and other characteristics of the machine. To prevent changes in the characteristics of the machine and consequent conversion errors, the magnetic circuit reluctance must be lower than the permanent reluctance of the air gap between the stator and the

rotor under all conditions. Permalloy is just the material capable of meeting this requirement.

The stator slots, as well as the rotor slots, accommodate two distributed windings spaced 90 electrical degrees apart. The arrangement of the rotary transformer windings in space is shown by Fig. 5.2, where s_1s_2 is the main stator winding, s_3s_4 is the auxiliary (quadrature) stator winding; r_1r_2 and r_3r_4 are, respectively, the sine and cosine rotor windings. The stator windings are usually made identical, that is, with an equal number of turns, equal cross-sectional area of magnet wire and similar connection of winding leads. The rotor windings are also identical. The rotor angle of turn θ is counted off between the sine winding axis and the stator quadrature winding axis.

The stator winding leads are brought out directly to terminal blocks. The rotor winding leads of slip-ring rotary transformers are brought out through a slip-ring assembly composed of four slip rings and brushes.

Fig. 5.1. Rotary transformer. Exploded view
1—stator; *2*—rotor; *3*—slip-ring assembly; *4*—rotating and locking mechanism

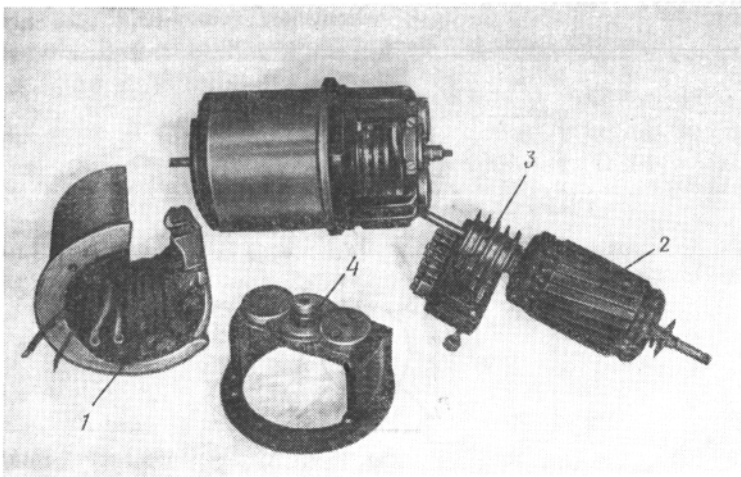

As for no-contact rotary transformers, their rotor voltage can be picked off by two methods:

(1) dy means of spiral springs;

(2) by means of intervening toroidal transformers (as in magslips, see Section 4.2).

In the former case, the rotor angle of turn is limited between 1.8 and 2 revolutions. In the latter case, it is unlimited. No-contact rotary transformers are more reliable and provide higher accuracy due to the absence of sliding contacts.

Inverted rotary transformers are also available. Their sine and cosine windings are placed on the stator, the quadrature winding is short-circuited, and the main winding leads are brought out through two sliding contacts or one intervening transformer.

Rotary transformers must be designed and manufactured so as to ensure variations in the mutual inductance of the stator and rotor windings, while the rotor is turned, according to the law of almost ideal sines. In most cases, errors exceeding 0.01 per cent must not be allowed, that is, the ordinates of the mutual inductance versus angle of rotor turn curve at any point must not differ from the ideal sine ordinates by more than 0.0001 of its peak value.

Most rotary transformers are two-pole machines. High-accuracy remote angle transmission systems, however, em-

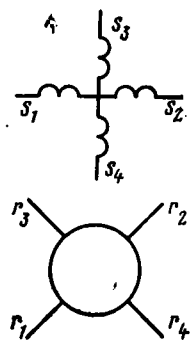

Fig. 5.2. Arrangement of rotary transformer windings

ploy multipole rotary transformers. These transformers afford a more accurate conversion of angular quantities into voltages because the effect of manufacturing errors in them is not so great due to averaging the emfs induced at all the poles ($2p$).

The discussions given below relate to two-pole rotary transformers. The results obtained are also valid for multipole rotary transformers, provided their characteristics are considered as functions of an angle in electrical degrees $\theta_{el} = p\theta$.

Rotary transformers of all the types are wound for 400-Hz supply.

5.3. Sine-Cosine Rotary Transformers

The operating principle of rotary transformers can be exemplified by obtaining a sine function of the rotor angle of turn (sine rotary transformer). In a sine rotary transformer the main stator winding s_1s_2 is connected to an a.c. source $\dot{V}_1$ supplying a constant voltage (Fig. 5.3*a*). The rotor winding r_1r_2 is connected to an external load characterized by an impedance $Z_{load\ 1} = R_{load\ 1} + jX_{load\ 1}$. The quadrature

Fig. 5.3. Sine rotary transformer
(*a*) schematic diagram; (*b*) equivalent circuit diagram

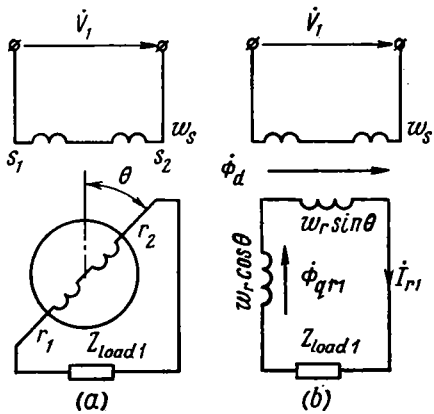

winding s_3s_4 and the rotor winding r_3r_4 are open and do not function at all (they are not shown on Fig. 5.3).

Assume that a rotary transformer is designed and manufactured so that the mutual inductance of the s_1s_2 and r_1r_2 windings varies with the rotor angle of turn θ strictly according to the law of sines. When this is the case

$$M = M_{max} \sin \theta \tag{5.1}$$

where M_{max} is mutual inductance when the axes of the s_1s_2 and r_1r_2 windings coincide.

Since maximum mutual inductance is proportional to the product of turns of inductively coupled coils, equation (5.1) can be transformed as follows:

$$M = \Lambda w_s w_r \sin \theta \tag{5.2}$$

where Λ is permeance which is independent of the rotor angle of turn because the air gap is uniform; w_s is effective number of turns of the stator winding; w_r is effective number of turns of the rotor winding.

As can be understood from the analysis of Eq. (5.2), the mutual inductance M varies in the same manner if the turns of the r_1r_2 winding are treated as a vector sum (Fig. 5.4) of direct-axis turns $w_r \sin \theta$, whose axis coincides with that of the s_1s_2 winding, and quadrature-axis turns $w_r \cos \theta$ whose axis

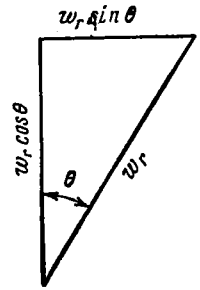

Fig. 5.4. Resolving the rotor winding into longitudinal and transverse turns

is normal to that of the s_1s_2 winding. Hence, the schematic diagram shown by Fig. 5.3*a* can be replaced by the equivalent circuit diagram of Fig. 5.3*b*.

Let us see how such a rotary transformer operates under no-load and on-load conditions.

1. *No-load operation* ($Z_{load\ 1} = \infty$; $I_{r1} = 0$). The emf $\dot{E}_{r1}$ of the rotor winding r_1r_2 depends only on the mutual inductance flux between the s_1s_2 winding and the direct-axis turns $w_r \sin \theta$, that is, on the direct-axis flux $\dot{\Phi}_d$ only. Then

$$\frac{E_{r1}}{E_{s1}} = \frac{w_r \sin \theta}{w_s} = k_{tr} \sin \theta \qquad (5.3)$$

where E_{s1} is main stator winding emf ($E_{s1} \approx V_1$); $k_{tr} = w_r/w_s$ is transformation ratio. Hence,

$$\dot{E}_{r1} = k_{tr}\dot{E}_{s1} \sin \theta \qquad (5.4)$$

that is, the emf of the rotor winding r_1r_2 in the given circuit varies as a sine function of the rotor angle of turn θ when the rotary transformer runs at no load.

2. *On-load running* ($Z_{load\ 1} \neq \infty$, $I_{r1} \neq 0$). The direct-axis flux $\dot{\Phi}_d$ is produced due to a joint action of the mmf of the stator winding s_1s_2 and that of the direct-axis turns $w_r \sin \theta$ and is almost equal to the flux under no-load conditions. The mutual inductance emf induced by this flux in the direct-axis rotor turns is determined, as in the case of the no-load running, by the equation

$$\dot{E}_{r1m} = k_{tr}\dot{E}_{s1} \sin \theta \qquad (5.5)$$

The current $\dot{I}_{r1}$ flowing in the quadrature-axis turns $w_r \cos \theta$ produces a quadrature-axis flux $\dot{\Phi}_{qr1}$ which is not linked with the s_1s_2 winding and, consequently, cannot be compensated for by increasing the current through this winding. The flux $\dot{\Phi}_{qr1}$ induces in the quadrature-axis turns a self-inductance emf

$$\dot{E}_{r1L} = -j\omega_1 L\dot{I}_{r1} \qquad (5.6)$$

where ω_1 is angular frequency of supply voltage ; L is inductance proportional to the square of turns and permeance Λ:

$$L = (w_r \cos\theta)^2 \Lambda \tag{5.7}$$

The total emf induced in the $r_1 r_2$ winding is determined as a sum of the mutual inductance and self-inductance emfs:

$$\dot{E}_{r1} = \dot{E}_{r1m} + \dot{E}_{r1L} = k_{tr}\dot{E}_{s1} \sin\theta - j\omega_1 \dot{I}_{r1} (w_r \cos\theta)^2 \Lambda \tag{5.8}$$

The rotor current

$$\dot{I}_{r1} = \frac{\dot{E}_{r1}}{Z_{load\,1} + Z_{r1}} \tag{5.9}$$

where $Z_{r1} = R_{r1} + jX_{r1}$ is impedance of the $r_1 r_2$ winding.

From Eq. (5.8) and taking into account Eq. (5.9) we obtain

$$\dot{E}_{r1} = \frac{k_{tr}\dot{E}_{s1} \sin\theta}{1 + \dot{b}\cos^2\theta} \tag{5.10}$$

where the complex multiplier

$$\dot{b} = j\frac{\omega_1 w_r^2 \Lambda}{Z_{load\,1} + Z_{r1}} = j\frac{\omega_1 w_r^2 \Lambda}{(R_{load\,1} + R_{r1}) + j(X_{load\,1} + X_{r1})} \tag{5.11}$$

Equation (5.10) shows that under on-load conditions the $\dot{E}_{r1}$ versus θ curve is not sinusoidal because the denominator contains $\dot{b}\cos^2\theta$. This distortion can be attributed to the quadrature-axis flux Φ_{qr1} (which appears during on-load running), that is, to the quadrature-axis reaction of the rotor. This distortion can be lowered by reducing the multiplier $\dot{b}$, which is possible only at high load impedances.

The relative error is defined as a difference between the ideal sinusoid equation with an amplitude of $k_{tr}E_{s1}$ and Eq. (5.10) referred to the ideal sinusoid amplitude

$$\Delta\dot{E}_r = \frac{k_{tr}\dot{E}_{s1}\sin\theta - \dfrac{k_{tr}\dot{E}_{s1}\sin\theta}{1 + \dot{b}\cos^2\theta}}{k_{tr}\dot{E}_{s1}} = \frac{\dot{b}\cos^2\theta \sin\theta}{1 + \dot{b}\cos^2\theta} \tag{5.12}$$

From Eq. (5.12) we can find the angle at which the error reaches its maximum value:

$$\theta_{max} = 35°16'; \ 144°44'; \ 215°16' \ldots$$

The actual portion of the $\Delta\dot{E}_r$ complex value is taken as an amplitude error, and the imaginary portion as a phase error of the rotary transformer.

The distortion of the output voltage amplitude under the effect of the quadrature-axis reaction of the rotary transformer rotor is illustrated by Fig. 5.5. where curve *1* is an ideal sine curve, while curves *2* and *3* are output characteristics of the rotary transformer according to Eq. (5.10) at $\dot{b}$ values of 0.25 and 1, respectively. Curves *4* and *5* exhibit the amplitude error ΔE_r as a function of the rotor angle of turn at the above-specified values of $\dot{b}$ and correspond to Eq. (5.12). Curve *4* is plotted as the difference between curves *1* and *2*, and curve *5* as the difference between curves *1* and *3*.

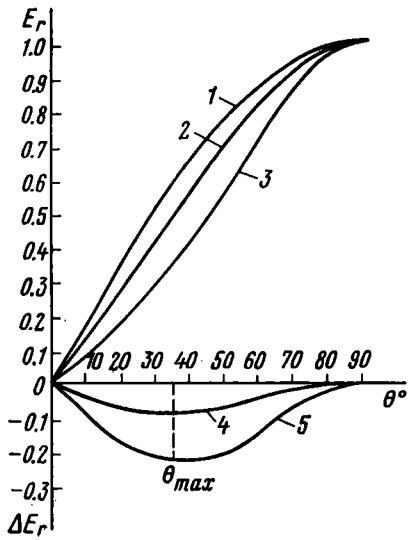

Fig. 5.5. Amplitude error of a loaded sine rotary transformer

The phase error occurs due to the resistances and inductive reactances of the stator windings and due to the quadrature-axis reaction of the rotor. Mathematically, the phase error is recognized by the fact that the multiplier $\dot{b}$ in equations (5.10) and (5.12) is a complex value. From the analysis of Eq. (5.11) we see that the argument of the denominator complex number in Eq. (5.10) changes with a change in the magnitude and type of load ($R_{load\ 1}$ and $X_{load\ 1}$ portions). Hence, the phase shift between vectors $\dot{E}_{r1}$ and $\dot{E}_{s1}$ also changes, that is, a phase error occurs. It also follows from Eq. (5.11) that the phase error can be reduced by increasing the inductive reactance share ($X_{load\ 1} + X_{r1}$) in the rotor circuit impedance ($Z_{load\ 1} + Z_{r1}$), which will greatly reduce the argument of the complex number $\dot{b}$. The phase error can be reduced to a minimum by using a purely inductive or purely capacitive load, but then the amplitude error would reach its maximum.

A similar discussion will be true for the case when the rotor winding r_3r_4 is functioning and the r_1r_2 winding is open. When this is the case, the mutual inductance of the windings s_1s_2 and r_3r_4 obeys the law of cosines, and the machine runs as a cosine rotary transformer. Here, the rotor emf under no-load conditions

$$\dot{E}_{r2} = k_{tr}\dot{E}_{s1}\cos\theta \tag{5.13}$$

and under on-load conditions

$$\dot{E}_{r2} = \frac{k_{tr}\dot{E}_{s1}\cos\theta}{1+\dot{b}\sin^2\theta} \tag{5.14}$$

Since the output voltage of rotary transformers must strictly follow the law of sines or cosines of the rotor angle of turn, the machines should be balanced out, that is, the quadrature-axis reaction of the rotor should be corrected so as to eliminate the error brought in by this reaction. Balancing adjustment of rotary transformers is also the best way to reduce the phase error.

5.4. Rotary Transformer Balancing Adjustment

Rotary transformers are balanced out either on the stator side (primary balancing adjustment) or on the rotor side (secondary balancing adjustment).

A *primary balancing adjustment* is made with the aid of the stator quadrature winding s_3s_4 which is shorted out through an external impedance Z_2 (Fig. 5.6*a*). Since the s_3s_4 axis is normal to the s_1s_2 axis, the turns w_s of this winding (Fig. 5.6*b*) and the quadrature-axis turns of the rotor winding r_1r_2 make up a transformer with its primary mounted on the rotor and its secondary on the stator. The current $\dot{I}_{r1}$ flowing through the quadrature-axis turns $w_r \cos\theta$ of the r_1r_2 winding creates a magnetic flux which is linked with the turns w_s of the s_3s_4 winding. A transformer emf is induced in the latter and a current $\dot{I}_{s2}$ starts flowing in this winding. The resultant quadrature-axis flux $\dot{\Phi}_q$ is defined as a vector

Fig. 5.6. Sine rotary transformer with primary balancing
(*a*) schematic diagram; (*b*) equivalent circuit diagram

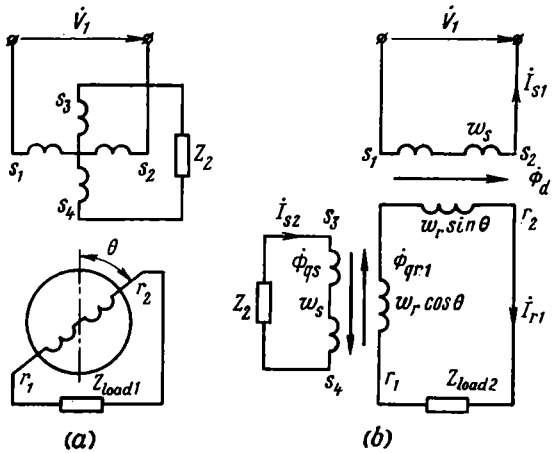

sum of the fluxes $\dot{\Phi}_{qr1}$ and $\dot{\Phi}_{qs}$ of both the windings. At a low value of Z_2, the transformer runs almost under short-circuit conditions and the demagnetizing action of the windings is so great that the resultant quadrature-axis flux $\dot{\Phi}_q$ tends to zero at any value of the load impedance $Z_{load\ 1}$. The effect of the quadrature-axis reaction of the rotor can be proved to fully disappear if we insert in the s_3s_4 winding the impedance $Z_2 = Z_1$, where Z_1 is the external impedance of the s_1s_2 field winding circuit, that is, the output impedance of the power source. When the rotary transformer is connected to the terminals of a heavy-power source, the output impedance of which approaches zero, then the primary balancing condition will be $Z_2 = 0$. Now we see that the balancing condition is independent of the load impedance.

The circuit arrangement illustrated by Fig. 5.7 can be used to test for the rotor quadrature-axis reaction correction under primary balancing conditions. The main stator winding s_1s_2 is disconnected from the power source and shorted out through the impedance Z_1 which equals the output impedance of the power source. The field voltage $\dot{V}_1$ is applied to the rotor winding r_3r_4, and a high-resistance voltmeter is connected across the terminals of the r_1r_2 winding. At an impedance Z_2 corresponding to the primary balancing condition, the resultant quadrature-axis flux, which is linked with the r_1r_2 winding, equals zero and the voltmeter must also read zero (accurate to the permissible error) for any position of the rotor. In the course of primary balancing adjustment the output impedance is independent of the rotor angle of turn. So, the ammeter inserted in the r_3r_4 circuit must read constant values. The field voltage across the rotor winding must be reduced to such a value that the current flowing in the transformer windings should not exceed the rated value.

It should be noted that in primarily balanced rotary transformers the input current and impedance depend on the rotor angle of turn. This feature involves certain problems when such transformers are used in multistep computers and automatic-control devices.

In the case of *secondary balancing* of a rotary transformer, whose winding r_1r_2 is connected to the terminals of a recei-

ver having an input impedance $L_{load\ 1}$ (Fig. 5.8*a*), a respective impedance $Z_{load\ 2}$ is also inserted in the circuit of the other rotor winding r_3r_4. As is seen from the equivalent circuit of Fig. 5.8*b*, the currents $\dot{I}_{r1}$ and $\dot{I}_{r2}$ flowing in the quadrature-axis turns $w_r\cos\theta$ and $w_r\sin\theta$ cause opposing quadrature-axis fluxes which act differentially. In order to fully eliminate the quadrature-axis flux ($\Phi_q = 0$), the quadrature-axis fluxes Φ_{qr1} and Φ_{qr2} of the rotor windings must be equalized. It means that the mmfs of the quadrature-axis turns must be equal:

$$\dot{I}_{r1}w_r\cos\theta = \dot{I}_{r2}w_r\sin\theta \qquad (5.15)$$

Since the output characteristics of the machine with a fully eliminated quadrature-circuit reaction of the rotor are

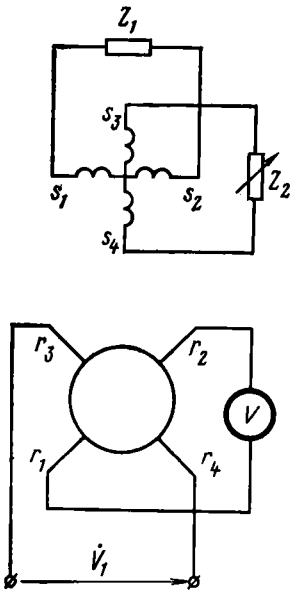

Fig. 5.7. Circuit arrangement to test for primary balancing adjustment

not distorted, we may state, disregarding the demagnetizing action of the direct-axis turns, that

$$\dot{I}_{r1} = \frac{k_{tr}\dot{E}_{s1}\sin\theta}{Z_{load\,1}+Z_{r1}} \tag{5.16}$$

$$\dot{I}_{r2} = \frac{k_{tr}\dot{E}_{s1}\cos\theta}{Z_{load\,2}+Z_{r2}} \tag{5.17}$$

Substitute equations (5.16) and (5.17) in Eq. (5.15):

$$\frac{k_{tr}\dot{E}_{s1}\sin\theta}{Z_{load\,1}+Z_{r1}} w_r\cos\theta = \frac{k_{tr}\dot{E}_{s1}\cos\theta}{Z_{load\,2}+Z_{r2}} w_r\sin\theta \tag{5.18}$$

Equation (5.18) is valid only when

$$Z_{load\,1}+Z_{r1} = Z_{load\,2}+Z_{r2} \tag{5.19}$$

Fig. 5.8. Sine-cosine rotary transformer with secondary-balancing adjustment
(a) schematic diagram; (b) equivalent circuit diagram

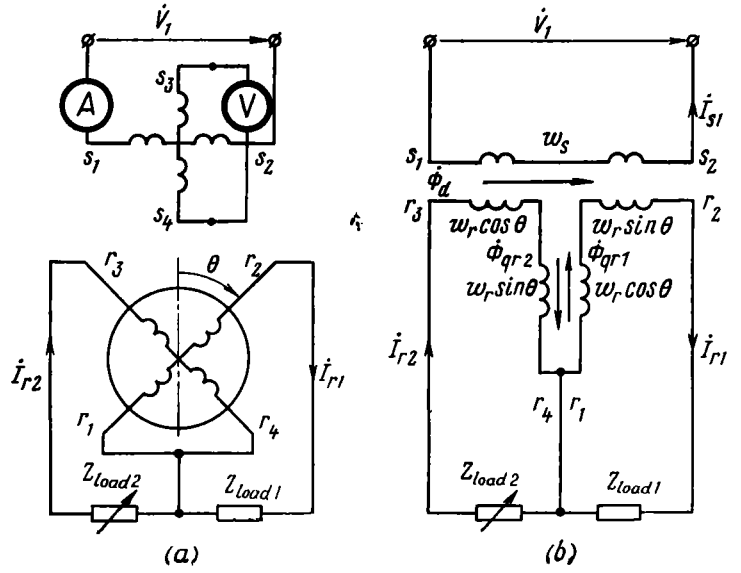

Equation (5.19) specifies the condition of full suppression of the quadrature-circuit rotor reaction in the case of secondary balancing adjustment of a rotary transformer.

The rotary transformer input impedance can be proved to be independent of the rotor angle of turn, that is, at a constant value of $\dot{V}_1$ the current $\dot{I}_{s1}$ flowing in the winding s_1s_2 is independent of the rotor angle of turn, provided the secondary balancing condition is complied with. In fact, disregarding the magnetizing component of the stator current, that is known to be independent of the angle θ because the magnetic system is balanced out, the balanced condition for the direct-axis mmfs will be

$$\dot{I}_{r1}w_r \sin\theta + \dot{I}_{r2}w_r \cos\theta = -\dot{I}_{s1}w_s \qquad (5.20)$$

Substitute currents from equations (5.16) and (5.17) in these equations to obtain

$$-\dot{I}_{s1} = \frac{k_{tr}^2 \dot{E}_{s1} \sin^2\theta}{Z_{load\,1} + Z_{r1}} + \frac{k_{tr}^2 \dot{E}_{s1} \cos^2\theta}{Z_{load\,2} + Z_{r2}} \qquad (5.21)$$

As the secondary balancing condition is equation (5.19), then

$$\dot{I}_{s1} = -\frac{k_{tr}^2 \dot{E}_{s1}}{Z_{load\,1} + Z_{r1}} \qquad (5.22)$$

that is, $\dot{I}_{s1}$ is independent of the angle θ.

If this condition is satisfied, the rotary transformer may be considered as secondarily balanced out (the ammeter inserted in the s_1s_2 winding circuit, as is shown by Fig. 5.8*a*, must read constant values).

The moment of a full suppression of the quadrature-axis flux can be determined more accurately by means of a high-resistance voltmeter connected across the stator quadrature axis s_3s_4 (Fig. 5.8*a*). If the machine is balanced out, the quadrature-axis flux equals zero and, hence, the quadrature-winding emf and the voltmeter readings will be zero too (or about zero within the permissible error limits) for any position of the rotor.

Secondary balancing adjustment is more difficult when the rotary transformer is connected to a varying external

load, because this load is incorporated in secondary balancing equation (5.19). In this case, primary balancing adjustment will be more efficient.

Minimum distortions of the output characteristics of a sine-cosine rotary transformer are obtained when both the primary and the secondary balancing adjustment are used.

So, balancing conditions being satisfied, the rotor winding emfs will also vary under on-load conditions strictly according to the law of sines and cosines of the rotor angle of turn θ. The rotary transformer output voltages $\dot{V}_{r1}$, $\dot{V}_{r2}$ picked off the terminals of the r_1r_2 and r_3r_4 windings will evidently obey the same law. At resistive and inductive loads the voltages $\dot{V}_{r1}$ and $\dot{V}_{r2}$ will be lower than the emfs $\dot{E}_{r1}$, $\dot{E}_{r2}$ due to the demagnetizing action of the direct-axis turns of the rotor windings and due to finite impedances of the windings:

$$\dot{V}_r = \dot{E}_r - \dot{I}_r Z_r = \frac{\dot{E}_r}{1 + Z_r/Z_{load}} \qquad (5.23)$$

In the case of a capacitive load, resonance voltages may occur, and then $V_r > E_r$ (as is the case for synchros and induction tachogenerators, Fig. 3.8).

The output voltage phase varies in steps of 180 deg. every 180 deg. of the rotor angle of turn.

5.5. Linear, Scale, and Vector-Computing Rotary Transformers

As has been already noted, a rotary transformer may perform a number of functions depending on the circuit arrangement used for the connection of its windings. The below-given description concerns the operation of linear, scale, and vector-computing rotary transformers.

5.5.1. Linear Rotary Transformer

Obtaining a linear output characteristic of a rotary transformer boils down to the determination of the relationship between the output voltage and the rotor angle of turn in

the form of a function

$$f(\theta) = \frac{\sin \theta}{1 + c \cos \theta} \tag{5.24}$$

where c is a constant independent of θ.

As can be understood from the analysis of this function, a minimum distortion of this function from the linear curve at angles ranging between —60 and +60 deg. is achieved at $c = 0.54$ and cannot be actually lower than 0.06 per cent. This is the reason why linear rotary transformers of the highest accuracy classes are not available.

The desired function can be obtained by using primary or secondary balancing adjustment circuits for linear rotary transformers.

Linear rotary transformer (LRT) with primary balancing adjustment (Fig. 5.9*a*). In this circuit arrangement, the main stator winding s_1s_2 and the cosine rotor winding r_3r_4 are connected in series. The quadrature stator winding s_3s_4 is shorted out through the impedance Z_2. The output voltage is the voltage picked off the terminals of the cosine rotor winding r_1r_2. The equivalent circuit of such a linear rotary transformer is shown by Fig. 5.9*b*. When the primary balancing condition is satisfied (usually at $Z_2 = 0$), the resultant quadrature-axis flux built up due to the quadrature-axis turns of the rotor windings r_1r_2, r_3r_4 and those of the stator winding s_3s_4 is zero. Hence, self-inductance emf in the quadrature-axis turns of the r_1r_2 winding is also zero. The direct-axis (main) flux $\dot{\Phi}_d$ is set up by the current $\dot{I}_{s1}$ flowing in the turns w_s of the stator winding s_1s_2 and in the direct-axis turns $w_r \cos \theta$ of the rotor winding r_3r_4. In other words, the resultant field winding has $w_s + w_r \cos \theta$ turns. Then the emf $\dot{E}_{r1}$ induced by the flux $\dot{\Phi}_d$ in the direct-axis turns of the r_1r_2 winding will be defined by the equation

$$\dot{E}_{r1} = \dot{E}_1 \frac{w_r \sin \theta}{w_s + w_r \cos \theta} \tag{5.25}$$

where $\dot{E}_1$ is emf of the resultant field winding ($E_1 \approx V_1$).

Upon the transformation of Eq. (5.25), considering that $w_r/w_s = k_{tr}$, we obtain

$$\dot{E}_{r1} = k_{tr}\dot{E}_1 \frac{\sin\theta}{1+k_{tr}\cos\theta}; \qquad (5.26)$$

Equation (5.26) is of exactly the same form as equation (5.24). Hence, the output characteristic of a rotary transformer using the above-described circuit arrangement is linear within the specified limits. Linear rotary transformers are manufactured with a transformation ratio $k_{tr} = 0.565$ at which the optimum value of the c constant is afforded.

Since the load impedance $Z_{load\ 1}$ across the output winding does not produce any effect on the primary balancing conditions, the LRT with primary balancing adjustment can

Fig. 5.9. Linear rotary transformer with primary balancing adjustment
(a) schematic diagram; (b) equivalent circuit diagram

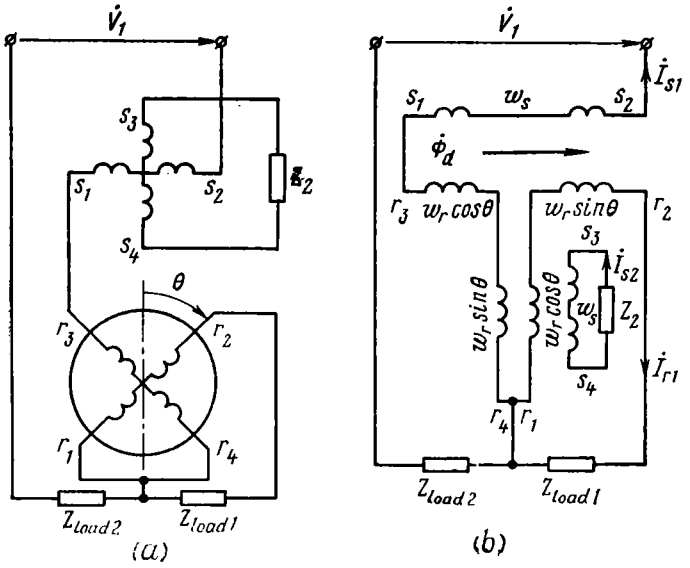

operate at a varying load without distorting a linear output characteristic, which is an essential advantage of the circuit under discussion.

When a linear rotary transformer is to operate in a multistep system, it should be borne in mind that in the case of a circuit with primary balancing adjustment the input impedance depends on the rotor angle of turn. This drawback can be eliminated by using linear rotary transformers with secondary balancing adjustment.

Linear rotary transformer with secondary balancing ad ustment (Fig. 5.10*a*). The field voltage is applied to the terminals of the main stator winding s_1s_2. The quadrature winding s_3s_4 of the stator and the sine winding r_1r_2 of the rotor are connected in series and make up a common circuit whose terminals are connected to a load impedance $Z_{load\ 1}$. The

Fig. 5.10. Linear rotary transformer with secondary balancing adjustment
(*a*) schematic diagram; (*b*) equivalent circuit diagram

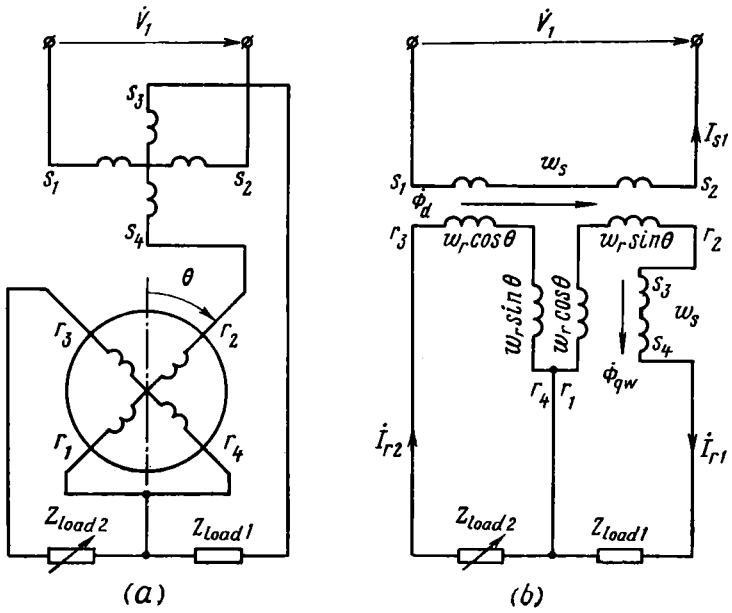

voltage picked off this impedance is the output voltage of the linear rotary transformer. The load impedance of the other rotor winding r_3r_4 must be selected so that the machine is fully balanced out on the rotor side, which can be recognized by a constant value of its input impedance. The equivalent circuit of a linear rotary transformer with secondary balancing adjustment is illustrated by Fig. 5.10*b*. In secondary balancing adjustment the quadrature-axis flux $\dot{\Phi}_q$ of the rotor windings is zero.

The resultant emf of the r_1r_2 winding

$$\dot{E}_{r1} = \dot{E}_{r1m} + \dot{E}_{r1q} \tag{5.27}$$

where $\dot{E}_{r1m}$ is emf induced in the direct-axis turns of the r_1r_2 winding due to the direct-axis flux $\dot{\Phi}_d$; its value can be found from Eq. (5.5); $\dot{E}_{r1q}$ is emf induced in the quadrature axis turns of the r_1r_2 winding due to the flux $\dot{\Phi}_q$ which is built up by the quadrature stator winding s_3s_4 when it carries a current $\dot{I}_{r1}$.

The magnitude of $\dot{E}_{r1q}$ depends on the mutual inductance M_q of the s_3s_4 winding and the quadrature-axis turns of the r_1r_2 winding:

$$\dot{E}_{r1q} = -j\omega_1 M_q \dot{I}_{r1} \tag{5.28}$$

where
$$M_q = w_s w_r \Lambda \cos\theta \tag{5.29}$$

Then

$$\dot{E}_{r1} = k_{tr}\dot{E}_{s1} \sin\theta - j\omega_1 w_s w_r \Lambda \cos\theta \dot{I}_{r1} \tag{5.30}$$

The magnitude of current in the r_1r_2 winding is determined by the equation

$$\dot{I}_{r1} = \frac{\dot{E}_{r1}}{Z_{load\,1} + Z_{r1} + Z_{s2}} \tag{5.31}$$

where Z_{s2} is impedance of the stator winding s_3s_4.

Substitute Eq. (5.31) in Eq. (5.30):

$$\dot{E}_{r1} = k_{tr}\dot{E}_{s1} \frac{\sin\theta}{1 + \dot{a}\cos\theta} \tag{5.32}$$

where $\dot{a}$ is complex multiplier independent of the angle θ:

$$\dot{a} = j \frac{\omega_1 w_s w_r \Lambda}{Z_{load\,1} + Z_{r1} + Z_{s2}} \tag{5.33}$$

It should be noted that the equation for $\dot{E}_{r1}$ as a function of the rotor angle of turn θ is of exactly the same form as Eq. (5.24). Consequently, at $a \approx 0.5$ the emf $\dot{E}_{r1}$ will be a linear function of the angle θ within the above-specified limits. The same law is valid for the output voltage across the impedance $Z_{load\,1}$.

A $Z_{load\,2}$ impedance required to meet the secondary balancing condition is to be found from the equation

$$Z'_{r2} + Z'_{load\,2} \approx 2(Z'_{r1} + Z'_{load\,1} + Z_{s2})$$

where all the impedances are given as referred to the number of turns of the main stator winding.

A disadvantage of the above-described circuit arrangement is that such a linear rotary transformer cannot be used where the load $Z_{load\,1}$ is variable, since a change in $Z_{load\,1}$ will

Fig. 5.11. Output characteristic of linear rotary transformer

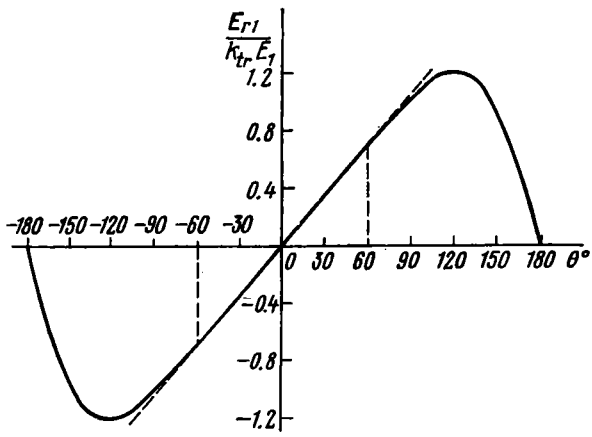

upset the balancing condition, with the result that the $\dot{E}_{r1}$ versus θ function will not be linear.

Figure 5.11 exhibits the output characteristic of a linear rotary transformer in which the balancing condition is satisfied.

5.5.2. Scale Rotary Transformer

Scale rotary transformers SRT are used where the scales of separate units of a system must be matched. It means that they must correlate the output voltage of the preceding step of a system with the desired input voltage of the next step without violating the voltage variation law. All the methods of matching the scales can be generally reduced to the following two procedures: (a) shaping signal voltages and (b) shaping bias voltages.

In the (a) procedure, the scale rotary transformer is connected as a usual sine rotary transformer with primary balancing adjustment (see Fig. 5.6*a*). The output voltage $\dot{V}_1$ of the preceding step is applied to the terminals of the main stator winding s_1s_2. The output voltage of the rotary transformer $\dot{V}_{r1}$, taken off the terminals of the r_1r_2 winding functions as an input signal for the next step of the system. According to Eq. (5.4), at a fixed angle θ the signal $\dot{V}_{r1}$ varies in proportion to the signal $\dot{V}_1$ with a scale factor $k_V \sin\theta$. The voltage transformation ratio is $k_V = V_{r1max}/V_1 \approx k_{tr}$, but its actual value depends on the magnitude and type of the load. The desired signal transmission scale is adjusted by gradually turning the rotor, whereupon the latter is locked in position. With the circuit arrangement described above, the scale factor may steplessly vary within the range of 0 to k_{tr}. The stepless scale-factor adjustment range can be extended by using special circuit arrangements.

Procedure (b) (Fig. 5.12*a*) is most frequently used to extend the operating range of linear rotary transformers in the event of an unambiguous variation of the input quantity (angle θ). The resultant output voltage $\dot{V}_{res}$ is obtained by adding the output voltage $\dot{V}_{out}$ of the linear rotary transformer with

a constant bias voltage $\dot{V}_{bias}$ which is equal to the maximum output voltage of a linear rotary transformer within the linear range of $\dot{V}_{out\ max}$, that is, at +60 deg. (Fig. 5.11). In the process, the zero position of the rotor is displaced 60 deg. to the left of the X axis from point O to point O'. As the rotor turns through 60 deg. from the new zero position, the output voltage of the linear rotary transformer drops to zero and the resultant voltage equals the bias voltage only. With the rotor turned through 120 deg., both the voltages are equal in phase and in magnitude. So, the resultant voltage will be equal to the sum of voltages

$$\dot{V}_{res} = 2\dot{V}_{out\ max}$$

Figure 5.12*b* illustrates a linear rotary transformer circuit using the bias voltage shaping procedure. The bias voltage $\dot{V}_{bias}$ is picked off the scale rotary transformer SRT whose rotor is turned to a position in which the desired output voltage is obtained. Both the rotary transformers are balanced out for the stator end.

Fig. 5.12. Bias voltage generation

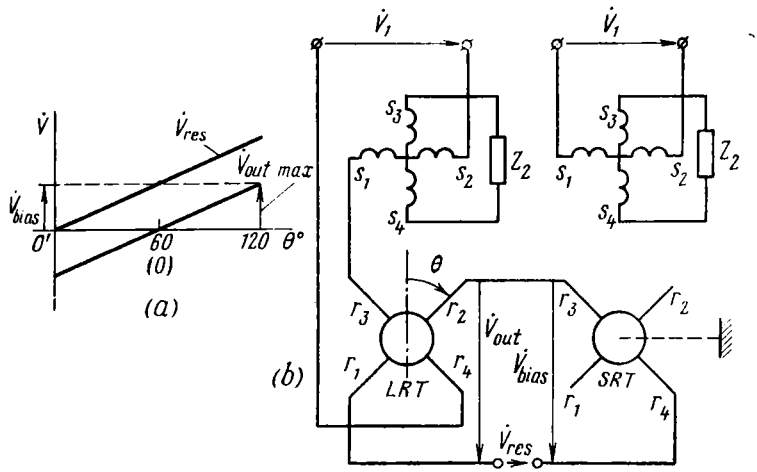

Because here the voltage variation as a function of angle θ is not essential, a scale rotary transformer of a low accuracy class may be used.

5.5.3. Vector-Computing Rotary Transformer

A vector-computing rotary transformer (see the schematic diagram of Fig. 5.13) is used to compute the size and the angle of a hypotenuse of a right-angled triangle whose two cathetuses are known. The stator windings s_3s_4 and s_1s_2 are connected to a single-phase supply via a voltage divider R, which makes it possible to set the desired voltages V_{s1} and V_{s2} at the input of the windings. The terminals of one of the rotor windings are connected to a voltmeter whose scale can be calibrated, whenever required, in terms of linear measures. The other winding of the rotor feeds the control winding CW of an induction servo motor SM whose field winding FW

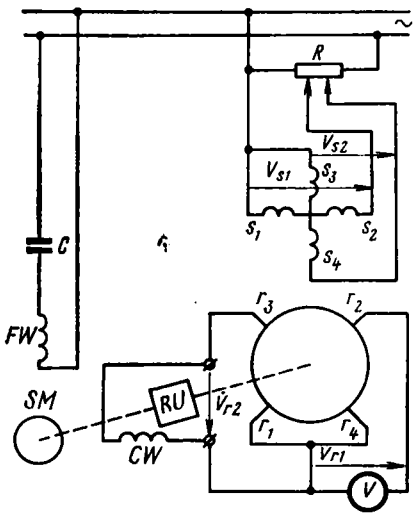

Fig. 5.13. Vector-computing rotary transformer. Schematic diagram

is connected via a capacitor to the same supply as the stator windings of the rotary transformer. The rotors of both the machines are mechanically coupled via a reduction unit. The system functions as follows. With cathetuses s_1 and s_2 of a right-angled triangle being known (Fig. 5.14*a*), find hypotenuse a of this triangle. The cathetuses are introduced into the system in the form of voltages V_{s1} and V_{s2} applied to the rotary transformer windings:

$$V_{s1} \sim s_1; \quad V_{s2} \sim s_2$$

The mmfs of the s_1s_2 and s_3s_4 windings produce fluxes Φ_{s1} and Φ_{s2} which are stationary in space and pulsating along the axes of the windings (Fig. 5.14*b*). As long as the magnetic circuit is not saturated, the modules of these fluxes are proportional to the voltages V_{s1}, V_{s2}. The vector sum of these fluxes yields a resultant flux Φ_a spaced at the same angles relative to the windings s_1s_2 and s_3s_4 as hypotenuse a of the original triangle. The magnitudes of fluxes Φ_{s1}, Φ_{s2}, and

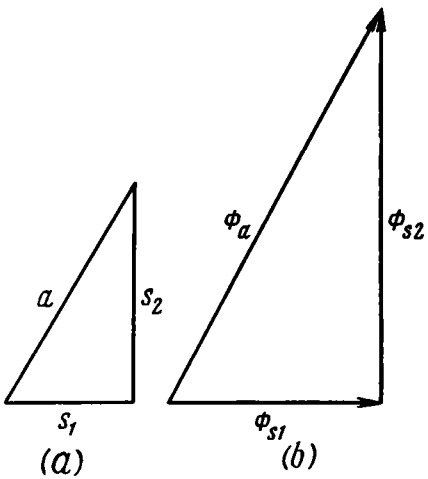

Fig. 5.14. Space diagram of fluxes in vector-computing rotary transformer

Φ_a are obviously proportional to the triangle legs s_1, s_2, and a. The flux Φ_a induces emfs E_{r1} and E_{r2} in the rotor windings.

Voltage V_{r2} is built up across the control winding terminals of the servo motor due to the emf E_{r2} of the r_3r_4 rotor winding. The motor rotor starts running and turns the rotary transformer rotor via the reduction unit. As soon as the r_3r_4 winding assumes a position in which its axis is normal to the Φ_a axis, the emf of this winding drops to zero and the servo motor stops running. In the action, the r_1r_2 winding axis is brought in coincidence with the Φ_a axis and the voltmeter will read the maximum possible value of V_{r1} which is proportional to the hypotenuse a of the given triangle. The rotor angle of turn will determine the angular position of the hypotenuse relative to the cathetuses.

The operation performed by the rotary transformer corresponds to determining a vector and its argument according to known components in a rectangular coordinate system.

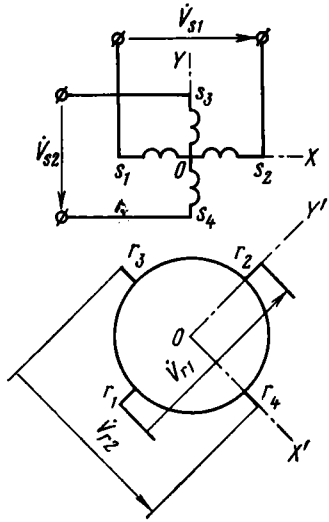

Fig. 5.15. Rotary transformer as coordinate converter

It means that the vector-computing rotary transformer can perform transformations from rectangular to polar coordinates.

A rotary transformer makes it possible to easily solve the problem of transformation from one rectangular coordinate system to another on turning their axes (Fig. 5.15). Align the frame of axes OX and OY of the given system with the stator windings and the frame of axes OX', OY', which is at an angle θ in respect to the former, with the rotor axis. With voltages V_{s1} and V_{s2} applied to the stator windings s_1s_2 and s_3s_4, the voltages across the rotor windings will depend on the mutual inductance between the rotor and the stator windings. According to equations (5.4) and (5.23), we have

$$\dot{V}_{r1} = k_V (\dot{V}_{s1} \sin \theta + \dot{V}_{s2} \cos \theta) \qquad (5.34)$$

$$\dot{V}_{r2} = k_V (\dot{V}_{s1} \cos \theta - \dot{V}_{s2} \sin \theta) \qquad (5.35)$$

The equations obtained represent formulas for the transformation of coordinates accurate within the scale factor. It should be noted that the balancing effect of a rotary transformer functioning as a vector-computing machine is achieved due to the fact that each stator winding is a correcting element in respect to the other stator winding, apart from being an inducing component in respect to the rotor windings.

5.6. Rotary Transformer Errors

Rotary transformers are usually employed by high-accuracy instruments and devices where the error problem is one of the most important considerations. There can be distinguished four types of errors that may occur in transforming an angular motion into electric voltage according to their physical nature.

1. Errors defined according to the functions performed by a particular rotary transformer. With sine-cosine rotary transformers, these errors are displayed as output characteristic distortions from the sine form as a result of inaccurate balancing adjustment [equation (5.12)]; with linear rotary transformers, these errors show themselves as output characteristic distortions from the linear form as a result of inaccurate approximation [equations (5.26) and (5.32)].

2. Design errors brought in as a result of the non-sinusoidal distribution of the winding mmfs over the machine circumference, variations in the air gap reluctance caused by slots on the stator and rotor surfaces, nonlinearity of the *B-H* curve, and hysteresis effect.

These errors can be reduced by using special sine windings obtained through skewing the stator and rotor slots by 1 or 1.5 tooth pitches, or by employing an unsaturated magnetic circuit for the rotary transformers.

3. Manufacturing errors. The main sources of these errors are eccentric stator and rotor bores, unbalanced magnetic circuit, inaccurate positioning and skewing of slots, turn-to-turn faults in windings and shorted-out stampings in magnetic circuits, incorrectly wound stator or rotor. The stator and rotor stacks should be assembled in a fanned manner with due consideration given to magnetic anisotropy of stampings. Turn-to-turn faults, shorted-out stampings, or incorrect number of winding turns must never be admitted.

The effect of manufacturing errors appears as a certain additional emf $\Delta\dot{E}_{add}$ in the output windings. This emf generally has two components, one being an error emf (voltage) $\Delta\dot{E}_e$, which is in phase with the output emf, and the other a residual emf $\Delta\dot{E}_{res}$, which is in phase quadrature with the former. At reference points where the output voltage is zero (zero points), the emf is other than zero.

The error emf $\Delta\dot{E}_e$ can be corrected by the main output emf, for which purpose the rotor should be turned through an additional angle at which $\dot{E}_{out} = -\Delta\dot{E}_e$, that is, through an angle determining asymmetry of zero points. This asymmetry primarily characterizes nonperpendicularity of stator and rotor windings.

The residual emf $\Delta\dot{E}_{res}$ cannot be corrected by turning the rotor through an additional angle. Therefore, the output voltage of rotary transformers never drops to zero within one revolution but only decreases to a certain minimum value.

Manufacturing errors may also cause nonperpendicularity of stator or rotor windings. When this is the case, the

field flux induces an emf in the quadrature winding.

4. Operational errors. Winding resistance varies due to the effect of ambient temperature fluctuations. Supply frequency variations cause a change in inductive reactances. Variations in supply voltage amplitude change the output voltage value.

The accuracy class is established for rotary transformers supposed to operate under normal conditions. In establishing an accuracy class the following characteristics are taken into account:

(1) error in generating a sine (cosine) function for sine-cosine rotary transformers taken in per cent of maximum output voltage $V_{out\ max}$;

(2) error in generating a linear function for linear transformers within a linear region in per cent of $V_{out\ max}$ corresponding to the end of the linear region;

(3) asymmetry of zero points in terms of angular units, which is a maximum deviation of angles with minimum voltage of output windings from the rated angles of 0, 90, 180, and 270 deg.;

(4) maximum emf of the quadrature winding in per cent of the field voltage V_1 with the rotor windings open;

(5) residual emf at zero points in per cent of the field voltage V_1.

The accuracy class is established by the worst of characteristics obtained. Table 5.1 gives basic accuracy characteristics for rotary transformers of different classes.

Table 5.1

Type of rotary transformer	Accuracy characteristics	Accuracy class				
		0.01	0.02	0.05	0.1	0.2
Sine-cosine	Maximum error in per cent of $V_{out\ max}$	±0.01	±0.02	±0.05	±0.1	±0.2
Linear	Maximum error in per cent of $V_{out\ max}$ . . .	—	—	±0.05	±0.1	±0.2

5.7. Sine-Cosine Rotary Transformers as Parts of Remote High-Accuracy Angular Displacement Transmission Systems

Remote angular displacement transmission systems incorporating synchro transformers (see Section 4.4) have an absolute error of at least 10-30′. The transmission error can be brought down to 1-5′ through the use of two-pole sine-cosine rotary transformers as transmitters and receivers. The system illustrated by Fig. 5.16 is identical to the above-discussed system employing synchro transformers as far as its principle of operation and output characteristic are concerned. Most systems incorporating rotary transformers employ stator windings s_1s_2 and s_3s_4 as synchronizing windings, while the rotor windings r_1r_2 and r_3r_4 function as field and output windings.

The accuracy of angular displacement transmission can be further increased by developing double-channel systems, one channel being used for coarse reading and the other for fine reading, with sine-cosine rotary transformers performing the functions of transmitters and receivers. Double-channel systems may use either a mechanical or an electrical reduction unit between the coarse and fine channels.

The description below concerns a double-channel system with a mechanical reduction unit (Fig. 5.17). The transmitters and receivers of both the channels are two-pole machines. The transmitter shafts of the coarse and fine channels are interconnected via a step-up reduction unit *RU2* with

Fig. 5.16. Single-channel system for remote transmission of angular motions

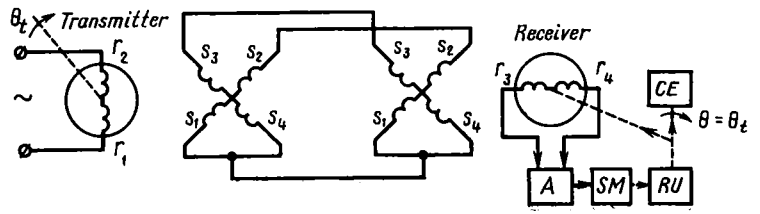

a gear ratio i, that is, the angle of turn of the coarse-channel transmitter, θ_{tc}, and that of the fine-channel transmitter, θ_{tf}, are in the following relationship:

$$\theta_{tf} = \theta_{tc} i \tag{5.36}$$

where $i \gg 1$.

The receiver shafts of the coarse and fine channels are interconnected in a similar way. Equations of voltages across the terminals of the coarse-channel (V_c) and fine-channel (V_f) windings, disregarding the error, can be derived from equations (4.29) and (5.36):

$$V_c = V_{c\,max} \sin \theta_c; \quad V_f = V_{f\,max} \sin (\theta_c i) \tag{5.37}$$

where θ_c is system error angle for the coarse channel.

The output characteristics of the coarse and fine channels corresponding to Eq. (5.37) are shown by Fig. 5.18.

The output voltages of the coarse and fine channels are delivered to the amplifier A (Fig. 5.17) feeding the control winding of the servo motor SM. The servo motor turns the equipment under control CE and the rotors of the receiver through a preset angle via the reduction unit $RU1$.

The amplifier functions so that at a small error angle θ_c the motor is controlled with the fine-channel output volta-

Fig. 5.17. Double-channel system for remote transmission of angular motions

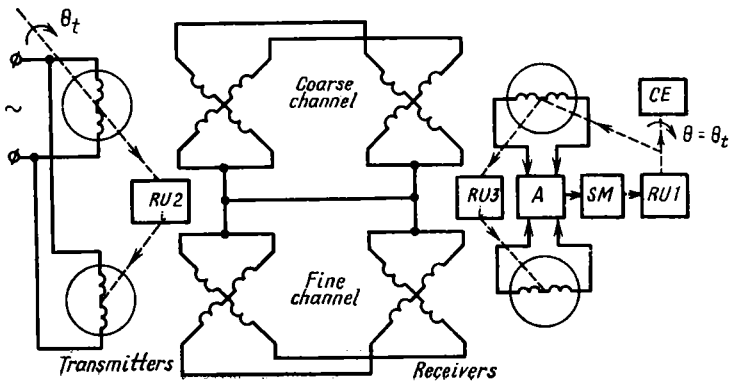

ge, and at a large error angle θ_c the motor control winding is changed over to the coarse-channel output voltage. In the action, the servo system is brought in alignment with the fine-channel error, while its self-synchronizing is provided by the coarse channel. The fine channel cannot afford self-synchronization of the system as it has i stable equilibrium positions within the transmitting shaft revolution $\theta_{tc} = 360$ deg. This can be easily understood from Eq. (5.37) and Fig. 5.18*a* and *b*, where the spatial cycle of the V_f curve is i times as short as that of the V_c curve.

At an odd gear ratio i (Fig. 5.18*a*) of reduction units *RU2* and *RU3* the unstable equilibrium point of the coarse channel, $\theta_c = 180$ deg., does not coincide with the stable equilibrium point of the fine channel, so the system self-synchronizing condition is fully satisfied.

At an even gear ratio i (solid lines on Fig. 5.18*b*), the stable equilibrium point of the fine channel coincides with the unstable equilibrium point of the coarse channel. If during the operation of the system point $\theta_c \approx 180$ deg., the fine channel brings it to $\theta_c = 180$ deg. and fixes it as a stable

Fig. 5.18. Output characteristics of coarse and fine channels

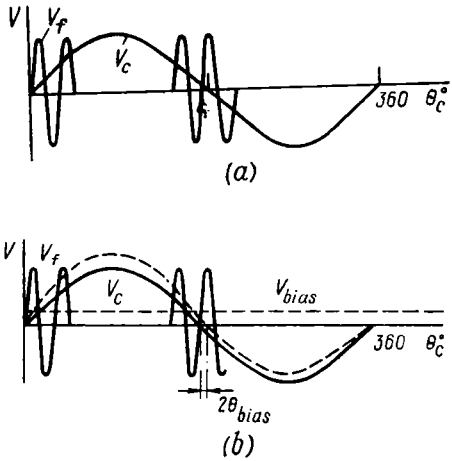

equilibrium position; so, false zero appears. This error can be eliminated as follows. A bias voltage V_{bias} of a constant amplitude (dash line on Fig. 5.18*b*) is added to the coarse channel output voltage.

An initial bias angle θ_{bias} is preset for the coarse channel transmitter or receiver. The coarse-channel output-voltage equation takes the form

$$V_c = V_{c\,max} \sin(\theta_c - \theta_{bias}) + V_{bias} \qquad (5.38)$$

If θ_{bias} and V_{bias} have been selected so that the $V_{bias} = V_{c\,max} \sin \theta_{bias}$ condition is satisfied, then in Eq. (5.38) $V_c = 0$ at $\theta_c = 0°$ and $(180° + 2\theta_{bias})$. It means that the stable equilibrium points of both the channels coincide and the unstable equilibrium point of the coarse channel is offset with respect to the nearest stable equilibrium point of the fine channel by an angle $2\theta_{bias}$ (dash line on Fig. 5.18*b*). The angle $2\theta_{bias}$ must be smaller than the spatial half-cycle of the fine-channel voltage curve, that is,

$$2\theta_{bias} < \frac{360°}{2i}$$

As has been already mentioned, the accuracy of a remote double-channel angle transmission system is determined by the fine-channel error. Manufacturing errors of rotary transformers and difference in their characteristics cause additional voltages across the receiver output in both the channels at a zero error angle ($\theta_c = 0$), with the result that the system turns the equipment under control through an angle $\theta \neq \theta_t$.

The analysis of errors (see Section 5.6) shows that such a turn takes place due to the components of additional voltages which are in phase with the respective error voltages $V_{c\,max}$ and $V_{f\,max}$. These additional voltage components are referred to as error voltages of the course and fine channels, ΔV_{ce} and ΔV_{fe}, respectively. The quadrature components of additional voltages (residual voltages) do not bring in angular errors themselves, but they reduce the system response and cause currents in the amplifier and servo motor control circuits with the system in a matched position.

When similar rotary transformers are used in the coarse and fine channels, the amplitudes of output voltages will

be equal to the amplitudes of error voltages:

$$V_{f\max} = V_{c\max} = V_{\max}$$
$$\Delta V_{ce} = \Delta V_{fe} = \Delta V_e$$

Taking into account Eq. (5.37), we have

$$V_c = V_{\max} \sin \theta_c + \Delta V_e \qquad (5.39)$$
$$V_f = V_{\max} \sin (\theta_c i) + \Delta V_e$$

The specific output voltage (steepness) of both the channels can be found in terms of angular minutes from the equations

$$V_{c\,sp} = \left(\frac{dV_c}{d\theta_c}\right)_{\theta_c \approx 0} = V_{\max} \qquad (5.40)$$
$$V_{f\,sp} = \left(\frac{dV_f}{d\theta_c}\right)_{\theta_c \approx 0} = iV_{\max}$$

that is, the output voltage steepness of the fine channel is i times as great as that of the coarse channel

$$V_{f\,sp} = iV_{c\,sp} \qquad (5.41)$$

The remote transmission angular error provided by each channel is defined as the ratio of the error voltage amplitude to the specific output voltage:

$$\Delta\theta_c = \Delta V_e / V_{c\,sp}; \quad \Delta\theta_f = \Delta V_e / V_{f\,sp} = \Delta V_e / iV_{c\,sp} \qquad (5.42)$$

It follows from Eq. (5.42) that

$$\Delta\theta_f = \Delta\theta_c / i \qquad (5.43)$$

that is, the static error of a double-channel system is i times as low as that of a single-channel system due to the fine channel.

Equation (5.43), however, is valid only if the angular engagement error of the reduction unit is zero. In actual reduction units the angular engagement error $\Delta\theta_{eng}$ is caused by poor finish of gears and by play. The angular error of the system, with allowance made for the reduction unit parameters, is to be found from the equation

$$\Delta\theta = \frac{\Delta\theta_c}{i} + \Delta\theta_{eng} \qquad (5.44)$$

As is seen from Eq. (5.44), an appreciable reduction of the error $\Delta\theta$ by increasing the gear ratio i is possible only as long as $\Delta\theta_f$ is not comparable with $\Delta\theta_{eng}$. Besides, velocity error due to the rotating emf induced in the synchronizing windings of the fine-channel transmitter and receiver rises with the gear ratio i. The reactionary torque opposing the system input shaft rotation rises at the expense of equivalent frictional torques of the fine-channel transmitter and reduction unit, which makes angle transmission from light-power units more difficult. Therefore, the gear ratio i of the reduction units employed in double-channel systems does not usually exceed 33.

The main trend in developing remote high-accuracy angle transmission systems with an error below 1 angular minute is to employ electrical reduction in double-channel systems. Characteristic features of a double-channel system with electrical reduction distinguishing it from a system with mechanical reduction unit illustrated by Fig. 5.17 are as follows:

(a) the fine-channel transmitter and receiver are multipole rotary transformers with pole pairs p_f;

(b) mechanical reduction units *RU2* and *RU3* are replaced by direct mechanical couplings with a transmission ratio of unity.

One revolution of the transmission shaft of such a system corresponds to one spatial cycle of the coarse-channel output voltage V_c and p_f spatial cycles of the coarse-channel output voltage V_f, that is, the channel-to-channel transmission ratio $i = p_f$. It means that equations (5.37) at $i = p_f$ are the output voltage equations of a double-channel system with electrical reduction, and the output characteristics are of the forms shown by Fig. 5.18. Hence, when rotary transformers of equal output voltage amplitudes and equal error voltages are used in coarse and fine channels, the ratio of coarse and fine channel errors can be estimated by using Eq. (5 43):

$$\Delta\theta_f = \Delta\theta_c / p_f \qquad (5.43')$$

Since there are no mechanical reduction units between the channels, the system error in Eq. (5.44) will be primarily

determined by the fine-channel angular error since $\Delta\theta_{eng} = 0$

$$\Delta\theta = \Delta\theta_f = \Delta\theta_c/p_f \qquad (5.44')$$

Thus, the system error in the case of electrical reduction can be reduced p_f times provided the transmitters and receivers used in both the channels have been properly designed. Besides, as has been already mentioned, the manufacturing errors of multipole rotary transformers are averaged. As a result, it may appear that the fine-channel error voltage $\Delta V_{fe} < \Delta V_{ce}$ and the system error $\Delta\theta < \Delta\theta_c/p_f$.

The reactionary torque opposing the input shaft turn is reduced due to the absence of a reduction unit between the coarse and fine-channel transmitters, which makes is possible to transmit angular motions from light-power units.

Conditions of self-synchronizing for a double-channel system with electrical reduction and consequent selection of the transmission ratio are the same as those for a system using a mechanical reduction unit.

Along with separate two-pole and multipole rotary transformers, the double-channel systems with electrical reduction make use of combined machines in which the two-pole and the multipole windings are placed on the same stator and rotor stacks and in the same slots. The total size and mass of the receivers and transmitters are reduced and the operation for matching zeros of the fine and coarse channels is eliminated. When a two-pole and a multipole winding build up sinusoidally distributed mmfs, self-inductance flux linkage between them does not exist and the coarse and fine channels operate independently.

5.8. Application of Rotary Transformers

Rotary transformers have found wide application in automatic computers designed to perform operations of the folowing three basic types:

(1) algebraic operations — addition, multiplication, division, raising to a power, root extraction;

(2) trigonometric operations — determination of voltage amplitudes as sine, arc sine, tangent, arc tangent, secant, and other functions of an angle of turn;

(3) conversion of coordinates,

The discussion below concerns an automatic multiplier of two variables X and Y, the block-diagram of which is shown by Fig. 5.19. The multiplier consists of two electric stages of rotary transformers, a comparison unit CU, and a decoding servo system. The first stage comprises linear rotary transformers LRT_1 and LRT_2; the second stage uses a linear rotary transformer LRT_3 and a scale rotary transformer SRT which functions to set the scale K; the servo system includes an electronic amplifier EA and a servo motor SM with a reduction unit. Signals are passed to the amplifier from the comparison unit CU, and the output voltage is applied to the servo motor control winding. The motor shaft is mechanically coupled with the LRT_3 rotor.

The multiplier operates as follows. Variable factors are introduced by turning the rotors of the LRT_1 and LRT_2; the LRT_1 rotor turns through an angle proportional to X and the LRT_2 rotor through an angle proportional to Y. Then, according to the operating principle of linear rotary transformers, the first stage output voltage will be V_1XY. The output voltage of the second stage will be V_1KZ, where Z is a value proportional to the angle of turn of the LRT_3 rotor. If the V_1KZ voltage is not equal to V_1XY, an error voltage is set up in the comparison unit. The amplified voltage is fed to the servo motor which turns the LRT_3 rotor.

Fig. 5.19. Block-diagram of automatic multiplier

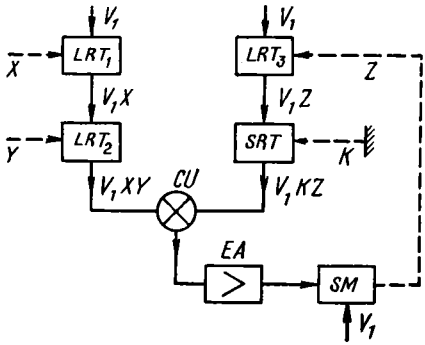

The angle is computed until the following equality is obtained:

$$V_1XY = V_1KZ \tag{5.45}$$

From Eq. (5.45) we obtain

$$Z = \frac{1}{K} XY \tag{5.46}$$

where $1/K$ is multiplication scale.

Proceeding from Eq. (5.46) we may conclude that the angle of turn of the LRT_3 is automatically set in proportion to the product of variables X and Y.

In selecting a rotary transformer type and its location in a computer system, bear in mind the following.

1. When building a computer stage, carry out primary or secondary balancing adjustment of all its components.

2. Since the input impedance of linear rotary transformers with primary balancing adjustment is not a constant value, such LRTs should better be inserted in the beginning of the stage. For the same reason, every two LRTs should better be connected in series.

3. Since the output voltages of rotary transformers placed in the middle of the stage may vary within a wide range, their magnetic circuits should be made of permalloy. Magnetic circuits of rotary transformers located in the beginning of the stage may be made of electric steel.

4. In order to obtain high accuracy in operation, the input impedance Z_{in2} of each concatenated rotary transformer should be 30 or 40 times as high as that of the preceding machine, Z_{in1}. Taking into account that at k_{tr} approaching unity

$$Z_{out} \approx 0.1 k_{tr}^2 Z_{in}$$

the above-given condition can be satisfied if the input impedances of concatenated machines are in the following relationship:

$$Z_{in2} \approx 3 k_{tr1}^2 Z_{in1}$$

Therefore, basic types of rotary transformers are manufactured in standard lines of different input impedances Z_{in}.

5. Conversion of voltages involves phase shifts of secondary voltages in respect to supply voltages in all the rotary transformers. Phase errors may accumulate in concatenated machines. As a result, voltages arriving at the comparison unit over different circuits may appear to be out of phase. Since the errors cannot be fully eliminated, the computer accuracy may reduce. So, measures should be taken to provide mutual phasing-out of signal voltages. The stage voltage is usually phased out at the end of the stage.

Now we shall see how a rotary transformer can be used in electronic devices taking as an example a path tracer unit (for the schematic diagram refer to Fig. 5.20).

The path tracer unit under discussion automatically draws the path of charged particles in electric and cross magnetic fields, which cannot be determined by analytic calculations. The knowledge of these paths is important in designing cathode-ray devices.

A path tracer unit consists of an electrolytic bath receiving the model of a set of electrodes to be studied, a resolver with

Fig. 5.20. Path tracer unit

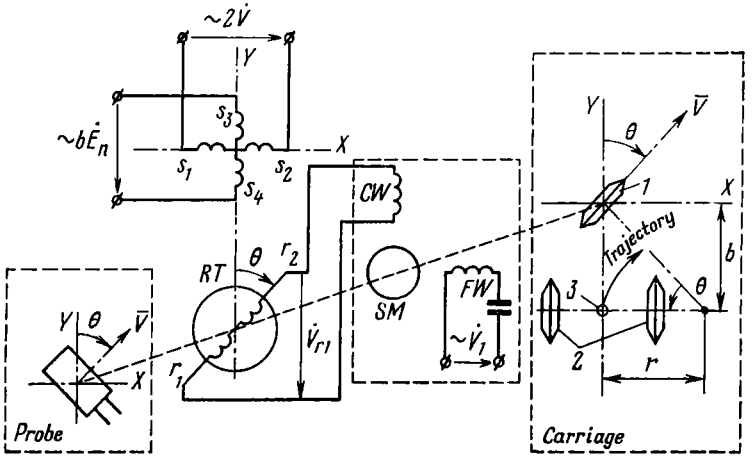

a self-moving carriage and electronic elements, and a two-pin probe which is free to move within the bath. The carriage is fitted with two loose thrust wheels *2* and a guide wheel *1* which is free to turn about the longitudinal axis *Y* of the carriage. The pin of the thrust wheels carries a path tracer *3*. A progressive motion over a plane surface is imparted to the carriage from a continuously running drive motor. According to Fig. 5.20, the instantaneous radius of the curve drawn by the tracer

$$r = \frac{b}{\tan \theta} \tag{5.47}$$

where θ is angle of turn of the guide wheel plane relative to the longitudinal axis of the carriage.

The probe is coupled with the carriage by means of a mechanical coordinate mechanism so that it moves continuously and the surface of its measuring pins is maintained parallel to the guide wheel axis and normal to the direction of motion (speed vector $\dot{V}$). The probe continuously measures two quantities, *viz.*, potential difference covered, V, and electric field strength component normal to the path, E_n. These quantities determine the instantaneous radius of the curve of a charged particle path in the field

$$r = \frac{2V}{E_n} \tag{5.48}$$

As is seen from equations (5.47) and (5.48), the path tracer will draw a curve that strictly follows the path of a charged particle moving in a simulated field, provided the following equation is satisfied at any point of the field:

$$\frac{b}{\tan \theta} = \frac{2V}{E_n} \tag{5.49}$$

This equation transformed to

$$2V \sin \theta = bE_n \cos \theta \tag{5.50}$$

is the main equation of the path tracer unit. The equation is automatically solved by means of a rotary transformer *RT* and a servo motor *SM* controlling the carriage wheels.

The V and E_n quantities measured by the probe within the bath are passed to the electronic amplifier wherein

they are corrected for appropriate factors and time shifts, amplified, and then delivered to the rotary transformer. The *RT* stator windings s_1s_2 and s_3s_4 are supplied with voltages proportional to $2\dot{V}$ and $b\dot{E}_n$, respectively, and shifted 180 deg. from each other. According to Eq. (5.34), the rotor winding r_1r_2 yields a voltage

$$\dot{V}_{r1} = k_v (2\dot{V} \sin \theta + b\dot{E}_n \cos \theta) \qquad (5.51)$$

This voltage is applied to the control winding *CW* of the servo motor *SM*.

The angle of turn, θ, of the *RT* rotor is preset by the guide wheel of the carriage by means of a mechanical linkage. When the angle θ is selected to satisfy equation (5.50), then $V_{r1} = 0$ and the angle of turn of the guide wheel does not change. If equation (5.50) is not satisfied, an error voltage $V_{r1} \neq 0$ is set up. The *SM* rotor starts running and turns the guide wheel of the carriage and the *RT* rotor until equation (5.50) is satisfied again. The instantaneous curve radius always satisfies Eq. (5.48) and the tracer stylus fixed on the carriage automatically draws the path to be known. The path can be traced accurate to 1 per cent, with the time taken to record one path not exceeding 3 or 5 min.

The rotary transformer functions in this system as a resolving element and a device measuring the error angle between the charged particle path and the direction of the carriage motion.

Rotary transformers are also used in high-accuracy remote angle transmission systems (see Section 5.7). The use of rotary transformers in remote transmission systems is also exemplified by Fig. 5.17.

Rotary transformers are often used in automatic-control and telemetering systems for building angle-voltage and angle-phase converters.

Bibliography

1. M. Kostenko, L. Piotrovsky. Electrical Machines (translated from the Russian), MIR Publishers, Moscow, 1968.
2. Seely Samuel. Electromechanical Energy Conversion. MCGRAW-HILL Book Company, INC, 1962.
3. Park R. H. To Reaction Theory of Synchronous Machines, pt. I, Trans. AIEE, 48, 1929; pt. II, Trans. AIEE, 52, 1933.
4. Davis S. A. Stepper Motors, Electromechanical Design, July, 1964.
5. McNaught D., Waloff D. A Review of Stepper Motors and Recent Developments in High Response Units, Instrument Practice, April, 1968.
6. Low-Speed Motor without Reduction Gearing, Electrical Manufacturer, 1965, vol. 9, No. 3.

Appendices

SPECIFICATIONS OF SOME FRACTIONAL-HORSEPOWER ELECTRICAL MACHINES

Table A.1

Amplidynes

Amplidyne type	Rated output, kW	Output voltage, V	Load current, A	Speed, r/min	Control windings				Type of construction
					qnty	input power, W	current, mA	gain	
ЭМУ-3А	0.22	60	3.33	2,850	2	0.35	10.0	570	Amplidyne is built integral in a common frame with a d.c. (П) or induction (А) motor
ЭМУ-3А	0.22	110	1.82	2,850	2	0.40	11.0	500	
ЭМУ-3П	0.35	60	5.00	5,000	2	0.20	8.0	1,500	
ЭМУ-3П	0.35	110	2.75	5,000	2	0.25	9.0	1,200	
ЭМУ-5А	0.55	60	8.30	2,850	2	0.20	8.5	2,500	
ЭМУ-5А	0.55	110	4.50	2,850	2	0.25	10.0	2,000	
ЭМУ-5П	0.75	60	11.70	5,000	2	0.20	8.5	3,600	
ЭМУ-5П	0.75	110	6.40	5,000	2	0.25	10.0	2,800	

Table A.2

Fractional-Horsepower Contactless Direct-Current Motors, Series МБ

Group	Motor type	V_r, V	T_r, N·m	n_r, r/min	I_r, A	Overall dimensions, mm	Commutator volume, cm³
I	МБ-11-Н2-01	27	0.004	2,000±1.5%	0.1	dia. 35×78	400
	МБ-12-Н2-01	27	0.01	2,000±1.5%	0.19	dia. 35×85	400
	МБ-21-Н2-01	27	0.02	2,000±1.5%	0.34	dia. 40×95	400
	МБ-22-Н2-01	27	0.04	2,000±1.5%	0.65	dia. 40×105.5	500
II	МБ-11-Н1-08	27	0.015	9,000	1.1	dia. 35×71	600
	МБ-11-Н3-01	27	0.003	5,000	0.14	dia. 35×80	700
	МБ-12-Ф1-06	14	0.004	4,500	0.26	dia. 42×78	400
	МБ-12-Ф1-08	14	0.008	8,000	0.95	dia. 42×78	500
	МБ-21-Н1-02	29	0.012	4,500	0.35	dia. 45.5×62	500
	МБ-41-Н1-01	27	0.1	2,000	1.8	dia. 70×87	800
	МБ-41-Н1-02	27	0.12	4,000	3.1	dia. 70×87	900
	МБ-21-15	27	0.0165	3,000	0.45	—	—
	МБ-21-16	27	0.025	3,000	0.55	—	—
	МБ-21-19	27	0.01	12,500	0.85	—	—
	МБ-21-25	25	0.008	4,500	0.29	—	—
	МБ-22-23	27	0.017	6,000	0.8	—	—
	МБ-11-26	27	0.004	3,000	0.1	—	—
	МБ-31-27	27	0.04	12,000	2.4	—	—

Note. Group I motors run at stabilized speed.

Table A.3

Disk-Armature Fractional-Horsepower Direct-Current Motors (Experimental Models)

Motor type	Electromechanical time constant, s	Rated speed, r/min	Rated torque, N·m	Rated output, W	Rated control current, A	Rated control voltage, V	Mass, kgf
МРМ-4	0.017	3,500	0.015	—	2	6	—
МРМ-61	—	3,000	—	50	7.5	12	—
ДП-30	—	3,500	0.1	—	6	12	—
ДПО-1	0.039	4,000	2.44	1,000	26	48	—
ДПО-2	0.018	3,000	2.28	700	7.85	110	—
ПДР-6	0.009	3,000	0.2	60	7	14	—
ПДР-3	0.006	3,000	1.35	400	15	39	—
ПЯ-5	0.016	3,000	—	5	1.67	6	0.355
ПЯ-20	0.015	3,000	—	20	5.67	6	0.78
ПЯ-50	0.019	3,000	—	50	7.5	12	1.1
ПЯ-125	0.021	3,000	—	125	16.0	12	1.96
ПЯ-250	0.013	3,000	—	250	31.7	12	6
ПЯ-500	0.013	3,000	—	500	13.8	48	9

Fractional-Horsepower Direct-Current Motors, Series ДПМ

Motor type	n, r/min	Volts						Mass, gf	Overall dimensions, mm
		27			12				
		T_r, N·m	I_r, A	T_{start}, N·m	T_r, N·m	I_r, A	T_{start}, N·m		
ДПМ-20	9,000	0.0015	0.15	0.006	0.0015	0.35	0.006	65	dia. 20×30
	6,000	0.002	0.15	0.005	0.002	0.30	0.005		
	4,500	0.002	0.15	0.004	0.0015	0.25	0.004		
	2,500	—	—	0.002	0.001	0.10	0.002		
ДПМ-25	9,000	—	—	0.015	0.0035	0.65	0.015	120	dia. 25×35
	6,000	0.005	0.3	0.015	0.0045	0.60	0.010		
	4,500	0.005	0.22	0.012	0.005	0.52	0.012		
	2,500	0.005	0.15	0.008	0.005	0.26	0.008		
ДПМ-30	9,000	—	—	0.035	0.007	1.2	0.035	220	dia. 30×45
	6,000	0.007	0.4	0.025	0.01	1.2	0.035		
	4,500	0.01	0.50	0.03	0.01	1.0	0.025		
	2,500	0.01	0.25	0.02	0.01	0.6	0.02		
ДПМ-35	9,000	0.015	1.3	0.07	0.015	2.8	0.07	340	dia. 35×50
	6,000	0.02	1.1	0.06	0.02	2.2	0.06		
	4,500	0.02	0.85	0.05	0.02	1.6	0.05		
	2,500	0.02	0.58	0.035	0.02	1.15	0.035		

Notes. Electromechanical time constant of the ДПМ motors is within the range of 0.035 to 0.055 s.
The series ДПМ motors are suitable for operation under the following conditions:
(1) ambient temperature of −60 to +60° C;
(2) relative humidity up to 98 per cent as referred to 20° C ambient;
(3) atmospheric pressure from 2 to 0.5 at;
(4) vibration of fastening joints in any direction at a frequency of 10 to 2,000 Hz at 10-g acceleration and an amplitude of oscillations not over 1 mm;
(5) linear acceleration up to 50 g in any direction.

Table A.5

Hollow-Armature Fractional-Horsepower Direct-Current Motors, Series ДПР

Motor type	n, r/min	$V = 12$ V			$V = 6$ V			Mass, gf	Overall dimensions, mm
		T_r, N·m	I_r, A	T_{start}, N·m	T_r, N·m	I_r, A	T_{start}, N·m		
ДПР-22	9,000	0.001	0.145	0.004	0.001	0.29	0.004	36	dia. 15×36
	6,000	0.0012	0.130	0.003	0.001	0.23	0.0026		
	4,500	—	—	—	0.001	0.175	0.0026		
	2,500	—	—	—	0.001	0.13	0.002		
		$V = 27$ V			$V = 12$ V				
ДПР-32	9,000	0.002	0.14	0.013	0.002	0.3	0.015	80	dia. 20×46
	6,000	0.0025	0.12	0.01	0.002	0.2	0.011		
	4,500	0.0025	0.095	0.0075	0.002	0.16	0.0075		
	2,500	—	—	—	0.002	0.115	0.0046		
ДПР-42	9,000	0.005	0.29	0.036	0.005	0.66	0.03	150	dia. 25×54
	6,000	0.005	0.20	0.022	0.005	0.45	0.024		
	4,500	0.005	0.16	0.017	0.005	0.35	0.019		
	2,500	0.005	0.11	0.0107	0.005	0.24	0.017		

Table A.5 (cont.)

Motor type	n, r/min	$V = 12$ V			$V = 6$ V			Mass, gf	Overall dimensions, mm
		T_r, N·m	I_r, A	T_{start}, N·m	T_r, N·m	I_r, A	T_{start}, N·m		
ДПР-52	9,000	0.01	0.53	0.12	0.01	1.2	0.108	260	dia. 30×64
	6,000	0.01	0.36	0.087	0.01	0.8	0.081		
	4,500	0.01	0.26	0.075	0.01	0.6	0.068		
	2,500	0.01	0.16	0.042	0.01	0.35	0.051		
ДПР-62	9,000	0.02	1.00	0.2	0.02	2.4	0.19	410	dia. 35×74
	6,000	0.02	0.72	0.17	0.02	1.5	0.177		
	4,500	0.02	0.55	0.147	0.02	1.2	0.125		
	2,500	0.02	0.33	0.082	0.02	0.73	0.081		
ДПР-72	6,000	0.04	1.35	0.35	0.04	3.0	0.32	600	dia. 40×84
	4,500	0.04	1.00	0.3	0.04	2.2	0.28		
	2,500	0.04	0.6	0.19	0.04	1.3	0.185		

Notes. Electromechanical time constant of the ДПР motors is within the range of 0.015 to 0.02 s.
The series ДПР motors are suitable for operation under the following conditions:
(1) ambient temperature of −60 to +60° C;
(2) relative humidity up to 98 per cent as referred to 40° C ambient;
(3) atmospheric pressure from 3 to 0.5 at;
(4) vibration of fastening joints in any direction at a frequency of 5 to 2,000 Hz, at 10-g acceleration and an amplitude of oscillations not over 1 mm;
(5) linear acceleration up to 100 g along the motor axis and up to 50 g in any direction;
(6) shock loads up to 50 g in any direction.

Fractional-Horsepower Induction

Motor type	Rated output (minimum), W	Rated voltage, V		Input current (maximum), A		Capacitance inserted in power winding, μF	Rated frequency, Hz
		power winding	control winding	power winding	control winding		
ДКМ 0.16-12	0.16	36	36	0.18	0.20	1.3	400
ДКМ 0.4-12	0.4	36	36	0.20	0.20	1.2	400
ДКМ 1-12	1	115	36	0.16	0.25	0.2	400
ДКМ 2.5-12	2.5	115	36	0.25	0.45	0.3	400
ДКМ 6-12	6	115	36	0.35	0.55	0.5	400
ДКМ 16-12	16	115	80	0.85	0.75	1.4	400
ДКМ 25-12	25	115	80	0.65	0.6	1.2	400
ДКМ 40-12	40	115	80	1.2	0.85	2	400

Fractional-Horsepower Induction Servo Motors

Motor type	Supply voltage (field circuit), V	Supply frequency, Hz	Rated output, W	Rated speed, r/min	Rated torque, N·m	Starting torque, N·m	Maximum control voltage, V
АДП-1	120	500	3.7	9,000	0.004	0.0055	35
АДП-120	110	400-500	2.4	4,000	0.006	—	—
АДП-123	110	400-500	4.1	4,000	0.01	0.014	110
АДП-262	110	50	9.5	1,850	0.05	0.09	125
АДП-263	110	500	24	6,000	0.04	0.054	165
АДП-362	110	50	19	1,950	0.095	0.17	120
АДП-363	110	500	35	6,000	0.057	0.07	120
АДП-563А	36	500	62	6,000	0.1	0.12	220

Table A.6

Servo Motors, Series ДКМ

Starting torque on the shaft (minimum), N·m	Rated torque on the shaft, N·m	Speed at rated torque, r/min	Electromechanical time constant, s	Mass, gf	Overall dimensions, mm
0.0007	0.0004	4,000	0.015	40	dia. 20 × 35
0.0015	0.0008	5,000	0.02	80	dia. 25 × 42
0.0045	0.0020	5,000	0.025	140	dia. 32 × 53
0.009	0.0045	5,500	0.03	250	dia. 40 × 64
0.016	0.0106	5,500	0.05	500	dia. 50 × 80
0.042	0.0285	5,500	0.05	900	dia. 60 × 95
0.05	0.04	6,100	0.10	1,600	dia. 80 × 100
0.06	0.05	8,000	0.15	2,200	dia. 80 × 118

Table A.7

with Hollow Nonmagnetic Rotor, Series АДП

Current, A		Field circuit capacitance, μF	Efficiency, %	No-load speed, r/min	Break-away voltage, V	Rotor moment of inertia, kg·m²	Electromechanical time constant, s	Mass, kgf	Overall dimensions, mm
control	field								
0.15	0.36	0.3	—	12,500	3	78×10^{-7}	0.048	0.75	dia. 50 × 87
—	0.3	0.3	—	—	—	—	—	0.65	dia. 50 × 108
0.27	0.22	0.3	—	—	—	—	—	0.55	dia. 50 × 90
0.58	0.23	2.5	20	2,650	2	166×10^{-7}	0.0055	1.6	dia. 70 × 122
0.75	0.38	—	32	8,800	3	166×10^{-7}	0.032	1.6	dia. 70 × 122
0.65	0.6	6.5	29	2,650	1.5	390×10^{-7}	0.006	2.6	dia. 85 × 135
1.2	0.55	—	34	8,600	3	390×10^{-7}	0.05	2.6	dia. 85 × 135
0.75	3.3	13	38.5	8,600	3	1180×10^{-7}	0.082	5.7	dia. 108 × 183

Fractional-Horsepower Induction Servo

Motor type	Rated output, W	Maximum control power, VA	Rated field voltage, V	Rated control voltage, V	Starting field current, A	Starting control current, A	Rated frequency, Hz	Starting torque on the shaft, N·m
ДИД 0.1ТА	0.1	2	36	30	0.08	0.07	400	0.00026
ДИД 0.5ТА	0.3	3.3	36	30	0.15	0.11	400	0.0007
ДИД 0.6ТА	0.6	3.0	36	30	0.155	0.1	400	0.0012
ДИД 1ТА	1	3.6	36	30	0.25	0.12	400	0.0016
ДИД 2ТА	2	7.0	36	30	0.4	0.23	400	0.0034
ДИД 3ТА	3	12	36	30	0.7	0.4	400	0.01
ДИД 5ТА	5	14	36	30	1.2	0.48	400	0.022
ДИД 10ТА	10	22.5	36	30	1.4	0.75	400	0.028

Fractional-Horsepower Induction Servo

Motor type	Rated field voltage, V	Rated control voltage, V	Breakaway voltage, V	Starting field current, A	Starting control current, A
ДМ-0.04	12	12	—	0.1	0.1
ДМ-0.1	36	18	—	0.09	0.07
ДМ-0.4	36	30	1	0.125	0.15
ДМ-1	36	30	1	0.24	0.29
ДМ-2.5	36	30	1	0.41	0.46

Motors, with Hollow Nonmagnetic Rotor, Series ДИД

Table A.8

Rated torque on the shaft, N·m	No-load speed, r/min	Rated efficiency, %	Breakaway voltage at 20° C, V	Rotor moment of inertia, kg·m²	Electromechanical time constant, s	Mass, gf	Overall dimensions, mm
0.00015	13,000	—	0.5	2.2×10^{-8}	0.09	25	dia. 18.5×38
0.00035	14,000	—	0.5	4.4×10^{-8}	0.09	50	dia. 22.2×44.8
0.00065	16,000	11	0.5	7.4×10^{-8}	0.05	60	dia. 26×45.5
0.0009	18,000	17.5	0.5	6.9×10^{-8}	0.038	110	dia. 33×54.5
0.0018	18,000	20	0.5	8.8×10^{-8}	0.032	160	dia. 33×68.5
0.0056	8,000	20	0.7	23.2×10^{-8}	0.026	350	dia. 48×70
0.012	6,000	20	0.7	245×10^{-8}	0.052	720	dia. 60×104
0.015	10,000	30	0.5	360×10^{-8}	0.05	1,000	—

Motors, Series ДМ (Heat-Resistant)

Table A.9

Rated frequency, Hz	Starting torque, N·m	No-load speed, r/min	Rated output, W	Electromechanical time constant, s	Mass, gf
400	2.5×10^{-4}	8,000	0.04	—	20
400	6×10^{-4}	8,500	0.1	—	40
400	20×10^{-4}	5,800	0.4	0.024	70
400	40×10^{-4}	5,800	1.0	0.03	175
400	100×10^{-4}	5,800	2.5	0.066	330

Fractional-Horsepower Induction

Motor type	Rated field voltage, V	Rated control voltage of series-connected windings, V	Rated control voltage of parallel-connected windings, V	Breakaway voltage, V	Starting power of field winding, W	Starting power of control winding, W	Rated frequency, Hz	Starting torque, N·m
АД-20	24	24	12	1	2.6	2.6	400	13×10^{-4}
АД-25		40	20	1				
	40				3.5	3.5	400	40×10^{-4}
		24	12	0.6				
АД-32		40	20	1				
	40				3.5	3.5	400	75×10^{-4}
		24	12	0.6				
АД-40		40	20					
	40			—	—	—	400	150×10^{-4}
		24	12					
АД-50		40	20					
	40			—	—	—	400	210×10^{-4}
		24	12					

Fractional-Horsepower Induction

Motor-amplidyne set type	Rated output, W	Supply voltage, V	Frequency, Hz	Rated stator current, A	Efficiency, %	Power factor or ($\cos\varphi$)	Capacitor capacitance, μF	Synchronous speed, r/min
РДУ-5-50	5	127	50	0.8	20	0.5	10	3,000
РДУ-10-50	10	127	50	1.0	20	0.5	20	3,000
РДУ-20-50	20	127	50	1.3	20	0.6	30	3,000
РДУ-40-50	40	127	50	1.5	35	0.8	70	3,000
РДУ-60-50	60	127	50	1.5	35	0.82	14	3,000
РДУ-90-50	90	127	50	1.6	38	0.85	25	3,000

Table A.10

Servo Motors, Series АД

No-load speed, r/min	Rated output, W	Rated efficiency, %	Starting power factor ($\cos\varphi$)	Static frictional torque, N·m	Rotor moment of inertia, kg·m²	Electromechanical time constant, s	Mass, gf	Overall dimensions, mm
6,000	0.3	6	0.85	10^{-4}	2×10^{-8}	0.015	30	dia. 20 × 25
6,500	0.9	18	0.6	10^{-4}	10×10^{-8}	0.020	74	dia. 25 × 35
7,000	1.7	21	0.5	10^{-4}	10×10^{-8}	0.010	130	dia. 32 × 38
5,000	2.5	20	—	—	50×10^{-8}	0.015	240	dia. 40 × 43.5
5,000	3.5	20	—	—	60×10^{-8}	0.016	450	dia. 50 × 52.5

Table A.11

Motor-Amplidyne Sets

Rotor type	Rotor moment of inertia, $\times10^4$, kg·m²	Speed control range	Continuous control current, mA	Maximum control current, mA	Power gain	Mass, kgf	Overall dimensions, mm
Hollow sleeve	0.2	1 : 20	20	100	200	10	dia. 100×150 Less shaft extensions
Same	0.203	1 : 20	20	100	200	13	dia. 160×150
Same	0.206	1 : 20	20	100	200	14.6	dia. 208×150
Squirrel-cage	4.3	1 : 20	20	100	300	12	dia. 125×200
							dia. 148×200
Same	4.05	1 : 20	20	100	300	13	
Same	5.4	1 : 20	20	100	400	14	dia. 170×200

Motor-amplidyne set type	Rated output, W	Supply voltage, V	Frequency, Hz	Rated stator current, A	Efficiency, %	Power factor or (cos φ)	Capacitor capacitance, μF	Synchronous speed, r/min
РДУ-120-50	120	127	50	2.2	40	0.9	32	3,000
РДУ-180-50	180	127	50	3.2	42	0.9	45	3,000
РТДУ-180-50	180	220	50	1.4	52	0.9	—	3,000
РТДУ-250-50	250	220	50	2	57	0.9	—	3,000
РТДУ-370-50	370	220	50	2.8	63	0.85	—	3,000
РТДУ-550-50	550	380	50	3.7	65	0.8	—	3,000
РТДУ-750-50	750	380	50	5	68	0.8	—	3,000
РДУ-5-400	5	115	400	0.4	20	0.85	1.5	6,000
РДУ-10-400	10	115	400	0.95	20	0.9	2.2	6,000
РДУ-20-400	20	115	400	1.4	20	0.9	5	6,000
РДУ-40-400	40	115	400	2.3	30	0.9	10	6,000
РДУ-60-400	60	115	400	1.6	40	0.85	5	6,000
РДУ-90-400	90	115	400	2.25	40	0.85	8	6,000
РДУ-120-400	120	115	400	2.8	42	0.90	10	6,000
РДУ-180-400	180	115	400	3.85	45	0.9	15	6,000
НДУ-60-50	60	127	50	1.3	40	0.95	5	3,000
НДУ-90-50	90	127	50	1.8	42	0.95	5	3,000
НДУ-120-50	120	127	50	2.4	42	0.95	14	3,000
НДУ-180-50	180	127	50	3.4	44	0.95	25	3,000
НДУ-250-50	250	127	50	4.7	44	0.95	32	3,000
НТДУ-250-50	250	220	50	2.0	63	0.94	—	3,000
НТДУ-370-50	370	220	50	2.7	63	0.95	—	3,000
НТДУ-550-50	550	220	50	3.5	64	0.95	—	3,000
НТДУ-750-50	750	380	50	4.0	65	0.96	—	3,000

Notes: 1. Designations: *P* — reversible, two-phase; *PT* — reversible three-phase;
2. The motors will operate normally at an ambient temperature of
3. The motors will sustain shocks at a rate of 80 shocks per minute

Table A.11 (cont.)

Rotor type	Rotor moment of inertia, $\times 10^4$, kg·m²	Speed control range	Continuous control current, mA	Maximum control current, mA	Power gain	Mass, kgf	Overall dimensions, mm
Squirrel-cage	6.25	1 : 20	20	100	400	16	dia. 208×200
Same	7.3	1 : 20	20	100	500	19	dia. 265×200
Same	31.8	1 : 20	50	150	150	23	dia. 360×260 Including
Same	36.3	1 : 20	50	150	150	26	dia. 380×260 shaft extensions
Same	41.5	1 : 20	50	150	150	31	dia. 420×260
Same	188	1 : 10	100	300	160	39	dia. 342×390
Same	225	1 : 10	100	300	200	56	dia. 402×390
Hollow sleeve	0.18	1 : 20	20	100	200	5.0	dia. 140×180 Less shaft extensions
Same	0.198	1 : 20	20	100	200	7.7	dia. 168×180
Same	0.203	1 : 20	20	100	200	10	dia. 180×180
Same	0.203	1 : 20	20	100	200	12.5	dia. 210×180
Squirrel-cage	3.8	1 : 20	20	100	1000	11	dia. 170×200
Same	4.3	1 : 20	20	100	1,100	13	dia. 185×200 Less shaft extensions
Same	4.85	1 : 20	20	100	1.300	14	dia. 200×200
Same	5.4	1 : 20	20	100	1,600	16	dia. 220×200
Same	3.2	1 : 20	20	100	1,200	11.5	dia. 110×200
Same	3.6	1 : 20	20	100	1,300	13.2	dia. 125×200
Same	3.75	1 : 20	20	100	1,500	14.0	dia. 148×200
Same	4.4	1 : 20	20	100	1,800	15.1	dia. 176×200
Same	3	1 : 20	20	100	2,000	16.8	dia. 208×200
Same	20.2	1 : 20	50	150	150	21	dia. 296×255 Including
Same	25.4	1 : 20	50	150	150	27	dia. 336×255 shaft extensions
Same	30.6	1 : 10	50	150	200	33	dia. 375×375
Same	127	1 : 10	100	300	150	55	dia. 333×375

H — nonreversible, two-phase; *HT* — nonreversible three-phase.
—50 to +40° C at a relative humidity of 80 per cent.
and a linear acceleration up to 9 *g*.

Table A.12

General-Purpose Fractional-Horsepower Induction Motors, Series УАД Three-Phase (star-connected, 220 V)

Motor type	P_r, W	n_r, r/min	I_r, A	Efficiency, %	T_{max}/T_r	T_{start}/T_r	I_{start}/I_r
УАД-12 . .	1.5	2,700	0.055	14	2.5	2.5	2
УАД-22 . .	4	2,700	0.08	28	2	1.5	2
УАД-32 . .	7	2,700	0.11	30	2	2	2.5
УАД-42 . .	13	2,700	0.13	45	2	2	3.2
УАД-52 . .	20	2,700	0.17	55	2	2	4.5
УАД-62 . .	40	2,700	0.25	60	1.5	1.5	6
УАД-72 . .	70	2,700	0.4	65	1.5	1.5	6
УАД-24 . .	1.2	1,280	0.05	9	2	1.5	1.5
УАД-34 . .	2.5	1,250	0.09	11	1.5	1.5	1.5
УАД-44 . .	6	1,280	0.13	20	1.5	1.5	2
УАД-54 . .	9	1,280	0.17	25	1.5	1.5	2.5
УАД-64 . .	20	1,280	0.23	40	1.5	1.5	3
УАД-74 . .	30	1,280	0.3	50	1.5	1.5	3.5

Single-Phase (220 V)

Motor type	P_r, W	n_r, r/min	I_r A	Efficiency, %	T_{max}/T_r	T_{start}/T_r	I_{start}/I_r	Capacitance, μF
УАД-12	1	2,750	0.055	10	2	0.5	2	0.5
УАД-22	3	2,750	0.08	20	2	0.5	2	1
УАД 32	5	2,750	0.11	25	1.5	0.3	2.5	1.5
УАД-42	10	2,750	0.13	44	1.5	0.3	3	1.5
УАД-52	18	2,750	0.19	50	1.5	0.3	3.5	2
УАД-62	30	2,750	0.3	54	1.5	0.2	4	4
УАД-72	50	2,750	0.42	60	1.5	0.1	5	5
УАД-24	1	1,280	0.055	9	1.5	0.5	1.5	0.5
УАД-34	2	1,280	0.09	11	1.5	0.5	1.5	1
УАД-44	4	1,300	0.14	14	1.5	0.5	1.5	2
УАД-54	8	1,300	0.16	25	1.5	0.5	2	2
УАД-64	15	1,300	0.23	35	1.5	0.3	2.5	3
УАД-74	25	1,300	0.3	45	1.5	0.2	3	4

Table A.13

Fractional-Horsepower Single-Phase Hysteresis Synchronous Motors, Series Г

Motor type	Rated output, W	Input power, W	Rated current, A	Speed, r/min	Overall dimensions, mm	Mass, kgf
Г-205	1	20	0.09	3,000	dia. 55×60	0.4
Г-314	8	35	0.18	3,000	dia. 72×90	0.9
Г-413	16	60	0.4	3,000	dia. 88×115	1.8
Г-509	40	100	0.7	3,000	dia. 103×145	3.5
Г-316	4	30	0.18	1,500	dia. 72×90	0.9
Г-415	12	50	0.4	1,500	dia. 88×115	1.8
Г-511	30	90	0.7	1,500	dia. 103×145	3.5

Note. Supply voltage 220 V, 50 Hz.

Table A.14

Fractional-Horsepower Reducing Synchronous Motors, Type ДСР (50 Hz, 220 V)

Motor type	Power system	Input current, A	Rated torque, N·m	Maximum and starting torque, N·m	cos φ	n, r/min	Starting, time, s	Mass, gf
ДСР-2	Single-phase	0.06	0.1	0.2	0.95	2	Maximum 0.1	700
	Three-phase	0.055	0.3	0.6	0.85			
ДСР-60	Single-phase	0.06	0.01	0.02	0.95	60	Maximum 0.1	650
	Three-phase	0.055	0.015	0.03	0.85			
ДСР-115	Single-phase	0.06	0.05	0.07	0.95	$115\frac{5}{13}$	Maximum 0.1	600
	Three-phase	0.055	0.075	0.01	0.85			

Table A.15

Stepper Motors with Permanent-Magnet Rotor (27-V supply)

Motor type	Stepping angle (increment), deg.	Number of phases	Maximum static torque, N·m	Rated load torque, N·m	Rotor moment of inertia, kg·m²	Rated moment of load inertia, kg·m²	Response frequency, Hz		Power input in statics, W	Overall dimensions, mm	Mass, kgf
							no-load	rated			
ДШ-0,025А	22.5	4	0.02	0.0025	2.5×10^{-7}	2.5×10^{-7}	550	450	24	dia. 40×57	0.22
ДШ-0,04А	22.5	4	0.035	0.004	3.5×10^{-7}	3.5×10^{-7}	500	350	20	dia. 40×67	0.25
ДШ-0,1А	22.5	4	0.08	0.01	19×10^{-7}	19×10^{-7}	400	300	32	dia. 50×80	0.5
ДШ-0,25А	22.5	4	0.15	0.025	58×10^{-7}	58×10^{-7}	300	250	40	dia. 60×95	0.9
ДШ-0,4А	22.5	4	0.21	0.04	125×10^{-7}	125×10^{-7}	250	200	80	dia. 80×100	1.6
ДШ-1А	22.5	4	0.6	0.1	420×10^{-7}	420×10^{-7}	200	150	145	dia. 100×130	3.0
ДШ-4А	18	4	1.6	0.4	$1{,}370\times10^{-7}$	$1{,}370\times10^{-7}$	150	100	320	dia. 120×190	8.1
ДШ-6А	18	4	2.1	0.6	$3{,}900\times10^{-7}$	$3{,}900\times10^{-7}$	100	80	270	dia. 155×200	11.5
ДШ-10А	18	4	3.0	1.0	$4{,}200\times10^{-7}$	$4{,}200\times10^{-7}$	80	70	340	dia. 160×248	14.8
ШДА-2-1	15	2	0.016	0.001	—	1×10^{-7}	—	400	11.7	dia. 32×35.5	0.14
ШДА-2-2	15	2	0.04	0.004	—	3×10^{-7}	—	350	18.0	dia. 40×45	0.28
ШДА-2-3	15	2	0.10	0.01	—	7×10^{-7}	—	320	36.5	dia. 50×55.5	0.55
ШДА-2-4	15	2	0.25	0.04	—	25×10^{-7}	—	300	85	dia. 60×69.5	1.0
ШДА-2-5	15	2	0.5	0.06	—	60×10^{-7}	—	250	162	dia. 80×84	2.0
ШДА-2-6	18	2	1.0	0.1	—	125×10^{-7}	—	200	208	dia. 100×92	3.15
ШДА-3-1	15	3	0.02	0.001	—	1×10^{-7}	—	500	8.5	dia. 32×38	0.14
ШДА-3-2	15	3	0.04	0.004	—	3×10^{-7}	—	450	13.5	dia. 40×48	0.28
ШДА-3-3	15	3	0.09	0.01	—	7×10^{-7}	—	350	17.5	dia. 50×58	0.55
ШДА-3-4	15	3	0.25	0.04	—	25×10^{-7}	—	150	27	dia. 60×72	1.0
ШДА-3-5	15	3	0.5	0.06	—	60×10^{-7}	—	150	34	dia. 80×87	2.0
ШДА-3-6	15	3	1.0	0.1	—	125×10^{-7}	—	100	50	dia. 100×95	3.5

Table A.16

Three-Phase Reluctance Stepper Motors, Series ШДР

Motor type	Stepping angle (increment), deg.	Maximum static torque, N·m	Rated load torque, N·m	Rotor moment of inertia, kg·m²	Rated moment of load inertia, kg·m²	Response frequency, Hz		Power input in statics, W	Rated voltage, V	Overall dimensions, mm	Mass, kgf
						no-load	rated				
ШДР-231	9	0.0125	0.004	0.83×10^{-7}	0.1×10^{-7}	1,500	700	20	28	dia. 35 × 58	0.18
ШДР-321	6.43	0.0045	0.002	—	0.1×10^{-7}	—	450	8.1	28	dia. 34 × 39	0.155
ШДР-521	9	0.054	0.016	3.1×10^{-7}	5×10^{-7}	1,500	600	56	28	dia. 48 × 85	0.45
ШДР-523	3	0.16	0.04	28×10^{-7}	45×10^{-7}	1,500	600	56	28	dia. 58 × × 116.5	0.5
ШДР-711	3	0.12	0.04	15×10^{-7}	15×10^{-7}	1,100	600	49	14	dia. 58 × 44	0.35
ШДР-721	3	0.19	0.06	21.5×10^{-7}	22×10^{-7}	1,100	600	70	14	dia. 58 × 58	0.5

Table A.17

Direct-Current Tachogenerators

Tachogenerator type	Field voltage, V	Field current, A	No-load gain, V/r/min	Maximum speed, r/min	Maximum load current, A	Armature winding resistance, Ohm	Mass, kgf	Moment of rotor inertia, kg·m²
СЛ-161	110	0.050	0.020	3,500	0.10	170	0.49	52×10^{-7}
СЛ-261	110	0.080	0.025	3,600	0.20	51	1.25	196×10^{-7}
ТД-101	110	0.065	0.021	1,500	0.10	330	0.70	62×10^{-7}
ТД-102	110	0.065	0.050	1,500	0.10	330	0.70	62×10^{-7}
ТД-103	110	0.060	0.100	1,500	0.10	660	0.70	196×10^{-7}
ТД-201	110	0.100	0.130	1,000	0.20	780	—	235×10^{-7}
ТГ-1	27	0.300	0.007	1,100	0.01	430	1.86	685×10^{-7}
ТГ-2	27	0.300	0.020	2,400	0.02	115	0.80	137×10^{-7}
ТГП-1	—	—	0.006	7,000	0.1	—	0.15	—

Notes: 1. Service life of series ТГ tachogenerators is 1,000 hours, that of remaining types is 2,000 hours.
2. Series ТД tachogenerators will operate trouble-free at an ambient temperature of −40 to +40 °C and a relative humidity up to 98 per cent; series ТГ tachogenerators will operate normally at an ambient temperature of −40 to +70°C and a relative humidity up to 98 per cent.
3. Type ТГ-1 tachogenerator has the same overall dimensions as the СЛ-369 fractional-horsepower direct-current motor.

Table A.18

Induction Tachogenerators

Tachogenerator type	Field voltage, V	Field current, A	Frequency, Hz	No-load gain, V/r/min	Output characteristic nonlinearity, %	Maximum speed, r/min	Mass, kgf
ТД-1	110	0.15	50	0.008	1.5	2,400	3.0
ТД-2	127	0.13	50	0.008	1.5	2,400	3.0
АТ-231	110	0.25	400-500	0.0085	0.1	4,000	2.10
АТ-261	110	0.22	400	0.0075	0.1	4,000	1.30
ТГ-4	110	0.30	400	0.0100	2.5	6,000	1.50
ТГ-5А	115	0.06	400	0.0110	2.5	9,000	0.28

Notes. 1. The ТГ-5А tachogenerator is fitted with an expansion device to eliminate output voltage temperature error.
2. The tachogenerators will operate trouble-free at an ambient temperature of −40 to +50°C (or −60 to +50°C for ТГ-5А type) and a relative humidity of up to 98 per cent.

Table A.19

Differential Synchros

Synchro type	Field voltage, V	Frequency, Hz	Secondary voltage, V	Specific torque, N·m/deg.	Maximum synchronizing torque, N·m	Mass, kgf	Overall dimensions, mm
ДИД-101	50	50	49	—	—	0.80	dia. 62 × 119
ДИД-505	57	50	68	—	—	2.65	dia. 100 × 150
ДИД-204	100	400→	—	—	—	—	dia. 45 × 109.5
НЭД-101	50	50	50	0.0006	0.03	0.80	dia. 62 × 119
НЭД-101Б	150	50	—	0.0004	0.025	0.80	dia. 62 × 119
НЭД-101П	100	400	—	0.001	0.065	—	dia. 62 × 119
НЭД-501	57	50	57	0.0035	0.255	2.50	dia. 100 × 150
НЭД-501Б	150	50	—	0.0017	0.125	2.60	dia. 100 × 150
СДС-1	90	400	90	—	—	2.22	dia. 86 × 160
СДСМ-1	58	400	58	—	—	0.20	dia. 36 × 66
ЭД-101	50	50	38	0.0002	0.016	0.80	dia. 62 × 119
ЭД-501	57	50	52	0.0017	0.125	2.65	dia. 100 × 150
ЭД-501Б	39	50	35.5	0.0015	0.075	2.65	dia. 100 × 150

Table A.20

Magslip Transmitters with Unipolar Excitation

Magslip type	Field voltage, V	Frequency, Hz	Field current, A	Input power, W	Secondary voltage, V	Rotor moment of inertia, $kg \cdot m^2$	Mass, kgf	Overall dimensions, mm
БД-404А	110	50	0.45	12.5	49	1.32×10^{-5}	1.20	dia. 62×119
БД-404Б	110	50	0.40	12.5	150	1.32×10^{-5}	1.25	dia. 62×119
БД-500	127	50	0.50	20.0	55	8.7×10^{-5}	2.20	dia. 100×86.5
БД-501А	110	50	1.20	25.0	55	14.2×10^{-5}	3.75	dia. 100×150
БД-501Б	110	50	1.20	25.0	150	14.2×10^{-5}	3.85	dia. 100×150

Notes. 1. The speed ensuring synchronous follow-up of transmitter rotor is 500 r/min.
2. The service life at an average operational speed of 10 r/min is 3,000 hours.
3. Magslip transmitters БД-500 will operate trouble-free at an ambient temperature of −40 to +50°C and a relative humidity up to 98 per cent, as referred to 20±5°C ambient; the remaining types of magslip transmitters will operate trouble-free at an ambient temperature of −40 to +40°C and a relative humidity up to 98 per cent as referred to 20±5°C ambient.

Table A.21

Magslip Receivers with Unipolar Excitation

Magslip type	Field voltage, V	Frequency, Hz	Field current, A	Input power, W	Secondary voltage, V	Specific torque, N·m/deg.	Maximum synchronizing torque, N·m	Rotor moment of inertia, kg·m²	Mass, kgf	Overall dimensions, mm
БС-404А	110	50	0.45	12.5	49	0.0005	0.024	1.32×10^{-5}	1.30	dia. 62 × 119
БС-404Б	110	50	0.45	12.5	150	0.0004	0.021	1.32×10^{-5}	1.30	dia. 62 × 119
БС-405	110	50	0.09	2.0	36	—	—	1.32×10^{-5}	1.25	dia. 62 × 119
БС-405Б	110	50	0.09	2.0	81	—	—	1.32×10^{-5}	1.25	dia. 62 × 119
БС-500	127	50	0.50	20.0	55	0.0017	0.08	8.7×10^{-5}	2.30	dia. 100 × 86.5
БС-501А	110	50	1.20	25.0	55	0.0032	0.18	38.5×10^{-5}	4.00	dia. 100 × 150
БС-501Б	110	50	1.20	25.0	150	0.0032	0.18	38.5×10^{-5}	4.10	dia. 100 × 150
СБМ-2	36	400	0.1	—	80	—	—	—	0.065	dia. 48 × 28.5
СБМ3-3	36	400	0.1	3.6 VA	2.5	—	—	—	—	—

Notes. 1. Basic specifications are given for the joint operation with a respective transmitter.
2. The speed ensuring synchronous follow-up of receiver rotor is 500 r/min.
3. The service life of magslips at an average operational speed of 10 r/min is 3,000 hours.
4. The magslip receivers will operate trouble-free at an ambient temperature of −40 to +40°C (−40 to +55°C for БС-500 and ДБС-500 magslips) and a relative humidity up to 98 per cent.

Table A.22

Magslips with Intervening Transformers

Magslip type	Function performed	Field voltage, V	Frequency, Hz	Field current, A	Input power, W	Specific torque, N·m/deg.	Specific output voltage, V	Mass, kgf	Overall dimensions, mm
БД-160А	Transmitter	110	400	0.30	10	—	—	0.465	dia. 45×80
БС-151А	Indicating receiver	110	400	0.30	7.5	$\frac{1.25\times10^{-4}}{1.4\times10^{-4}}$	—	0.41	dia. 45×68
БС-155А	Transformer receiver	—	400	0.15	4	—	0.7	0.365	dia. 45×68

Notes. 1. The БД-160А transmitter can operate as a magslip transformer with one receiver БС-155А or as a magslip indicator with two receivers БС-151А.
2. Specific output voltage of БС-151А is specified for a load resistance of 1,000 ohms.
3. Specific torque of magslip БС-155А is given in the numerator when operating in conjunction with a transmitter of the same type and that given in the denominator concerns the magslip receiver operating in conjunction with a БД-160А transmitter.

Table A.23

Sine-Cosine Rotary Transformers

Transformer type	Supply voltage, V	Frequency, Hz	No-load input resistance, Ohm	Transformation ratio	Overall dimensions, mm
2,5ВТ	12	400	200	1	dia. 25×64
	27		400		
	27		800		
	27		1,600		

Table A.23 (cont.)

Transformer type	Supply voltage, V	Frequency, Hz	No-load input resistance, Ohm	Transformation ratio	Overall dimensions, mm
3,2BT	27	400	200	1	dia. 32 × 72
	27		400		
	40		800		
	40		1,600		
	40		3,200		
4BT	27	400	200	1	dia. 40 × 87
	40		400		
	40		800		
	40		1,600		
	40		3,200		
5BT	60	400	200	1	dia. 50 × 100
	127		400		
	60		800		
	127		1,600		
	127		3,200		
6BT	127	400	200	1	dia. 60 × 110
	127		400		
	127		800		
	127		1,600		
	127		3,200		

Note. The magnetic circuit of these rotary transformers is made of permalloy.

Index

Adjustable-frequency speed control system, 190, 191
Aerodynamic noise, 136
Amplidyne, 24, 31-44
Amplidyne dynamic characteristic, 36-44
Amplidyne motor-generator set, 45
Amplidyne response, 41
Amplidyne static characteristics, 36-44
Amplification, 23
Amplifier quality factor, 23
Amplifier response, 23
Amplitude-and-phase control method (see capacitor control method), 102, 103-107
Amplitude control method, 101-107
Amplitude error, 198, 199, 273
Angular engagement error, 298
Angular error, 251
Armature control method, 63-68
Asymmetric field, 150
Automatic multiplier, 301, 302
Auxiliary motor, 49
Auxiliary single-phase motors:
  induction with starting elements, 181-186
  split-and-shaded-pole, 176-180

Backward-rotating field, 94
Backward-sequence system of vectors, 97
Balancing adjustment, 274-280
Balancing of windings, 82, 83
Bias voltage shaping, 286, 287

Calculators, 227
Capacitor control method (see amplitude-and-phase control method), 103-107
Capacitor motor, 181
Capacitor motor speed-torque characteristic, 181
Circular field, 93
Commutator motor, 48
Compensated amplidyne, 33
Compensating field, 32
Compensating loop, 42
Compensation factor, 33
Contactless motors, 54-63
Continuous control, 63
Continuous-running synchronous motors, 116-138, 145
Cosine rotary transformer, 274
Critical angle, 25, 27
Critical slip, 87, 189
Cross-magnetized amplifier (see amplidyne), 22, 24
Current gain, 23

Damping factor, 174
Damping torque, 174
Data transmission line, 239, 252, 260
Differential synchro, 236, 252-254
Differentiator, 228
Disk-armature motor, 50, 53, 54
Drag torque, 94
Dynamic synchronizing torque, 245

Eccentric rotor, 150
Electromagnetic coupling, 42
Electromagnetic damping, 173
Electromagnetic-field motor, 54
Electromagnetic synchronizing torque, 139
Electromechanical time constant, 81, 113, 114
Elliptical field, 93, 94
Endurance (electrical and mechanical), 19
Error angle, 239
Exciting power, 109

Factor of proportionality, 67
False zero, 297
Ferraris motor, 49, 87
Field control method, 68-73
Fine-channel error, 297
Forward-rotating field, 94
Forward-sequence system of vectors, 97
Fractional-horsepower motors, 48-197
Full-pitch amplidyne, 31-36

General-purpose machines, 9

Harmonic-drive motor, 155-161
Heteropolar switching, 164
Hollow ferromagnetic rotor motor, 93
Hollow nonmagnetic armature motor, 50, 54
Hollow nonmagnetic rotor motor, 89-91
Hunting, 138-140
Hysteresis loop, 130, 133
Hysteresis motor, 128-138

Hysteresis motor speed-torque characteristic, 130, 132
Hysteresis torque, 129-132

Increment (see step angle), 166
Indicating transmission system, 252-256
Induction motor-amplifier set, 186-189
Induction regulator, 46
Induction servo motor control characteristic, 107, 108
Induction servo motor dynamic characteristic, 112-116
Induction servo motor speed-torque characteristic, 106, 107
Induction servo motors, 87-116
Inertial running, 95, 114, 115
Inherent damping factor, 66, 67, 71
Instability of rotor speed, 144
Instantaneous rotor speed, 138
Integrators, 193-195
Intensity of failures, 14-16
Intercommutating interval, 58
Intervening-transformer magslip, 235, 236
Inverted rotary transformers, 268

Linear rotary transformers, 265, 266, 280-286
Low-inertia induction servo motor, 89
Low-inertia motors, 50-54

Magnetic lag, 129
Magnetic shunt, 179
Magslips, 233-236
Motor-amplifier set speed-torque characteristic, 188, 190
Multiplex reception, 245
Multiplex transmission system, 259

No-contact rotary transformer, 268
No-failure probability, 14
Nonmagnetic barrier, 234
Nonrepairable equipment, 13, 14
No-trouble probability, 14
No-trouble time, 18
No-voltage signal, 217, 219

Output voltage ripples:
  armature, 205
  commutator, 206
  tooth, 205
Output voltage unbalance, 204, 207
Overcompensated amplidyne, 33

Path tracer unit, 303-305
Permanent-magnet motor angular characteristic, 120, 121
Permanent-magnet motors, 55, 60, 117-121
Phase control method, 102
Phase error, 198, 199, 273, 274
Phase-shifting network, 85
Pole shader, 177
Position detector, 54-56, 60
Power gain, 23, 36-38
Primary balancing adjustment, 275, 276
Printed armature winding, 53
Program-control systems, 195-197
Pulsating field, 95
Pulsating torque, 142
Pulsed control, 63, 73-77

Radar antenna drive system, 226, 227
Radar relative bearing data transmission, 260-263
Radioactive level gauge, 259, 260
Rate of response, 175, 176
Reactionary torque, 256
Receiver error, 244
Reducing motor, 145-149
Reliability, 13, 14, 17-21
Reluctance motor, 122-128
Reluctance motor angular characteristic, 125-127
Reluctance torque, 124-127
Reluctance torque equation, 157
Remote angular displacement transmission system, 294-300
Remote transmission angular error, 298
Repairable equipment, 13, 14
Requirements to fractional-horsepower machines, 12, 13
Rotary amplifiers, 22-47
Rotary transformer errors:
  design, 292
  manufacturing, 292
  operational, 293
  output characteristic distortion, 291, 292
Rotary transformers, 265-305
  accuracy classes of, 293
Rotor wheels, 150

Scale rotary transformer, 265, 280, 286-288
Secondary balancing adjustment, 276-279
Self-excited rotary amplifier, 24-31
Service life, 17, 21
Servo motor control characteristic, 75-77
Servo motor dynamic characteristic, 77-82
Servo motor speed control, 63-77
Servo motor speed-torque characteristic, 76, 78
Servo motors, 49, 50, 60-82
Servo system, 10, 11
Signal voltage shaping
Sine-cosine rotary transformers, 265, 269-280, 294-300
Sine rotary transformer, 269-273
Single-step angle generation, 171
Slip-ring rotary transformer, 267

Slip-ring synchro, 231-233
Slip-torque characteristic, 181
Space control method, 102-107
Spark-discharge machine, 192, 193
Specific synchronizing torque, 142, 243
Squirrel-cage induction servo motor, 88
Stability of rotor speed, 138, 143
Stable equilibrium, 243
Stable equilibrium point, 297
Static angular error, 244
Static stability, 170
Stator-to-rotor tooth ratio, 221
Stator tracks, 150
Steady state gain, 67, 70, 202
Steady state stability, 87
Step angle (see increment), 166
Step number, 166
Stepper motor angular characteristic, 169-171
Stepper motor static condition, 169
Stepper motor steady state condition, 173
Stepper motor transient condition, 175, 176
Stepper motors:
  inductor, 168
  permanent-magnet, 162-166
  reluctance, 166-168
Stepping angle, 170
Steromotor, 149-155
Switching device, 161
Synchro indicator dynamic characteristic, 256-259
Synchro indicators, 237-247
Synchro-motor set, 254, 255
Synchro receiver, 237-241
Synchro transformers, 247-252
Synchro transmitter, 237-241
Synchronizing torque, 241-243
Synchronous motor speed control, 138-145
Synchronous motor-transformer set, 190-192
Synchronous motors, 48, 116-176
Synchros, 230-264

Tachogenerator as accelerometer, 207
Tachogenerator as automatic computer element, 227-229
Tachogenerator as inertial differentiator, 223
Tachogenerator as speed counter, 225, 226
Tachogenerator as speed regulation system element, 226, 227
Tachogenerator dynamic characteristic, 222-224
Tachogenerators, 198-229
  direct-current, 199-208
  induction, 208-220
  synchronous, 221-222
Threshold torque/pulse rate curve, 174, 175
Through construction, 88
Torque equilibrium equation, 77
Transformer coupling, 217
Transient overshoot, 172
Transient process, 41
Transistor commutator, 54-63
Transistor switch, 190
Transmitter error, 244

Undercompensated amplidyne, 33
Unipolar excitation magslip, 233-235
Unipolar switching, 164
Universal commutator motors, 82-86
Unstable equilibrium, 243
U-shaped characteristic, 135

Vector-computing rotary transformer, 265, 280, 288-291
Voltage gain, 23

Wire annealing installation, 225, 226

TO THE READER

Mir Publishers welcome your comments on the content, translation, and design of the book.

We would also be pleased to receive any suggestions you care to make about our future publications.

Our address is: USSR, 129820, Moscow, I-110, GSP, Pervy Rizhsky Pereulok, 2, Mir Publishers.

Printed in the Union of Soviet Socialist Republics